



SAPIENZA
UNIVERSITÀ DI ROMA

Exotic hadron spectroscopy

Scuola di Dottorato in Scienze Matematiche, Fisiche e Naturali
"Vito Volterra"

Dottorato di Ricerca in Fisica – XXVIII Ciclo

Coordinatore Prof. M. Testa

Candidate

Alessandro Pilloni

ID number 696196

Thesis Advisor

Prof. A.D. Polosa

A thesis submitted in partial fulfillment of the requirements
for the degree of Doctor of Philosophy in Physics

December 2015

Thesis not yet defended

Exotic hadron spectroscopy

Ph.D. thesis. Sapienza – University of Rome

© 2015 Alessandro Pilloni. All rights reserved

This thesis has been typeset by \LaTeX and the Sapthesis class.

Author's email: alessandro.pilloni@roma1.infn.it

Acknowledgments

*My comeback to Physics was neither easy nor trivial, and the list of people I am indebted to would be as long as this thesis itself. For the sake of brevity, I will restrict to thank a few of them. Firstly, I need to thank my supervisor, prof. Antonello Polosa. The creative, energetic and pragmatic way he affords any physical problem has influenced me deeply. But more than that, he invested so much on me, and gave me much more freedom than any other supervisor I have heard about. I mainly owe him my comeback to physics. I will never forget the first time I received an email from him, saying he had some work for me. I was really tempted not to answer, because I was almost sure he had written to me by mistake. Sometimes, I still think that, but *alea iacta fuit* already.*

I thank Fulvio Piccinini, his humanitas, and the modest way to cast doubts on his own work, even when discussing with students, in spite of his deep competence in physics. I thank Riccardo Faccini for not throwing me out of his office, despite the number of times I harassed him for questions on statistics and data analysis. I am particularly grateful to prof. Luciano Maiani, for having interacted and spent himself with an orders-of-magnitude less experienced student like me. The discussions with him form the core of my scientific knowledge.

I thank Fabio Anulli and Luca Cavoto for allowing me to join the BABAR Collaboration, despite my formation as a theorist. What I have learned performing data analysis on my own, is definitely much more valuable than many abstract speculations. I thank Marco Bochicchio for sharing his noncommon sight on nonperturbative QCD.

Special thanks go to Angelo Esposito and Andrea Leonardo Guerrieri for tolerating me, and in particular for sustaining me during last year. Our discussions have been funny and deep, and I definitely would be more sad and ignorant without them. I wish to thank many other students, researchers and professors I met and I discussed with along these years, and I owe them part of my scientific formation: (in strict alphabetic order) Antonio Augusto Alves Jr., Alessandro Caloi, Gianluca Filaci, Isabella Garzia, Ivan Girardi, Paolo Lami, Matteo Mori, Mauro Papinutto, Niccolò Scopigno, Nazario Tantalò, Massimo Testa.

I thank the INFN sez. Roma, in particular Marco Rescigno, Gianni Salmé and Luca Silvestrini, and the doctoral school “Vito Volterra” for giving me support to go to much more schools and conferences than I deserved to go.

I conclude thanking my company partners, who unawaresly persuaded me to come back to university, and my family and friends for not giving up with me.

Contents

Introduction	1
1 Ordinary quarkonia	5
1.1 The birth of the quark model	5
1.2 Deep inelastic scattering and the discovery of partons	7
1.3 Color and QCD	9
1.4 The discovery of J/ψ	10
1.5 Quarkonia	11
2 Four-Quark states in Large-N QCD	13
2.1 A short guide to Large- N QCD	13
2.2 Weinberg’s observation	16
2.3 Flavor structure of narrow tetraquarks	20
2.4 Hypothetical non-perturbative contributions to tetraquark operators	21
2.5 Flavored tetraquarks in Corrigan-Ramond Large- N limit	23
2.6 Flavored tetraquarks in ‘t Hooft Large- N limit	26
3 Experimental overview	29
3.1 $Z(4430)$	35
3.2 Charged states in the 3900-4300 MeV region	37
3.3 Charged bottomonium states: $Z_b(10610)/Z'_b(10650)$	41
3.4 Pentaquark states	44
3.5 The $X(3872)$ saga	44
3.5.1 More on the $X(3872)$ spin [1]	54
3.6 Vector resonances	54
3.7 The 3940 family	57
3.8 Other states	59
4 Lattice QCD status of exotics	61
5 Phenomenology	65
5.1 Molecule	65
5.1.1 Low-energy universality and line shapes of the $X(3872)$	67
5.1.2 Non-Relativistic Effective Field Theory	69
5.1.3 Candidates	71
5.2 Hadro-quarkonium	72
5.2.1 Candidates	73

5.3	Hybrids and Born-Oppenheimer tetraquarks	74
5.3.1	Candidates	78
5.4	Alternative explanations	78
6	The prompt production of $X(3872)$	81
6.1	Pion rescattering and $X(3872)$ production [2, 3]	83
6.2	Comparison with deuteron and light nuclei [4]	87
7	Tetraquarks	95
7.1	Tetraquark production [3, 5]	96
7.2	Diquarks	99
7.3	Diquark-antidiquark States with $L = 0$	102
7.3.1	The X tetraquark	102
7.3.2	The Z tetraquark	104
7.3.3	Scalar and Tensor states	105
7.4	Spectrum of $L = 0$ states	107
7.5	Diquark-antidiquark States with $L = 1$	109
7.6	Spectrum of $L = 1$ states	110
7.6.1	The $Y(4220)$ state [6]	112
7.7	A brief note on the Z_c in the type-I tetraquark model [7]	116
7.8	The $b\bar{b}$ sector	117
7.9	Multi-diquark states	118
7.10	Amplitudes in the compact tetraquark model	120
7.10.1	Constituent Counting Rules	121
7.10.2	Brief review on QCD sum rules	122
7.11	Probing the nature of the Z_c via the $\eta_c \rho$ decay [8]	123
8	Production of exotic states at hadron colliders	127
8.1	Possible production of doubly charmed states [9, 10]	127
8.2	Compact tetraquarks and meson molecules in heavy ion collisions . .	134
	Conclusions	141
A	One-loop β of QCD by the background field method	143
B	Heavy meson chiral Lagrangians	151
C	NREFT amplitudes and loop integrals	153
	Bibliography	155

Introduction

Since the discovery of the $X(3872)$, a decade ago, more than 20 new charmonium-like resonances have been registered. Most of them have features which do not match what expected from standard charmonium theory. A few resonances have been found in the beauty sector too. Some authors just claim that most of the so called XYZ states are not even resonances but kind of effects of kinematical or dynamical origin, due to the intricacies of strong interactions. According to them, data analyses are naïvely describing and fitting as resonances what are indeed the footprints of such complicated effects.

On the other hand, the $X(3872)$, for example, is an extremely narrow state, $\Gamma \lesssim 1$ MeV, and it is very difficult, in our understanding, to imagine how this could be described with some sort of strong rescattering mechanism. We do not know of other clear examples of such phenomena in the field of high-energy physics and in this review we will give little space to this kind of interpretations, which we can barely follow. We shall assume instead that what experiments agree to be a resonance is indeed a resonance.

Moreover, we find very confusing the approach of mixing the methods proper of nuclear theory to discuss what we learned with the observations of XYZ resonances especially at Tevatron and LHC. It is true that X seems to be an extreme version of deuterium as its mass happens to be fine-tuned on the value of the $D^0 D^{0*}$ threshold, but one cannot separate this observation from the fact that X is observed at CMS after imposing kinematical transverse momentum cuts as large as $p_T \simeq 15$ GeV on hadrons produced. Is there any evidence of a comparable prompt production of deuterium within the same kinematical cuts, in the same experimental conditions? The ALICE experiment could provide in the near future a compelling measurement of this latter rate (and some preliminary estimates described in the text are informative of what the result will be).

Some of the XYZ , those happening to be close to some threshold, are interpreted as loosely-bound molecules, regardless of the great difficulties in explaining their production mechanisms in high energy hadron collisions. Some of them are described just as bound hadron molecules, once they happen to be below a close-by open flavor meson threshold. Other ones, even if sensibly above the close-by thresholds, have been interpreted as molecules as well: in those cases subtle mistakes in the experimental analysis of the mass have been advocated.

As a result the field of the theoretical description of XYZ states appears as an heterogeneous mixture of ad-hoc explanations, mainly post-dictions and contradictory statements which is rather confusing to the experimental community and probably self-limiting in the direction of making any real progress.

It is our belief instead that a more simple and *fundamental* dynamics is at work in the hadronization of such particles. More quark body-plans occur with respect to usual mesons and baryons: compact tetraquarks. The diquark-antidiquark model in its updated version, to be described in Chapter 7, is just the most simple and economical description (in terms of new states predicted) that we could find and we think that the recent confirmation of $Z(4430)^+$ especially, and of some more related charged $J^{PG} = 1^{++}$ states, is the smoking gun for the intrinsic validity of this idea.

The charged $Z(4430)$ was the most uncomfortable state for the molecular interpretation for at least two reasons: *i*) it is charged and molecular models have never provided any clear and consistent prediction about charged states; *ii*) it is far from open charm thresholds. However, if what observed (by Belle first and confirmed very recently by LHCb) is not an “effect” but a real resonance, we should find the way to explain and put it in connection to all other ones.

The $Z(4430)$ appears extremely natural in the diquark-antidiquark model, which in general was the only approach strongly suggesting the existence of charged states years before their actual discovery.

We think otherwise that open charm/beauty meson thresholds should likely play a role in the formation of XYZ particles. We resort to the Feshbach resonance mechanism, as mediated by some classic studies in atomic physics, to get a model on the nature of this role. The core of our preliminary analysis, as discussed in Chapter 7, is the postulated existence of a discrete spectrum of compact tetraquark levels in the fundamental strong interaction Hamiltonian. The occurrence of open charm/beauty meson thresholds in the vicinity of any of these levels might result in an enhanced probability of resonance formation.

The thesis is organized as follows:

- In Chapter 1 we sketch a general introduction on the quark model and QCD, and describe the ordinary quarkonium systems.
- In Chapter 2 we review a recent discussion on the existence of tetraquarks in Large- N QCD: for a long time multiquark states have been expected to be extremely broad in the large- N limit, but recently this theoretical obstacle has been suggesting that even tetraquarks might have order $1/\sqrt{N}$ decay amplitudes for they occur as subleading poles in the connected diagrams of the $1/N$ expansion.
- Chapter 3 is devoted to a comprehensive experimental overview. We underscore that a genuine tetraquark appears in the physical spectrum, the $Z(4430)$. We also discuss the recent discovery of two pentaquark states.
- Chapter 4 discuss the recent lattice studies in the XYZ field, which appear to be still in their infancy. Lattices of $2 \div 3$ fm in size cannot by definition allow loosely bound molecules and it is not yet tested how those deeply bound lattice-hadron-molecules, that some studies claim to observe in lattice simulations, will tend to become loosely bound states in some large volume limit. Moreover it is not clear how one can safely distinguish on the lattice between a tetraquark operator, a standard charmonium and a meson-meson operator, as they all happen to mix with each other.

- Chapter 5 reviews the various phenomenological models in the literature: mainly nuclear-theory inspired molecular models, hybrids, hadro-quarkonia.
- Chapter 6 discusses the discriminative problem of producing loosely bound molecules at hadron colliders, which is considered as one of the most compelling motivations to go towards compact tetraquarks. This chapter is composed mainly by our original Monte Carlo simulations about the rescattering of pions and their influence for the X production cross section. We also discuss our comparison between the X and light nuclei cross sections at hadron colliders.
- Chapter 7 is devoted to the tetraquark model. After a presentation of the Feshbach mechanism, which might provide some new selection rules to explain the nonobservation of many predicted states, we show the general formalism, and discuss the updated spectrum. We then present some results obtained for particular resonances or decay channel, within the diquark-antidiquark model.
- In Chapter 8, we discuss our proposal of searching for doubly charmed states, inspired by the problem of simulating tetraquarks on lattices. Some hints from the physics of heavy-ion collisions are also considered.

Chapter 1

Ordinary quarkonia

In this chapter we aim at giving a brief overview about the quark model description of the standard hadrons, focusing on the heavy $Q\bar{Q}$ system. For a historical review, see [11].

1.1 The birth of the quark model

Heisenberg introduced the approximate $SU(2)$ *isospin* symmetry, that would be respected by strong interactions and violated by electromagnetic and weak processes. The proton and the neutron would transform like a doublet in this new internal space. This explained the small mass difference between the two, and justified the presence of both nucleons inside the nuclei. The Yukawa particle, discovered in the 3 states of charge π^+ , π^- and π^0 , was considered the mediator of strong interactions, and transformed indeed in the adjoint representation of $SU(2)$.

However, in late '50s the number of strongly interacting particles started increasing, and a zoo of new mesons and baryons challenged the understanding of the hadron sector. It was noticed that some of these particles were produced in pair with cross sections typical of strong processes, but decayed much more slowly with typical weak-interaction lifetimes. Gell-Mann, Nakano and Nishima realized that this could be understood if an additional quantum number were introduced, called *strangeness* S , conserved by strong and electromagnetic interactions but not by weak interactions. The introduction of the Cabibbo angle [12] and the discovery of parity violations in weak decays enriched the framework of weak physics, but left the hadron spectrum in a non-understood state.

To infer a pattern, Sakata proposed to embed the $SU(2)$ isospin symmetry and the $U(1)$ strangeness in a larger $SU(3)$ group, with p , n and the strange baryon Λ to transform in the fundamental representation of the group. The discovery of many other baryons and mesons discredited this model, but Gell-Mann and Ne'eman included all the known mesons and baryons with the same quantum numbers, either in the adjoint representation of the group (the *eightfold way*), or in other representations based on this, for example the decuplet or the 27-plet (indeed, $\mathbf{8} \otimes \mathbf{8} = \mathbf{1} \oplus \mathbf{8} \oplus \mathbf{8} \oplus \mathbf{10} \oplus \bar{\mathbf{10}} \oplus \mathbf{27}$). The weight diagrams are shown in (Figure 1.1). Furthermore, using the breaking of $SU(3) \rightarrow SU(2)_I \otimes U(1)_S$, Gell-Mann was able to derive relations between the masses of the various multiplets. For example the

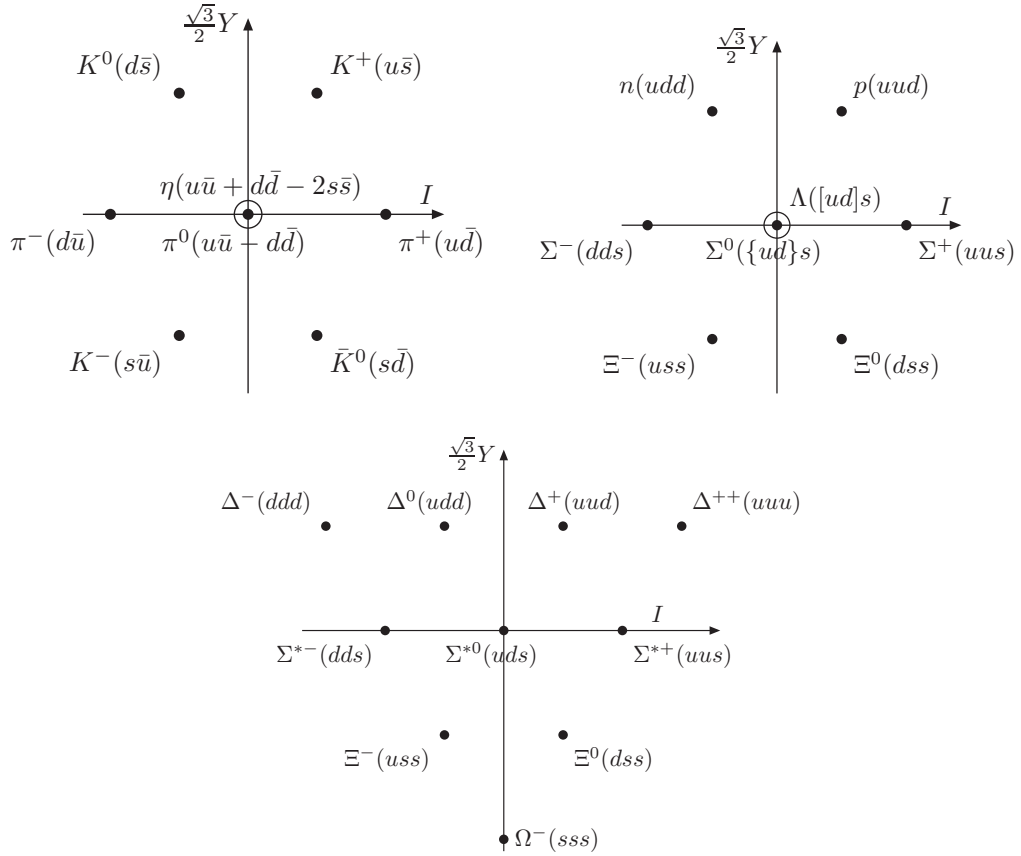


Figure 1.1. Weight diagrams for $J^{PC} = 0^{-+}$ mesons (in the $\mathbf{8}$), $J^P = 1/2^+$ baryons (in the $\mathbf{8}$), and $J^P = 3/2^+$ baryons (in the $\mathbf{10}$). A flavor-singlet η' meson, which completes the nonet, was later discovered.

Gell-Mann-Okubo formula [13], which implies

$$2(m_N + m_\Xi) = 3m_\Lambda + m_\Sigma, \quad (1.1a)$$

$$m_{\Sigma^*} - m_\Delta = m_{\Xi^*} - m_{\Sigma^*} = m_{\Omega^-} - m_{\Xi^*} \quad (1.1b)$$

for the octet and decuplet of baryons, respectively. This leads the prediction of a Ω^- baryon with $Q = -1$ and $S = -3$ and of mass ~ 1670 MeV. The discovery of a particle with these very same characteristics in 1964 delivered the Nobel Prize to Gell-Mann.

Soon after, Gell-Mann and Zweig considered what kind of particles might transform in the fundamental representation of $SU(3)$ [13]. These unobserved particles, called *quarks*, would carry baryonic number $B = 1/3$, and fractional charge as well. The *up* (u) and *down* (d) quarks are an isospin doublet, and carry $S = 0$, while the *strange* (s) quark is an isospin singlet, and carries $S = -1$. The weight diagrams are shown in (Figure 1.2). The hypercharge Y is defined to be $B + S$ and is related to the electric charge by the Nishima relation,

$$Q = I_3 + \frac{Y}{2}, \quad (1.2)$$

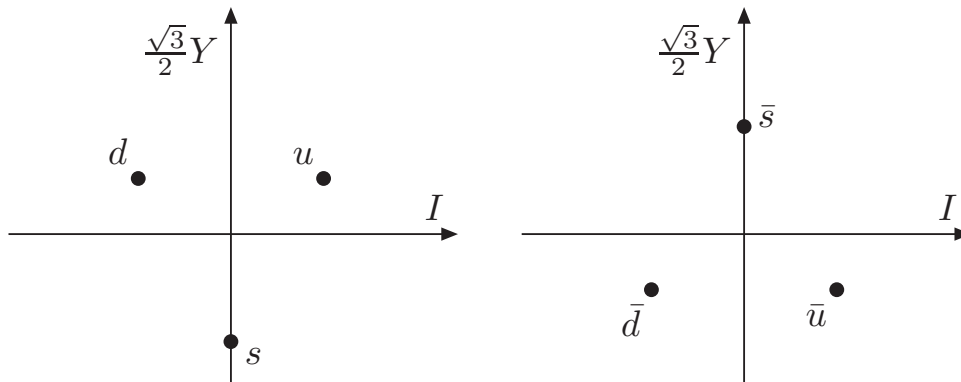


Figure 1.2. Weight diagrams for quarks (in the $\mathbf{3}$) and antiquarks (in the $\bar{\mathbf{3}}$).

so that the u quark has $Q = 2/3$, and the d, s have $Q = -1/3$.

With this fundamental constituents, it is possible to build integer-charge baryons and mesons according to

$$\text{Mesons :} \quad \mathbf{3} \otimes \bar{\mathbf{3}} = \mathbf{1} \oplus \mathbf{8} \quad (1.3a)$$

$$\text{Baryons :} \quad \mathbf{3} \otimes \mathbf{3} \otimes \mathbf{3} = \mathbf{1} \oplus \mathbf{8} \oplus \mathbf{8} \oplus \mathbf{10} \quad (1.3b)$$

Moreover, if the quarks are fermions, baryons are fermions as well, while mesons are bosons, as expected.

In his original paper, Gell-Mann stressed how these quarks might have no physical content, and could be considered as mere mathematical entities. The motivations of this *caveat* were twofold: at the time, the most popular theoretical framework in strong interactions was the so-called S -matrix theory. Geoffrey Chew, in particular, proposed that talking about constituents of hadrons was meaningless, and that it was possible to calculate the full spectrum of hadrons by assuming some kind of inter-hadron potential, building the most general S -matrix fulfilling the requirements of analyticity, unitarity, and crossing symmetry, and then obtaining the hadron poles in a self-consistent evaluation (the so-called *bootstrap* program). Moreover, the idea of hadron constituents recalled a description in terms of elementary quantum fields. Whereas this was proved to work for electrodynamics, the application to strong interactions was seriously challenged by Landau and the discovery of Landau poles. Another Gell-Mann's concern was that there was no experimental sign of fractional charged particles.

1.2 Deep inelastic scattering and the discovery of partons

From mid-'50s to late '60s, the Stanford universities was the theater of many important discoveries using an accelerated electron beam on hydrogen and helium targets. In 1956, McAllister and Hofstadter measured the elastic form factor of the proton. The tree-level cross-section of relativistic electrons on point-like protons is

given by

$$\left(\frac{d\sigma}{d\Omega}\right)_{\text{point-like}} = \frac{\alpha^2 \cos^2 \frac{\theta}{2}}{4E^2 \sin^4 \frac{\theta}{2}} \frac{E'}{E} \left[1 - \frac{q^2}{2M} \tan^2 \frac{\theta}{2} \right] \quad (1.4)$$

where E (E') is the energy of the ingoing (outgoing) electron in the laboratory frame, $q^2 = -Q^2 = -4EE' \sin^2 \frac{\theta}{2}$ is the square of the transferred 4-momentum, and M is the proton mass. If the proton is not pointlike, the hadronic current can be parametrized in terms of form factors,

$$J_{\text{had}}^\mu = \bar{u}(P_f) \left(F_1(q^2) \gamma^\mu + i \frac{q_\nu \sigma^{\mu\nu} \kappa}{2M} F_2(q^2) \right) u(P_i) \quad (1.5)$$

where P_i and P_f are the initial and final proton 4-momenta, and $\kappa = 1.79$ is the anomalous magnetic coupling in units of the nuclear magneton $\frac{e}{2M}$. The form factors are normalized to $F_1(0) = F_2(0) = 1$. The resulting cross-section is the Rosenbluth formula:

$$\left(\frac{d\sigma}{d\Omega}\right)_{\text{Rosenbluth}} = \frac{\alpha^2 \cos^2 \frac{\theta}{2}}{4E^2 \sin^4 \frac{\theta}{2}} \frac{E'}{E} \left[\left(F_1^2 + \frac{\kappa^2 Q^2}{4M^2} F_2^2 \right) + \frac{Q^2}{2M} (F_1 + \kappa F_2)^2 \tan^2 \frac{\theta}{2} \right] \quad (1.6)$$

For an exponential charge distribution, $\rho(\vec{r}) = \exp(-r/r_p)$, the form factors are expected to fall as $F \propto 1/(1 + r_p Q^2)$. This led to the expectation that the cross section had become smaller and smaller after the resonances region. However, in 1969 the same experiment was performed in the deep-inelastic region, *i.e.* observing the $e^- \rightarrow p \rightarrow e^- X$ process, where X is whatever hadronic final state, generally undetected. The cross section is now

$$\frac{d\sigma}{d\Omega dE'} = \frac{\alpha^2 \cos^2 \frac{\theta}{2}}{4E^2 \sin^4 \frac{\theta}{2}} \left[W_2(\nu, Q^2) + 2W_1(\nu, Q^2) \tan^2 \frac{\theta}{2} \right] \quad (1.7)$$

with $\nu = E' - E$ the exchanged energy, and W_1 and W_2 two form factors with the dimension of the inverse of an energy. The experiment observed that the adimensional variables $F_2 = \nu W_2$ and $F_1 = M W_1$ did not fall with increasing Q^2 , but instead tended to a value that depended on the single adimensional variable $x = \frac{Q^2}{2M\nu}$. This behavior, named “scaling”, was predicted by Bjorken in the case of scattering over pointlike particles. Feynman christened these quasi-free constituents “partons”, and showed that x is the fraction of momentum of the proton carried by the stroked parton. Calling $x f_q(x)$ the related probability density, the form factors are

$$F_2(x) = \sum_q e_q^2 x f_q(x) \quad (1.8a)$$

$$F_1(x) = \sum_q \frac{e_q^2}{2} f_q(x) \quad (1.8b)$$

where q runs over the different partons. We can identify the partons with Gell-Mann quarks, and for the proton we get the sum rules

$$\int dx [f_u(x) - f_{\bar{u}}(x)] = 2 \quad (1.9a)$$

$$\int dx [f_d(x) - f_{\bar{d}}(x)] = 1 \quad (1.9b)$$

$$\int dx [f_s(x) - f_{\bar{s}}(x)] = 0 \quad (1.9c)$$

which replaced the statement that the proton was composed of two u quarks and a d quark. Thus in Feynman's model these *valence* quarks were supplemented by a *sea* of quark-antiquark pairs. Finally, the Callan-Gross relation holds, *i.e.* $F_2 = 2x F_1$, which proves the Dirac nature of the quarks. If the quarks were the only kind of partons, the momenta of the quarks have to sum up to the total momentum of the proton, *i.e.*

$$\int dx x [f_u(x) + f_{\bar{u}}(x) + f_d(x) + f_{\bar{d}}(x) + f_s(x) + f_{\bar{s}}(x)] = 1 \quad (1.10)$$

but instead, is ~ 0.54 . The remaining fraction of the proton momentum has to be carried by neutral partons (which do not contribute to the form factors), and can be identified with the mediators of the strong interactions, the *gluons*.

1.3 Color and QCD

The discovery of the Δ^{++} , *i.e.* a baryon with completely symmetric wave function uuu , led to the introduction of a new quantum number to enforce the Fermi statistics, the *color*. Each quark transforms according to the fundamental representation of a new $SU(3)$ symmetry. For the Δ^{++} , the most simple wave function is $\epsilon_{ijk} u^i u^j u^k$, with ijk the new color indices. Because of the Levi-Civita symbol, the Fermi statistics is restored. The hadrons are expected to be color singlet, in order not to triplicate the existing physical spectrum. Another hint of the existence of the color is given by the Drell ratio, *i.e.*

$$R = \frac{\sigma(e^+e^- \rightarrow \text{hadrons})}{\sigma(e^+e^- \rightarrow \mu^+\mu^-)} \sim \sum_q e_q^2 \quad (1.11)$$

according to the quark model at tree-level. Thus, at energies of $\sqrt{s} \sim 2$ GeV, the ratio was expected to be $(\frac{2}{3})^2 + (-\frac{1}{3})^2 + (-\frac{1}{3})^2 = \frac{2}{3}$. A value of $R \sim 2$ was instead observed in the data, consistent with the expectation for three different quark colors. The Sixties witnessed different attempts to describe the strong interactions via a non-abelian Yang-Mills gauge theory. The observation of three $\rho^{\pm,0}$ vector mesons, which dominate the electromagnetic form factor of the pion (*vector meson dominance*, or VMD) led Sakurai to consider the ρ as the gauge boson of the $SU(2)$ isospin symmetry. However, the approximate nature of isospin, and the relatively large mass of the ρ meson did not favor this interpretation. On the other hand, the (apparently exact) $SU(3)$ color symmetry looked like a more promising candidate, although the 8 massless gauge bosons, called *gluons* had not been observed. An important

breakthrough happened in early '70s: 't Hooft and Veltman proved the renormalizability of Yang-Mills theories [14], in the case of both exact and spontaneously broken symmetries. Soon after, Gross and Wilczek [15], and Politzer [16] evaluated for the first time the β function of Yang-Mills theory, which describes the evolution of the QCD coupling constant according to the Renormalization Group as a function of the scale of the process:

$$\beta(g) = \mu \frac{dg}{d\mu} = \beta_0 g^3 + O(g^5) \quad (1.12)$$

In QED and in $\lambda\phi^4$ $\beta_0 > 0$, which means that at higher energies (or short distances) the effective coupling is larger and larger, whereas at low scales the coupling becomes small enough to allow for reliable perturbative calculations. Surprisingly, Gross, Wilczek and Politzer found that

$$(\beta_0)_{\text{QCD}} = -\frac{\frac{11}{3}N_c - \frac{2}{3}n_f}{(4\pi)^2} \quad (1.13)$$

where N_c is the number of colors and n_f the number of quark flavors, so that $\beta_0 < 0$ for $\frac{n_f}{N_c} < \frac{11}{2}$. The calculation of the QCD beta function is reported in Appendix A. So, the effective coupling is smaller at high energies, and this explains why observation consistent with quark objects were seen in the high-energy deep-inelastic scattering experiments. On the other hand, at low energies the coupling constant increases, and the hadron spectrum happens to be in the nonperturbative (incalculable) regime. This phenomenon is the so-called *asymptotic freedom*. The requirement that no colored particles appear in the physical spectrum is the *confinement* property of QCD, and forbids the direct observation of quarks and gluons.

1.4 The discovery of J/ψ

Back in 1970, Glashow, Iliopoulos and Maiani [17] introduced a fourth quark, the *charm* (c), to explain the absence of tree-level flavor-changing neutral currents (FCNC), which would be large according to the simplest combination of the Glashow-Weinberg-Salam theory of weak interactions [18] with the Cabibbo theory of hadronic currents [12]. The upper limit on the $K_L \rightarrow \mu^+ \mu^-$ branching ratio allowed for an estimate of the charm mass $m_c \sim 2$ GeV.

In early '70s, data seemed to disfavor the quark model. Some preliminary data showed that the R ratio started to increase, challenging the quark model prediction of a piecewise constant function. It was proposed that the raise might be due to a very narrow resonance, which the experimental resolution did not allow to resolve. In 1974, two different experiments in Brookhaven and SLAC announced the discovery of a new narrow resonance at a mass of 3.1 GeV. Ting led the Brookhaven group, and found what he called the J particle [19] using a high intensity proton beam on a Berillium target, $p + Be \rightarrow e^+ e^- X$, at $\sqrt{s} \sim 7$ GeV. A narrow peak showed up in the $e^+ e^-$ invariant mass spectrum at 3.1 GeV.

At the same time, Burton christened a new ψ resonance observed in $e^+ e^-$ collisions at SLAC, during an energy scan in the region around 3.1 GeV [20]. They observed a sharp narrow peak in $e^+ e^- \rightarrow e^+ e^-$, $e^+ e^- \rightarrow \mu^+ \mu^-$, and $e^+ e^- \rightarrow$ hadrons.

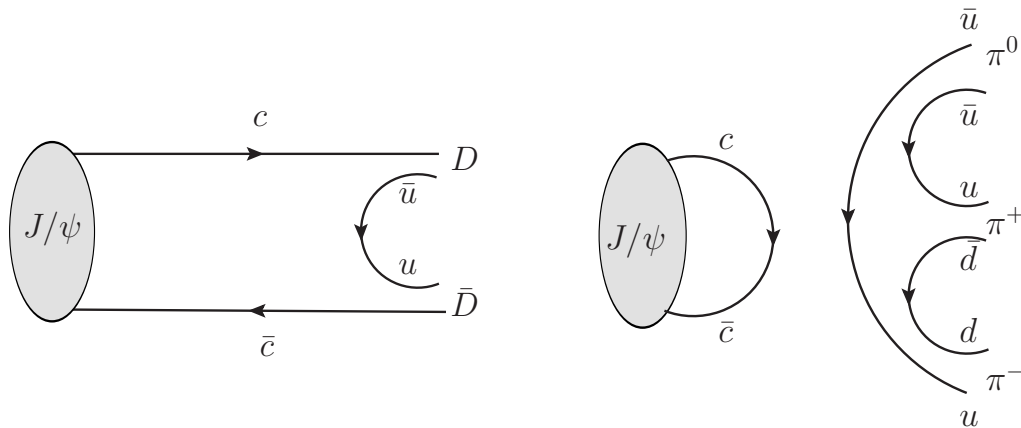


Figure 1.3. OZI allowed (left) and OZI forbidden (right) J/ψ decays. The latter is forbidden by phase space.

The natural width of this newly discovered particle, which was politely called J/ψ , was much smaller than the experimental resolution of the two experiments, but the indirect measure of the cross section allowed for an estimate $\Gamma_\psi \sim 90$ keV. The angular distribution for $e^+e^- \rightarrow \mu^+\mu^-$ were consistent with a $J^{PC} = 1^{--}$, whereas the observation of $J/\psi \rightarrow p\bar{p}$ and $J/\psi \rightarrow \rho^0\pi^0$ established an isosinglet assignment. Such surprising narrow state stimulated the theorists' fantasy. Appelquist and Politzer [21] proposed that the J/ψ could be a $c\bar{c}$ bound state in the spin triplet configuration.

The narrow width of the J/ψ can be qualitatively understood by the OZI rule, which explained the suppression of the $\Upsilon \rightarrow 3\pi$ mode with respect to the $\phi \rightarrow KK$ one, despite the much larger phase space. In (Figure 1.3) we show the different decay modes. The one in the left panel is OZI-allowed, the other one is OZI-suppressed, because it involves the annihilation of the $c\bar{c}$ pair. However, if the J/ψ happens to be below the open charm threshold, the former decay is phase-space forbidden. Two years later, the open-charm D mesons were indeed observed at SLAC at a mass of 1.87 GeV [22]. The other crucial ingredient added by Appelquist and Politzer is the asymptotic freedom: the $c\bar{c}$ pair has to annihilate in at least three gluons¹, so the hadronic width carries a factor $\alpha_s^3(m_c)$. Since we are already in the perturbative regime, this is further suppressed.

In 1977 the E288 collaboration observed a new narrow resonance, the Υ meson, with $m_\Upsilon = 9.5$ GeV and $\Gamma_\Upsilon = 54$ keV [23]. It was immediately described as a $b\bar{b}$ bound state, b being the fifth quark (*bottom* or *beauty*).

1.5 Quarkonia

In the static limit $m_Q \rightarrow \infty$, the quark-antiquark potential is a meaningful quantity, which can be related to the vacuum expectation value of a Wilson loop on a rectangular path with the long side in the time direction, much longer than the

¹The $c\bar{c}$ pair is a color singlet, and does not couple to one gluon. Two gluons have only $C = +$ signature, whereas the $c\bar{c}$ pair in J/ψ has $C = -$.

spatial side. The leading order perturbative calculation (one-gluon exchange) gives

$$V(r)_{\text{OGE}} = -\frac{4\alpha_s}{3r} \quad (1.14)$$

which is expected to hold at small distances. Higher-order corrections give only logarithmic corrections to α_s (running coupling). If so, the quarkonia would be a simple replica of an hydrogen atom. The ordinary quarkonium spectroscopy uses indeed the hydrogenoid notation for the levels, namely $n^{2S+1}L_J$, with $L = S, P, D, F \dots$. The idea of quark confinement has driven some of these models. The most successful choice is that of a linearly growing potential $V(r) = \sigma r$, where σ is the string tension of the chromoelectric flux tube connecting the quark and the antiquark. One of the most developed models uses the Cornell potential [24], which is build up as a simple sum of the OGE potential and of a linearly confining term

$$V(r)_{\text{Cornell}} = -\frac{\alpha}{r} + \sigma r \quad (1.15)$$

with α Nowadays, the potential can be calculated with remarkable precision in lattice QCD, and it is possible to estimate corrections to this simple formula (for example the Lüscher term, or the logarithmic corrections to α_s , and the $O(1/m_Q^2)$ corrections, see [25] and references therein). If m_Q is finite, the potential is no longer strictly defined. However, as long as $m_Q \gg \Lambda_{QCD}$, one can consider a Born-Oppenheimer-like approximation: the heavy quark pair motion to happen on much slower timescales than the color field; this allows us to solve the Schrödinger equation with the finite m_Q mass, using as background potential the Cornell one, obtained by studying the dynamic of the color fields as a function of the parametric distance r between the quark and the antiquark. The relativistic corrections at order $1/c^2$ can be included, obtaining a Breit-Pauli like Hamiltonian.

The annihilation of a quark-antiquark pair into photons and gluons can be evaluated in leading-order perturbative QCD, as a function of the value of the wave-function in the origin. Exclusive radiative and hadronic transitions can be estimated using QCD multipole expansion (see [26] for a review). All these ideas can be discussed in a proper effective Quantum Field Theory framework, like the Non-Relativistic QCD (NRQCD) [27]. For an updated review on theoretical and experimental state of quarkonia, see [28, 29].

Chapter 2

Four-Quark states in Large- N QCD

2.1 A short guide to Large- N QCD

Quantum Chromodynamics (QCD) in the limit of a large number, N , of colors [30] has been used in the past 40 years as a simplified though reliable model of the strong interaction phenomena [31]. The perturbative expansion in Feynman diagrams is simplified by a number of selection rules holding when $N \rightarrow \infty$. Nevertheless, the theory thus obtained is non-trivial and shows asymptotic freedom, being non-perturbative in the infrared region. Assuming that confinement persists also in the $N \rightarrow \infty$ limit, it can be shown that the following peculiar properties hold:

- Mesons and glueballs (bound states of just gluons as explained in Sec. 5.3) are stable and non-interacting at leading order in the $1/N$ expansion.
- Meson decay amplitudes are of order $1/\sqrt{N}$ and meson-meson elastic scattering amplitudes are of order $1/N$.
- OZI rule is exact and the mixing of mesons with glue states is suppressed.
- Baryons are heavier than mesons: they decouple from the spectrum having a mass growing as N .

All of these statements can be proven without computing explicitly Feynman diagrams, but simply counting their color factors. To do this and to follow the theoretical arguments reported in this section, it is first necessary to analyze in greater detail the content of QCD with $SU(N)$ gauge group.

Quark and antiquark fields have N color components, while gluon fields are $N \times N$ matrix-valued fields with $(N^2 - 1) \sim N^2$ independent components¹. As a result, the gluon bubble diagram, Figure 2.1a, brings a color factor N^2 since that is the number of possible intermediate gluon states. In contrast, a quark bubble diagram, Figure 2.1b, brings a color factor N being that the number of possible intermediate quarks. The interaction vertices $g\bar{q}q$ and ggg scale as $1/\sqrt{N}$

¹This approximation is justified because, as shown by 't Hooft [30], the traceless condition plays no role in the limit $N \rightarrow \infty$.

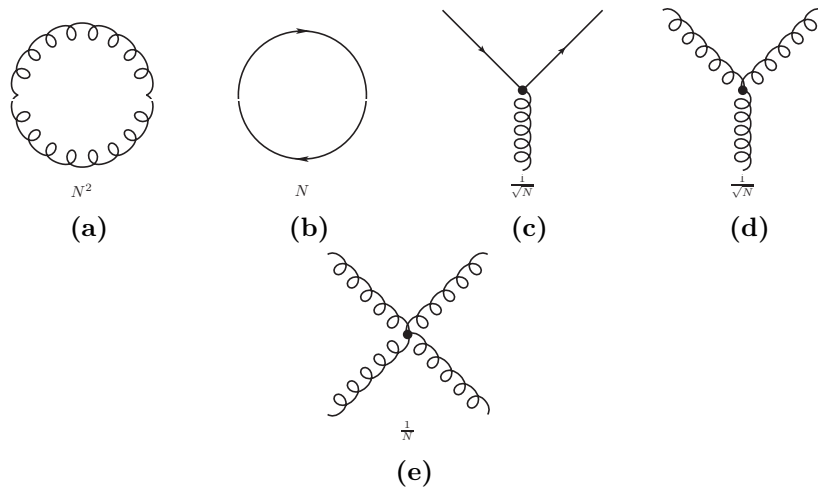


Figure 2.1. Basic rules for the counting of color factors in Feynman diagrams.

– Figure 2.1c and 2.1d – and the four-gluon vertex as $1/N$ – Figure 2.1e. These factors appearing in the interaction vertices are a consequence of the rescaling of the coupling constant, $\lambda = g/\sqrt{N}$, necessary to avoid further positive powers of N in the perturbative expansion in the rescaled Yang-Mills coupling λ . For instance, the perturbative expansion in λ of the gluon propagator is at most of order N^0 although, at this order in $1/N$, infinite diagrams with different orders in g contribute.

The simplest way to take properly into account all the combinatoric color factors is to introduce the ‘t Hooft double line representation [30]. As already observed, gluons are $N \times N$ matrices, thus, as far as the color factors are concerned, they are indistinguishable from $q\bar{q}$ pairs when N is large. For this reason one can substitute each gluon line with a couple of lines oriented in opposite directions. Examples of this representation are shown in Figure 2.2, 2.3 and 2.4. The gluon self energy diagram in Figure 2.2 is of order $N^2 \times g^4/N^2 = g^4$: the factor N^2 is consequence of the two color loops and g^4/N^2 of the four interaction vertices.

The diagram in Figure 2.3 is of order g^2/N , arising from the vertices only. In fact, in the double line representation, this diagram has no closed fermion lines and hence no powers N coming from loops. The comparison of this diagram with that in Figure 2.2 shows the difference between the weak-coupling and the Large- N expansion: a sub-leading term in the former, Figure 2.2, is not so in the latter, Figure 2.3, and viceversa. Moreover, $1/N$ is a good expansion parameter regardless of the running of g .

In Figure 2.4 it is shown an example of non-planar diagram. Non-planar means that it is impossible to draw it without line crossings. In this case the counting of color factors gives $N \times g^2/N \times g^2/N^2 = g^4/N^2$. Again, beside the vertices, the single factor of N comes from the only fermionic closed line present in the diagram. It can be shown that this relative suppression of the non-planar diagrams compared to the planar ones is true in general. This is one of the most important simplifications induced by the Large- N expansion.

The above discussion can be summarized in few important rules:

- Planar diagrams with only gluon internal lines are all of the same order in the $1/N$ expansion.
- Diagrams containing quark loops are subleading: the theory is quenched in the limit $N \rightarrow \infty$.
- Non-planar diagrams are also subleading.

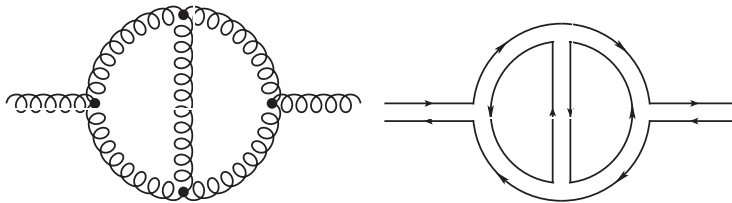


Figure 2.2. Planar diagram contributing to the gluon self energy at leading order in $1/N$ expansion, in usual and 't Hooft color line notation. The counting of color factors and couplings gives $N^2 \times g^4/N^2 = g^4$.

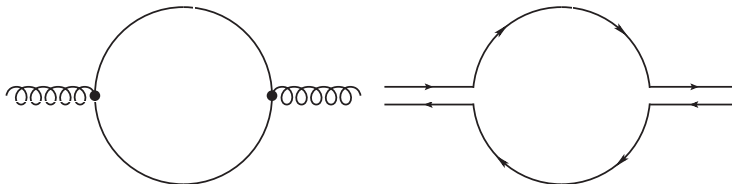


Figure 2.3. Example of a diagram with a quark loop, suppressed with respect to a planar diagram with gluon internal lines. The counting of color factors and couplings gives g^2/N , showing that although this diagram is leading in the coupling g expansion compared to the diagram in Figure 2.2, it is sub-leading in the $1/N$ counting.

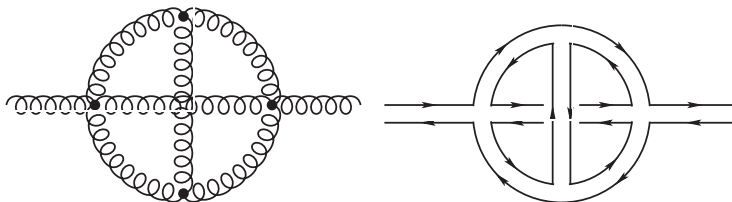


Figure 2.4. Non-planar contribution to the gluon self energy. The counting of color factors and couplings gives $N \times g^2/N \times g^2/N^2 = g^4/N^2$.

2.2 Weinberg's observation

In his classic Erice lectures [32], Coleman justifies the non-existence of exotic mesons noticing that the application of local gauge-invariant quark quadri-linear operators to the vacuum state creates meson pairs and nothing else. The argument was as follows.

By Fierz rearrangement of fermion fields, any color-neutral operator formed from two quark and two antiquark fields

$$Q(x) = \epsilon^{abc} \epsilon^{ade} q^b q^c \bar{q}^d \bar{q}^e \quad (2.1)$$

can be rewritten in the form

$$Q(x) = \sum_{ij} C_{ij} B_i(x) B_j(x), \quad (2.2)$$

where C_{ij} are numerical coefficients and

$$B_i(x) = \bar{q}(x) \Gamma_i q(x) \quad (2.3)$$

is some generic color-neutral quark bilinear with spin-flavor structure determined by the matrix Γ_i .

Let us look at the two-point correlation function of the Q operators, $\langle T(Q(x)Q^\dagger(y)) \rangle$, and perform the fermionic Wick contractions first². For simplicity, also suppose that the expectation value of single fermion bilinears vanishes, *i.e.* $\langle B_i(0) \rangle = 0$. The two-point function $\langle T(Q(x)Q^\dagger(y)) \rangle$ is a sum of terms that can be grouped in two different classes: double trace terms of the form

$$\left\langle \langle T(B_i(x)B_k(y)) \rangle_\psi \langle T(B_j(x)B_l(y)) \rangle_\psi \right\rangle_A \quad (2.4a)$$

$$= \langle \text{Tr}[S(x-y)\Gamma_i S(y-x)\Gamma_k] \rangle_A \langle \text{Tr}[S(x-y)\Gamma_j S(y-x)\Gamma_l] \rangle_A \quad (2.4b)$$

and single trace terms

$$\langle T(B_i(x)B_j(x)B_k(y)B_l(y)) \rangle_{\psi,A} \quad (2.5a)$$

$$= \langle \text{Tr}[S(x-y)\Gamma_i S(y-x)\Gamma_j S(x-y)\Gamma_k S(y-x)\Gamma_l] \rangle_A, \quad (2.5b)$$

where the flavor of the quark propagator $S(x-y)$ is implied to simplify the notation. The subscripts A and ψ indicate a functional integration over the corresponding fields (gauge fields and fermions respectively). It is worth noticing that in the Large- N limit the contribution in (2.4) has a perturbative expansion in $1/N$ of the form

$$\left\langle \langle T(B_i(x)B_k(y)) \rangle_\psi \langle T(B_j(x)B_l(y)) \rangle_\psi \right\rangle_A \quad (2.6a)$$

$$= \langle T(B_i(x)B_k(y)) \rangle_{\psi,A} \langle T(B_j(x)B_l(y)) \rangle_{\psi,A} + \mathcal{O}(N^0). \quad (2.6b)$$

The first term of the right hand side in Eq. (2.6) is the product of two non-interacting meson bubbles (Figure 2.5, left panel) and is of order N^2 . The next-to-leading order term for this double trace contribution is the sum of planar diagrams

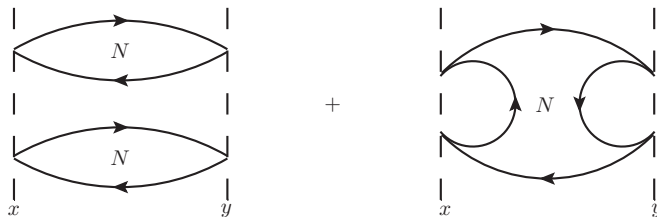


Figure 2.5. Diagrammatic representation of the two-point correlation function of tetraquark operators at the leading and next-to-leading order in the Large- N expansion. Everywhere it is understood that the insertion of any number of planar gluon *internal* lines does not change the order of the diagrams.

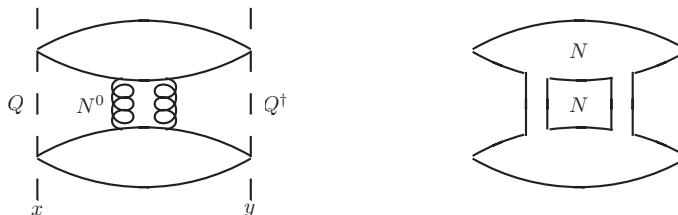


Figure 2.6. Example of subleading contribution to the double-trace term in the tetraquark two-point correlation function. The color factor is $N^2 \times g^4/N^2 = g^4$.

like that in Figure 2.6 that are at most of order $N^2 \times 1/N^2 = 1$. For this reason we will refer to the leading contribution of this correlation function as “disconnected”, implying that there are no gluon lines connecting the two meson bubbles. The contribution in Eq. (2.5) is, instead, of order N : in Figure 2.5, right panel, it is shown one of these possible single trace subleading terms (the shape of the diagram depends on the flavor structure of the quark bilinears). It is important to stress that the addition of any number of gluon lines *internal* to the fermion loops does not spoil the order of the diagram in the $1/N$ expansion because of the cancellation between the positive powers coming from the additional loops and the negative powers coming from the additional quark-gluon vertices. Therefore, as long as the $1/N$ expansion is considered, it will always be understood that any possible number of internal gluon lines, not changing the order of the expansion itself, will be included. Hence, since the leading order contribution to the single trace term in Eq. (2.5) is made of all the possible planar diagrams with internal gluon lines we will refer to it as the “connected” contribution. The complete two-point tetraquark correlation function can then be written as

$$\langle T(Q(x)Q^\dagger(y)) \rangle = \sum_{ijkl} C_{ij} C_{kl} \left[\langle T(B_i(x)B_k(y)) \rangle_{\psi,A} \langle T(B_j(x)B_l(y)) \rangle_{\psi,A} \quad (2.7a)$$

$$+ \langle T(B_i(x)B_j(x)B_k(y)B_l(y)) \rangle_{\text{conn},\psi,A} \right] + \mathcal{O}(N^0), \quad (2.7b)$$

where the subscript “conn” stands for connected. The disconnected term contains only information about the propagation of two non-interacting mesons. This can be seen cutting in half the first diagram in Figure 2.5: assuming confinement, the

²This is always possible because the fermionic action is quadratic.

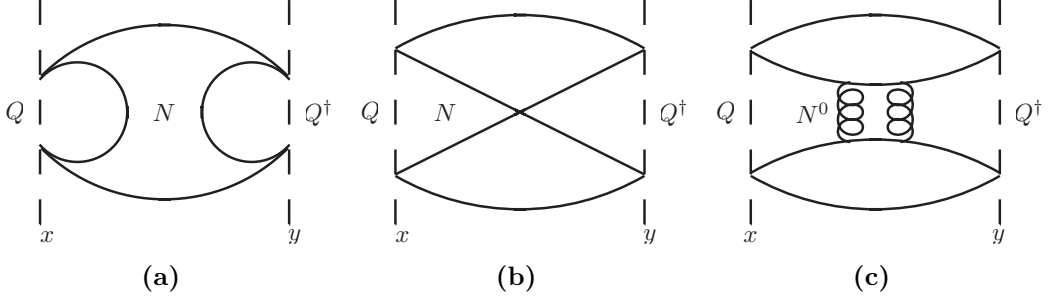


Figure 2.7. (a) Tetraquark correlation function with flavor $B = C$, for instance $(\bar{u}c)(\bar{c}d)$. Cutting vertically this diagram reveals the contribution from both tetraquark and meson intermediate states. (b) Tetraquark correlation function with flavor $A = C$, for instance $(\bar{c}u)(\bar{c}d)$ [9]. (c) Tetraquark correlation function with all different flavors, $(\bar{c}u)(\bar{s}d)$. The leading order connected diagrams, in this case, need the exchange of at least two gluons between the two meson bubbles.

only way to put on-shell the two bubbles is to form two non-interacting mesons. In contrast, there are different ways of cutting in half the second diagram of Figure 2.5 and it is possible to put on-shell simultaneously four quark propagators. For this reason, if a one-tetraquark pole exists, it contributes only to the connected term of the correlation function, which is of order N , relatively vanishing if compared to the disconnected one, which is of order N^2 . Consequently, Coleman [32] concludes that such exotic mesons do not exist when $N \rightarrow \infty$.

However, Weinberg recently pointed out [33] that Coleman's argument seems not to be conclusive. To make an analogy, consider the meson-meson scattering in the Large- N limit. The scattering amplitude is dominated by the analogous of the disconnected term in Eq. (2.7), with the difference that all quark bilinears are now located in different points. Terms of interaction between meson bubbles are subleading in the $1/N$ expansion. This essentially means that, when $N \rightarrow \infty$, the mesons are non-interacting, but surely we do not infer that mesons do not scatter at all in the physical world, when $N = 3$. In other words, one should compute a scattering amplitude first and then take the Large- N limit, otherwise the result would vanish right from the beginning, being the mesons non-interacting in this limit.

To better understand this point and what follows we will give some further details. Consider the scattering amplitude with B_1, B_2 ingoing and B_3, B_4 outgoing mesons:

$$\tilde{\mathcal{A}}_{B_1 B_2 \rightarrow B_3 B_4} = \lim_{N \rightarrow \infty} \prod_{i=1}^4 \lim_{q_i^2 \rightarrow m_i^2} (q_i^2 - m_i^2) \frac{1}{\sqrt{Z_{B_i}}} \tilde{G}_4(q_i^2; s, t), \quad (2.8)$$

where \tilde{G}_4 is the Fourier transform of the four-point correlation function

$$G_4(x, y, z, w) = \langle T (B_1(x) B_2(y) B_3(z) B_4(w)) \rangle, \quad (2.9)$$

s, t are the two independent Mandelstam variables characterizing the scattering process. Moreover, G_4 can be expanded in the parameter $1/N$, as the two-point function in Eq. (2.7). The renormalization constants Z_{B_i} bring a color factor of

N . This follows from the definition of Z_{B_i} in terms of the two-point function, $G_2(x) = \langle T(B_i(x)B_i(0)) \rangle$, whose Fourier transform reads:

$$\tilde{G}_2(p^2) = \frac{iZ_{B_i}}{p^2 - m_i^2 + i\epsilon} + \dots, \quad (2.10)$$

where the dots stand for additional poles or cut contributions. Since the leading order contribution to $G_2(x)$ is the bubble in Figure 2.1b, with the insertion of any number of internal gluon lines not changing the N -counting, it follows that

$$\langle T(B_i(x)B_i(y)) \rangle \propto Z_{B_i} \propto N. \quad (2.11)$$

Therefore, the Z_{B_i} in Eq. (2.8) bring a factor of $1/N^2$. As in Eq. (2.7), the leading disconnected contribution to G_4 is proportional to N^2 and hence it produces a term of order one in the amplitude. However, this term corresponds to a couple of freely-propagating mesons. For this reason, it doesn't contribute to the cross section since it corresponds to the identity part of the S -matrix, $S = \mathbb{1} + iT$, that is subtracted in the LSZ formalism. The connected subleading term is, instead, of order N and thus contributes as $1/N$ to the amplitude. This is the real leading term in the scattering matrix. On the other hand, if we had taken the limit $N \rightarrow \infty$ first and applied the LSZ formalism after, we would have got $\mathcal{A} = 0$ because, as we mentioned, QCD in the Large- N limit is a theory of non-interacting mesons and glueballs. In other words, taking $N \rightarrow \infty$ beforehand kills all the contribution but the one describing the two mesons propagating without interacting.

In this spirit, Weinberg shows that, admitting the existence of a one-tetraquark pole in some connected correlation function of the kind mentioned above, the Large- N expansion can actually be used to learn more about the phenomenology of tetraquark in the physical situation of finite N . Consider the decay amplitude of a tetraquark into two ordinary mesons. As just observed, the quark bilinear entering in the LSZ formulation has to be normalized as $N^{-1/2}B(x)$. The same happens for tetraquark interpolating operators, where, for the connected term, holds

$$\langle T(Q(x)Q^\dagger(y)) \rangle \propto Z_Q \propto N, \quad (2.12)$$

Z_Q being the residue at the tetraquark pole. The properly normalized operator for the creations or annihilation of a tetraquark is $N^{-1/2}Q(x)$, as for an ordinary meson.

The amplitude for the decay of a tetraquark is then proportional to a suitable Fourier transform, \tilde{G}_3 , of the three-point function

$$\begin{aligned} \frac{1}{N^{3/2}} \langle T(Q(x)B_n(y)B_m(z)) \rangle &= \frac{1}{N^{3/2}} \sum_{ij} C_{ij} \langle T(B_i(x)B_n(y)) \rangle_{\psi,A} \langle T(B_j(x)B_m(z)) \rangle_{\psi,A} \\ &+ \frac{1}{N^{3/2}} \langle T(Q(x)B_n(y)B_m(z)) \rangle_{\text{conn},\psi,A} + \mathcal{O}\left(\frac{1}{N}\right). \end{aligned} \quad (2.13)$$

The disconnected term is leading and hence the decay width has a color factor proportional to $(N^2 \times 1/N^{3/2})^2 = N$. Therefore, it seems that tetraquarks would be

very broad states, *i.e.* they would be unobservable in the Large- N limit. However, when we amputate the tetraquark external leg,

$$\mathcal{A}(Q \rightarrow B_1 B_2) \propto \lim_{q^2 \rightarrow m_Q^2} \frac{1}{\sqrt{Z_Q}} (q^2 - m_Q^2) \tilde{G}_3, \quad (2.14)$$

this term vanishes: \tilde{G}_3 at leading order is just the convolution of two meson propagators, and thus contains meson poles only. Therefore the factor $q^2 - m_Q^2$ makes the amplitude vanish in the on-shell limit. On the other hand, if a tetraquark pole actually exists in the connected subleading term (the second term in (2.13)), it would have a decay rate proportional to $(N \times 1/N^{3/2})^2 = 1/N$ and it would be stable in the Large- N limit, just like an ordinary meson.

2.3 Flavor structure of narrow tetraquarks

In the previous section we showed that if a tetraquark exists, then it has a decay width proportional, at most, to $1/N$. In this kind of analysis the flavor quantum numbers play a crucial role in predicting their decay widths.

Here we summarize some recent results about the classification of all possible flavor structures of tetraquarks [34]. In order to simplify the discussion, we define a quark bilinear with flavor quantum numbers A and B as

$$B_{AB}(x) = \bar{q}_A(x) \Gamma q_B(x). \quad (2.15)$$

We will also assume that the flavor indices A, B are different so that the vacuum expectation value $\langle B_{AB}(x) \rangle$ identically vanishes. The tetraquark interpolating field will be denoted as

$$Q_{AB;CD}(x) = B_{AB}(x) B_{CD}(x). \quad (2.16)$$

Since $A \neq B$ and $C \neq D$, we have only three non-trivial possibilities for the flavor structure of the couple CD :

$$C = B, \quad C = A, \quad A \neq B \neq C \neq D. \quad (2.17)$$

These three possibilities imply different quark contractions in the correlation functions involving tetraquark operators since contractions between different flavors are forbidden, and hence determine different Large- N behaviors. The resulting predictions are summarized in Table 2.1 and can be derived looking at Figure 2.7a, 2.7b and 2.7c. For a detailed derivation one should refer to the original work [34].

The remarkable aspect of this analysis is that a careful treatment of the flavor quantum numbers reveals the presence of even narrower tetraquarks than those decaying as $1/N$. This happens in those situations in which the tetraquark is made out of quarks with all different flavors, for instance $[cs] [\bar{u}\bar{d}]^3$. Let us perform a detailed analysis for this case, the extension to the other flavor structures follows straightforwardly.

³The notation $[q_1 q_2][\bar{q}_1 \bar{q}_2]$ is introduced to distinguish between a tetraquark written in the diquark-antidiquark basis – see Chapter 7 – against the notation $(\bar{q}_1 q_2)(\bar{q}_3 q_4)$ – see Table 2.1.

Type	Decay width	$\sqrt{Z_Q}$	Tetraquark-Meson mixing	Example
$C = B$	$1/N$	\sqrt{N}	N^0	$(\bar{u}c)(\bar{c}d)$
$C = A$	$1/N$	\sqrt{N}	absent	$(\bar{c}u)(\bar{c}d)$
$A \neq B \neq C \neq D$	$1/N^2$	N^0	absent	$(\bar{c}u)(\bar{s}d)$

Table 2.1. Flavor structure and associated decay width for tetraquarks as reported by Knecht and Peris [34]. The notation $(\bar{q}_1 q_2)(\bar{q}_3 q_4)$ is used when the tetraquark is written in the meson-meson basis.

In order to determine the decay width of such a tetraquark it is sufficient to take only the leading connected contribution to the amplitude, in the sense specified in Sec. 2.2, with properly normalized operators. In this case, $Z_Q \sim N^0$ because (Figure 2.6) the color factor of $\langle T(Q^\dagger(x)Q(y)) \rangle$ is $N^2 \times g^4/N^2 \sim N^0$ – also recall that the Large- N order of Z_Q must be evaluated from the two-point function as in Sec. 2.2. The color factor of the decay amplitude, Eq. (2.14), is:

$$\mathcal{A}_{Q \rightarrow BB} \sim \frac{1}{\sqrt{Z_Q}} \frac{1}{Z_B} \tilde{G}_3 \sim \frac{1}{N^0} \times \frac{1}{N} \times N^0 \sim \frac{1}{N}, \quad (2.18)$$

where the color factor of \tilde{G}_3 is N^0 since the decay diagram of a tetraquark of this kind is analogous to Figure 2.7c – see again the original reference [34] for details. Finally, in this case a tetraquark-meson mixing is absent: cutting vertically the diagram in Figure 2.7c it is impossible to have a cut involving only two color lines, thus there is no meson intermediate state contribution. The decay width of this kind of tetraquarks goes as $1/N^2$, being the decay amplitude of order $1/N$, Eq. (2.18).

As a final note, we comment the Large- N behavior of the diagram in Figure 2.7b. At a first look, it seems a subleading non-planar contribution, since there are line crossings. However, the planarity is a topological property of the diagram, being its $1/N$ order associated to its Euler characteristic χ , as shown by ‘t Hooft [30, 32], through the power law

$$N^\chi \quad \text{with} \quad \chi = L - I + V, \quad (2.19)$$

where L is the number of loops, I the internal lines and V the vertices of the diagrams. It hence follows that the one showed in Figure 2.7b is clearly a connected planar diagram (there are many examples of non-trivial planar diagrams, for instance in Maiani *et al.* [35]).

2.4 Hypothetical non-perturbative contributions to tetraquark operators

In a recent paper by Lebed [36] a potential incongruence is found in considering the normalization of the tetraquark wave functions created by LSZ normalized operators.

The fact that $Z_B \sim N$ is equivalent to the conclusion that LSZ reduction identifies the operator $N^{-1/2}B(x)$ as the one creating or destroying properly normalized

asymptotic states. This prefactor also produces correctly normalized meson states

$$\frac{1}{\sqrt{N}} B_i |0\rangle = \frac{1}{\sqrt{N}} \sum_{a=1}^N \bar{q}^a \Gamma_i q^a |0\rangle. \quad (2.20)$$

Nevertheless, also $Z_Q \sim N$ – see Eq. (2.12), leading to a properly normalized tetraquark operator $N^{-1/2} Q(x)$. However, its application to the vacuum creates states with norm squared N

$$\frac{1}{\sqrt{N}} Q |0\rangle = \frac{1}{\sqrt{N}} \sum_{ij} \sum_{a=1}^N \sum_{b=1}^N C_{ij} \bar{q}^a \Gamma_i q^a \bar{q}^b \Gamma_j q^b |0\rangle. \quad (2.21)$$

Lebed [36] pointed out that, in order to obtain the additional $1/\sqrt{N}$ suppression needed for the correct normalization of the state in Eq. (2.21), the definition of the tetraquark operator as a local product of fermion bilinears must be revisited. We have already shown that, when the Large- N limit is involved together with another different limit procedure, they must be treated carefully. In particular, in the LSZ formalism one has to take the infrared limit first, otherwise all the scattering amplitudes would identically vanish. In this spirit, one could ask if the Large- N commutes with the definition of composite operators: an operation that involves a limit procedure. For example, in the ϕ^4 scalar theory one may define the composite operator $:\phi^2(0):$ as

$$:\phi^2(0): = \lim_{x \rightarrow 0} \left(\phi(x)\phi(0) - \frac{C}{x^2} \mathbf{1} \right), \quad (2.22)$$

in order to obtain finite renormalized correlation functions with its insertions ⁴.

Lebed [36] suggests that the non-commutativity of the limit $N \rightarrow \infty$ and the local limit in the definition of the composite tetraquark operator $Q(x)$ is crucial in resolving the lack of the additional $1/\sqrt{N}$ suppression factor in the tetraquark wave function in Eq. (2.21). Consider the product of operators

$$B_i(x)B_j(0) \sim \dots + C_{ij}(x)B_i(0)B_j(0) + \dots, \quad (2.23)$$

when $x \rightarrow 0$ ⁵ and allow the coefficients $C_{ij}(x)$ to have a contribution of the form

$$\delta C_{ij} \sim e^{-N^m \Lambda_{QCD}^2 x^2}. \quad (2.24)$$

For any finite separation $x^2 \geq \frac{1}{\Lambda_{QCD}^2}$ this contribution is vanishing when $N \rightarrow \infty$, in order to preserve the usual N -counting for the correlation function of two mesons.

If one defines the tetraquark operator smearing the product $B(x)B(0)$ over a small spatial region of size $\mathcal{O}(1/\Lambda_{QCD})$

$$Q(x) = \int_{\Lambda_{QCD}^3} d^3y \sum_{ij} C_{ij}(y-x) B_i(x) B_j(x), \quad (2.25)$$

⁴The operator product expansion is blind to contact terms of the form $\square^n \delta(x)$, for some power n : an additional reason to define composite operators through a limit procedure.

⁵We are ignoring the mixing with operators of dimension less than 6 because we are dealing with properly defined composite operators, Eq. (2.22).

the above mentioned four-point correlation function, in the limit $x \rightarrow 0$, gets a contribution of $N^{-m/2}$ for each spatial integral of the gaussian factor δC_{ij} . If $m = 1/3$ one obtains precisely the desired additional suppression $1/\sqrt{N}$ in order to obtain properly normalized tetraquark wave functions.

We remark that the coefficients δC_{ij} are non-perturbative in the N -counting and cannot be inferred from perturbation theory. The mechanism proposed is only a possibility and there are no reasons to believe that it happens in this precise way. Nevertheless, it suggests that in order to allow the existence of one-tetraquark poles in the connected piece of the correlation functions considered so far, some non-perturbative mechanism in the $1/N$ expansion must occur.

2.5 Flavored tetraquarks in Corrigan-Ramond Large- N limit

So far we discussed in detail the Large- N physical behavior of meson and tetraquark states in the so-called ‘t Hooft limit [30]. Another well studied limit is that of Veneziano [37], with $N_f \rightarrow \infty$ flavors, $N_c \rightarrow \infty$ colors, provided that N_f/N_c is fixed. In both these formulations, a simple definition of baryons does not exist, in contrast with what happens for mesons and tetraquarks. In fact, in generic $SU(N)$ gauge theories color-neutral states composed of only quarks – *i.e.* baryons – are made of N quarks in a totally antisymmetric combination

$$\epsilon_{i_1 i_2 \dots i_N} q^{i_1} q^{i_2} \dots q^{i_N}. \quad (2.26)$$

As shown by Witten [31], they have very distinctive properties in the Large- N limit. As already mentioned, their mass goes as N , thus they disappear from the hadronic spectrum when $N \rightarrow \infty$.

As firstly proposed by Corrigan and Ramond [38], it could be important to have, for every value of N , color-neutral bound states composed of only three quarks. A simple way to do it is to introduce new fermions, originally called “larks” [38], transforming as the $N(N-1)/2$ (antisymmetric) representation of $SU(N)$. This choice is motivated by the observation that, when $N = 3$, the dimension of this representation is 3 and coincides with the $\bar{\mathbf{3}}_c$ conjugate representation

$$q_{ij} = \epsilon_{ijk} q^k \quad i, j, k = 1, 2, 3. \quad (2.27)$$

In this formulation, the baryons for Large- N are constructed out of

$$\bar{q}_{ij} q^i q^j \quad (2.28)$$

color-neutral states, which look more like physical baryonic states. Moreover, just like quarks, larks only couple to gluons with a minimal coupling. The introduction of a lark sector in the Large- N extrapolation of QCD, not only allows to define three-quark states, but also modifies the N -counting. The reason is simple. If we introduce the ‘t Hooft double line representation [30] to understand the color flow of this theory, we notice immediately that lark lines split in two with arrows pointing in the same direction since both color indices in Eq. (2.27) belong to the same representation, in contrast with gluons, represented as two oriented lines pointing

in opposite directions since their color indices always appear as a color-anticolor combination. Apart from the different orientation of the color flows, lark loops have a color factor N^2 like gluon loops. This implies that leading order planar diagrams contain any possible internal gluons as well as lark loop corrections to these gluon lines. In other words, we can also introduce an arbitrary number of lark “bubbles” in the middle of a gluon propagator. The reason is again simple: each insertion of a lark loop in a gluon line counts as N but each lark-gluon vertex counts as $1/\sqrt{N}$ and hence a lark loop in the middle of a gluon line does not change the N -counting of the considered diagram – see Sec. 2.2. This is in contrast with quark loops, whose insertion inside a gluon propagator suppresses the order of the diagram in the $1/N$ expansion. For this reason we also see how including other antisymmetric tensors is dangerous for the $1/N$ expansion since they contribute in loops as N^m , where m is the number of antisymmetric color indices, thus spoiling the perturbative expansion of the correlators of the theory ⁶. In fact, the fine cancellation between positive powers coming from loops and negative powers coming from couplings does not work for $m \neq 2$.

It was recently shown [39] that in the Corrigan-Ramond Large- N formulation, *i.e.* the ‘t Hooft limit with quarks in the antisymmetric $SU(N)$ representation, (sometimes called QCD(AS)) it is possible to unambiguously define narrow tetraquark states. Consider a source operator of the form

$$Q(x) = C_{AB} \bar{q}^{ij} \Gamma_{Aqjk} \bar{q}^{kl} \Gamma_{Bqli}, \quad (2.29)$$

where lowercase letters indicate color indices and $\Gamma_{A,B}$ are matrices in the Dirac and flavor space. Spin and flavor quantum numbers of the operator are fixed by a suitable choice of C_{AB} . This combination is gauge invariant, *i.e.* is a color singlet, if we notice that

$$q_{ij} \rightarrow \Omega_i^k \Omega_j^l q_{kl}, \quad (2.30a)$$

$$\bar{q}^{ij} \rightarrow \bar{q}^{kl} (\Omega^\dagger)_k^i (\Omega^\dagger)_l^j, \quad (2.30b)$$

under a generic $SU(N)$ gauge transformation Ω . Moreover, lark color indices are saturated in such a way that the operator given by Eq. (2.29) can never be split into two independent color singlets for $N > 3$ ⁷. In other words, the two-point correlation function with sources as in Eq. (2.29) cannot be separated in disconnected pieces. In Figure 2.8a we show the leading order contribution to the correlation function $\langle Q(x)Q^\dagger(0) \rangle$. Using the ‘t Hooft double line representation, Figure 2.8b, we see that it is impossible to rearrange the colors in order to obtain two disconnected color singlet diagrams. This essentially means that operators like the one in Eq. (2.29) unambiguously interpolate tetraquarks (or tetralarks in a generic $SU(N)$) states, without mixing with ordinary mesons.

Counting the lark loops we find that the color factor of this diagram is N^4 . As usual in the Large- N expansion, the N -counting does not change if we consider all

⁶Larks can be considered as additional quark species: they couple to gluons with the same coupling constant of the quarks, but with the $SU(N)$ generators in the covariant derivative belonging to the antisymmetric representation. The same can be done for other species belonging to different representations of $SU(N)$.

⁷As already mentioned, the case $N = 3$ is equivalent to the diquark-antidiquark formulation.

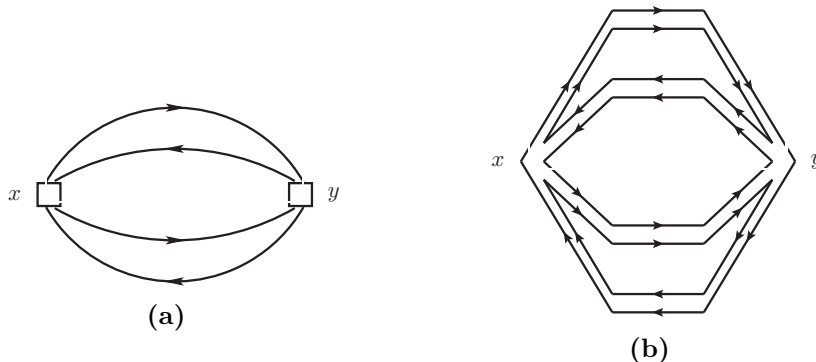


Figure 2.8. “Tetralark” operator two-point correlation function. It is clear from the diagram that it is not possible to separate the lark lines in gauge invariant subdiagrams.

the planar diagrams with the insertion of an arbitrary number of gluon internal lines. It is remarkable to notice again that this counting does not change even if we add any number of planar lark loops in the middle of these gluon lines for the reasons explained before.

At this point, we can easily show that an operator source like that in Eq. (2.29) can create out of the vacuum single tetralarks at leading order in the Large- N expansion. We must be careful that, if the flavor of the sources allows lark-antilark annihilations, there are other diagrams besides that in Figure 2.8a. In that case, however, it would not be possible to unambiguously disentangle the contribution of tetralark intermediate states from those of mesons. Imagine cutting vertically the diagram in Figure 2.8b. Assuming confinement, the only way to form a gauge invariant combination of the lark lines involved in the cut is to group the four larks in a single hadron. This statement holds even if we insert an arbitrary number of gluon internal lines in the diagram in figure name 2.8b. In that case the generic gauge-invariant contribution to the cut would have the form

$$\text{Tr} [q A \dots A \bar{q} A \dots A q A \dots A \bar{q}], \quad (2.31)$$

with A the gluon field. This is still a color-singlet combination with four larks. Since the two-point function $\langle T(Q(x)Q^\dagger(0)) \rangle$ brings a color factor $N^4 \sim Z_Q$ (as shown by the power counting of Figure 2.8b) we also find that the LSZ properly normalized tetralark operators are $N^{-2}Q(x)$. Since lark loops are not suppressed, there are also flavor-singlet contribution of states with an arbitrary number of lark-antilark couples. This means that the tetralark states found are not pure, but rather they are a superposition of infinite states, with arbitrary even number of larks, *i.e.* the analogous of “sea quarks” in the lark sector. However, they are unambiguously exotic states, since mesons made of larks cannot contribute to their two-point correlation function.

Finally, we show that tetralarks in the Corrigan-Ramond Large- N limit are

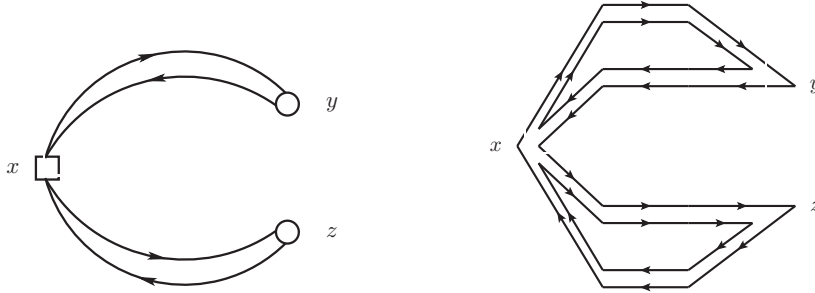


Figure 2.9. Three point correlation function $\langle Q(x)B(y)B(z) \rangle$ for the decay of a “tetralark” in two mesons.

actually narrow states. To see this, consider the three point correlation function

$$\langle T(Q(x)B(y)B(z)) \rangle, \quad (2.32)$$

where the operator B interpolates a lark-antilark couple (we use the same notation of ordinary meson operators to stress the analogy among them). One of the leading order diagrams contributing to Eq. (2.32) is shown in Figure 2.9. The counting of the color loops gives a factor N^3 , instead of N^4 obtained for the two-point correlation function of “tetralark” operators. Normalizing properly the amplitude, we obtain a total color factor $1/N^2 \times (1/N)^2 \times N^3 = 1/N$, where we have used the result that $N^{-1}B(x)$ is the LSZ normalized lark-antilark meson operator (we have not shown this, but it can be easily proven). The resulting decay width is then proportional to $1/N^2$, showing that in the limit $N \rightarrow \infty$ Corrigan-Ramond tetralarks are narrow states.

2.6 Flavored tetraquarks in ‘t Hooft Large- N limit

From a field theory point of view, it is a challenging task to identify operators interpolating only tetraquarks with flavor content $c\bar{c}u\bar{d}$. This is because such an operator would interpolate also mesonic states as $u\bar{d}$ having the same quantum numbers.

This is one of the major difficulties in treating these states using Lattice QCD, although some recent works on the subject has been presented [40–44]. Nevertheless, a class of operators that do not overlap with ordinary mesons and that unambiguously contain four valence quarks can be found [9].

It is the same class of operators already introduced in Corrigan-Ramond QCD(AS) formulation and considered in a recent work by Cohen and Lebed [45]. The authors show that the leading order connected diagrams contributing to the scattering amplitude of mesons with the appropriate exotic quantum numbers do not contain any tetraquark s -channel cut. A careful and detailed analysis of the argument can be found in the original paper [45]. Here we will sketch the same argument referring to a specific case, in order to make the discussion more concrete.

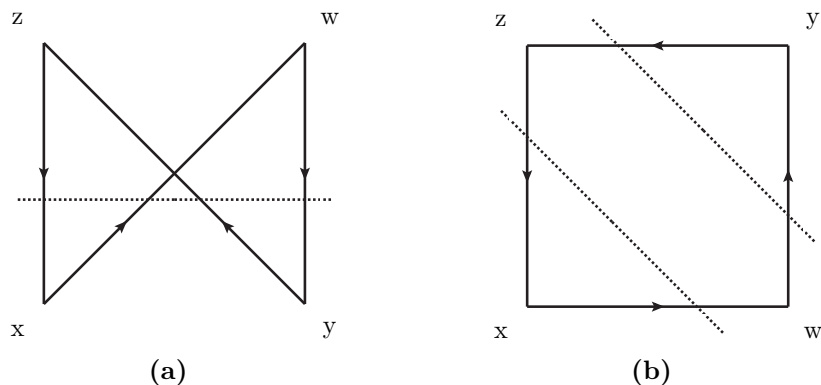


Figure 2.10. Leading order connected contribution to the meson meson scattering amplitude with exotic quantum numbers. The dashed lines represent the cut in the s -channel.

Consider the following four-point correlation function – see Figure 2.10 – that can be used, for instance, to compute the elastic scattering amplitude of $D_s^+ D^0$ mesons

$$G_4(x, y, z, w) = \langle T (\bar{c}\Gamma_1 s(z) \bar{c}\Gamma_2 u(w) \bar{s}\Gamma_3 c(x) \bar{u}\Gamma_4 c(y)) \rangle, \quad (2.33)$$

with $\Gamma_1, \Gamma_2, \Gamma_3, \Gamma_4$ appropriate Dirac matrices. We are looking for a possible s -channel cut contributing to the four-point amplitude in which an on-shell tetraquark with flavor content $[cc][\bar{s}\bar{u}]$ propagates. We also notice that a t -channel cut cannot reveal the presence of a tetraquark with these exotic flavor quantum numbers.

Imagine to cut the diagram in Figure 2.7b separating the incoming mesons in x, y from the outgoing mesons in z, w . The resulting cut is shown in Figure 2.10a. Apparently, we are led to say that in the considered scattering amplitude there is a contribution from a tetraquark cut. However, drawing the diagram in a different, topologically equivalent, way (Figure 2.10b), we see that the effect of the cut is to put on shell the corners of the diagram, thus separating all the meson sources from each other.

Recalling that the scattering amplitude is obtained, in momentum space, from Eq. (2.33) multiplying it for the inverse of the propagators of the mesons in the external legs, we have

$$\mathcal{A}(s, t) = \prod_i \lim_{q_i^2 \rightarrow m_i^2} (q_i^2 - m_i^2) \frac{1}{\sqrt{Z_i}} \tilde{G}_4(\{q_i^2\}; s, t), \quad (2.34)$$

with $\tilde{G}_4(\{q_i^2\}; s, t)$ the Fourier transform of G_4 in Eq. (2.33). The factors $q_i^2 - m_i^2$ cancel exactly the contribution of the sources to the s -channel and the on-shell contributions come only from meson intermediate states.

Drastically different is the situation for a tetraquark with flavor $(\bar{c}u)(\bar{d}\bar{c})$, as the recently discovered charged resonance $Z(4430)$. The resulting connected leading order diagram is similar to the diagram in Figure 2.7a. In that case a cut in the s -channel reveal either a meson or a tetraquark intermediate state.

To summarize, a pure tetraquark intermediate state, *i.e.* with flavor quantum numbers that can only be interpreted as exotic, cannot contribute to the leading

order connected contribution to meson-meson elastic scattering amplitude. It is remarkable to notice that the experimental situation is drastically different. Until now, there is no evidence for such exotic resonances with all four different flavors and the considerations illustrated here are not applicable to the current experimental situation.

The key points of this section are schematically summarized in Table 2.2.

Coleman [32]/Witten [31]	Tetraquarks do not exist, (subleading in the large- N QCD expansion)
...	...
Weinberg [33]	Even if subleading, tetraquarks can exist. The width is $\propto 1/N$ (like mesons)
Knecht-Peris [34]	4-flavored tetraquarks are as narrow as $1/N^2$
Lebed [36]	Non-perturbative effects in $1/N$ might affect tetraquark wave function
Cohen-Lebed 1 [45]	Tetraquarks naturally exist in Corrigan-Ramond limit (larks in the antisymmetric representation)
Cohen-Lebed 2 [39]	Production of tetraquarks in scattering amplitudes is sub-subleading only.

Table 2.2. The current status of Large- N tetraquarks.

Chapter 3

Experimental overview

As shown in the previous section, recently a good deal of work has been done to understand the phenomenology of tetraquark states in Large- N QCD. In particular, some doubts were raised about a possible broadness of these particles, that would make them experimentally undetectable. However, as we will show in the following sections, in the past eleven years many different experiments, both at lepton and hadron colliders, reported evidences for a large number of particles having properties which can hardly be embedded in the known charmonia frameworks. A pictorial representation of this is visible in Figure 3.1. In particular, the charged states reported in the second panel are manifestly exotic. Some states, like the $X(3872)$ or the $X(3915)$, have more or less the correct mass and quantum numbers to be identified with (otherwise missing) ordinary charmonia; on the other hand, in the vector sector we have much more levels than expected. In any case, the decay pattern of these states is not compatible with charmonia predictions, and so it needs some exotic assignment.

Besides finding the states, the measurement of the quantum numbers is needed to establish their exotic nature. While prompt production at hadron colliders can produce particles with any quantum numbers, exclusive production modes, in particular at e^+e^- colliders, can constrain the assignment. For example, a generic state X could be produced:

- Directly with $e^+e^- \rightarrow X$, if the center-of-mass energy coincides with the mass of the state (typically at τ - c factories), or in association with Initial State Radiation (ISR) which lowers the center of mass energy, $e^+e^- \rightarrow e^+e^-\gamma_{\text{ISR}} \rightarrow X\gamma_{\text{ISR}}$, typically at B -factories. In the first case an invariant mass distribution can be studied by varying the energy of the beam, which does not allow to collect many data points with high statistics, while in the second the same distribution is studied as a function of the γ_{ISR} energy. In both cases, the quantum numbers must be the same as the photon, *i.e.* $J^{PC} = 1^{--}$.
- In the fusion of two quasi-real photons, $e^+e^- \rightarrow e^+e^-\gamma\gamma \rightarrow e^+e^-X$, where e^+ and e^- are scattered at a small angle and are not detected; the signal events have no tracks and neutral particles but the daughters of X . If the photons are quasi-real, Landau-Yang theorem holds [47], and $J \neq 1$; moreover $C = +$ is constrained.

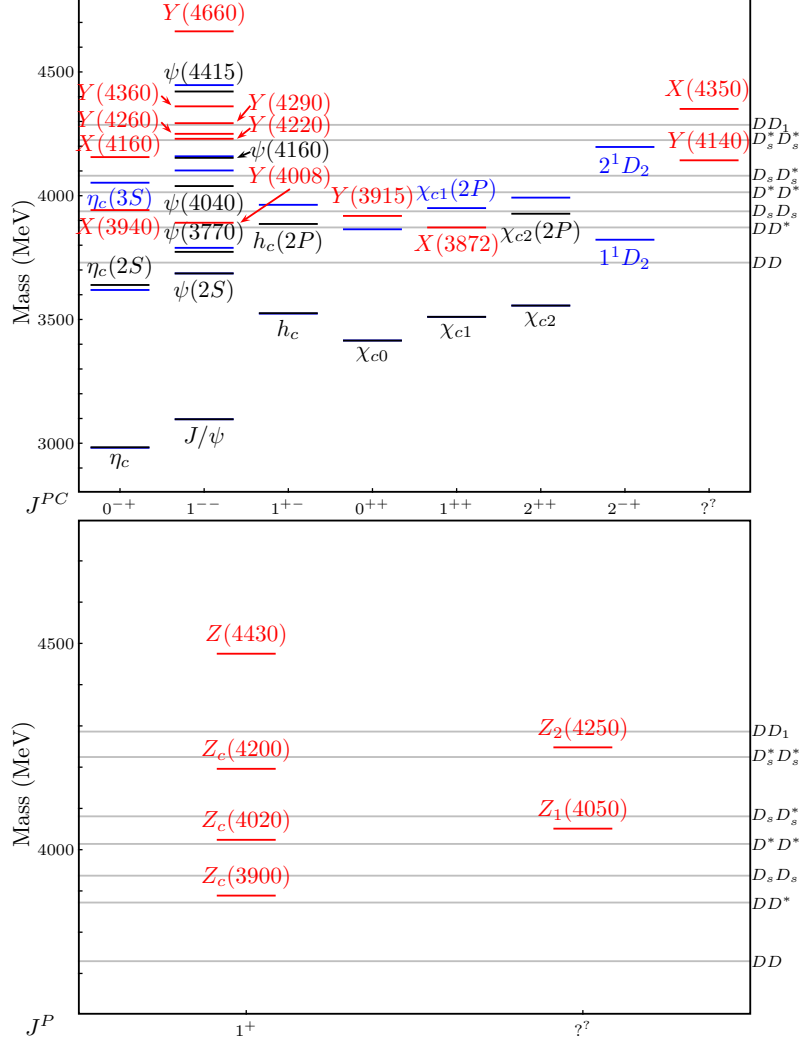


Figure 3.1. Charmonium sector. In the upper panel, we show ordinary charmonia and neutral exotic states, in the lower panel charged exotic states. Black lines represent observed charmonium levels, blue lines represent predicted levels according to Radford and Repko [46], red line are exotic states. The open charm thresholds are reported on the right.

-
- In double charmonium production, for example $e^+e^- \rightarrow J/\psi X$, which constrains X to have C opposite to the one of the associated charmonium.

The production in B decays allows X to have any J^{PC} , albeit low values of the spin are preferred.

Hadron colliders, instead, produce charmonia states both directly and in B decays, and the search is typically carried out inclusively.

A summary of the resonances we will talk about is reported in Table 3.1-3.3. We start our review from the charged ones, first the recently confirmed $Z(4430)$ in Sec. 3.1, then we move to the charged states in the 3900-4200 MeV region (Sec. 3.2) and the corresponding ones in the bottomonium sector (Sec. 3.3). The newly discovered pentaquark states are discussed in Sec. 3.4, the $X(3872)$ is extensively described in Sec. 3.5, as well as the vector states in Sec. 3.6. Finally, the other resonances around 3940 MeV are described in Sec. 3.7, and the remaining ones in Sec. 3.8. Other information can be found in some reviews [48–50]; a complete treatise about the physics of *BABAR* and *Belle* can be found in the recent review book [29].

State	M (MeV)	Γ (MeV)	J^{PC}	Process (mode)	Experiment ($\#\sigma$)
$X(3823)$	3823.1 ± 1.9	< 24	$?^{? -}$	$B \rightarrow K(\chi_{c1}\gamma)$	Belle [51] (4.0)
$X(3872)$	3871.68 ± 0.17	< 1.2	1^{++}	$B \rightarrow K(\pi^+\pi^- J/\psi)$ $p\bar{p} \rightarrow (\pi^+\pi^- J/\psi) \dots$ $pp \rightarrow (\pi^+\pi^- J/\psi) \dots$ $B \rightarrow K(\pi^+\pi^-\pi^0 J/\psi)$ $B \rightarrow K(\gamma J/\psi)$ $B \rightarrow K(\gamma\psi(2S))$ $B \rightarrow K(D\bar{D}^*)$	Belle [52, 53] (>10), BABAR [54] (8.6) CDF [55, 56] (11.6), DØ [57] (5.2) LHCb [58, 59] (np) Belle [60] (4.3), BABAR [61] (4.0) Belle [62] (5.5), BABAR [63] (3.5) LHCb [64] (> 10) BABAR [63] (3.6), Belle [62] (0.2) LHCb [64] (4.4) Belle [65] (6.4), BABAR [66] (4.9)
$Z_c(3900)^+$	3888.7 ± 3.4	35 ± 7	1^{+-}	$Y(4260) \rightarrow \pi^-(D\bar{D}^*)^+$ $Y(4260) \rightarrow \pi^-(\pi^+ J/\psi)$	BES III [67] (np) BES III [68] (8), Belle [69] (5.2) CLEO data [70] (>5)
$Z_c(4020)^+$	4023.9 ± 2.4	10 ± 6	1^{+-}	$e^+e^- \rightarrow \pi^-(\pi^+ h_c)$ $e^+e^- \rightarrow \pi^-(D^*\bar{D}^*)^+$	BES III [71] (8.9) BES III [72] (10)
$Y(3915)$	3918.4 ± 1.9	20 ± 5	0^{++}	$B \rightarrow K(\omega J/\psi)$ $e^+e^- \rightarrow e^+e^-(\omega J/\psi)$	Belle [73] (8), BABAR [61, 74] (19) Belle [75] (7.7), BABAR [76] (7.6)
$Z(3930)$	3927.2 ± 2.6	24 ± 6	2^{++}	$e^+e^- \rightarrow e^+e^-(D\bar{D})$	Belle [77] (5.3), BABAR [78] (5.8)
$X(3940)$	3942_{-8}^{+9}	37_{-17}^{+27}	$?^{?+}$	$e^+e^- \rightarrow J/\psi(D\bar{D}^*)$	Belle [79, 80] (6)
$Y(4008)$	3891 ± 42	255 ± 42	1^{--}	$e^+e^- \rightarrow (\pi^+\pi^- J/\psi)$	Belle [69, 81] (7.4)
$Z(4050)^+$	4051_{-43}^{+24}	82_{-55}^{+51}	$?^{?+}$	$\bar{B}^0 \rightarrow K^-(\pi^+\chi_{c1})$	Belle [82] (5.0), BABAR [83] (1.1)

Table 3.1. Summary of quarkonium-like states. For charged states, the C -parity is given for the neutral members of the corresponding isotriplets.

State	M (MeV)	Γ (MeV)	J^{PC}	Process (mode)	Experiment ($\#\sigma$)
$Y(4140)$	4145.6 ± 3.6	14.3 ± 5.9	$?^{?+}$	$B^+ \rightarrow K^+(\phi J/\psi)$	CDF [84, 85] (5.0), Belle [86] (1.9), LHCb [87] (1.4), CMS [88] (>5) DØ [89] (3.1)
$X(4160)$	4156_{-25}^{+29}	139_{-65}^{+113}	$?^{?+}$	$e^+e^- \rightarrow J/\psi (D^*\bar{D}^*)$	Belle [80] (5.5)
$Z(4200)^+$	4196_{-30}^{+35}	370_{-110}^{+99}	1^{+-}	$\bar{B}^0 \rightarrow K^-(\pi^+ J/\psi)$	Belle [90] (7.2)
$Y(4220)$	4196_{-30}^{+35}	39 ± 32	1^{--}	$e^+e^- \rightarrow (\pi^+\pi^- h_c)$	BES III data [91, 92] (4.5)
$Y(4230)$	4230 ± 8	38 ± 12	1^{--}	$e^+e^- \rightarrow (\chi_{c0}\omega)$	BES III [93] (>9)
$Z(4250)^+$	4248_{-45}^{+185}	177_{-72}^{+321}	$?^{?+}$	$\bar{B}^0 \rightarrow K^-(\pi^+\chi_{c1})$	Belle [82] (5.0), BABAR [83] (2.0)
$Y(4260)$	4250 ± 9	108 ± 12	1^{--}	$e^+e^- \rightarrow (\pi\pi J/\psi)$	BABAR [94, 95] (8), CLEO [96, 97] (11) Belle [69, 81] (15), BES III [68] (np)
				$e^+e^- \rightarrow (f_0(980)J/\psi)$	BABAR [95] (np), Belle [69] (np)
				$e^+e^- \rightarrow (\pi^- Z_c(3900)^+)$	BES III [68] (8), Belle [69] (5.2)
				$e^+e^- \rightarrow (\gamma X(3872))$	BES III [98] (5.3)
$Y(4290)$	4293 ± 9	222 ± 67	1^{--}	$e^+e^- \rightarrow (\pi^+\pi^- h_c)$	BES III data [91, 92] (np)
$X(4350)$	$4350.6_{-5.1}^{+4.6}$	13_{-10}^{+18}	$0/2^{?+}$	$e^+e^- \rightarrow e^+e^-(\phi J/\psi)$	Belle [86] (3.2)
$Y(4360)$	4354 ± 11	78 ± 16	1^{--}	$e^+e^- \rightarrow (\pi^+\pi^-\psi(2S))$	Belle [99] (8), BABAR [100] (np)
$P_c(4380)^+$	$4380 \pm 8 \pm 29$	$205 \pm 18 \pm 86$	$3/2^-$	$\Lambda_b^0 \rightarrow K^-(J/\psi p)$	LHCb [101] (9)
$Z(4430)^+$	4478 ± 17	180 ± 31	1^{+-}	$\bar{B}^0 \rightarrow K^-(\pi^+\psi(2S))$	Belle [102, 103] (6.4), BABAR [104] (2.4) LHCb [105] (13.9)
				$\bar{B}^0 \rightarrow K^-(\pi^+ J/\psi)$	Belle [90] (4.0)
$P_c(4450)^+$	$4449.8 \pm 1.7 \pm 2.5$	$39 \pm 5 \pm 19$	$5/2^+$	$\Lambda_b^0 \rightarrow K^-(J/\psi p)$	LHCb [101] (12)
$Y(4630)$	4634_{-11}^{+9}	92_{-32}^{+41}	1^{--}	$e^+e^- \rightarrow (\Lambda_c^+\bar{\Lambda}_c^-)$	Belle [106] (8.2)
$Y(4660)$	4665 ± 10	53 ± 14	1^{--}	$e^+e^- \rightarrow (\pi^+\pi^-\psi(2S))$	Belle [99] (5.8), BABAR [100] (5)

Table 3.2. (Continued).

State	M (MeV)	Γ (MeV)	J^{PC}	Process (mode)	Experiment ($\#\sigma$)
$Z_b(10610)^+$	10607.2 ± 2.0	18.4 ± 2.4	1^{+-}	$\Upsilon(5S) \rightarrow \pi(\pi\Upsilon(nS))$	Belle [107, 108] (>10)
				$\Upsilon(5S) \rightarrow \pi^-(\pi^+h_b(nP))$	Belle [107] (16)
				$\Upsilon(5S) \rightarrow \pi^-(B\bar{B}^+)$	Belle [109] (8)
$Z_b(10650)^+$	10652.2 ± 1.5	11.5 ± 2.2	1^{+-}	$\Upsilon(5S) \rightarrow \pi^-(\pi^+\Upsilon(nS))$	Belle [107] (>10)
				$\Upsilon(5S) \rightarrow \pi^-(\pi^+h_b(nP))$	Belle [107] (16)
				$\Upsilon(5S) \rightarrow \pi^-(B^*\bar{B}^+)$	Belle [109] (6.8)

Table 3.3. (Continued).

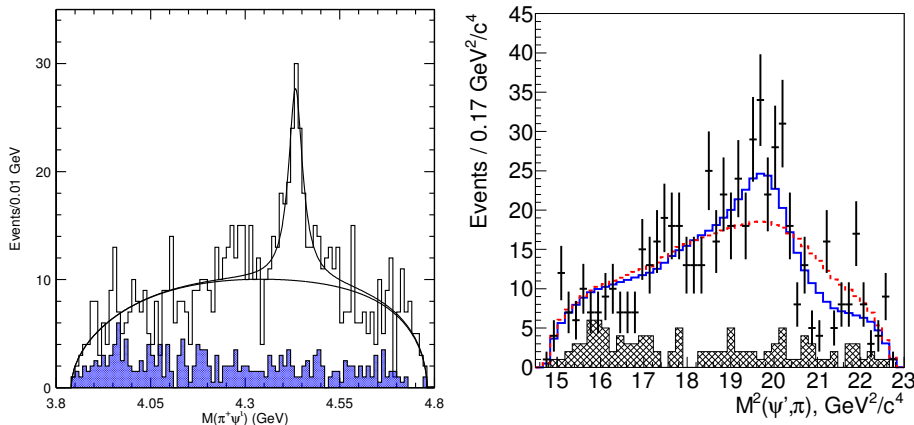


Figure 3.2. Invariant mass distributions in $\psi(2S)\pi^-$ channel according to first [110] (left), and last [103] (right) Belle analyses. The fit shows that an additional resonances is needed to describe the data. In the right panel, the blue solid (red dashed) curve shows the fit with (without) the additional $Z(4430)$ resonance. In both figures, a K^* veto has been applied.

3.1 $Z(4430)$

In April 2014, LHCb confirmed the existence of a charged resonance in the $\psi(2S)\pi^-$ channel [105].¹ This announcement solved a controversy between Belle, which discovered [110] and confirmed [102, 103] the existence of this state, and *BABAR*, which did not observe any new structure and criticized some aspects of Belle’s analysis [104]. A state decaying into a charmonium and a charged light meson has undoubtedly a four-quark content, being the production of a heavy quark pair from vacuum OZI suppressed. As we will discuss later, the very existence of such an exotic state far from usual open-charm thresholds is extremely interesting for phenomenological interpretations. We now briefly review the experimental history of this and other charged states.

The original Belle paper [110] studies the $B \rightarrow \psi(2S)\pi K$ decays, and reports a peak in the $\psi(2S)\pi$ invariant mass distribution, with $M = (4430 \pm 4 \pm 2)$ MeV and $\Gamma = (45_{-13}^{+18+30})$ MeV (Figure 3.2). This kind of analysis is particularly difficult, because the rich structure of $K\pi$ resonances could reflect into the $\psi(2S)\pi$ channel and create many fake peaks. However, Belle considered that the events with $M(\psi(2S)\pi^-) \sim 4430$ MeV correspond to events with $\cos\theta_{K\pi} \simeq 0.25$, *i.e.* an angular region where interfering $L = 0, 1, 2$ partial waves cannot produce a single peak without creating other larger structures elsewhere. Belle named this state $Z(4430)$, and reported the product branching fractions

$$\mathcal{B}(B^0 \rightarrow K^+ Z(4430)^-) \times \mathcal{B}(Z(4430)^- \rightarrow \psi(2S)\pi^-) = (4.1 \pm 1.0 \pm 1.4) \times 10^{-5}. \quad (3.1)$$

BABAR reviewed this analysis [104], by studying in detail the efficiency corrections

¹Unless specified, the charged conjugated modes are understood.

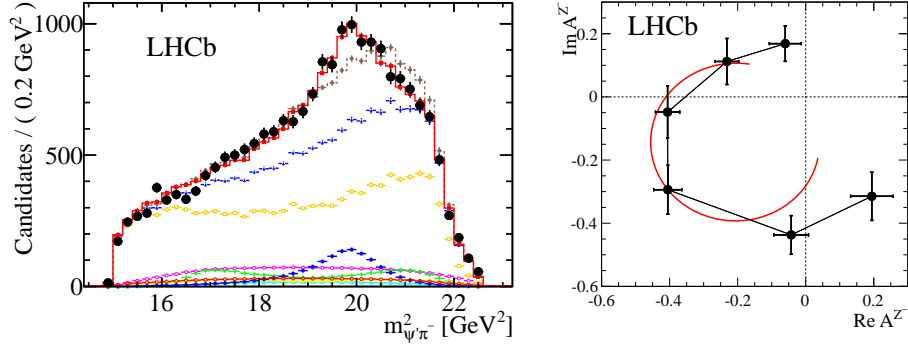


Figure 3.3. Invariant mass distributions in $\psi(2S)\pi^-$ channel (left) and resonant behavior (right) according to LHCb [105]. In the left panel, the red solid (brown dashed) curve shows the fit with (without) the additional $Z(4430)$ resonance. In the right panel, the complex value of the $Z(4430)$ fitted amplitude for six bins of $M(\psi(2S)\pi)$ is shown. The red curve is the prediction from the Breit-Wigner formula with a resonance mass (width) of 4475 (172) MeV.

and the shape of the background, relying for the latter on data as much as possible. Hints of a structure near 4430 MeV appeared, even though not statistically significant, thus leading to a 95% C.L. upper limit on the production branching fraction

$$\mathcal{B}(B^0 \rightarrow K^+ Z(4430)^-) \times \mathcal{B}(Z(4430)^- \rightarrow \psi(2S)\pi^-) < 3.1 \times 10^{-5}. \quad (3.2)$$

After that, Belle revised the analysis [102] studying in detail the 3-body Dalitz plot, and adding all known $K\pi$ resonances, both with and without a coherent amplitude for the $Z(4430)$ in the $\psi(2S)\pi^-$ channel. Belle confirmed the presence of a peak with a statistical significance of 6.4σ . The Breit-Wigner parameter from the Dalitz analysis are $M = (4443_{-12}^{+15+19})$ MeV and $\Gamma = (109_{-43}^{+86+74})$ MeV. A more recent 4D re-analysis by Belle [103] shows that the $J^P = 1^+$ hypothesis is favored, modifying mass and width values to $M = 4485_{-22}^{+22+28}$ MeV and $\Gamma = 200_{-46}^{+41+26}$ MeV (Figure 3.2). The production branching fraction is instead

$$\mathcal{B}(B^0 \rightarrow K^+ Z(4430)^-) \times \mathcal{B}(Z(4430)^- \rightarrow \psi(2S)\pi^-) = (6.0_{-2.0}^{+1.7+2.5}) \times 10^{-5}. \quad (3.3)$$

LHCb confirmed this last result with a similar 4D analysis of the same decay channel. The $Z(4430)^+$ is confirmed with a significance of 13.9σ at least, and the fitted mass and width are $M = (4475 \pm 7_{-25}^{+15})$ MeV and $\Gamma = (172 \pm 13_{-34}^{+37})$ MeV. Also the $J^P = 1^+$ signature is confirmed with high significance. The average *à la* PDG of Belle's and LHCb's mass and width are:

$$M = (4478 \pm 17) \text{ MeV}, \quad \Gamma = (180 \pm 31) \text{ MeV}. \quad (3.4)$$

Since some theoretical papers [111] cast doubts on the resonant nature of the peak, in this analysis the complex value of the $Z(4430)$ amplitude has been plotted as a function of $M(\psi(2S)\pi)$ (Figure 3.3). The behavior is compatible with the Breit-Wigner prediction with the fitted values of mass and width. The same analysis also shows hints for a $Z(4200)$ peak with quantum numbers likely $J^P = 0^-$, mass

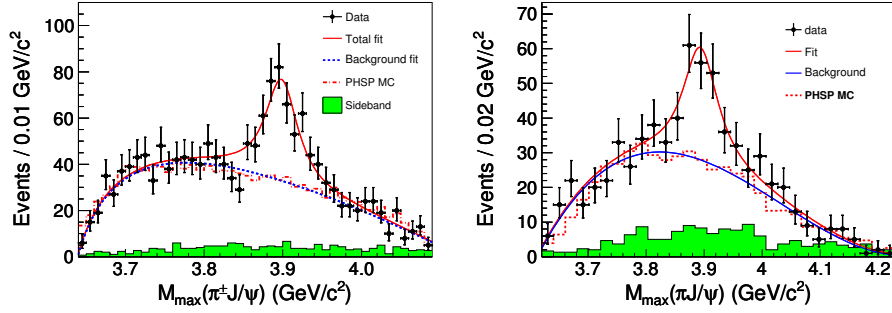


Figure 3.4. Distributions of $M_{\max}(J/\psi \pi^\pm)$, *i.e.* the larger one of the two $M(J/\psi \pi^\pm)$ in each event, according to BES III [68] (left) and Belle [69] (right) in the $Y(4260) \rightarrow J/\psi \pi^+ \pi^-$ decay. The red solid curve is the result of the fit, the blue dotted curve is the background component, the green histogram shows the normalized J/ψ sideband events.

and width $M = (4239 \pm 18_{-10}^{+45})$ MeV, $\Gamma = (220 \pm 47_{-74}^{+108})$ MeV; however, since the Argand diagram is not conclusive about its resonant nature, LHCb has decided not to claim the discovery of another state.

Recently, Belle published a similar analysis of the $B \rightarrow J/\psi \pi K$ decays [90]. Hints of a $Z(4430)$ have been reported in $M(J/\psi \pi)$ invariant mass, with branching fraction

$$\mathcal{B}(B^0 \rightarrow K^+ Z(4430)^-) \times \mathcal{B}(Z(4430)^- \rightarrow J/\psi \pi^-) = (5.4_{-1.0-0.6}^{+4.0+1.1}) \times 10^{-6}. \quad (3.5)$$

The fact that the $Z(4430)$ is found in different decay channels gives solidity to its existence. In the same analysis, Belle claimed the discovery of a broad $Z(4200)$ state with quantum numbers likely $J^P = 1^+$, mass and width $M = (4196_{-29-13}^{+31+17})$ MeV, $\Gamma = (370_{-70-132}^{+70+70})$ MeV, with a significance of 6.2σ , possibly related to the LHCb hint. The reported branching fraction is

$$\mathcal{B}(B^0 \rightarrow K^+ Z(4200)^-) \times \mathcal{B}(Z(4200)^- \rightarrow J/\psi \pi^-) = (2.2_{-0.5-0.6}^{+0.7+1.1}) \times 10^{-5}. \quad (3.6)$$

3.2 Charged states in the 3900-4300 MeV region

In March 2013, BES III [68] and Belle [69] claimed the discovery of a charged resonance in the channel $J/\psi \pi^+$ at a mass of about 3900 MeV, *i.e.* slightly above the DD^* threshold (Figure 3.4). BES III takes data at the $Y(4260)$ pole, and analyzes the process $e^+e^- \rightarrow Y(4260) \rightarrow J/\psi \pi^+ \pi^-$; Belle instead produces $Y(4260)$ in addition with initial state radiation (ISR), and analyzes the process $e^+e^- \rightarrow Y(4260)\gamma_{\text{ISR}} \rightarrow J/\psi \pi^+ \pi^- \gamma_{\text{ISR}}$. The measured mass and width of the resonance are

$$M = (3899.0 \pm 3.6 \pm 4.9) \text{ MeV}, \quad \Gamma = (46 \pm 10 \pm 20) \text{ MeV} \quad (\text{BES III}), \quad (3.7a)$$

$$M = (3894.5 \pm 6.6 \pm 4.5) \text{ MeV}, \quad \Gamma = (63 \pm 24 \pm 26) \text{ MeV} \quad (\text{Belle}), \quad (3.7b)$$

and production branching fractions

$$\begin{aligned} & \frac{\mathcal{B}(Y(4260) \rightarrow Z_c(3900)^+ \pi^-) \times \mathcal{B}(Z_c(3900)^+ \rightarrow J/\psi \pi^+)}{\mathcal{B}(Y(4260) \rightarrow J/\psi \pi^+ \pi^-)} \\ & = (21.5 \pm 3.3)\% \quad (\text{BES III}) = (29.0 \pm 8.9)\% \quad (\text{Belle}). \end{aligned} \quad (3.8)$$

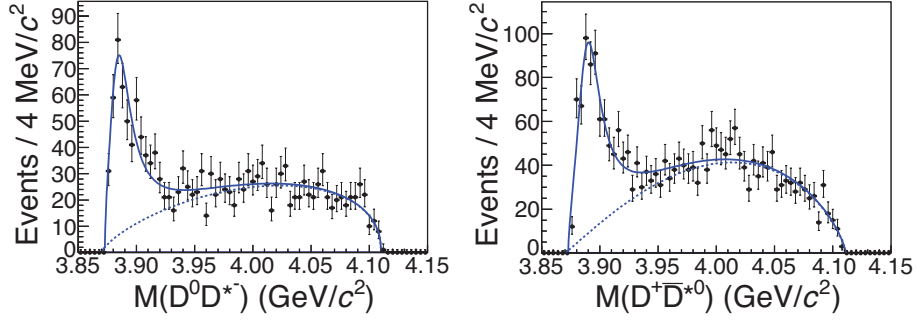


Figure 3.5. Invariant mass distributions of $D^0 D^{*-}$ (left) and $D^+ \bar{D}^{*0}$ (right), according to BES III [67]. The solid curve is the result of the fit, the blue dotted curve is the background component.

This is the first time that a charged manifestly exotic state has been confirmed by two independent experiments, which has given some excitement to the charmonium community. The resonance was called $Z_c(3900)$. No measurement of quantum numbers has been performed, but $J^P = 1^+$ is most likely if the decay $Z_c(3900) \rightarrow J/\psi \pi^+$ is assumed to be in S -wave. Soon after, an analysis of CLEO- c data confirms [70] the presence of the charged $Z_c(3900)^+$ in the $\psi(4160) \rightarrow J/\psi \pi^+ \pi^-$ decay and provides evidence for a neutral partner in the $\psi(4160) \rightarrow J/\psi \pi^0 \pi^0$ decay, with fitted parameters

$$M(Z_c^+) = (3886 \pm 4 \pm 2) \text{ MeV}, \quad \Gamma = (37 \pm 4 \pm 8) \text{ MeV}, \quad (3.9a)$$

$$M(Z_c^0) = (3904 \pm 9 \pm 5) \text{ MeV}, \quad \Gamma = 37 \text{ MeV (fixed)}. \quad (3.9b)$$

A preliminary result by BES III confirm the existence of the neutral partner in $Y(4260) \rightarrow Z_c(3900) \pi^0 \rightarrow J/\psi \pi^0 \pi^0$ [112]. A similar signal has been observed by BES III in $e^+ e^- \rightarrow (D \bar{D}^*)^+ \pi^-$, as a resonance in the $(D \bar{D}^*)^+$ invariant mass [67], with mass and width $M = (3883.9 \pm 1.5 \pm 4.2) \text{ MeV}$ and $\Gamma = (24.8 \pm 3.3 \pm 11.0) \text{ MeV}$ (Figure 3.5). The signature $J^P = 1^+$ is favored, and if this state is assumed to be the same as in the $J/\psi \pi^+$ channel, we have

$$\frac{\mathcal{B}(Z_c(3900) \rightarrow D \bar{D}^*)}{\mathcal{B}(Z_c(3900) \rightarrow J/\psi \pi)} = 6.2 \pm 1.1 \pm 2.7. \quad (3.10)$$

The resulting PDG averaged mass and width are [113]:

$$M = (3888.7 \pm 3.4) \text{ MeV}, \quad \Gamma = (35 \pm 7) \text{ MeV (PDG)}. \quad (3.11)$$

In the same period, BES III studied the $e^+ e^- \rightarrow (D^* \bar{D}^*)^+ \pi^-$ process, and observed another charged resonance in the $D^* \bar{D}^*$ channel [72], at a mass slightly above the $D^* D^*$ threshold, with quantum numbers likely $J^P = 1^+$. Soon after, BES III reported a similar peak in the $e^+ e^- \rightarrow h_c \pi^+ \pi^-$ reaction as a resonance in $h_c \pi^+$ invariant mass [71]. This state is dubbed $Z_c'(4020)$ (Figure 3.6), and the

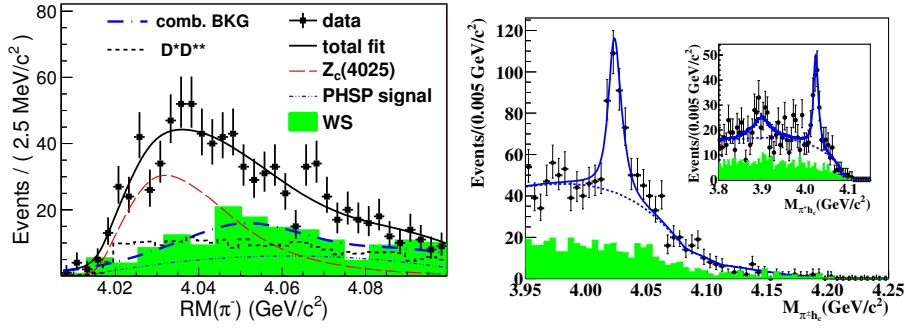


Figure 3.6. Left panel: unbinned maximum likelihood fit to the π recoil mass spectrum, in the $e^+e^- \rightarrow (D^*\bar{D}^*)^+\pi^-$ analysis by BES III [72]. Right panel: fits to the $M(h_c\pi)$ distributions by BES III [71]; the inset shows the sum fits if allowing for an additional $Z_c(3900)$ resonance.

measured masses and widths are:

$$M = (4026.3 \pm 2.6 \pm 3.7) \text{ MeV}, \quad \Gamma = (24.8 \pm 5.6 \pm 7.7) \text{ MeV} \quad (Z'_c \rightarrow D^*\bar{D}^*), \quad (3.12a)$$

$$M = (4022.9 \pm 0.8 \pm 2.7) \text{ MeV}, \quad \Gamma = (7.9 \pm 2.7 \pm 2.6) \text{ MeV} \quad (Z'_c \rightarrow h_c\pi), \quad (3.12b)$$

$$M = (4023.9 \pm 2.4) \text{ MeV}, \quad \Gamma = (10 \pm 6) \text{ MeV} \quad (\text{PDG}). \quad (3.12c)$$

Moreover, BES III has recently reported some evidence for the neutral isospin partner $Z'_c(4020)^0$, with $M = (4023.9 \pm 2.2 \pm 3.89) \text{ MeV}$ and the width fixed to $\Gamma(Z'_c(4020)^+)$ [114]. The $Z_c(3900)$ is also searched [71] in the $h_c\pi$ final state. A peak occurs at 2.1σ level, thus not statistically significant. A 90% C.L. upper bound on the production cross section is established:

$$\sigma(e^+e^- \rightarrow Z_c(3900)^+\pi^- \rightarrow h_c\pi^+\pi^-) < 11 \text{ pb}, \quad (3.13)$$

to be compared with

$$\sigma(e^+e^- \rightarrow Z_c(3900)^+\pi^- \rightarrow J/\psi\pi^+\pi^-) = (13.5 \pm 2.1) \text{ pb}. \quad [68] \quad (3.14)$$

Similarly, no $Z'_c(4020)$ has been seen by BES III and Belle decaying into $J/\psi\pi$, as it is shown in Figure 3.4.

It is worth noticing that no $Z_c(3900)$ has been seen by Belle in the $B \rightarrow KJ/\psi\pi$ channel [90], and the 90% C.L. upper bound on the branching fraction is:

$$\mathcal{B}(B^0 \rightarrow K^+Z(3900)^-) \times \mathcal{B}(Z(3900)^- \rightarrow J/\psi\pi^-) < 9 \times 10^{-7}. \quad (3.15)$$

Moreover, the COMPASS collaboration reported a search for $\gamma N \rightarrow Z_c^+(3900)N$, where the photon is obtained with scattering of positive muons at 160 and 200 GeV on a target of LiD or NH_3 [115]. No signal is observed, and a 90% C.L. upper bound is put:

$$\frac{\mathcal{B}(Z_c(3900) \rightarrow J/\psi\pi^+) \times \sigma(\gamma N \rightarrow Z_c^+(3900)N)}{\sigma(\gamma N \rightarrow J/\psi N)} < 3.7 \times 10^{-3} \quad (3.16)$$

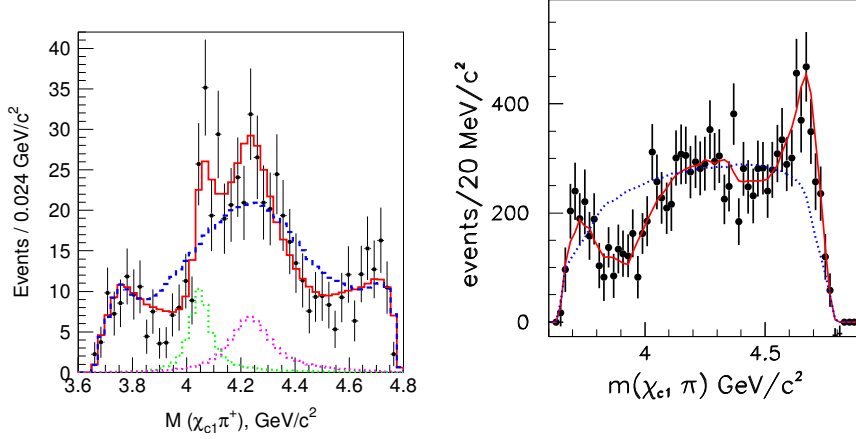


Figure 3.7. Invariant mass distributions of $\chi_{c1}\pi^\pm$, with fit results showing the charged resonances in the Belle (left) [82] and *BABAR* (right) [83] analyses. The region of the $K^*(890)$ and $K^*(1410)$ peaks are removed. In left panel, the solid red histogram shows the results of the fit that includes coherent Z_1 and Z_2 amplitudes; the dashed blue curve is the result of the fit using $K\pi$ amplitudes only. In right panel, the solid curve fits data using $K\pi$ amplitudes only.

at $\sqrt{s_{\gamma N}} \simeq 13.8$ GeV.

In a Dalitz-plot analysis of $B \rightarrow \chi_{c1}\pi^+K$ decays, Belle could get an acceptable fit only by adding two resonances in the $\chi_{c1}\pi^+$ channel, which were named $Z_1(4050)$ and $Z_2(4250)$ [82]. The fitted masses and widths are

$$M = (4051 \pm 14^{+20}_{-41}) \text{ MeV} \quad \Gamma = (82^{+21+47}_{-17-22}) \text{ MeV} \quad (Z_1^+), \quad (3.17a)$$

$$M = (4248^{+44+180}_{-29-35}) \text{ MeV} \quad \Gamma = (177^{+54+316}_{-39-61}) \text{ MeV} \quad (Z_2^+), \quad (3.17b)$$

and reported the production branching fractions

$$\mathcal{B}(B \rightarrow Z_1^- K^+) \times \mathcal{B}(Z_1^- \rightarrow \chi_{c1}\pi^-) = (3.0^{+1.2+3.7}_{-0.8-1.6}) \times 10^{-5}, \quad (3.18a)$$

$$\mathcal{B}(B \rightarrow Z_2^- K^+) \times \mathcal{B}(Z_2^- \rightarrow \chi_{c1}\pi^-) = (4.0^{+2.3+19.7}_{-0.9-0.5}) \times 10^{-5}. \quad (3.18b)$$

The same decay was investigated by *BABAR*, which carefully studied the effects of interference between resonances in the $K\pi$ system [83]. Considering interfering resonances in the $K\pi$ channel only, *BABAR* obtained good fits to data without adding any $\chi_{c1}\pi$ resonance. Upper limits at 95% C.L. on the product branching fractions of Z_1 and Z_2 can be evaluated if incoherent resonant amplitudes for these two states are added to the fit:

$$\mathcal{B}(B \rightarrow Z_1^- K^+) \times \mathcal{B}(Z_1^- \rightarrow \chi_{c1}\pi^-) < 1.8 \times 10^{-5}, \quad (3.19a)$$

$$\mathcal{B}(B \rightarrow Z_2^- K^+) \times \mathcal{B}(Z_2^- \rightarrow \chi_{c1}\pi^-) < 4.0 \times 10^{-5}. \quad (3.19b)$$

Part of the discrepancy between the two experiments may be due to the fact that in the *BABAR* analysis the Z_1 and Z_2 terms are added incoherently and do not interfere

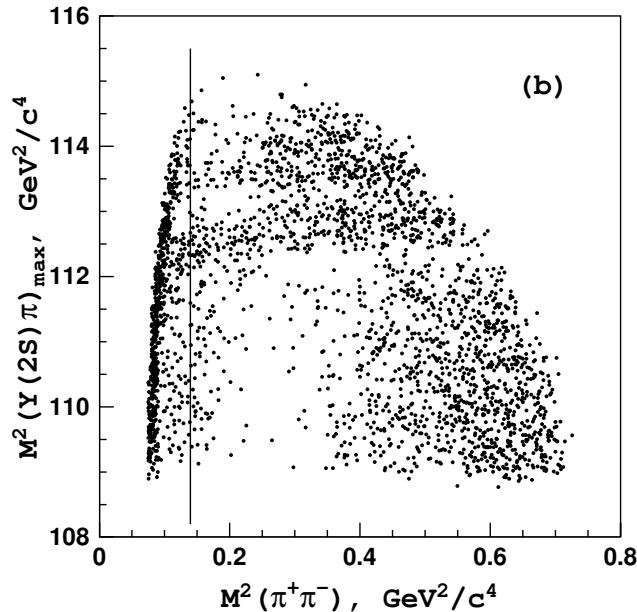


Figure 3.8. Dalitz plot for $\Upsilon(2S)$ events in the signal region. Events to the left of the vertical line are excluded. From Belle [107].

with the $K\pi$ amplitudes, while in the Belle analysis, significant constructive and destructive interference between the $Z_{1,2}$ amplitudes and the $K\pi$ resonances is more relevant (see the dips and peaks of the solid red curve in Figure 3.7).

Finally, we report a 3.5σ peak in the $\psi(2S)\pi^+$ invariant mass, in the $e^+e^- \rightarrow \psi(2S)\pi^+\pi^-$ full statistics analysis by Belle [116], with best fit parameters $M = (4054 \pm 3 \pm 1)$ MeV and $\Gamma = (45 \pm 11 \pm 6)$ MeV.

3.3 Charged bottomonium states: $Z_b(10610)/Z'_b(10650)$

The $Z_c(3900)$ and the $Z'_c(4020)$ could have their counterparts in the bottomonium sector. Belle reported the observation of anomalously high rates for the $\Upsilon(5S) \rightarrow \pi^+\pi^-\Upsilon(nS)$ ($n = 1, 2, 3$) [117] and $\Upsilon(5S) \rightarrow \pi^+\pi^-h_b(nP)$ ($n = 1, 2$) [118] transitions. The measured partial decay widths $\Gamma(\Upsilon(5S) \rightarrow \Upsilon(nS)\pi^+\pi^-) \simeq 0.5$ MeV are about two orders of magnitude larger than typical widths for dipion transitions among the four lower (nS) states. Furthermore, the observation of $\pi^+\pi^-h_b(nP)$ final states with rates comparable to $\pi^+\pi^-\Upsilon(nS)$ violates heavy-quark spin conservation. Belle searched for exotic resonant substructures in these decays [107]. In order to have a relatively background-free sample, the $\Upsilon(nS)$ states are observed in their $\mu^+\mu^-$ decay only, whereas the $h_b(nP)$ are reconstructed inclusively.

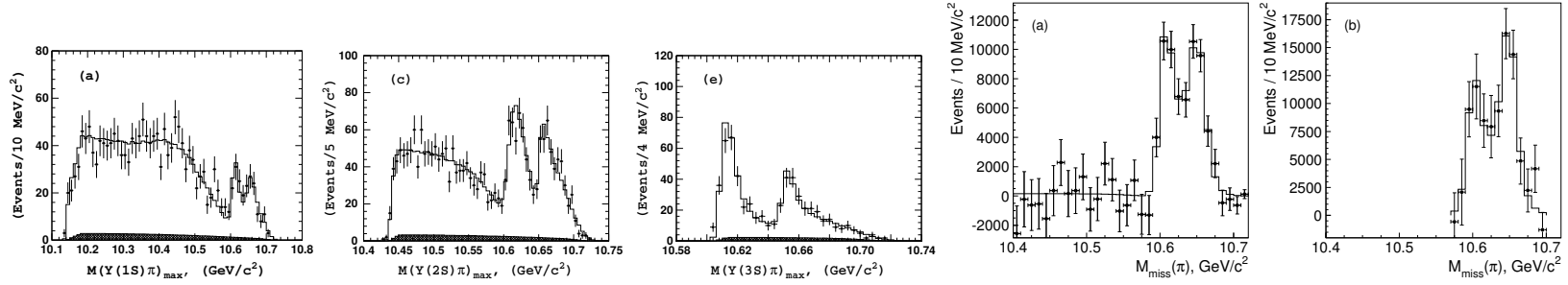


Figure 3.9. Comparison of fit results (open histogram) with experimental data (points with error bars) for events in the $\Upsilon(nS)$ (first 3 plots) and $h_b(nP)$ (last 2 plots) regions. From Belle [107].

Final state	$\Upsilon(1S)\pi^+\pi^-$	$\Upsilon(2S)\pi^+\pi^-$	$\Upsilon(3S)\pi^+\pi^-$	$h_b(1P)\pi^+\pi^-$	$h_b(2P)\pi^+\pi^-$
$M[Z_b(10610)], \text{ MeV}$	$10611 \pm 4 \pm 3$	$10609 \pm 2 \pm 3$	$10608 \pm 2 \pm 3$	$10605 \pm 2^{+3}_{-1}$	10599^{+6+5}_{-3-4}
$\Gamma[Z_b(10610)], \text{ MeV}$	$22.3 \pm 7.7^{+3.0}_{-4.0}$	$24.2 \pm 3.1^{+2.0}_{-3.0}$	$17.6 \pm 3.0 \pm 3.0$	$11.4^{+4.5+2.1}_{-3.9-1.2}$	13^{+10+9}_{-8-7}
$M[Z_b(10650)], \text{ MeV}$	$10657 \pm 6 \pm 3$	$10651 \pm 2 \pm 3$	$10652 \pm 1 \pm 2$	$10654 \pm 3^{+1}_{-2}$	10651^{+2+3}_{-3-2}
$\Gamma[Z_b(10650)], \text{ MeV}$	$16.3 \pm 9.8^{+6.0}_{-2.0}$	$13.3 \pm 3.3^{+4.0}_{-3.0}$	$8.4 \pm 2.0 \pm 2.0$	$20.9^{+5.4+2.1}_{-4.7-5.7}$	$19 \pm 7^{+11}_{-7}$
Rel. normalization	$0.57 \pm 0.21^{+0.19}_{-0.04}$	$0.86 \pm 0.11^{+0.04}_{-0.10}$	$0.96 \pm 0.14^{+0.08}_{-0.05}$	$1.39 \pm 0.37^{+0.05}_{-0.15}$	$1.6^{+0.6+0.4}_{-0.4-0.6}$
Rel. phase, degrees	$58 \pm 43^{+4}_{-9}$	$-13 \pm 13^{+17}_{-8}$	$-9 \pm 19^{+11}_{-26}$	187^{+44+3}_{-57-12}	$181^{+65+74}_{-105-109}$

Table 3.4. Comparison of results on $Z_b(10610)$ and $Z_b'(10650)$ parameters obtained from $\Upsilon(5S) \rightarrow \Upsilon(nS)\pi^+\pi^-$ and $\Upsilon(5S) \rightarrow h_b(nP)\pi^+\pi^-$ analyses [107].

Channel	Fraction, %	
	$Z_b(10610)$	$Z'_b(10650)$
$\Upsilon(1S)\pi^+$	0.32 ± 0.09	0.24 ± 0.07
$\Upsilon(2S)\pi^+$	4.38 ± 1.21	2.40 ± 0.63
$\Upsilon(3S)\pi^+$	2.15 ± 0.56	1.64 ± 0.40
$h_b(1P)\pi^+$	2.81 ± 1.10	7.43 ± 2.70
$h_b(2P)\pi^+$	4.34 ± 2.07	14.8 ± 6.22
$B^+\bar{B}^{*0} + \bar{B}^0B^{*+}$	86.0 ± 3.6	–
$B^{*+}\bar{B}^{*0}$	–	73.4 ± 7.0

Table 3.5. List of branching fractions for the $Z_b^+(10610)$ and $Z'_b(10650)$ decays. From Belle [109].

The Dalitz plots in the signal region (see for example Figure 3.8) is fitted with a sum of interfering resonances: the $f_0(980)$, the $f_2(1270)$ in $\pi\pi$ channel, two new charged resonances in the $\Upsilon(nS)[h_b(nP)]\pi^\pm$ channel, and a nonresonant background. The result of each fit is reported in Table 3.4; all the studied channels show the highly significant presence of both charged resonances, dubbed $Z_b(10610)$ and $Z'_b(10650)$, with compatible masses and widths. The one-dimensional invariant mass projections for events in each $\Upsilon(nS)$ and $h_b(nP)$ signal region are shown in Figure 3.9. The average of all channels gives for $Z_b(10610)$ a mass and width of $M = (10607.2 \pm 2.0)$ MeV, $\Gamma = (18.4 \pm 2.4)$ MeV, and for $Z'_b(10650)$ a mass and width of $M = (10652.2 \pm 1.5)$ MeV, $\Gamma = (11.5 \pm 2.2)$ MeV.

The $Z_b(10610)$ production rate is similar to that of the $Z'_b(10650)$ for each of the five decay channels. Their relative phase is consistent with zero for the final states with the $\Upsilon(nS)$ and consistent with 180 degrees for the final states with $h_b(nP)$. Production of the Z_b 's saturates the $\Upsilon(5S) \rightarrow h_b(nP)\pi^+\pi^-$ transitions and accounts for the high inclusive $h_b(nP)$ production rate reported by Belle [118]. Analyses of charged pion angular distributions [107, 119] favor the $J^P = 1^+$ spin-parity assignment for both the states.

Belle searched these states also in pairs of open bottom mesons [109]. The Dalitz plots of $\Upsilon(5S) \rightarrow (BB^*)^-\pi^+$ and $\Upsilon(5S) \rightarrow (B^*B^*)^-\pi^+$ report a 8σ signal of $Z_b^-(10610) \rightarrow (BB^*)^-$ and a 6.5σ signal of $Z'_b(10650) \rightarrow (B^*B^*)^-$, respectively, whereas $Z'_b(10650) \rightarrow (BB^*)^-$ is compatible with zero². The best estimate for the branching ratios are reported in Table 3.5.

Recently, Belle has been able to find the neutral isospin partner $Z_b(10610)^0$ [108] in $\Upsilon(5S) \rightarrow \Upsilon(2,3S)\pi^0\pi^0$ decays, at a significance of 6.5σ if mass and width are fixed to the averaged values of the $Z_b(10610)^+$. If the mass is let free, the fitted value is $M = (10609 \pm 4 \pm 4)$ MeV, consistent with the charged partner mass. On the other hand, no significant signal of $Z'_b(10650)^0$ is seen.

² $Z_b^-(10610) \rightarrow (B^*B^*)^-$ is phase-space forbidden.

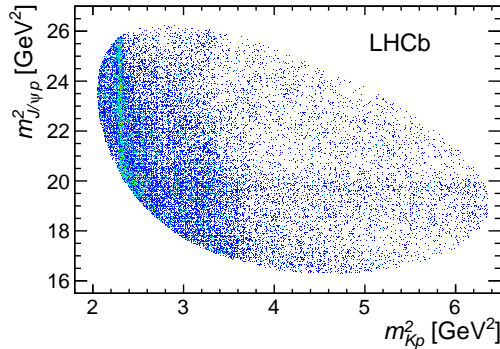


Figure 3.10. Invariant mass squared of Kp versus $J/\psi p$ for candidates within ± 15 MeV of the Λ_b^0 mass [101].

3.4 Pentaquark states

In July 2015, LHCb reported the observation of two peaks, denoted $P_c(4380)^+$ and $P_c(4450)^+$, in the invariant mass of $J/\psi p$ in the $\Lambda_b^0 \rightarrow J/\psi p K^-$ decay [101]. In the Dalitz plot in Figure 3.10 a band in the $J/\psi p$ is indeed visible, and looks far from the Λ^* region ($m_{Kp}^2 < 4 \text{ GeV}^2$). The full amplitude fit cannot satisfactorily describe data without including these two Breit-Wigner shaped resonances (Figure 3.11). The lighter state has a mass of $4380 \pm 8 \pm 29 \text{ MeV}$ and a width of $205 \pm 18 \pm 86 \text{ MeV}$, while the heavier one has a mass of $4449.8 \pm 1.7 \pm 2.5 \text{ MeV}$ and a width of $39 \pm 5 \pm 19 \text{ MeV}$. The parities of the two states are opposite, and the preferred J^P are $(\frac{3}{2}^-, \frac{5}{2}^+)$, although $(\frac{3}{2}^+, \frac{5}{2}^-)$ and $(\frac{5}{2}^+, \frac{3}{2}^-)$ are not excluded. The higher mass state has a fit fraction of $(4.1 \pm 0.5 \pm 1.1)\%$, and the lower mass state of $(8.4 \pm 0.7 \pm 4.2)\%$, of the total sample. To study the resonant behavior of the two states, the amplitudes are represented as the combination of independent complex numbers at six equidistant points in the range $\pm\Gamma_0 = 39 \text{ MeV}$ around the as determined in the default fit. Real and imaginary parts of the amplitude are interpolated in mass between the fitted points. The resulting Argand diagram, shown in Figure 3.12, is consistent with a rapid counter-clockwise change of the $P_c(4450)^+$ phase when its magnitude reaches the maximum, whereas no conclusion can be drawn for the wider $P_c(4380)^+$.

3.5 The $X(3872)$ saga

The queen of exotic states is the $X(3872)$. It was discovered by Belle while studying the $B \rightarrow K J/\psi \pi^+ \pi^-$ decays [52], as an unexpected resonance in the $J/\psi \pi^+ \pi^-$ invariant mass distribution (see Figure 3.14, left panel). It was then confirmed both in B decays [120] and in inclusive prompt $p\bar{p}$ [57, 121] and pp production [58, 122] – see Chapter 6 for a long-standing controversy about the theoretical interpretation of that. First of all, an exotic nature was suggested by its narrow width, $\Gamma < 2.3 \text{ MeV}$ at 90% C.L. [52], despite being above threshold for the decay into a charmed meson pair. Furthermore, both $\pi^+ \pi^-$ invariant mass distribution [52, 123] and angular analyses [55] show that the $\pi^+ \pi^-$ amplitude is dominated by the ρ meson, *i.e.*

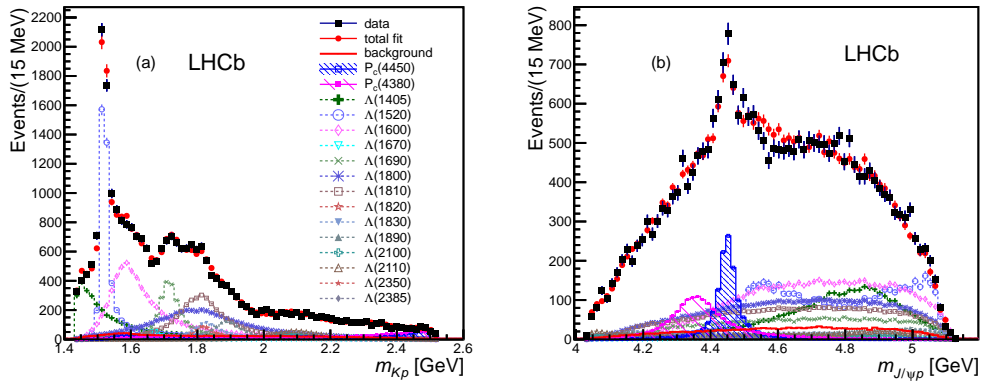


Figure 3.11. Results for the full amplitude fit in the m_{Kp} (left) and $m_{J/\psi p}$ variables. The data are shown as (black) squares with error bars, while the (red) circles show the results of the fit. The error bars on the points showing the fit results are due to simulation statistics [101].

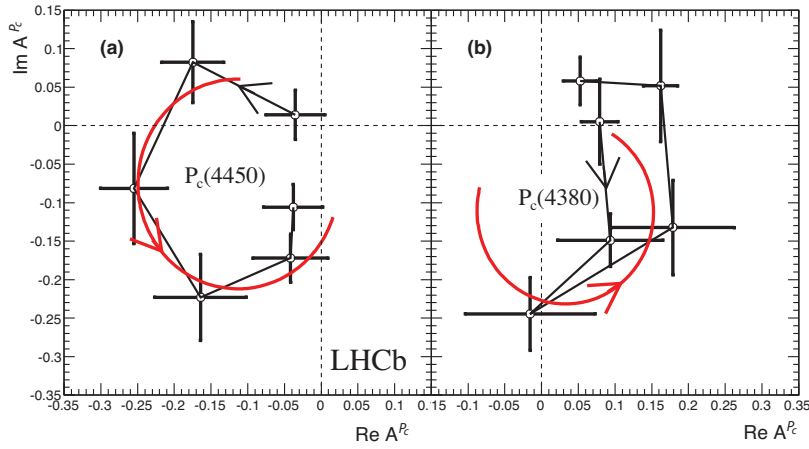


Figure 3.12. Fitted values of the real and imaginary parts of the amplitudes for the favored spin fit for the $P_c(4450)^+$ state (left) and for the $P_c(4380)^+$ state (right), each divided into six $m_{J/\psi p}$ bins of equal width shown in the Argand diagrams as connected points with error bars ($m_{J/\psi p}$ increases counterclockwise). The solid (red) curves are the predictions from the Breit-Wigner formula [101].

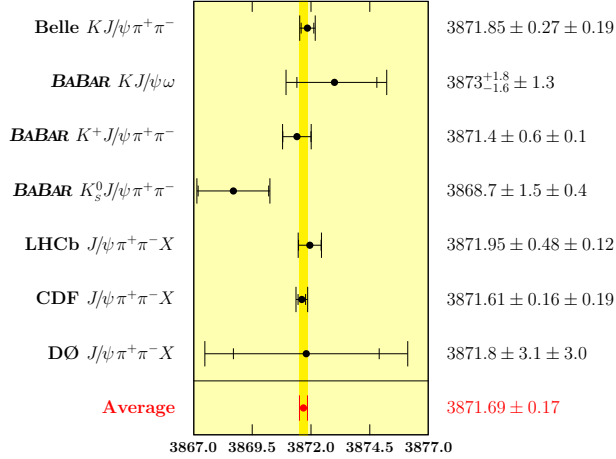


Figure 3.13. Measured mass of the $X(3872)$. We show the measurements which contribute to the average in PDG [113].

a $I = 1$ resonance. If the $X(3872)$ were an ordinary charmonium with $I = 0$, such a decay would badly violate isospin symmetry. The size of isospin breaking was quantified by the measurement of the $X(3872) \rightarrow J/\psi \omega$ branching fraction by Belle [60] and BABAR [61]:

$$\frac{\Gamma(X(3872) \rightarrow J/\psi \omega)}{\Gamma(X(3872) \rightarrow J/\psi \pi^+ \pi^-)} = 0.8 \pm 0.3. \quad (3.20)$$

The $C = +$ assignment was confirmed by the observation of the $X(3872) \rightarrow J/\psi \gamma$ decay [60, 124], and by the non-observation of $X(3872) \rightarrow \chi_{c1} \gamma$ [52]. As for the spin, a preliminary angular analysis of the $X(3872) \rightarrow J/\psi \pi^+ \pi^-$ by Belle [125] favored 1^{++} assignment. Soon after, a more detailed analysis by CDF [55] was able to rule out all but the 1^{++} and 2^{-+} assignments. The latter could not be excluded because of the additional complex parameter given by the ratio between the two independent amplitudes for $X(2^{++}) \rightarrow J/\psi \pi^+ \pi^-$, which could not be constrained in inclusive $X(3872)$ production; on the other hand, the former was preferred by theoretical models. Instead, the analysis of the $J/\psi \omega$ invariant mass distribution by BABAR [61] favored the 2^{-+} hypothesis, and stimulated a discussion on its theoretical feasibility [1, 49, 126–128]. However, a $J = 2$ assignment would allow $X(3872)$ to be produced in $\gamma\gamma$ fusion, but CLEO has found no significant signal in $\gamma\gamma \rightarrow X(3872) \rightarrow J/\psi \pi^+ \pi^-$ [129]. A statistically improved analysis of angular distributions in $X(3872) \rightarrow J/\psi \pi^+ \pi^-$ has been made by Belle [53], again favoring 1^{++} . The limited statistics forced Belle to consider three different one-dimensional projections of the full angular distribution, which were not able to rule out 2^{-+} .

Finally, LHCb has recently published an analysis of a large $B^+ \rightarrow K^+ X(3872)$ sample [59]. This study is based on an event-by-event likelihood ratio test of 1^{++} and 2^{-+} hypotheses on the full 5D angular distribution, and favors the 1^{++} over 2^{-+} at 8σ level. The additional complex parameter in the 2^{-+} distributions is treated as a nuisance parameter; its best value extracted from the fit is found to be consistent with the value obtained if the events are MC generated with a 1^{++} assumption;

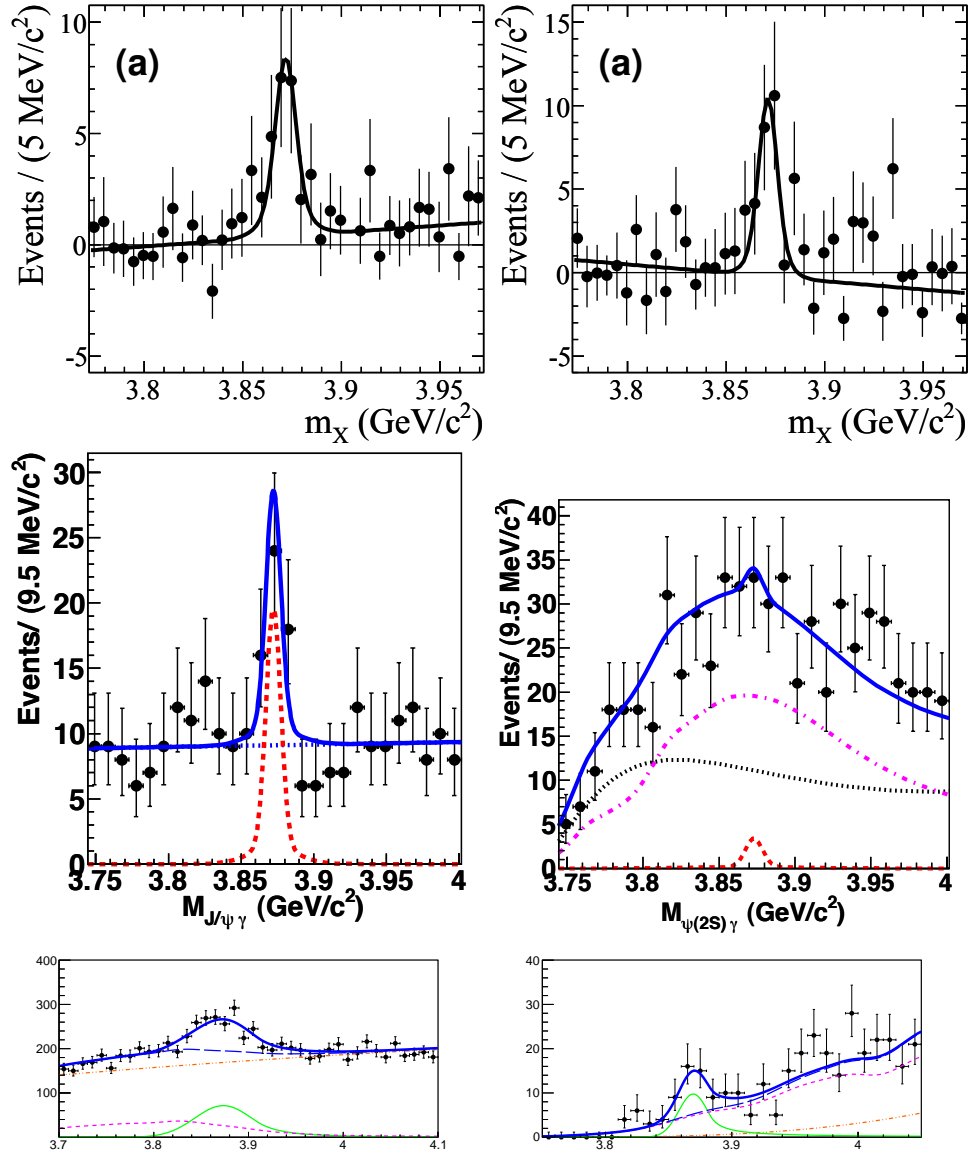


Figure 3.15. Invariant mass spectra of $J/\psi\gamma$ (left) and $\psi(2S)\gamma$ (right) in $B^+ \rightarrow \psi^{(\prime)}\gamma K^+$, according to *BABAR* [63] (upper), *Belle* [62] (middle) and *LHCb* [64] (lower).

We just discuss the case of $X(3872) \rightarrow \psi(2S)\gamma$, which is of interest for theoretical interpretations. *BABAR* [63] and LHCb [64] find a signal with a relative branching fraction of:

$$\frac{\mathcal{B}(X(3872) \rightarrow \psi(2S)\gamma)}{\mathcal{B}(X(3872) \rightarrow J/\psi\gamma)} = 3.4 \pm 1.4 \quad (\text{BABAR}), \quad (3.21a)$$

$$= 2.46 \pm 0.64 \pm 0.29 \quad (\text{LHCb}), \quad (3.21b)$$

$$< 2.1 \quad (\text{Belle}). \quad (3.21c)$$

In particular, for the decay $X(3872) \rightarrow \psi(2S)\gamma$, Belle [62] sees no significant signal and puts a 90% C.L. upper limit (see Figure 3.15).

Other production mechanisms like $B^0 \rightarrow K^+\pi^-X(3872)$ have also been studied. Such decays are seen, but with a smooth distribution in $K^+\pi^-$ invariant mass; an upper limit is set on $\mathcal{B}(B^0 \rightarrow K^*(892)^0X(3872))$ [134]. This is in contrast to ordinary charmonium states, where $B \rightarrow K^*c\bar{c}$ and $Kc\bar{c}$ branching fractions are comparable, and K^* dominates over nonresonant $K\pi$. We also mention the decay $Y(4260) \rightarrow \gamma X(3872)$ seen by BES III [98], with a production cross section of $\sigma(e^+e^- \rightarrow Y(4260) \rightarrow \gamma X(3872)) \times \mathcal{B}(X(3872) \rightarrow J/\psi\pi^+\pi^-) = (0.33 \pm 0.12 \pm 0.02)$ pb.

In Table 3.6 we show estimates for the absolute branching fractions of the $X(3872)$ we evaluated in [50]. These can be obtained from measured product branching fractions of $X(3872)$ by exploiting the upper limit on $B \rightarrow X(3872)K$ measured by *BABAR* from the spectrum of the kaons recoiling against fully reconstructed B mesons [135], $\mathcal{B}(B^\pm \rightarrow K^\pm X(3872)) < 3.2 \times 10^{-4}$ at 90% C.L.. Combining the likelihood from the measurements of the product branching fractions in the observed channels, the $B \rightarrow X(3872)K$ upper limit and the $X(3872)$ width distribution [69], with a bayesian procedure we extracted the likelihood for the absolute $X(3872)$ branching fractions and the widths in each of the decay modes. Then, we used the probability distributions obtained with this procedure to set limits on the not observed channels. The full shape of the experimental likelihoods was used whenever available, while gaussian errors and poissonian counting distributions have been assumed elsewhere. The 68% confidence intervals (defined in such a way that the absolute value of the PDF is the same at the upper and lower bound, unless one of them is at the boundary of the physical range) are summarized in Table 3.6 for each of the decay modes. Some of the likelihoods are shown in Figure 3.16.

The searches for partner states of the $X(3872)$ have been motivated by the predictions of the tetraquark model (see Chapter 7). For example, it has been hypothesized that the X state produced in B^+ decays was different from the X state produced in B^0 decays. If so, the two X should have different masses. Both *BABAR* [54, 136] and Belle [53, 134] have performed analyses distinguishing the two samples. The most recent results set the mass difference of the two X at

$$\begin{aligned} \delta M &\equiv M(X | B^+ \rightarrow K^+ X) - M(X | B^0 \rightarrow K^0 X) \\ &= (+2.7 \pm 1.6 \pm 0.4) \text{ MeV} \quad (\text{BABAR}), \end{aligned} \quad (3.22a)$$

$$= (-0.7 \pm 1.0 \pm 0.2) \text{ MeV} \quad (\text{Belle}), \quad (3.22b)$$

$$= (+0.2 \pm 0.8) \text{ MeV} \quad (\text{mean}). \quad (3.22c)$$

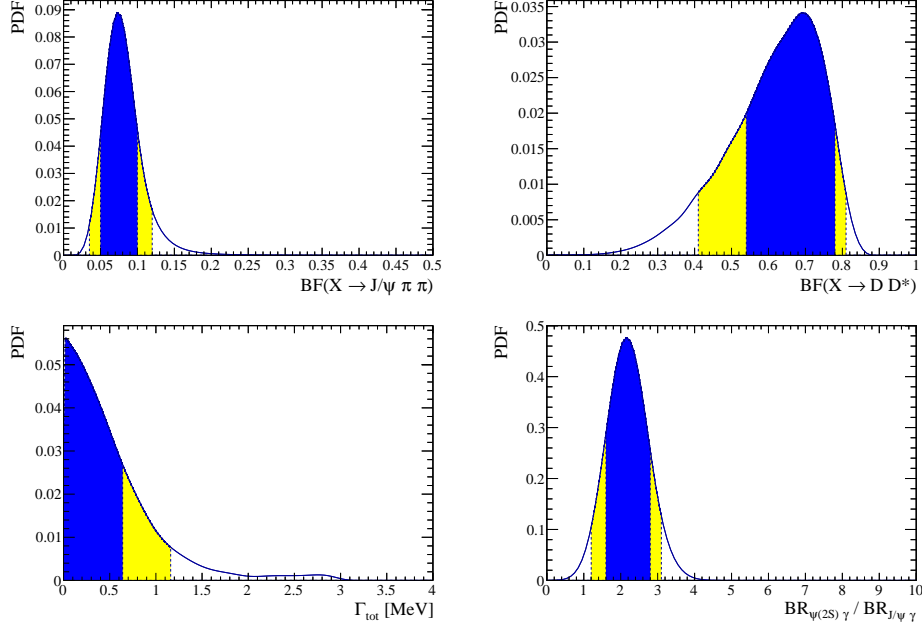


Figure 3.16. Likelihood function of the $X(3872)$ branching fraction in $J/\psi\pi\pi$ and $D^{*0}\bar{D}^0$, the total width and the ratio $\mathcal{B}(X(3872) \rightarrow \psi(2S)\gamma)/\mathcal{B}(X(3872) \rightarrow J/\psi\gamma)$ [50]. The dark (light) filled area corresponds to the 68% (90%) C.L. region.

Moreover, an inclusive analysis by CDF [56], of the $J/\psi\pi^+\pi^-$ spectrum, gives no evidence for any other neutral state, setting an upper limit on the mass difference of 3.6 MeV at the 95% C.L..

The same analyses provide measurements of the ratio of product branching fractions

$$\frac{\mathcal{B}(B^0 \rightarrow K^0 X) \times \mathcal{B}(X \rightarrow \pi^+\pi^- J/\psi)}{\mathcal{B}(B^+ \rightarrow K^+ X) \times \mathcal{B}(X \rightarrow \pi^+\pi^- J/\psi)} = 0.41 \pm 0.24 \pm 0.05 \quad (\text{BABAR}), \quad (3.23a)$$

$$= 0.50 \pm 0.14 \pm 0.04 \quad (\text{Belle}). \quad (3.23b)$$

Searches for charged partners have also been performed by both *BABAR* [137] and *Belle* [53]. No evidence for such a state is seen, with limits on the product branching fractions of

$$\mathcal{B}(\bar{B}^0 \rightarrow K^- X^+) \times \mathcal{B}(X^+ \rightarrow \rho^+ J/\psi) < 5.4 \times 10^{-6} \quad (\text{BABAR}), \quad (3.24a)$$

$$< 4.2 \times 10^{-6} \quad (\text{Belle}), \quad (3.24b)$$

$$\mathcal{B}(B^+ \rightarrow K^0 X^+) \times \mathcal{B}(X^+ \rightarrow \rho^+ J/\psi) < 22 \times 10^{-6} \quad (\text{BABAR}), \quad (3.24c)$$

$$< 6.1 \times 10^{-6} \quad (\text{Belle}), \quad (3.24d)$$

to be compared with

$$\begin{aligned} \mathcal{B}(B^+ \rightarrow K^+ X) \times \mathcal{B}(X \rightarrow \rho^0 J/\psi) \\ = (8.4 \pm 1.5 \pm 0.7) \times 10^{-6} \quad (\text{BABAR}), \quad (3.25a) \end{aligned}$$

$$= (8.6 \pm 0.8 \pm 0.5) \times 10^{-6} \quad (\text{Belle}) \quad (3.25b)$$

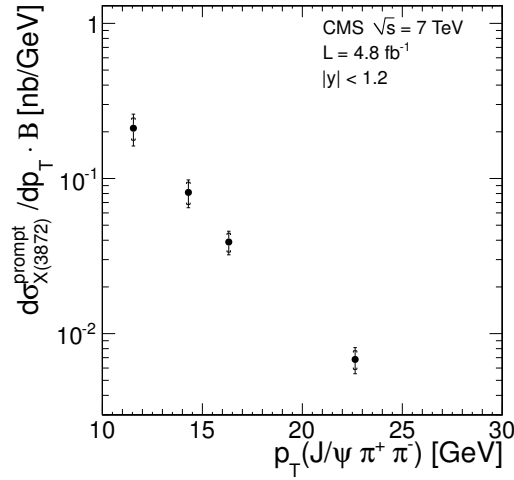


Figure 3.17. Measured differential cross section for prompt $X(3872)$ production times branching fraction $\mathcal{B}(X(3872) \rightarrow J/\psi \pi^+ \pi^-)$ as a function of p_T , from CMS [122].

for the discovery mode, measured by *BABAR* [54] and Belle [53].

We conclude this section on the $X(3872)$ with the inclusive production at hadron colliders: the prompt production has been studied at CDF [138] and CMS [122], giving

$$\frac{\sigma^{\text{prompt}}(p\bar{p} \rightarrow X(3872) + \text{all})}{\sigma(p\bar{p} \rightarrow X(3872) + \text{all})} = (83.9 \pm 4.9 \pm 2.0)\% \text{ at } \sqrt{s} = 1.96 \text{ GeV}, \quad (3.26a)$$

$$\frac{\sigma^{\text{prompt}}(pp \rightarrow X(3872) + \text{all})}{\sigma(pp \rightarrow X(3872) + \text{all})} = (73.7 \pm 2.3 \pm 1.6)\% \text{ at } \sqrt{s} = 7 \text{ GeV}. \quad (3.26b)$$

CMS published also the value for the prompt production cross section, $\sigma^{\text{prompt}}(pp \rightarrow X(3872) + \text{all}) \times \mathcal{B}(X(3872) \rightarrow J/\psi \pi^+ \pi^-) = (1.06 \pm 0.11 \pm 0.15) \text{ nb}$ at $\sqrt{s} = 7 \text{ GeV}$ (see Figure 3.17).

The same measurement is not present in the CDF note, but it has been estimated by Bignamini *et al.* [139]: $\sigma^{\text{prompt}}(pp \rightarrow X(3872) + \text{all}) \times \mathcal{B}(X(3872) \rightarrow J/\psi \pi^+ \pi^-) = (3.1 \pm 0.7) \text{ nb}$ at $\sqrt{s} = 1.96 \text{ GeV}$.

B decay mode	X decay mode	product branching fraction ($\times 10^5$)	B_{fit}	R_{fit}
$K^+ X$	$X \rightarrow \pi\pi J/\psi$	0.86 ± 0.08 (<i>BABAR</i> [54], Belle [53])	$0.081^{+0.019}_{-0.031}$	1
		$0.84 \pm 0.15 \pm 0.07$ <i>BABAR</i> [54]		
		$0.86 \pm 0.08 \pm 0.05$ Belle [53]		
$K^0 X$	$X \rightarrow \pi\pi J/\psi$	0.41 ± 0.11 (<i>BABAR</i> [54]; Belle [53])		
		$0.35 \pm 0.19 \pm 0.04$ <i>BABAR</i> [54]		
		$0.43 \pm 0.12 \pm 0.04$ Belle [53]		
$(K^+\pi^-)_{NR} X$	$X \rightarrow \pi\pi J/\psi$	$0.81 \pm 0.20^{+0.11}_{-0.14}$ Belle [134]		
$K^{*0} X$	$X \rightarrow \pi\pi J/\psi$	< 0.34 , 90% C.L. Belle [134]		
KX	$X \rightarrow \omega J/\psi$	$R = 0.8 \pm 0.3$ <i>BABAR</i> [61]	$0.061^{+0.024}_{-0.036}$	$0.77^{+0.28}_{-0.32}$
$K^+ X$		$0.6 \pm 0.2 \pm 0.1$ <i>BABAR</i> [61]		
$K^0 X$		$0.6 \pm 0.3 \pm 0.1$ <i>BABAR</i> [61]		
KX	$X \rightarrow \pi\pi\pi^0 J/\psi$	$R = 1.0 \pm 0.4 \pm 0.3$ Belle [60]		
$K^+ X$	$X \rightarrow D^{*0} \bar{D}^0$	8.5 ± 2.6 (<i>BABAR</i> [66]; Belle [65])	$0.614^{+0.166}_{-0.074}$	$8.2^{+2.3}_{-2.8}$
		$16.7 \pm 3.6 \pm 4.7$ <i>BABAR</i> [66]		
		$7.7 \pm 1.6 \pm 1.0$ Belle [65]		
$K^0 X$	$X \rightarrow D^{*0} \bar{D}^0$	12 ± 4 (<i>BABAR</i> [66]; Belle [65])		
		$22 \pm 10 \pm 4$ <i>BABAR</i> [66]		
		$9.7 \pm 4.6 \pm 1.3$ Belle [65]		

Table 3.6. Measured $X(3872)$ product branching fractions, separated by production and decay channel. Our averages are in boldface. The last two columns report the results in terms of absolute $X(3872)$ branching fraction (B_{fit}) and in terms of the branching fraction normalized to $J/\psi\pi\pi$ (R_{fit}) as obtained from the global likelihood fit described in the text. For non-zero measurements we report the mean value, and the 68% C.L. range in form of asymmetric errors. The limits are provided at 90% C.L. The $X(3872) \rightarrow \pi\pi\pi^0 J/\psi$ is dominated by $\omega J/\psi$, but no limits on the non-resonant $\pi\pi\pi^0 J/\psi$ component have been set. The ratio R' given by LHCb [140] is the ratio $\mathcal{B}(X(3872) \rightarrow \psi(2S)\gamma) / \mathcal{B}(X(3872) \rightarrow J/\psi\gamma)$.

B decay mode	X decay mode	product branching fraction ($\times 10^5$)		B_{fit}	R_{fit}
$K^+ X$	$X \rightarrow \gamma J/\psi$	0.202 ± 0.038	(<i>BABAR</i> [63]; Belle [62])	$0.019^{+0.005}_{-0.009}$	$0.24^{+0.05}_{-0.06}$
$K^+ X$		$0.28 \pm 0.08 \pm 0.01$	<i>BABAR</i> [63]		
		$0.178^{+0.048}_{-0.044} \pm 0.012$	Belle [62]		
$K^0 X$		$0.26 \pm 0.18 \pm 0.02$	<i>BABAR</i> [63]		
		$0.124^{+0.076}_{-0.061} \pm 0.011$	Belle [62]		
$K^+ X$	$X \rightarrow \gamma \psi(2S)$	0.44 ± 0.12	<i>BABAR</i> [63]	$0.04^{+0.015}_{-0.020}$	$0.51^{+0.13}_{-0.17}$
$K^+ X$		$0.95 \pm 0.27 \pm 0.06$	<i>BABAR</i> [63]		
		$0.083^{+0.198}_{-0.183} \pm 0.044$	Belle [62]		
		$R' = 2.46 \pm 0.64 \pm 0.29$	LHCb [64]		
$K^0 X$		$1.14 \pm 0.55 \pm 0.10$	<i>BABAR</i> [63]		
		$0.112^{+0.357}_{-0.290} \pm 0.057$	Belle [62]		
$K^+ X$	$X \rightarrow \gamma \chi_{c1}$	$< 9.6 \times 10^{-3}$	Belle [51]	$< 1.0 \times 10^{-3}$	< 0.014
$K^+ X$	$X \rightarrow \gamma \chi_{c2}$	< 0.016	Belle [51]	$< 1.7 \times 10^{-3}$	< 0.024
KX	$X \rightarrow \gamma \gamma$	$< 4.5 \times 10^{-3}$	Belle [141]	$< 4.7 \times 10^{-4}$	$< 6.6 \times 10^{-3}$
KX	$X \rightarrow \eta J/\psi$	< 1.05	<i>BABAR</i> [142]	< 0.11	< 1.55
$K^+ X$	$X \rightarrow p\bar{p}$	$< 9.6 \times 10^{-4}$	LHCb [140]	$< 1.6 \times 10^{-4}$	$< 2.2 \times 10^{-3}$

Table 3.7. (Continued).

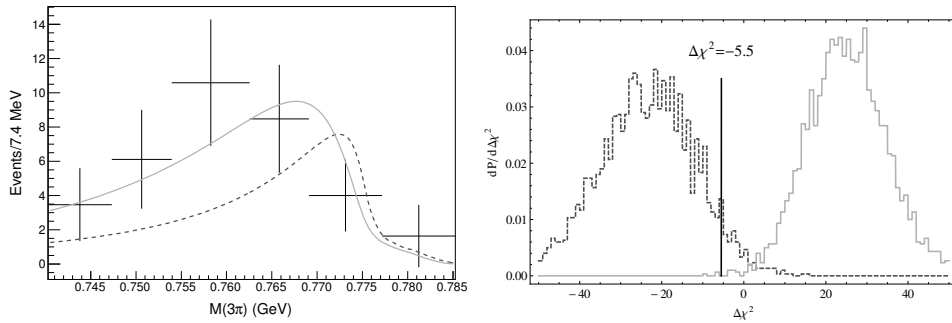


Figure 3.18. Left panel: fit to the $m_{3\pi}$ distribution in the $X(3872) \rightarrow J/\psi \omega$ [1]. The dashed curve refers to the 1^{++} hypothesis whereas the solid one is for the 2^{-+} . Right panel: distribution of the $\Delta\chi^2 = \chi^2(1^{++}) - \chi^2(2^{-+})$ resulting from the combined fits to Monte Carlo data samples [1]. The solid (dashed) histogram corresponds to events generated assuming the X to be a 2^{-+} (1^{++}) state. We mark with a line the position of the experimental $\Delta\chi^2$.

3.5.1 More on the $X(3872)$ spin [1]

In 2012, before that the high-statistics analysis by LHCb [59] was published, we reanalyzed the available Belle [143] and *BABAR* [61] on the spin of the $X(3872)$, starting from a general parametrization of the decay amplitudes for the axial and tensor quantum numbers of the X . The level of agreement of the two spin hypotheses with data is interpreted with a rigorous statistical approach based on Monte Carlo simulations in order to be able to combine all the distributions regardless of their different levels of sensitivity to the spin of the X . Our analysis returned a probability of 5.5% and 0.1% for the agreement with data of the axial and tensor hypotheses, respectively, once we combine the whole information (angular and mass distributions) from both channels (Figure 3.18). The separate analysis of the Belle $J/\psi \rho$ data (angular and mass distributions) indicates that the 2^{-+} assignment is excluded at the 99.9% C.L. Also the new LHCb analysis ruling out the 2^{-+} hypothesis is performed in the $J/\psi \rho$ channel. A separate analysis of the *BABAR* $J/\psi \omega$ mass distribution excludes instead the 1^{++} hypothesis at the 99.9%. This might be an indication that the two decay modes are due to different degenerate states. An independent analysis of the $J/\psi \omega$ mass and angular distribution, by LHCb or Belle, will enlighten on this.

3.6 Vector resonances

Many states with unambiguous $J^{PC} = 1^{--}$ have been discovered via direct production in e^+e^- collisions. The B -factories can investigate a large mass range, by searching events with an additional energetic photon γ_{ISR} emitted by the initial state, which lowers the center-of-mass energy down to the mass of the particle. The $\tau - c$ factories can instead scan the mass range by varying their center-of-mass energy. A graphic summary of all these states is in Figure 3.19.

In 2005 *BABAR* observed an unexpected vector charmonium state decaying into $J/\psi \pi^+ \pi^-$ named $Y(4260)$ [94], with a mass of $M = (4259 \pm 8_{-6}^{+2})$ MeV and a

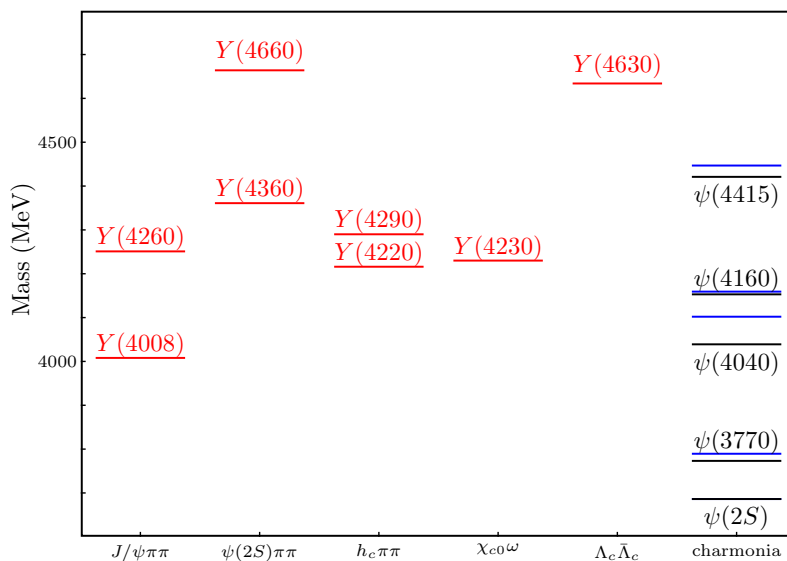


Figure 3.19. Exotic vector states divided by decay channel. In the right column, we report observed (black) and predicted (blue) charmonium levels. Red line are exotic states.

width of $\Gamma = (88 \pm 23_{-4}^{+6})$ MeV. Soon after it was confirmed by CLEO [96, 97], which reported evidence also for $Y(4260) \rightarrow J/\psi \pi^0 \pi^0$. *BABAR* performed a similar analysis in the $e^+e^- \rightarrow \psi(2S)\pi^+\pi^-$ channel [144], finding no evidence of $Y(4260)$; instead, a heavier state was observed at a mass $M = (4324 \pm 24)$ MeV and a width $\Gamma = (172 \pm 33)$ MeV, dubbed $Y(4360)$. The absence of $Y(4360) \rightarrow J/\psi \pi^+\pi^-$ is significant: $\mathcal{B}(Y(4360) \rightarrow J/\psi \pi^+\pi^-)/\mathcal{B}(Y(4360) \rightarrow \psi(2S)\pi^+\pi^-) < 3.4 \times 10^{-3}$ at the 90% C.L. [145], and is hard to understand in an ordinary charmonium framework. This pattern has been confirmed in an update of *BABAR*'s analysis [100].

Belle confirmed both these vector states [81, 99], and observed another resonance, called $Y(4660)$, in the $\psi(2S)\pi^+\pi^-$ channel, which *BABAR* was not able to see because of limited statistics, with mass $M = (4664 \pm 11 \pm 5)$ MeV and width $\Gamma = (48 \pm 15 \pm 3)$ MeV. It also found a broad structure in $J/\psi \pi^+\pi^-$ named $Y(4008)$, at mass $M = (4008 \pm 40_{-28}^{+114})$ MeV and width $\Gamma = (226 \pm 44 \pm 87)$ MeV. This last state has not been seen by *BABAR* [95], but it has been confirmed in the full statistics analysis by Belle [69], with $M = (3890.8 \pm 40.5 \pm 11.5)$ MeV and $\Gamma = (254.5 \pm 39.5 \pm 13.6)$ MeV. The PDG [113] averaged mass and width for the $Y(4260)$ are based on the most recent analyses by Belle [69], *BABAR* [95] and CLEO [97] and are $M = (4251 \pm 9)$ MeV and $\Gamma = (120 \pm 12)$ MeV. The full statistics analysis in $\psi(2S)\pi^+\pi^-$ by Belle [116] gives for the $Y(4360)$ a mass and width of $M = (4347 \pm 6 \pm 3)$ MeV and $\Gamma = (103 \pm 9 \pm 5)$ MeV, and for the $Y(4660)$ a mass and width of $M = (4652 \pm 10 \pm 8)$ MeV and $\Gamma = (68 \pm 11 \pm 1)$ MeV. In Figure 3.20 we report some distributions of $J/\psi \pi^+\pi^-$ and $\psi(2S)\pi^+\pi^-$ by Belle.

Motivated by the tetraquark predictions, Belle searched for vector resonances decaying into $\Lambda_c \bar{\Lambda}_c$ [106]. A structure (the $Y(4630)$) has actually been found near the baryon threshold, with Breit-Wigner parameters $M = (4634_{-7-8}^{+8+5})$ MeV and $\Gamma = (92_{-24-21}^{+40+10})$ MeV. A combined fit of the $\psi(2S)\pi^+\pi^-$ and $\Lambda_c \bar{\Lambda}_c$ spectra concluded that the two structures $Y(4630)$ and $Y(4660)$ can be the same state, with

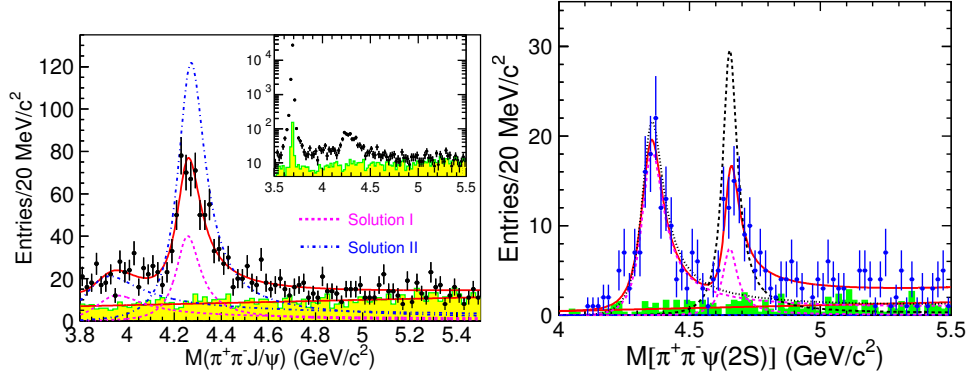


Figure 3.20. Belle analyses of $e^+e^- \rightarrow J/\psi \pi^+\pi^-$ (left) [69] and $\rightarrow \psi(2S)\pi^+\pi^-$ (right) [116].

a strong preference for the baryonic decay mode: $\mathcal{B}(Y(4660) \rightarrow \Lambda_c \bar{\Lambda}_c)/\mathcal{B}(Y(4660) \rightarrow \psi(2S)\pi^+\pi^-) = 25 \pm 7$ [145].

The vector states mentioned before are considered to be exotic. In fact, there are no unassigned 1^{--} charmonia below 4500 MeV, and the branching ratios into open charm mesons are too small for above-threshold charmonia: *BABAR* sees no evidence for a signal [146, 147], and set 90% C.L. upper limits:

$$\mathcal{B}(Y(4260) \rightarrow D\bar{D})/\mathcal{B}(Y(4260) \rightarrow J/\psi \pi^+\pi^-) < 1.0, \quad (3.27a)$$

$$\mathcal{B}(Y(4260) \rightarrow D^*\bar{D})/\mathcal{B}(Y(4260) \rightarrow J/\psi \pi^+\pi^-) < 34, \quad (3.27b)$$

$$\mathcal{B}(Y(4260) \rightarrow D^*\bar{D}^*)/\mathcal{B}(Y(4260) \rightarrow J/\psi \pi^+\pi^-) < 40, \quad (3.27c)$$

$$\mathcal{B}(Y(4260) \rightarrow D_s^+ D_s^-)/\mathcal{B}(Y(4260) \rightarrow J/\psi \pi^+\pi^-) < 0.7, \quad (3.27d)$$

$$\mathcal{B}(Y(4260) \rightarrow D_s^- D_s^{*-})/\mathcal{B}(Y(4260) \rightarrow J/\psi \pi^+\pi^-) < 44, \quad (3.27e)$$

$$\mathcal{B}(Y(4260) \rightarrow D_s^{*+} D_s^{*-})/\mathcal{B}(Y(4260) \rightarrow J/\psi \pi^+\pi^-) < 30, \quad (3.27f)$$

whereas the limits set by Belle [148] are:

$$\mathcal{B}(Y(4260) \rightarrow D^0 D^{*-} \pi^+)/\mathcal{B}(Y(4260) \rightarrow J/\psi \pi^+\pi^-) < 9, \quad (3.28a)$$

$$\mathcal{B}(Y(4360) \rightarrow D^0 D^{*-} \pi^+)/\mathcal{B}(Y(4360) \rightarrow \psi(2S)\pi^+\pi^-) < 8, \quad (3.28b)$$

$$\mathcal{B}(Y(4660) \rightarrow D^0 D^{*-} \pi^+)/\mathcal{B}(Y(4660) \rightarrow \psi(2S)\pi^+\pi^-) < 10, \quad (3.28c)$$

to be compared with $\mathcal{B}(\psi(3770) \rightarrow D\bar{D})/\mathcal{B}(\psi(3770) \rightarrow J/\psi \pi^+\pi^-) \gtrsim 480$ for an ordinary above-threshold vector charmonium. As for radiative decays, $Y(4260) \rightarrow \gamma X(3872)$ has been observed by BES III. Some clean events of $e^+e^- \rightarrow \gamma X(3872)$ have been measured. Moreover, the production cross section $\sigma(e^+e^- \rightarrow \gamma X(3872)) \times \mathcal{B}(X(3872) \rightarrow J/\psi \pi^+\pi^-)$ scales as a function of the center-of-mass energy consistently with a Breit-Wigner with $Y(4260)$ mass and width as parameters, consequently the observed events come from the intermediate resonant state and not from the continuum. The $Y(4260)$ has been searched without success in many other final states, which we report in Table 3.8.

Another important question to understand the nature of these vector states is whether or not the pion pair comes from any resonance. The updated *BABAR* analysis in $J/\psi \pi^+\pi^-$ [95] finds some evidence of a $J/\psi f_0(980)$ component. Since the decay

Final state	Upper limit (90% C.L.)	Experiment
$\Gamma_{ee} \times \mathcal{B}(Y(4260) \rightarrow f)$ (eV)		
$J/\psi K^+ K^-$	1.2	Belle [149]
$J/\psi \eta$	14.2	Belle [150]
$\phi \pi^+ \pi^-$	0.4	BABAR [151]
$K_S^0 K^+ \pi^-$	0.5	BABAR [152]
$K^+ K^- \pi^0$	0.6	BABAR [152]
$\mathcal{B}(Y(4260) \rightarrow f) / \mathcal{B}(Y(4260) \rightarrow J/\psi \pi^+ \pi^-)$		
$h_c \pi^+ \pi^-$	1.0	CLEO [153]
$p\bar{p}$	0.13	BABAR [154]
$\sigma(e^+ e^- \rightarrow f)$ (pb)		
$\chi_{c1} \omega$	18 ($\sqrt{s} = 4.31$ GeV)	BES III [93]
$\chi_{c2} \omega$	11 ($\sqrt{s} = 4.36$ GeV)	BES III [93]

Table 3.8. Upper limits for $Y(4260)$ into different final states. The decays into open charm mesons are discussed in the text.

$Y(4260) \rightarrow \psi(2S)f_0(980)$ is phase-space forbidden, this could partially explain why the $Y(4260)$ does not decay into $\psi(2S)\pi^+\pi^-$ (although the relevant non-resonant component could allow this decay). Some indications of an $f_0(980)$ component in the $Y(4660)$ appear in Belle's $\psi(2S)\pi^+\pi^-$ analysis [99], while no definite structure is recognizable for the other resonances.

BES III also measured the $e^+e^- \rightarrow h_c \pi^+ \pi^-$ cross sections at center-of-mass energies varying from 3.9 to 4.42 GeV [71] (see Figure 3.21). The values of the cross sections are similar to the $e^+e^- \rightarrow J/\psi \pi^+ \pi^-$, but the line shape is completely different and does not show any signal for the $Y(4260)$. The $h_c \pi^+ \pi^-$ has been fitted by Yuan [91, 92], which found a significant signal for a new $Y(4220)$ state. The fit improves if a second $Y(4290)$ resonance is added, however the lack of experimental data above 4.4 GeV makes hard to distinguish this second peak from a non-resonant background. The values of the mass and width according to the one peak hypothesis are $M = (4216 \pm 7)$ MeV and $\Gamma = (39 \pm 17)$ MeV. If there are two peaks, the best fitted values are $M_1 = (4216 \pm 18)$ MeV, $\Gamma_1 = (39 \pm 32)$ MeV and $M_2 = (4293 \pm 9)$ MeV, $\Gamma_2 = (222 \pm 67)$ MeV.

A somewhat similar signal has been seen by BES III in $e^+e^- \rightarrow \chi_{c0} \omega$ [93] at a mass of $M = (4230 \pm 8)$ MeV and a width of $\Gamma = (38 \pm 12)$ MeV, again not compatible with $Y(4260)$ parameters.

3.7 The 3940 family

Some resonances with $C = +$ have been observed around 3940 MeV. Even if they could be likely interpreted as ordinary charmonium states, some peculiarities in their decay patterns favor a more exotic assignment.

The $X(3940)$ was observed by Belle in double-charmonium production events

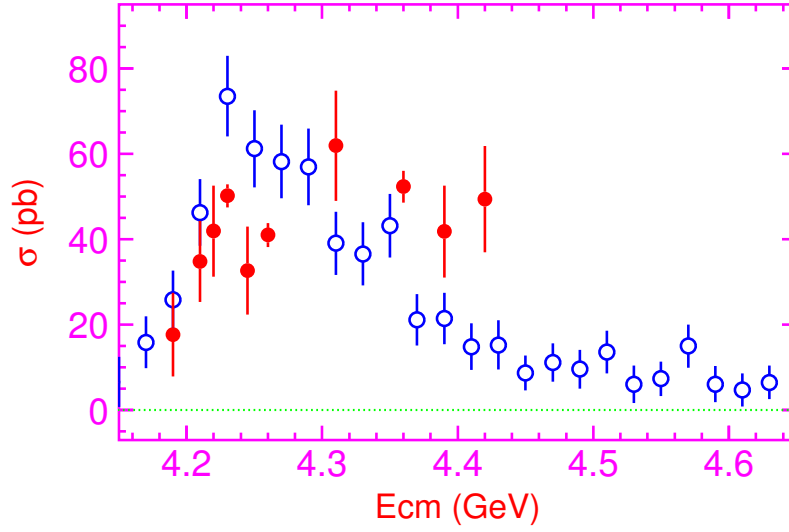


Figure 3.21. BES III data of $e^+e^- \rightarrow h_c \pi^+ \pi^-$ (red dots) [71] compared to Belle data of $e^+e^- \rightarrow J/\psi \pi^+ \pi^-$ (blue circles) [69]. From Yuan [91, 92].

as a peak in the $M_{J/\psi}$ recoiling mass [79, 80], with $M = (3942_{-6}^{+7} \pm 6)$ MeV and $\Gamma = (37_{-15}^{+26} \pm 8)$ MeV. A partial reconstruction technique in this production channel showed that $X(3940) \rightarrow D^* \bar{D}$ is a prominent decay mode (see Figure 3.22, right panel), whereas $X(3940) \rightarrow D \bar{D}$, $J/\psi \omega$ show no signal. The production mechanism $e^+e^- \rightarrow \gamma^* \rightarrow J/\psi X(3940)$ constrains the state to have $C = +$. All known states observed via this production mechanism have $J = 0$, so a tentative J^{PC} assignment for this state is 0^{-+} , where the parity is suggested by the absence of $D \bar{D}$ decays.

Belle observed another state at a similar mass in $B \rightarrow J/\psi \omega K$ decays as a resonance in the $J/\psi \omega$ invariant mass, with $M = (3943 \pm 11 \pm 13)$ MeV and $\Gamma = (87 \pm 22 \pm 26)$ MeV [73]. The fact that such a state is not seen in $B \rightarrow D^* \bar{D} K$ strongly suggests that it is not the $X(3940)$, whence it was dubbed $Y(3940)$. The decay into two vectors constrains a $C = +$ assignment, whereas $J = 0, 1, 2$ and $P = \pm$ are equally allowed. *BABAR* confirmed the state in $B \rightarrow J/\psi \omega K$ [61, 74], even if at a lower mass and with narrower width, $M = (3919.4_{-3.4}^{+3.8} \pm 2.0)$ MeV and $\Gamma = (31_{-8}^{+10} \pm 5)$ MeV, compatible at 2σ level with Belle measurement (see Figure 3.22, left panel). This discrepancy could be due to different assumptions about the shape of the background. Another state called $Y(3915)$ was observed in $\gamma\gamma$ fusion by both Belle [75] and *BABAR* [76], with mass and width compatible with the *BABAR* $Y(3940)$ result. The PDG, which assumes the resonances seen in $\gamma\gamma$ fusion and in B decays to be the same state (called $Y(3915)$), gives an averaged mass and width of $M = (3918.4 \pm 1.9)$ MeV and $\Gamma = (20 \pm 5)$ MeV [113]. The study of angular correlations by *BABAR* favors a $J^{PC} = 0^{++}$ assignment [76], which would make this state a candidate for $\chi_{c0}(2P)$. However, the $\chi_{c0}(2P)$ is expected to have $\Gamma(\chi_{c0}(2P) \rightarrow D \bar{D}) \sim 30$ MeV, *i.e.* wider than the total width measured of the $Y(3915)$. Even if no upper bound on $\mathcal{B}(Y(3915) \rightarrow D \bar{D})$ has been reported, no signs of a signal for such a decay appear in the measured $D \bar{D}$ invariant mass distributions for $B \rightarrow D \bar{D} K$ decays published by *BABAR* [66] and Belle [155]. Moreover, if the $Z(3930)$ (see below) is identified as the $\chi_{c2}(2P)$ state, the hyperfine splitting

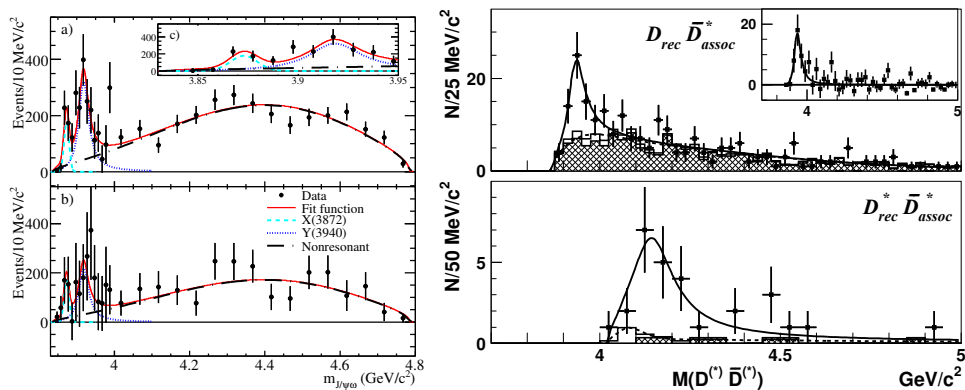


Figure 3.22. Left panel: observation of $Y(3915)$ (at the time called $Y(3940)$) in the invariant mass distribution of $J/\psi\omega$ in $B \rightarrow J/\psi\omega K$ decay, by BABAR [61]. Right Panel: observation of $X(3940)$ and $X(4160)$ in the invariant mass distribution of $D^*\bar{D}$ (upper) and $D^*\bar{D}^*$ (lower) in $e^+e^- \rightarrow J/\psi D^*\bar{D}^*$ events, by Belle [80].

$\chi_{c2}(2P) - \chi_{c0}(2P)$ would be only 6% with respect to the $\chi_{c2}(1P) - \chi_{c0}(1P)$ splitting. This is much smaller than the similar ratio in the bottomonium system ($r \sim 0.7$), and than the potential model predictions [156] ($0.6 < r < 0.9$). These facts challenge the ordinary charmonium interpretation [157, 158].

Another state, at the time called $Z(3930)$, was seen by Belle in $\gamma\gamma \rightarrow D\bar{D}$ [77], and confirmed by BABAR [78], at an averaged mass and width of $M = (3927.2 \pm 2.6)$ MeV and $\Gamma = (24 \pm 6)$ MeV. The angular analysis by BABAR favors a 2^{++} assignment. This state is compatible with the $\chi_{c2}(2P)$ assignment.

3.8 Other states

The analysis by Belle of double charmonium events which discovered the $X(3940)$ observed also a state called $X(4160)$ in the $D^*\bar{D}^*$ invariant mass [80] (see Figure 3.22, right panel). The fitted mass and width are $M = (4156^{+25}_{-20} \pm 15)$ MeV and $\Gamma = (139^{+111}_{-61} \pm 21)$ MeV. The production mechanism constrains $C = +$ and favors $J = 0$, thus making this state a good candidate for a $\eta_c(nS)$ state.

The CDF experiment announced a resonance close to threshold in $J/\psi\phi$ invariant mass, in the channel $B \rightarrow J/\psi\phi K$ [84, 85]. Since the creation of a $s\bar{s}$ pair is OZI suppressed, the very existence of such states likely requires exotic interpretations. This state is called $Y(4140)$, and has mass and width $M = (4143.0 \pm 2.9 \pm 1.2)$ MeV and $\Gamma = (11.7^{+8.3}_{-5.0} \pm 3.7)$ MeV. The natural quantum number would be $J^{PC} = 0^{++}$, but the exotic assignment $J^{PC} = 1^{-+}$ is not excluded. Belle searched this state in $\gamma\gamma$ fusion, driven by a molecular prediction [159], but found no $Y(4140)$ signal and put a 90% C.L. upper bound for $\Gamma_{\gamma\gamma} \times \mathcal{B}(\phi J/\psi) < 41$ (6) eV for $J^P = 0^+$ (2^+) [86]. Instead, a peak with a 3.2σ significance was seen at $M = (4350.6^{+4.6}_{-5.1} \pm 0.7)$ MeV and $\Gamma = (13^{+18}_{-9} \pm 4)$ MeV (see Figure 3.23), and dubbed $X(4350)$.

Several experiments have searched for the $Y(4140)$: $D\phi$ [89] and CMS [88] have recently confirmed the observation, and reported mass and width $M = (4159.0 \pm 4.3 \pm 6.6)$ MeV, $\Gamma = (19.9 \pm 12.6^{+3.0}_{-8.0})$ MeV, and $M = (4148.0 \pm 2.4 \pm 6.3)$ MeV, $\Gamma =$

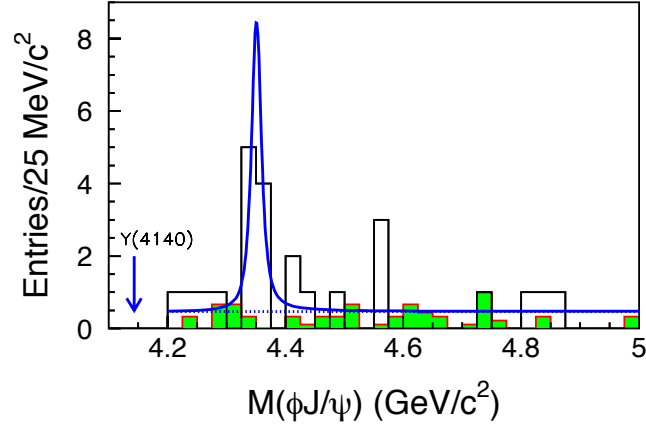


Figure 3.23. Invariant mass distributions of $J/\psi\phi$, from Belle [86]. No evidence for $Y(4140)$ is seen, whereas the peak of $X(4350)$ is fitted.

$(28_{-11}^{+15} \pm 19)$ MeV, with significances of $\sim 3\sigma$ and $> 5\sigma$, respectively. On the other hand, neither LHCb [87] nor BABAR [160] are able to see any significant signal, and put 90% C.L. upper limits on the relative branching fractions of

$$\frac{\mathcal{B}(B^+ \rightarrow Y(4140)K^+) \times \mathcal{B}(Y(4140) \rightarrow J/\psi\phi)}{\mathcal{B}(B^+ \rightarrow J/\psi\phi K^+)} < 0.07 \text{ (LHCb)}, \quad (3.29a)$$

$$< 0.135 \text{ (BABAR)}, \quad (3.29b)$$

to be compared with a ~ 0.1 measured by CMS. We mention also a preliminary null result of BES III in the $J/\psi\phi$ invariant mass in $e^+e^- \rightarrow \gamma Y(4140)$ process [161].

The averaged values of mass and width *à la* PDG [113] from the experiments that have claimed the observation are $M = (4145.6 \pm 3.6)$ MeV and $\Gamma = (14.3 \pm 5.9)$ MeV.

Last state we review is the $X(3823)$ seen by Belle in $B \rightarrow (\chi_{c1}\gamma)K$ radiative decays, with mass and width of $M = (3823.1 \pm 1.8 \pm 0.7)$ MeV and $\Gamma < 24$ MeV at 90% C.L., with a significance of 4σ [51]. Nothing prevents the identification of this state as the 2^{--} ordinary charmonium.

Chapter 4

Lattice QCD status of exotics

Lattice QCD has recently reached some preliminary results about exotics, albeit the non-trivial numerical and theoretical difficulties. In fact, from a field theoretical point of view, there is no way to distinguish between a meson and a tetraquark with the same quantum numbers, as we discussed for Large- N QCD (see Chapter 2). For instance, the charged resonance $Z_c(3900)^+$, with quark content $c\bar{c}u\bar{d}$, has the same quantum numbers as the $a_1^+(980)$ (the lightest $I = 1$ axial vector), so that any operator able to resolve the Z_c interpolates also the excitations of a_1 . In principle, the existence of the Z_c can be revealed by extracting all the excited a_1 levels up to the mass of the Z , but this is not numerically feasible. A numerically reliable approximation, widely used in heavy quarkonium spectroscopy, is to neglect charm annihilation diagrams [162], which are expected to be small because of OZI suppression. Under this approximation, it is possible to deal with these states using a field theory approach. In current lattice simulations one considers the vacuum expectation value of two-point functions for a set of interpolating operators with given quantum numbers. For each of them, the spectral representation gives

$$C_{ij}(t) = \langle O_i^\dagger(x, t) O_j(0) \rangle = \sum_n \sqrt{Z_i^{n*} Z_j^n} e^{-E_n t}. \quad (4.1)$$

From a single correlation function it is possible to extract only the lowest lying state using the effective mass method: when the time t is large, the function

$$m_{\text{eff}} = -\ln \frac{C_{ij}(t)}{C_{ij}(t-1)} \quad (4.2)$$

has a plateau at the energy of the ground state. The excited energy levels are extracted using the generalized eigenvalue problem [163]. If we have N_{op} different operators with the same quantum numbers, we can compute the correlation function matrix C_{ij} , ($i, j = 1, \dots, N_{op}$). The solution of the eigenvalue problem

$$C(t)\psi = \lambda(t, t_0)C(t_0)\psi, \quad (4.3)$$

gives N_{op} levels of the energy spectrum: in fact, the resulting eigenvalues λ_n decay exponentially with the n^{th} energy level, up to exponentially suppressed deviations:

$$\lambda_n(t, t_0) \sim e^{-E_n(t-t_0)}. \quad (4.4)$$

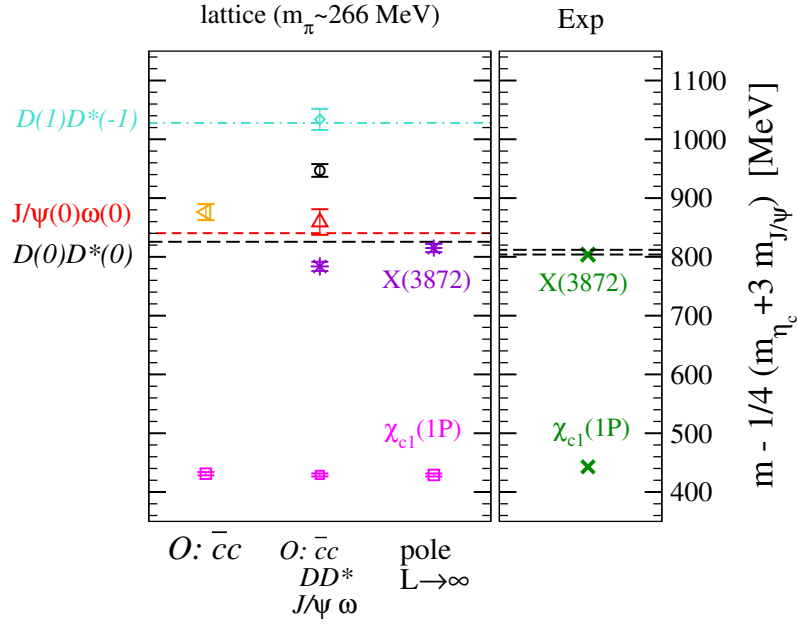


Figure 4.1. Energy levels computed in lattice simulations in the $J^{PC} = 1^{++}$, $I = 0$ channel (left panel), to compare with the experimental mass of the $\chi_{c1}(1P)$ and $X(3872)$ (right panel). On the x axis the operator basis used in simulations is sketched. From Prelovsek *et al.* [41]

The larger is the basis of operators, the larger is the number of computable excited levels. For numerical reasons, the operators have to be also as different as possible. If we were interested in below-threshold states, this is enough. If we instead are interested in above-threshold resonances, we have to look at all 2-particle levels with the same quantum numbers as the resonance. While at infinite volume these levels form a continuum¹, on the lattice these levels have a rather peculiar behavior as a function of the size of the volume. In particular, their energy is related to the infinite volume scattering phase [166, 167]. Roughly speaking in fact, by varying the size of the lattice, we vary the relative momentum of the 2-particle states ($\propto \frac{2\pi}{L}$), hence we simulate a “scattering” experiment at different momenta.

Currently, the only positive result in charmonium lattice spectroscopy is the confirmation of an energy level compatible with the $X(3872)$ in the $J^{PC} = 1^{++}$ channel with isospin $I = 0$ [41] – see Figure 4.1. It is argued that the energy level found on the lattice is a real shallow bound state because of the large positive shift in energy of the state $D(0)D^*(0)$ [168]. The signal of a level below the DD^* threshold seems to indicate the presence of the $X(3872)$ in QCD spectrum. It is worth noticing that this result is very sensitive to lattice artifacts, in particular the charm mass (and consequently the threshold) is affected by large discretization effects: for example this level could go away from threshold when approaching the physical point. Moreover, there is no way to distinguish such state from the ordinary $\chi_{c1}(2P)$: even if the level were confirmed, Lattice QCD cannot say whether it has

¹In fact, no information about resonances can be deduced from Euclidean correlators in the thermodynamic limit [165].

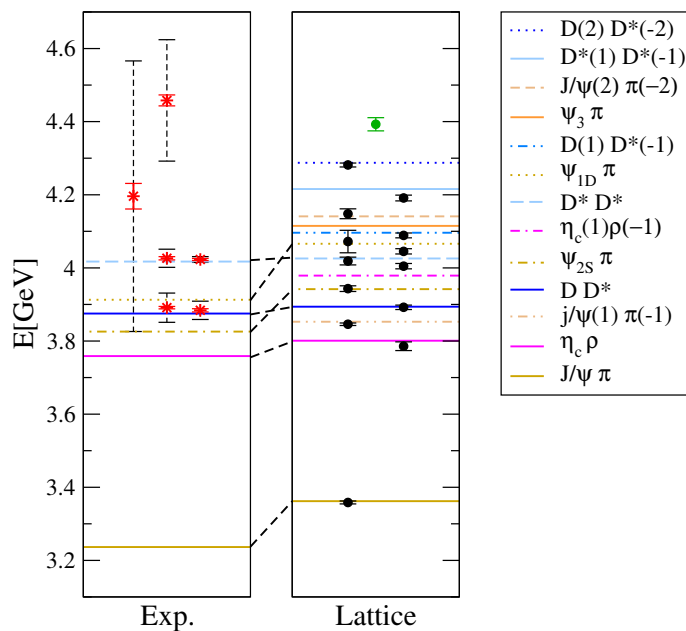


Figure 4.2. Experimental spectrum of the charged exotic resonances (left panel), and energy levels of charged states computed in lattice simulations, in the $J^{PC} = 1^{+-}$, $I = 1$ channel (right panel). From Prelovsek *et al.* [164]

the exotic features of the $X(3872)$.

For the $J^{PC} = 1^{+-}$ sector with $I = 1$ the situation is still unclear: the analysis of the energy levels does not reveal any additional state, expected in presence of a resonance [164, 169] (Figure 4.2). However, this level could be obscured by the presence of many different two-particle mesonic channels.

Furthermore, the above-mentioned approximation of neglecting charm annihilation contributions, unavoidable in practice, could make tetraquark states hard to be found. This statement is motivated by a Large- N analysis. Consider the 2-point correlation function $\langle Z_c^\dagger(x) Z_c(0) \rangle$. The leading and subleading contributions to this correlation function are shown in Figure 4.3. In Sec. 2.6, we showed that both the disconnected and the crossed diagrams (first and third in Figure 4.3) receive contributions from two meson states only. However, a tetraquark pole could appear in

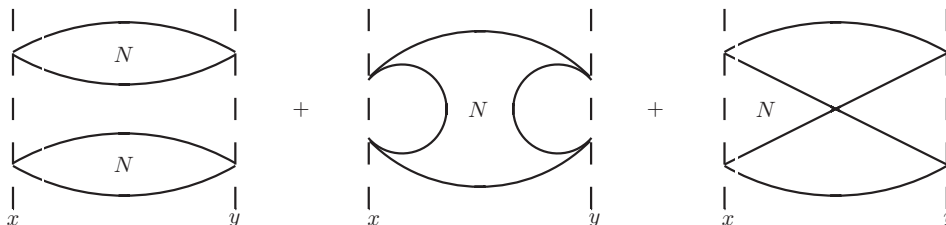


Figure 4.3. Diagrams contributing to the 2-point correlation function $\langle cc\bar{u}\bar{d}(x) \bar{c}\bar{u}d(y) \rangle$. In the large- N limit, only the second diagram could contain any tetraquark pole. However, this diagram cannot be included in lattice simulations, because the light meson content would obscure the information about heavier states. For details, see Sec. 2.6.

(subleading) diagrams which present any quark annihilations (second in Figure 4.3). Such kind of diagrams are neglected in $I = 1$ simulations (it is not numerically feasible to take into account charm annihilation), whereas in the $I = 0$ channel the light quarks are able to annihilate. This suggests that the possible tetraquark pole could be out of reach of current $I = 1$ simulations.

Chapter 5

Phenomenology

5.1 Molecule

Soon after the first observation of the $X(3872)$ in 2003, its closeness to the $D^0\bar{D}^{*0}$ threshold suggested to many authors that it might be the very first example of a loosely bound meson molecule. The possible existence of such states has been proposed many years ago by Tornqvist [170, 171] looking for hypothetical $K\bar{K}^*$, $\rho\rho$, $\rho\omega$, etc. bound states. It has been argued that the one-pion-exchange potential is likely to bind some states composed of ground state mesons, the idea being driven by the analogy with the time-honored case of deuterium where one knows that this potential is the dominant one. The same idea can also be extended to the heavy sector [172–175]. In particular, it has been found [174] that one-pion-exchange alone is strong enough to form at least *deuteron-like* $B\bar{B}^*$ and $B^*\bar{B}^*$ states with binding energy of about 50 MeV. Composites made of $D\bar{D}^*$ and $D^*\bar{D}^*$ and bound by pion exchange alone – *i.e.* neglecting the contribution from other kinds of potential – are expected near threshold, while molecular states composed of light mesons would require a stronger additional short range attraction and hence are likely not to be formed if only pions are taken into account.

Using an effective Lagrangian for pions one can find the following potentials in momentum space for the interaction between pseudo-scalar (P) and vector (V) mesons [174]:

$$U_{\pi}^{(VV)}(\mathbf{q}) = -U_{\pi}^{(V\bar{V})}(\mathbf{q}) = \frac{g^2}{f_{\pi}^2} (\boldsymbol{\tau}_1 \cdot \boldsymbol{\tau}_2) (\boldsymbol{\Sigma}_1 \cdot \mathbf{q}) (\boldsymbol{\Sigma}_2 \cdot \mathbf{q}) \frac{1}{\mathbf{q}^2 + m_{\pi}^2}; \quad (5.1a)$$

$$U_{\pi}^{(PV \rightarrow VP)}(\mathbf{q}) = \frac{g^2}{f_{\pi}^2} (\boldsymbol{\tau}_1 \cdot \boldsymbol{\tau}_2) (\boldsymbol{\epsilon}_1 \cdot \mathbf{q}) (\boldsymbol{\epsilon}_2^* \cdot \mathbf{q}) \frac{1}{\mathbf{q}^2 + m_{\pi}^2 - (m_V - m_P)^2}, \quad (5.1b)$$

where $f_{\pi} \simeq 132$ MeV is the pion decay constant and $g \simeq 0.5 \div 0.7$ is some axial effective strong coupling. $\boldsymbol{\Sigma}$ are the spin-1 matrices, $\boldsymbol{\tau}$ are the Pauli isospin matrices and $\boldsymbol{\epsilon}$ is the polarization vector for the vector meson. It should be stressed that the PP potential is forbidden by parity conservation. It is worth noticing that, in coordinate space, the potential is singular, and needs an ultraviolet cutoff $\Lambda = 0.8 \div 1.2$ GeV. The existence of loosely bound molecules can crucially depend on the choice of the cutoff [170, 176, 177]. The complete evaluation shows that the coupling happens to be proportional to $C[I(I+1) - 3]$, where C and I are the charge conjugation

and the isospin of the heavy pair. This means that we expect attraction in the isosinglet channel when $C = +$, and a three times weaker attraction in the isotriplet channel with $C = -$. The latter was for longtime considered too weak to actually produce a bound state, thus explaining the lack of charged molecular states. This was withdrawn as soon as charged exotic states were actually discovered.

In Table 5.1 we report the expected bound states according to this one-pion-exchange framework [178]. As one can see the $X(3872)$ would perfectly fit into this picture. This motivated a great amount of work done on the topic. In the following sections we will present some phenomenological models and their consequences, assuming these exotic states to be mesonic molecules.

Bound state	J^{PC}	Mass [MeV]	Bound state	J^{PC}	Mass [MeV]
$D\bar{D}^*$	0^{-+}	$\simeq 3870$	$B\bar{B}^*$	0^{-+}	$\simeq 10545$
$D\bar{D}^*$	1^{++}	$\simeq 3870$	$B\bar{B}^*$	1^{++}	$\simeq 10562$
$D^*\bar{D}^*$	0^{++}	$\simeq 4015$	$B^*\bar{B}^*$	0^{++}	$\simeq 10582$
$D^*\bar{D}^*$	0^{-+}	$\simeq 4015$	$B^*\bar{B}^*$	0^{-+}	$\simeq 10590$
$D^*\bar{D}^*$	1^{+-}	$\simeq 4015$	$B^*\bar{B}^*$	1^{+-}	$\simeq 10608$
$D^*\bar{D}^*$	2^{++}	$\simeq 4015$	$B^*\bar{B}^*$	2^{++}	$\simeq 10602$

Table 5.1. Bound states expected by the one-pion-exchange model [178]. The masses are predicted to be near threshold for the case of D mesons and about 50 MeV below threshold in the case of B mesons. We show the states with isospin $I = 0$ only.

A somehow complementary approach was established by Barnes and Swanson [179, 180]: meson-meson interactions can be obtained as the sum of effective potentials between the constituent quarks of the mesons. The hamiltonian is given by

$$H = \frac{1}{2} \sum_{i \neq j} (U_{1g} + U_{\text{conf}} + U_{\text{hyp}})_{ij} \quad (5.2a)$$

$$= \frac{1}{2} \sum_{i \neq j} \frac{\lambda_i \lambda_j}{2} \left(\frac{\alpha_s}{r_{ij}} - \frac{3b}{4} r_{ij} - \frac{8\pi\alpha_s}{3m_i m_j} \mathbf{S}_i \cdot \mathbf{S}_j \frac{\sigma^3}{\pi^{3/2}} e^{-\sigma^2 r_{ij}^2} \right) \quad (5.2b)$$

where U_{1g} is the one-gluon exchange potential at Born level, U_{conf} is the (non-perturbative) linear potential which takes into account confinement, and U_{hyp} parametrizes the hyperfine splitting of the charmonium levels. Even if constituent quark models are commonly used in quarkonium physics, it is unclear whether they can describe strong interactions on the scale of loosely bound molecules (~ 10 fm); it is more likely that quark can interact with each other on the typical scale of strong interactions, *i.e.* ~ 1 fm, but if so, the distinction between hadronic molecules and tetraquarks would become just a matter of language, the only difference between the two being the way in which color is saturated. It is worth noticing that this interaction is not strong enough to bind the $X(3872)$, and a contribution from one-pion-exchange has to be added [181].

Finally, in the heavy sector one can use heavy quark spin symmetry to obtain predictions for molecular spectrum and decay patterns, regardless of the details of

the binding potential [182–184].

5.1.1 Low-energy universality and line shapes of the $X(3872)$

As we mentioned before different potential models predict the presence of bound molecular states. Among these possible molecules the $X(3872)$, interpreted as an S -wave $D^0\bar{D}^{*0}$ state, would have a whole set of striking features due to the closeness to its constituents threshold. Its binding energy (simply given by the difference between its measured mass and the mass of its constituents) would be [185] $E_X = (-0.142 \pm 0.220)$ MeV. The natural energy scale for a pionic interaction is given by $m_\pi^2/m_D \simeq 10$ MeV and hence is much larger than E_X .

Bound states with such a feature share some common properties – the so-called *low-energy universality*¹ – coming from non-relativistic Quantum Mechanics and, in particular, many of their characteristic can be described via a single parameter: the scattering length, a . When the scattering length gets bigger and bigger (or analogously when the binding energy, E , gets smaller and smaller) we have that

$$E \longrightarrow \frac{1}{2\mu a^2}. \quad (5.3)$$

For the case of the $X(3872)$ we have $\mu = 966.6$ MeV and this leads to an unusually large scattering length, $a \simeq 12$ fm $\gg 1/m_\pi \simeq 1.5$ fm, the last one being the typical range of the interaction between the two D mesons². Such a striking feature necessarily requires some kind of fine tuning. Moreover, the wave function for the constituents assumes the universal form

$$\psi_{DD^*}(r) \longrightarrow \frac{1}{\sqrt{2\pi a}} \frac{e^{-r/a}}{r}. \quad (5.4)$$

Note that this also implies that a loosely bound molecule is an extremely extended object, having a typical radius $r_0 \simeq a$.

It has been pointed out [187] that the most generic quantum mechanical state for the $X(3872)$ can be written as

$$|X\rangle = \sqrt{Z_{DD^*}} \int \frac{d^3p}{(2\pi)^3} \tilde{\psi}(p) \frac{1}{\sqrt{2}} \left(|D^0(\mathbf{p})\bar{D}^{*0}(-\mathbf{p})\rangle + |\bar{D}^0(\mathbf{p})D^{*0}(-\mathbf{p})\rangle \right) \quad (5.5a)$$

$$+ \sum_H \sqrt{Z_H} |H\rangle, \quad (5.5b)$$

where $\tilde{\psi}(p)$ is the wave function of the D mesons in momentum space and $|X\rangle$ are other possible states (discrete or continuous) having the same quantum numbers $J^{PC} = 1^{++}$, e.g. $|D^+(\mathbf{p})D^{*-}(-\mathbf{p})\rangle$ or $|\chi_{c1}(2P)\rangle$. The constants Z_i are the probabilities for a certain configuration. Using an effective field theory approach, it can

¹ It should be mentioned that low-energy universality has been exploited for the first time by Voloshin [186] to compute the momentum distribution for the $X \rightarrow D^0\bar{D}^0\pi^0$ and $X \rightarrow D^0\bar{D}^0\gamma$ decays.

² It has been shown [2] that the scattering length obtained with this formalism can hardly be reconciled with the one obtained by the experimental data on the $X(3872)$ width, which appears to be smaller by (at least) a factor of $3 \div 4$.

be shown [187] that such suppression factors go as $Z_H \sim 1/\nu_H a$, where ν_H is the energy gap between the state H and the $D^0\bar{D}^{*0}$ threshold.

Two mechanisms to explain the large scattering length of the $X(3872)$ has been proposed [187]:

1. If all the other states H have an energy gap $\nu_H > m_\pi^2/m_D$ then, for a fairly large a , $Z_H \simeq 0$ and $Z_{DD^*} \simeq 1$, *i.e.* the $X(3872)$ would be purely a molecule. In this case the fine tuning necessary to explain the value of a would be something related to the interaction between the two components only, *e.g.* the depth or the width of the potential or the mass of the D mesons. In particular, one can consider m_u as a tuning parameter since it influences both the one-pion potential and the mass of the two mesons.
2. If one of the states H has mass very close to the $D^0\bar{D}^{*0}$ threshold, the ν_H factor would compensate the suppression due to the scattering length and lead to an almost equal mixture of this state and of the molecule, $Z_{DD^*} \simeq 1 - Z_H$. This mechanism is the analogous of the well-known Feshbach resonances which are used in atomic physics to control the scattering length [188]. It has been hypothesized that this state might be the (still undiscovered) charmonium $\chi_{c1}(2P)$. However, potential models predict the mass of this particle to be ~ 90 MeV above the threshold and hence we would need a fortuitous shift of this by at least ~ 80 MeV, in order to achieve $\nu_\chi < m_\pi^2/m_D$.

Since the second mechanism requires a large amount of luck (the discovery of the $\chi_{c1}(2P)$ with a mass value quite smaller than the expected one) we would only consider the first one, hence assuming that all the states appearing in Eq. (5.5) can be neglected except for the molecular one.

This model is also able to explain the narrowness of the $X(3872)$. In fact, one finds that the following partial widths are given by [187]

$$\Gamma(X \rightarrow D^0\bar{D}^0\pi^0) = Z_{DD^*}C_\pi\Gamma(D^{*0} \rightarrow D^0\pi^0); \quad (5.6a)$$

$$\Gamma(X \rightarrow D^0\bar{D}^0\gamma) = Z_{DD^*}C_\gamma\Gamma(D^{*0} \rightarrow D^0\gamma), \quad (5.6b)$$

where C_π and C_γ are coefficients taking into account the interference from the charge conjugate components. In particular, they both depend on the value of the binding energy of $X(3872)$ but they are of order one. While these final states receive a non-zero contribution from the decay of the D^{*0} component, other channels like $\psi(2S)\gamma$, $\eta_c(2S)\gamma$, $J/\psi\rho$ and $J/\psi\omega$ must occur either thanks to a short distance interaction between the two components, which is suppressed by the large separation of the two D mesons, or thanks to one of the charmonium states $|H\rangle$ appearing in Eq. (5.5), which are suppressed by $1/a$. Therefore, this could explain the small width of the $X(3872)$, which would then be of order $\Gamma_X \sim \Gamma_{D^*} \simeq 65$ keV.

In later works [131, 189–191] the previous analysis has been extended considering the possibility for the $X(3872)$ to be an above threshold resonant state – *i.e.* allowing for negative scattering lengths. It has been proposed [131, 190, 191] that the discrimination between these two cases can be done using the *line shapes* for different decay channel, meaning the shape of the invariant mass distributions of the final products.

It is known from non-relativistic Quantum Mechanics that the shape of a resonance near threshold is proportional to $|f(E)|^2$, $f(E)$ being the analytic continuation of the scattering amplitude as a function of the total energy of the particles in their center-of-mass system. The previously mentioned low-energy universality for S -wave states implies

$$f(E) = \frac{1}{-\gamma + \sqrt{-2\mu(E + i\epsilon)}}, \quad (5.7)$$

with $\gamma = 1/a$ and E the energy with respect to the threshold. If $\gamma > 0$ the resonance shape, $|f(E)|^2$, has a peak below the $D^0\bar{D}^{*0}$ threshold, corresponding to a real bound state, while if $\gamma < 0$ it has a pole right above it, corresponding to a virtual resonance. A more accurate analysis of the problem showed [190] that, in order to include the effects of the non-zero width of the D^{*0} and possible inelastic scatterings for the charmed mesons, the previous expression must be modified to

$$f(E) = \frac{1}{-(\gamma_{\text{re}} + i\gamma_{\text{im}}) + \sqrt{-2\mu(E + i\Gamma_{D^*}/2)}}, \quad (5.8)$$

where we introduced the width of the D^{*0} and an imaginary part for γ .

Using this approach one can study the invariant mass distribution for different decay channels and compare the experimental results with the theoretical ones under the hypothesis of a real bound state or a virtual resonance. This analysis has been performed [190, 191] for the $J/\psi\pi^+\pi^-$ and $D^0\bar{D}^0\pi^0$ final states as reported by the Belle collaboration [52] and the resulting fit has favored a peak of the line shapes below the threshold, thus pointing to a possible real bound state.

It should be mentioned that a similar approach was also used to study the line shapes of the exotic $Z(4430)$ under the hypothesis of a $D_1\bar{D}^*$ bound state [192]. However, the most recent measures of the mass of such particle, as well as the confirmation of the $J^{PC} = 1^{+-}$ signature [105], have casted some serious doubts on the validity of this analysis since the mass gap for the $Z(4430)$ is now shifted to a much higher value, $\nu_Z \simeq 47$ MeV, which prevents from using the low-energy universality and put in jeopardy its interpretation in terms of a molecular state.

5.1.2 Non-Relativistic Effective Field Theory

During the past years a fairly large amount of work [8, 193–198] has been done to develop and apply a Non-Relativistic Effective Field Theory (NREFT) for the study of exotic mesons in the molecular framework. The goal is to build a set of tools to describe the interaction between exotic, heavy and light mesons. The resulting theory combines the time-honored Heavy Meson Chiral Theory [199] adding terms describing the interaction of the exotic states with their constituents.

In the following we summarize the main aspects of such a formalism:

- The first key ingredient is that all the considered exotic mesons are intended as near-threshold molecular states and therefore the problem can be treated in a non-relativistic fashion. Since the velocities involved are small (see below) one can replace the HQET fields in the Lagrangian with their non-relativistic counterparts. Such limit is obtained by letting $v \rightarrow (1, \mathbf{0})$ in the usual HQET

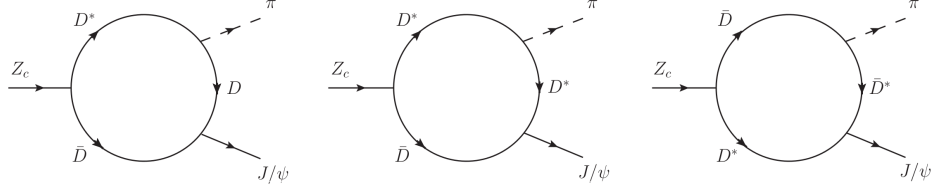


Figure 5.1. Example of heavy meson loops used the NREFT formalism. In the picture the decay $Z_c(3900) \rightarrow J/\psi \pi$ can only happen via an intermediate DD^* pair because of the molecular nature of the Z_c itself.

bi-spinors [200]. In particular, the non-relativistic Lagrangians involving the exotic mesons X , Y , Z and Z' are

$$\mathcal{L}_X = \frac{x}{\sqrt{2}} X^{i\dagger} (\bar{P}V^i + P\bar{V}^i) + h.c. \quad (5.9a)$$

$$\mathcal{L}_Y = \frac{y}{\sqrt{2}} Y^{i\dagger} (\bar{P}V^i - P\bar{V}^i) + h.c. \quad (5.9b)$$

$$\mathcal{L}_{Z_f} = \frac{z_f}{\sqrt{2}} Z^{i\dagger} (\bar{P}V^i - P\bar{V}^i) + h.c. \quad (5.9c)$$

$$\mathcal{L}_{Z'_f} = iz'_f \epsilon^{ijk} (Z')^{i\dagger} \bar{V}^j V^k + h.c. \quad (5.9d)$$

The fields X^i , Y^i and $Z_f^{(i)}$ annihilate the exotic mesons states while P (\bar{P}) and V^i (\bar{V}^i) annihilate a (anti-)pseudoscalar and a (anti-)vector state according to $P|P(k)\rangle = \sqrt{m_P}|0\rangle$ and $V^i|V(k, \epsilon)\rangle = \epsilon^i \sqrt{m_V}|0\rangle$. Also i , j and k are spatial indices and x , y and $z_f^{(i)}$ are some unknown effective couplings. Lastly, $f = c, b$ is a flavor index.

- The previous Lagrangians are dictated by symmetry considerations only – *i.e.* by the quantum numbers of the particles involved – and hence they describe the interaction of exotic mesons regardless of their internal structure. The essential information on the hypothetical molecular nature of these states comes from the requirement that the X , Y and Z states *only couple to their constituents*. This automatically implies that every hadronic transition must occur via heavy meson loops like the ones shown in Figure 5.1.

Since the problem is non-relativistic the propagators appearing in such loops must be the non-relativistic ones, namely:

$$\frac{i}{p^2 - m^2 + i\epsilon} \longrightarrow \frac{1}{2m} \frac{i}{p^0 - \frac{p^2}{2m} - m + i\epsilon} \quad (5.10)$$

- The typical velocities involved in the decay/creation of a certain particle with mass M are given, in this context, by $v \simeq \sqrt{|M - 2m|/m}$, where m is the mass of the open flavor mesons appearing in the loop. Since our states are close to the threshold such velocities turn out to be small, thus allowing a the use of a non-relativistic approach and of a power counting procedure to estimate the relevance of a certain Feynman diagram [195]. In particular, every meson loop

counts as $v^5/(4\pi)^2$ while the heavy meson propagators scale as $1/v^2$. Moreover, depending on the possible presence of derivatives in the interaction vertices, the diagram might also scale as a power of one of the external momenta, q , or as an additional power of v .

Since the interaction Lagrangians are non-perturbative some diagrams might be too challenging to be calculated and therefore, using this power counting technique, one can estimate the relevance of that particular process and hence determine an uncertainty related to its omission.

The open flavor heavy mesons can therefore interact with light pseudoscalar and vector mesons, with the usual Heavy Quark Chiral Lagrangians [199] (see also Appendix B). This formalism has been quite powerful in computing the decay width of many hadronic [8, 194, 195, 197] and radiative [195, 198] processes involving exotic mesons, assuming their internal structure to be a bound state of open flavor mesons. In particular, some attempts have been made to estimate the effective couplings appearing in Eqs. (5.9). The x and y constants have been extrapolated from the experimental value of the binding energies [198]:

$$|x| = \left(0.97_{-0.97}^{+0.40} \pm 0.14\right) \text{ GeV}^{-1/2}; \quad |y| = \left(3.28_{-0.28}^{+0.25} \pm 1.39\right) \text{ GeV}^{-1/2}, \quad (5.11)$$

while z_f and z'_f have been computed from experimental widths both in the charm and bottom sectors [8, 195]:

$$|z_c| = (1.28 \pm 0.13) \text{ GeV}^{-1/2}; \quad |z'_c| = (0.67 \pm 0.21) \text{ GeV}^{-1/2}; \quad (5.12a)$$

$$|z_b| = (0.79 \pm 0.05) \text{ GeV}^{-1/2}; \quad |z'_b| = (0.62 \pm 0.07) \text{ GeV}^{-1/2}. \quad (5.12b)$$

It is interesting to note that $|z_c/z'_c| = 1.91 \pm 0.60$ and $|z_b/z'_b| = 1.27 \pm 0.16$ which indicates a large degree of spin symmetry violation. This is expected for very-near-threshold states, since small mass variations can lead to large changes in binding energies and hence in the couplings.

Lastly, it should be mentioned that another, slightly different, NREFT has been developed in some papers [187, 193]. The main difference between such approach and the one explained above lies in how the molecular hypothesis is implemented. In particular, instead of requiring the presence of intermediate meson loops, the $X(3872)$ interpolating operator has been chosen to be explicitly $X^i \sim D\bar{D}^{*i} + \bar{D}D^{*i}$. We could refer to this model as a Non-Relativistic Effective Field Theory Type II (NREFT-II).

5.1.3 Candidates

The $X(3872)$ is the long-standing $\frac{1}{\sqrt{2}} \left(\bar{D}^0 D^{*0} + D^0 \bar{D}^{*0}\right)$ molecule [178, 187]. The $Z_c(3900)$ and $Z'_c(4020)$ are considered the $\frac{1}{\sqrt{2}} \left(\bar{D}D^* - D\bar{D}^*\right)$ and $D^* \bar{D}^*$ molecular candidates, respectively [197]. The binding energy of the $X(3872)$ is compatible with zero, whereas the other two states are above-threshold, which calls for new data or a more complicated description of the phenomenon. The signature of these three states is compatible with the one-pion exchange prediction, *i.e.* that the

isosinglet has $C = +$ and the isotriplet $C = -$. The $Y(4260)$ has been proposed to be a $\bar{D}D_1$ molecule [197], or a $\chi_{c1}\omega$ state [201]. The $Y(4630)$ might be a $\psi(2S)f_0(980)$ molecule [202]. The two Z_b states are compatible with a $\bar{B}^{(*)}B^*$ interpretation [182, 194].

5.2 Hadro-quarkonium

Another interpretation has been proposed [203, 204] for the $J^{PC} = 1^{--}$ resonances (namely $Y(4260)$, $Y(4360)$ and $Y(4660)$) and for the manifestly exotic $Z(4430)$. These states have always been observed in final states with a specific excitation of the charmonium spectrum, either J/ψ or $\psi(2S)$. In particular, for the $Y(4260)$ all the observed decays contain a J/ψ , while for the other exotic particles their decay products only contain a $\psi(2S)$. This feature motivated a model that describes these systems as composed of a heavy charmonium “core” surrounded by a “cloud” of light hadronic matter. Such a configuration is known as *hadro-charmonium* and it is an extension of a model for the binding of a J/ψ or $\psi(2S)$ around a nucleus [205]. Note that, the distinction between a molecular states and a compact tetraquark is determined by the clustering of the constituents. For the case of the hadro-quarkonium, instead, the distinction between the heavy and light degrees of freedom is due to their size (instead of their superposition region), the light excitation being more extended than the quarkonium core.

The interaction between the central heavy quarks and the surrounding excitation is a QCD analogous of the van der Waals force and is supposed to be strong enough to allow a bound state but also weak enough to mostly maintain the nature of the charmonium, thus explaining the absence of other excitations in the final states. Since the $c\bar{c}$ state is color neutral, such an interaction can be treated using a multipole expansion, in close analogy with the well-known electromagnetic case. The heavy quark pair, that from now on we will call generically as ψ , has a chromo-electric dipole moment proportional to the chromo-electric gluon field generated by the surrounding light excitation and this dipole will interact with the field itself, thus producing an effective Hamiltonian

$$H_{\text{eff}} = -\frac{1}{2}\alpha^{(\psi)}E_i^a E_i^a, \quad (5.13)$$

where E_i^a is the chromo-electric field generated by the surrounding light matter and $\alpha^{(\psi)}$ is the chromo-electric polarizability. Here and in the following we indicate with $\alpha^{(\psi)}$ a generic element of the polarizability; in general we will have different components, $\alpha^{(\psi_1\psi_2)}$, both diagonal and off-diagonal. Such a polarizability is still unknown from first principles. We can only estimate its off-diagonal values for the charmonium and bottomonium case from the $\psi(2S) \rightarrow J/\psi\pi\pi$ and $\Upsilon(2S) \rightarrow \Upsilon\pi\pi$ transitions [206], where one finds $\alpha^{(J/\psi\psi')} \simeq 2 \text{ GeV}^{-3}$ and $\alpha^{(\Upsilon\Upsilon')} \simeq 0.6 \text{ GeV}^{-3}$. The diagonal terms are usually expected to be larger than the off-diagonal ones.

Using the well-known expression for the conformal QCD anomaly in terms of the chromo-electric and chromo-magnetic fields, E_i^a and B_i^a

$$\theta_\mu^\mu = -\frac{9}{32\pi^2}F_{\mu\nu}^a F^{a\mu\nu} = \frac{9}{16\pi^2}(E_i^a E_i^a - B_i^a B_i^a), \quad (5.14)$$

one can compute a lower bound [203] for the expectation value of the previous Hamiltonian (5.13) over a generic hadron X :

$$\langle X | \frac{1}{2} E_i^a E_i^a | X \rangle \geq \frac{8\pi^2}{9} M_X. \quad (5.15)$$

In particular, we used the fact that $\langle X | \theta_\mu^\mu(\mathbf{q} = 0) | X \rangle = M_X$ and that the expectation value of $B_i^a B_i^a$ must be non-negative. This can also be used to determine a condition for the presence of a bound state due to the van der Waals interaction. One finds that it must be

$$\alpha^{(\psi)} \frac{M_X \bar{M}}{R} \geq C, \quad (5.16)$$

with M_X the mass of the light hadronic excitation, $\bar{M} = M_X M_\psi / (M_X + M_\psi)$ the reduced mass of the charmonium-light hadron system and C a (model dependent) constant of order 1. From Eq. (5.16) one immediately notices that bound states are favored for higher values of M_X , *i.e.* for higher light hadronic excitations, but also for higher values of $\alpha^{(\psi)}$, which is in general considered to be larger for higher quarkonium levels. This last point would explain why three out of four of the previously mentioned exotic resonances decay into $\psi(2S)$.

Using a square well ansatz for the interaction potential and a reference value $\alpha^{(\psi)} = 2 \text{ GeV}^{-3}$ one finds [203] that bound states might appear for $M_X \gtrsim 2 \text{ GeV}$ or for lower M_X but higher excitations of the central core. For the case of the bottomonium, since $\alpha^{(\Upsilon)}$ is much smaller, one needs much higher hadronic resonances in order to allow a bound state, making an experimental analysis quite challenging. However, it is still expected for lower values of M_X but higher excitations of the $b\bar{b}$ pair (in particular with a $\Upsilon(3S)$ core).

It is worth noting that, so far we assumed that the nature of the heavy quarkonium does not change because of the gluonic field. However, it turns out that the interaction in Eq. (5.13) might cause a transition $\psi(2S) \rightarrow J/\psi$ via the off-diagonal polarizability $\alpha^{(J/\psi\psi')}$ with a width of a few MeV. Therefore, the present model also predicts the $Y(4360)$, $Y(4660)$ and the $Z(4430)$ to decay into J/ψ but with a much lower (even though still detectable) branching ratios.

Lastly, using a holographic QCD approach [204] one can show that the decays of hadroquarkonium states into open flavor mesons are suppressed by a factor $e^{-\sqrt{M_Q/\Lambda_{QCD}}}$ in the large M_Q limit. This could explain why such final states are not observed experimentally. Recently, such a model has been applied to the $Y(4260)$ and $Y(4360)$ system by Voloshin and Li [207].

5.2.1 Candidates

This model was introduced to explain why the Y states do not decay into open charm pairs. The $Y(4260)$ and the $Y(4360)$ are identified as two mixed hadrocharmonia states [207]. The same was proposed for the $Z_c(3900)$ [208] before that the $(DD^*)^+$ decay mode was observed.

5.3 Hybrids and Born-Oppenheimer tetraquarks

Quark model describes mesons as a quark and an antiquark which saturates color with each other. However, the QCD Lagrangian contains also the gluons, as dynamical degrees of freedom mediating strong interactions. From the point of view of the quark model, one might treat gluons as static degrees of freedom as well, belonging to the adjoint representation of the color group: since the tensor product of any number of adjoint fields always contains a singlet ($\mathbf{8}_c \otimes \mathbf{8}_c \otimes \dots = \mathbf{1}_c \oplus \dots$), we can form hadrons made up of just gluons, the so-called *glueballs*. Moreover, we can add $q\bar{q}$ pairs in the color octet which saturates the gluon color, generating what it is usually called a *hybrid meson*. The addition of a gluon allows such mesons to have quantum numbers forbidden by ordinary quark model, *e.g.* 0^{+-} , 1^{-+} and so on. In the following we present a set of models developed during the years to describe these peculiar states.

The existence of hybrid mesons in the light sector was suggested in 1976 by Jaffe and Johnson [209] in the context of the MIT bag model. Some calculation [210, 211] predict the lightest hybrid multiplet to have a mass ~ 1.5 GeV (it is worth noticing the observation of an exotic $\pi_1(1400)$ with the exotic $J^{PC} = 1^{-+}$ exactly at $M = 1354$ MeV). The exotic J^{PC} quantum numbers are due to the boundary conditions in the bag.

For the heavy quarks a spherical bag would be quite unrealistic, and thus an adiabatic bag model was introduced by Hasenfratz *et al.* [212]. In this model the bag was allowed to deform in the presence of a fixed $Q\bar{Q}$ source. The resulting potential is used in a Schrödinger equation to compute the mass of the states, as in usual quarkonium spectroscopy. The lightest hybrid was found at ~ 3.9 GeV for $c\bar{c}$ and at ~ 10.5 GeV for $b\bar{b}$. Some recent results on adiabatic potentials in QCD string models can be found in the literature [213].

In the framework of constituent quark models, we can analogously consider constituent gluons. These models were pioneered by Horn and Mandula [214] and later developed [215–219]. The gluon has a fixed orbital angular momentum relatively to the $q\bar{q}$ pair, usually called l_g , and the $q\bar{q}$ is in a defined orbital configuration $l_{q\bar{q}}$ and spin configuration $s_{q\bar{q}}$. The quantum numbers of such bound states are $P = (-1)^{l_g + l_{q\bar{q}}}$ and $C = (-1)^{l_{q\bar{q}} + s_{q\bar{q}} + 1}$. The lightest hybrid state within this model has $l_g = 0$ and thus non-exotic quantum numbers such as 1^{--} are obtained using P -wave $q\bar{q}$ states with $s_{q\bar{q}} = 1$, while exotic 1^{-+} states have $s_{q\bar{q}} = 0$.

The most effective pictorial representation of hybrid mesons can be achieved via the flux-tube model. Lattice QCD simulations show that two static quarks at large distances are confined by approximately cylindrical regions of color fields. More specifically, if a gauge is fixed, the magnitude of chromoelectric field has cylindrical symmetry. The flux tube models this feature by approximating the confining region between quarks with an oscillating string. If one assumes Nambu-Goto action, *i.e.* the action to be proportional to the area spanned by the string in coordinate space, one gets an exact potential for large values of the separation, r , between the sources:

$$V_\Lambda(r) = \sqrt{\sigma^2 r^2 - \frac{\pi\sigma(12n-1)}{6}}, \quad (5.17)$$

where σ is the usual string tension, and n parametrizes the quantized excitation

of the string. For $n = 0$ we get a linear rising potential, which corresponds to ordinary quarkonium spectrum. Higher excitations of the string would correspond to excitations of the color field, and so can be associated to hybrids.

The previous potential is obtained as a function of the distance r between the sources. In the first studies with this model an adiabatic separation of the quark and gluon degrees of freedom was carried on. Such approximation is allowed because of the large difference between the time scales of the fast dynamical response of the flux tube degrees of freedom and of the slow motion of the heavy quarks. This allows to fix the $Q\bar{Q}$ separation at some value r (now considered as a parameter) and compute the eigenenergy of the system in some fixed configuration of the flux tube: $E_\Lambda(r)$, Λ being the quantum numbers of the flux tube. This eigenenergy is then treated as an effective potential $E_\Lambda(r) = V_\Lambda(r)$ acting on the heavy quark pair. The ground state $\Lambda = 0$ gives the ordinary meson spectrum. Hybrids are obtained for $\Lambda > 0$ and can be studied using the excited potential $V_\Lambda(r)$. This is nothing but the QCD analogous of the time-honored Born-Oppenheimer (BO) approximation for hydrogen molecules. This approximation has been successfully used since the first estimates of the charmonium spectrum on the lattice in the infinite mass limit (static potentials). The lightest hybrid state is the one in which the string has a single orbital excitation about the $Q\bar{Q}$ axis. In initial models the adiabatic potentials were determined in the approximation of small fluctuations relatively to the $Q\bar{Q}$ axis. This approximation was later removed by Barnes, Close and Swanson [220].

Some insight on the spectrum of hybrids might be obtained from Lattice QCD simulations, which are supposed to give the most reliable predictions for absolute masses. In the heavy quark sector, when the $Q\bar{Q}$ pair is kept fixed while the gluonic degrees of freedom are allowed to be excited, the lightest charmonium hybrid was predicted [221] to have a mass of 4.2 GeV for $c\bar{c}$ and 10.81 GeV for $b\bar{b}$. In general, in the charmonium family hybrids are predicted in the mass region around 4.3 GeV, while the bottom sector they are predicted in the region 10.7-11.0 GeV.

Unfortunately many problems have to be faced when dealing with hybrids on the lattice since, from a field theory point of view, hybrids with ordinary quantum numbers suffer the same problem than tetraquarks: they are indistinguishable from mesons. One possible solution to this difficulty is to look at the overlap (the prefactors $\sqrt{Z_i^* Z_j}$ in Eq. (4.1)) of those hybrid states with suitable operators. This has been recently done [162] in lattice simulations (see Figure 5.2) where a hybrid candidate with $J^{PC} = 1^{--}$ is found close to the mass of the $Y(4260)$ resonance. Although this evidence, it is not possible to conclude that the observed state is a hybrid meson instead of, for instance, a tetraquark. The observation of four hybrid candidates nearly degenerate with $J^{PC} = (0, 1, 2)^{-+}$ and $J^{PC} = 1^{--}$ (see the red boxes in Figure 5.2) is in agreement with the pattern predicted for the lightest states in the bag model [211] and in the P -wave quasi-particle approach [222]. They appear at a mass scale 1.2 – 1.3 GeV above the lightest conventional charmonia.

The picture of hybrids borrowed from Lattice QCD has been employed to try to explain some of the observed XYZ resonances [223, 224]. In particular, it has been proposed that the $Y(4260)$ might indeed be an example of a hybrid composed of a $c\bar{c}$ pair with $J^{PC} = 0^{-+}$ and a gluonic excitation with $J^{PC} = 1^{+-}$. This interpretation

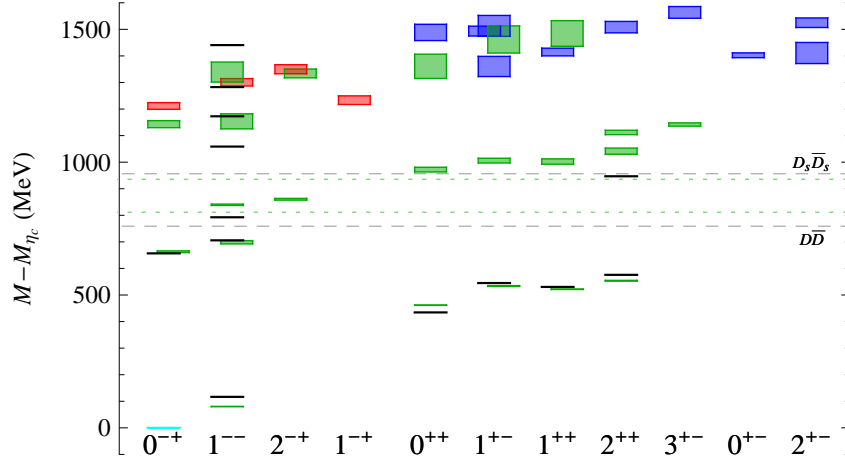


Figure 5.2. Charmonium spectrum for masses around 4.5 GeV. Red and blue boxes are identified as gluonic hybrids (ground and first excited states respectively). Green boxes are other charmonium states and black lines are experimentally observed levels. The $D\bar{D}$ and $D_s\bar{D}_s$ thresholds are also shown. From Liu *et al.* [162]

would explain some of the striking properties of this resonance. In particular, the smallness of the $c\bar{c}$ wave function at the origin, $r = 0$, would explain why the $Y(4260)$ is observed with a small production rate in e^+e^- annihilation and why its decays into light hadrons are suppressed. Moreover, it is also known [225] that the decays of gluonic hybrids into a pair of S -wave mesons are suppressed and hence the dominant decay (if allowed) should be into an S -wave and a P -wave charmed mesons. However, for the $Y(4260)$ the decay into $D_1\bar{D}$ is phase space forbidden and the decay into $D^*\bar{D}$ is suppressed by a D -wave coupling. The only drawback of this interpretation was that the decays into charmonium plus light hadrons were also expected to be suppressed and this is in striking contrast with the observed large branching fraction for the $J/\psi\pi\pi$ channel.

This problem found a solution with the discovery of the $Z_c(3900)$. It has, in fact, been hypothesized that this particle might be a different example of hybrid, a so-called *tetraquark hybrid*. The main idea is that the excited gluon can be replaced with a $q\bar{q}$ pair of light quarks belonging to the adjoint, $\mathbf{8}_c$, representation of the color group. In this context, the Z_c would be made out of a $c\bar{c}$ pair with $J^{PC} = 0^{-+}$ and a $q\bar{q}$ pair with $J^{PC} = 1^{+-}$, this last assignment being motivated by the analogy with the gluonic hybrid, where the lowest energy excitation has these quantum numbers. If this idea were true, the $Y(4260) \rightarrow Z_c(3900)\pi$ decay would be explained as a transition of the gluon within the hybrid into a $q\bar{q}$ by pion emission, thus explaining the observed branching fraction.

A similar interpretation has also been given for the Z_b and Z'_b states, even though in this case their closeness to the $\bar{B}^*B^{(*)}$ would also provide them with a strong molecular component.

As previously anticipated, the spectrum for gluonic and tetraquark hybrids can be computed under the BO approximation. To do that, one considers the $Q\bar{Q}$ pair to simply be a fixed source of color field, with a separation r and solve for the eigenenergy of the gluonic (tetraquark) excitation. Once this is done this energy is

taken as the effective potential suffered by the $Q\bar{Q}$ pair. Such a potential is given by Eq. (5.17) for large value of r and by a Coulomb-like expression for small r :

$$V_\Lambda(r) = \frac{\alpha_s(1/r)}{6r} + E_\Lambda, \quad (5.18)$$

where $\alpha_s(1/r)$ is the strong coupling constant evaluated at a scale $\mu = 1/r$ and E_Λ is the so-called *gluehump*, *i.e.* an additive term that depends on the quantum numbers (Λ) of the considered gluonic field (see for example Marsh and Lewis [226]). The parameters related to the previous potential can be fitted from lattice QCD results by Morningstar *et al.* [227]. Once this is done one can solve the Schrödinger equation for the $Q\bar{Q}$ pair with this potential:

$$\left[-\frac{1}{m_Q} \left(\frac{d}{dr} \right)^2 + \frac{\langle \mathbf{L}_{Q\bar{Q}}^2 \rangle_{\Lambda,r}}{m_Q r^2} + V_\Lambda(r) \right] rR(r) = ErR(r), \quad (5.19)$$

where $\langle \mathbf{L}_{Q\bar{Q}}^2 \rangle_{\Lambda,r}$ is the orbital angular momentum of the $Q\bar{Q}$ pair computed for certain quantum numbers Λ and for a separation r . $R(r)$ is the usual radial wave function. We will not go into the details of this calculation since it is rather involved and does not add anything interesting to our discussion. In Figure 5.3 we report the spectrum for the excited gluonic hybrid obtained from this calculation in the charm and bottom sectors. For the charmonium case the lowest energy level is estimated to be 4246 MeV, while for the bottomonium case it is 10559 MeV.

In the tetraquark hybrid case we have no insight on the actual shape of the potential $V_\Lambda(r)$ generated by the two quark-antiquark in the adjoint representation. It has been proposed [223, 224] to assume a similar behavior as in the gluonic case. From this assumption and from a certain number of input values one can try again to derive a spectrum for this second kind of hybrids, and some generic selection rules. However, it is worth noticing that the hybrid potential computed on the lattice relies on quenched simulations (*i.e.* without dynamical fermions), or on simulations with unphysical light quarks masses (typically $m_\pi \sim 500$ MeV). The excited level corresponding to the hybrid state becomes more and more noisy, and the potential becomes more and more difficult to extract when approaching the physical point. In particular, at the physical pion mass the potential could be rather different from the present computations.

While the masses of hybrid mesons are computable in all the models listed above, and in particular in Lattice QCD, the decay dynamics is more difficult to study.

The only model which offers a description of the decay dynamics is again the flux-tube model. In fact, in this picture, the decay occurs when the flux-tube breaks at any point along its length, producing in the process a $q\bar{q}$ pair in a relative $J^{PC} = 0^{++}$ state. Again this is just the well-know Lund model for ordinary mesons. The distance from the $Q\bar{Q}$ axis at which the light pair is created is controlled by the transverse distribution of the flux-tube. This distribution varies when going from the non-excited flux-tube to the first excited flux-tube configuration. Exploiting the empirical success of this model in describing the ordinary mesons decay dynamics, Close and Page [228] derived the decay pattern for hybrids. They found that in

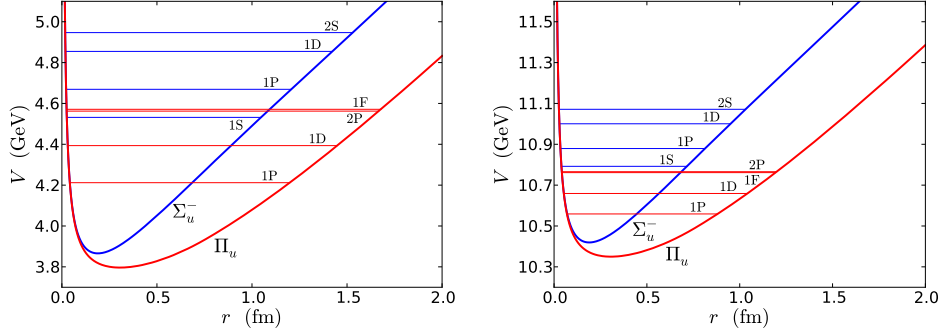


Figure 5.3. Lowest energy levels for the gluonic hybrids in the charm (left panel) and bottom (right panel) sector. The notation for the quantum numbers of the gluonic degrees of freedom is borrowed from atomic physics. Π_u has eigenvalue $+1$ for the operator $|\mathbf{r} \cdot \mathbf{J}_g|$, where \mathbf{J}_g is the total angular momentum of the gluon excitation, and $(CP)_g = -1$ for the gluon with respect to the center of the $Q\bar{Q}$ system. Σ_u^- , instead, has eigenvalue zero for $|\mathbf{r} \cdot \mathbf{J}_g|$, $(CP)_g = -1$ and is also odd under reflection of the gluon field with respect to the plane containing the $Q\bar{Q}$ pair. The usual nL notation for radial and angular quantum numbers has been used. From Braaten *et al.* [224]

a two-meson decay the unit of orbital angular momentum of the incoming hybrid around the $Q\bar{Q}$ axis is exactly absorbed by the component of the angular momentum of one of the two outgoing mesons along this axis. They treated explicitly the light flavor case [228], but a generalization to hybrid charmonia is straightforward. The final state should be in this case $D^{(*,**)}\bar{D}^{*,**}$, where D^{**} indicates D -meson which are formed from P -wave $c\bar{q}$ ($q = u, d$) pairs. However, since the masses predicted in the flux-tube model are about ~ 4.3 GeV, *i.e.* below the DD^{**} threshold, it is possible that this decay is kinematically forbidden giving a rather narrow resonance decaying in charmonium and light hadrons. These modes offer a clear experimental signature and furthermore should have large branching fractions if the total width is sufficiently small.

5.3.1 Candidates

The Born-Oppenheimer tetraquarks are still in an embryonic state, because of the lack of reliable calculation of the potential in the presence of light quarks. As we said, one of the most accepted interpretation for the $Y(4260)$ is a $c\bar{c}g$ hybrid [162, 222]

5.4 Alternative explanations

It should be mentioned that there are other interpretations about the nature of the XYZ states. In particular, it is worth spending a few words about cusp effect. Some of these exotic states, in fact, lie slightly above their open flavor threshold. This suggested to some authors [111, 180, 229, 230] that the experimental signals seen by the various collaborations might not be due to actual particles but to a dynamical effect. Cusps, in fact, can occur in amplitudes at threshold and these can manifest themselves as bumps in the cross sections right above the threshold. The

proximity of many of these states to their open flavor threshold suggested to these authors that the cusp option might be taken seriously. Such possibility has been studied for the $X(3872)$ [111, 229], for the $Z(4430)$ [111, 231] and most recently for the $Z_c^{(\prime)}$ and $Z_b^{(\prime)}$ [230]. This interpretation has been recently challenged by Hanhart *et al.* [232]. A more detailed analysis has been done in [233], where it is shown that a particularly strong final-state rescattering in the $\pi\pi$ system might produce peaks in the $J/\psi\pi$ and $\Upsilon\pi$ invariant mass.

Finally, some authors try to describe the exotic neutral candidates like $X(3872)$ as ordinary charmonia whose properties are deformed by the thresholds, see for example the Unquenched Quark Model by Ferretti *et al.* [234].

Chapter 6

The prompt production of $X(3872)$

In this section we discuss the controversy about the molecular interpretation of the $X(3872)$. The main drawback of this picture, in fact, lies in the unexpectedly high production cross section measured at Tevatron and LHC that, for many years, has been seen as the definitive proof of the inconsistency of the molecular interpretation.

The description of the $X(3872)$ in terms of a very loosely bound meson molecule is often compared to the well-known case of the deuteron, both being bound by strong interactions and having very small binding energies [113, 185], $E_X = (-0.142 \pm 0.220)$ MeV and $E_d = (-2.2245 \pm 0.0002)$ MeV.

The deuteron can be described by means of the phenomenological *coalescence model* [235, 236], according to which a neutron and a proton will bind together if they are produced with a relative momentum smaller than a *coalescence momentum*, $k_0 \simeq 80$ MeV. Because of the close analogy between the deuteron and the $X(3872)$ we might wonder if a similar approach could be valid for the latter as well. In particular, in both cases, one might expect to have a very small yield of such loosely bound molecules in high energy hadron collisions, since their component will naturally tend to be produced with a very high relative momentum, thus preventing the system from binding.

It is exactly this qualitative expectation that casted many doubts on the interpretation of the $X(3872)$ in terms of loosely bound meson molecule. Such particle was, in fact, observed both by CDF [55, 138] and CMS [122] with a very large prompt – *i.e.* directly produced at the collision vertex – production cross section, $\sigma \simeq 30$ nb. This experimental fact seems at odds with the previous conclusion about the deuteron and, more in general, about hadronic molecules with very small binding energy.

In particular, it is possible to estimate an upper bound for the production cross section of the X as follows [139]:

$$\sigma(p\bar{p} \rightarrow X(3872)) \leq \sigma^{\max}(p\bar{p} \rightarrow X(3872)) \sim \int_{\mathcal{R}} |\langle D\bar{D}^*(\mathbf{k}) | p\bar{p} \rangle|^2, \quad (6.1)$$

where \mathbf{k} is the relative momentum between the two D mesons and \mathcal{R} is the domain where the two-body wave function for the molecular $X(3872)$ is significantly different from zero.

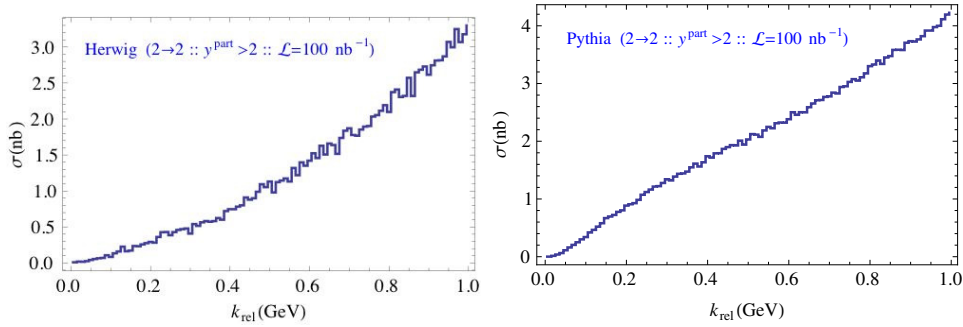


Figure 6.1. Integrated cross section for the production of a $D^0 \bar{D}^{*0}$ pair as a function of their relative momentum computed with HERWIG (left panel) and PYTHIA (right panel). These plots are obtained generating 55×10^9 events and applying final cuts on the D mesons such that the produced molecule has $p_T > 5$ GeV and $|y| < 0.6$. From Bignamini *et al.* [139]

Such an upper bound can be estimated by simply counting the number of $D^0 \bar{D}^{*0}$ ¹ produced with a relative momentum lower than a certain k_0 value. This has been done [139], again, using HERWIG [237] and PYTHIA [238] (see Figure 6.1), taking \mathcal{R} to be a ball or radius $[0, 35]$ MeV, on the basis of a naïve gaussian shape for the two-body wave function of the X . The result of the MC simulation was a production cross section of 0.071 nb for HERWIG and 0.11 nb for PYTHIA, which are both smaller than the experimental value by more than two orders of magnitude.

However, the previous approach was later criticized and it was shown [239] that the theoretical and experimental cross sections might be matched resorting to Final State Interactions (FSI) [240]. The possible presence of FSI, in fact, casts doubts on the applicability of the simple coalescence picture to the case of the $X(3872)$, since the two components of the molecule could be bound by final state rescattering even when their relative momentum is large. In particular, the Migdal-Watson theory would change the previous results in two different ways:

1. The cross section for the production of the X should be modified to

$$\sigma(p\bar{p} \rightarrow X(3872)) \simeq [\sigma(p\bar{p} \rightarrow X(3872))]_{k_0 < k_0^{\max}} \times \frac{6\pi\sqrt{-2\mu E_X}}{\Lambda}, \quad (6.2)$$

where $[\sigma(p\bar{p} \rightarrow X(3872))]_{k_0 < k_0^{\max}}$ is the upper bound evaluated in (6.1) and $\Lambda \sim m_\pi$ is the typical range of the interaction between the components;

2. Instead of being the inverse of the spread of the spatial wave function, the maximum value for the relative momentum should be given by the inverse of the range of the interaction, $k_0^{\max} \simeq c\Lambda$, with $c = \mathcal{O}(1)$.

By setting $k_0 = 2.7\Lambda \simeq 360$ MeV one can increase the theoretical cross section up to 32 nb, which is in agreement with the experimental value.

However, this approach has some flaws [241]: it can be shown that the use of Eq. (6.2) should enhance the occurrence of a new hypothetical molecule, the $D_s \bar{D}_s^*$, which otherwise would be suppressed, as one could infer by looking at data on D_s

¹Here and in what follows we will omit the charge conjugate system, $\bar{D}^0 D^{*0}$, for simplicity.

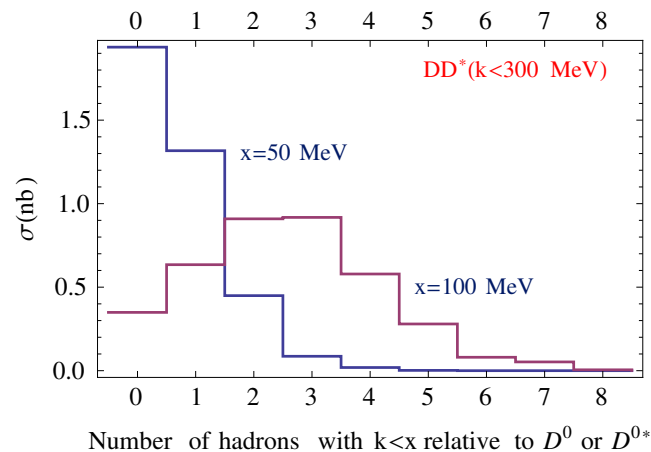


Figure 6.2. Integrated cross section for the production of hadrons with relative momentum $k < x$ with respect to either the D^0 or the \bar{D}^{*0} composing the molecular $X(3872)$. From Bignamini *et al.* [241]

production at Tevatron [242]. In fact, the theoretical production cross section for this X_s would be $\sigma \simeq 1 \div 3$ nb and should be detected by the CDF experiment. No hint for such a particle has been found. Furthermore, the applicability of the Migdal-Watson theorem requires that, (i) the two final particles should be in an S -wave state and (ii) they should be free to interact with each other up to relative distances comparable to the interaction range. First of all, the inclusion of relative momenta up to $k_0^{\max} \simeq 360$ MeV means to include relative orbital angular momenta up to $\ell \sim k_0^{\max}/m_\pi \simeq 2 \div 3$, thus violating the hypothesis (i). Moreover, using again the MC softwares HERWIG and PYTHIA, one can show [241] that in high energy collisions, such as those occurring at Tevatron and LHC, there are on average $2 \div 3$ more hadrons having a relative momentum with respect to one of the two components smaller than 100 MeV, thus violating the hypothesis (ii) – see Figure 6.2.

Even though the presence of other hadrons (mainly pions) surrounding the system does not allow the use of FSI, it might still play an important role in explaining the unnaturally high prompt production of the $X(3872)$.

6.1 Pion rescattering and $X(3872)$ production [2, 3]

In [2] we proposed that the possible elastic scattering of these “comoving” pions with one of the components of the molecule might decrease their relative momentum, hence increasing the number of would-be molecules. This possibility can be understood intuitively referring to the distribution of D meson pairs as a function of k_0 as reported in Figure 6.1. The idea is that the interaction might push the pair both to higher and to lower values of k_0 . However, since the majority of would-be molecules are produced with high relative momenta, even if a small fraction of them would be pushed to smaller momenta, that could cause a feed-down of pairs towards the lower bins of the distribution, where the $X(3872)$ candidates live. For a pictorial representation of the considered rescattering mechanism see Figure 6.3.

It is worth noting that, if we assume the initial total energy \mathcal{E} of the pair to be

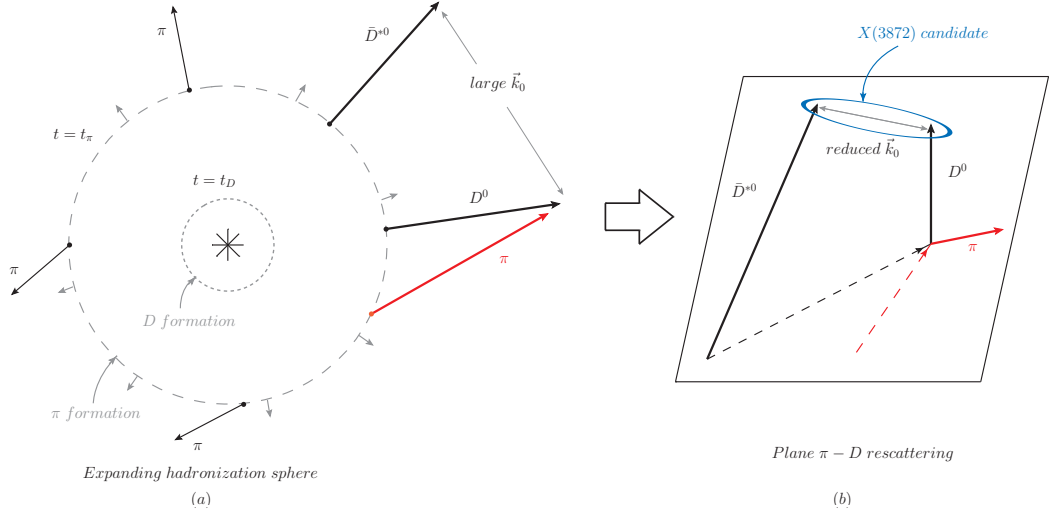


Figure 6.3. Pictorial representation of the rescattering mechanism. After the main high-energy interaction has taken place, the final state particles can be thought of as belonging to an expanding sphere. The hadronization time of a certain particle goes as $t_{\text{hadr}} \propto 1/m$. Therefore the D mesons hadronize at an earlier time t_D whereas pions hadronize at a later time t_π (dotted and dashed spheres respectively). In figure (a) the $D^0\bar{D}^{*0}$ pair starts with a large relative momentum \mathbf{k}_0 . However, the D^0 might interact with one of the comoving pions (red arrow). The $\pi - D$ rescattering (figure (b)) can deviate the D^0 and reduce the relative momentum \mathbf{k}_0 thus producing a possible $X(3872)$ candidate.

positive, the decrease in k_0 due to the elastic scattering may bring it to negative values, hence assuring the binding of the molecule. Therefore, in this model the $X(3872)$ would be a genuine, negative energy $D^0\bar{D}^{*0}$ bound state, whose lifetime would be entirely regulated by the lifetime of its shorter lived component, the \bar{D}^{*0} . Hence, this mechanism also predicts a narrow width, $\Gamma_X \sim \Gamma_{D^*} \simeq 65$ keV, in accordance with the experiments.

Once again, we tested this idea [2, 3] with the already mentioned MC algorithms. In particular, the recipe used to implement the interaction with the pions is as follows: first of all the 10 most coplanar pions to the $D^0\bar{D}^{*0}$ plane are selected, then the pion which will interact with (say the D^0) is randomly chosen and lastly the most parallel pion to the non-interacting meson (say the \bar{D}^{*0}) is selected. One expects this configuration to be the most effective in physical events. Moreover, in order to prevent that D mesons belonging to different jets (separated in coordinate space) would get closer by the scattering with a hard pion, one also requires $\Delta R_{DD^*} \equiv \sqrt{(\Delta y_{DD^*})^2 + (\Delta \phi_{DD^*})^2} < 0.7$. The πD interaction in the center of mass is given by

$$\langle \pi(p)D(q) | D^*(P, \eta) \rangle = g_{\pi DD^*} \eta \cdot p, \quad (6.3a)$$

$$\langle \pi(p)D^*(q, \lambda) | D^*(P, \eta) \rangle = \frac{g_{\pi D^* D^*}}{M_{D^*}} \epsilon_{\alpha\beta\gamma\delta} \lambda^\alpha \eta^\beta p^\gamma q^\delta, \quad (6.3b)$$

with $g_{\pi DD^*} \simeq 11$ and $g_{\pi D^* D^*} \simeq 17$ [199].

First of all, it has been checked [3] that this new mechanism does not spoil the high energy behavior of the relevant D meson distribution, as shown in Figure 6.4. It was

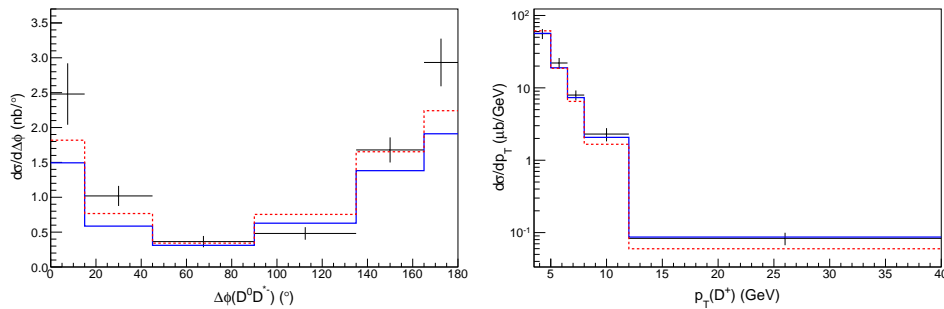


Figure 6.4. Differential cross sections of D^0 and D^0D^{*-} pairs at CDF obtained not including (blue, solid) and including (red, dashed) the interaction with one pion per D^0/D^0D^{*-} event [3]. Both distribution have been rescaled by the same normalization factor, K , obtained by minimizing the combined χ^2 . It is clear that the inclusion of one elastic scattering does not weaken the agreement of the MC simulations to the experimental data.

actually showed that the inclusion of one elastic scattering improves the agreement of the simulation with the experimental data from CDF – see Table 6.1. This is a strong hint of the fact that this mechanism actually takes place in real physical events and should hence be considered when studying final hadronic distributions.

The effect was studied by generating 10^{10} $p\bar{p} \rightarrow c\bar{c}$ events [2], and later by generating 6×10^9 $p\bar{p} \rightarrow 2$ partons (full QCD) events [3]. The parton cut are as loose as possible, $p_{\perp}^{\text{part}} > 2$ GeV and $|y^{\text{part}}| < 6$. The hadron cut have been fixed to the experimental ones in [138], $p_{\perp} > 5$ GeV and $|y| < 0.6$. As one can see from Figure 6.5 and Figure 6.6 the proposed mechanism is actually effective in feeding down the lower $k_0 < 50$ MeV bin, the one containing the would-be molecules. The mechanism is extremely effective for the $p\bar{p} \rightarrow c\bar{c}$ events [2], where the two charmed mesons carry much of the original parton energy $\sqrt{\hat{s}}$. In the complete the full QCD simulation in [3], whose molecular candidates likely originate from a $c\bar{c}$ pair recoiling against a gluon, the effect is milder.

It is also possible to estimate how many of these interactions may take place. In particular, considering a model where all the produced hadrons are flying away from each other on the surface of a sphere – see again Figure 8.4 – and taking into account the range of the interaction, one finds [2] that the simulations suggest an average of 3 scatterings per event. These consecutive interactions can be reproduced by implementing a Markov chain [2]: for each molecule candidate, we wish to evaluate $k_0^{(n)}$ after n interactions. We do it according to the probability distribution functions (PDF) as extracted from $\mathcal{P}(k_0, \Delta k_0)$. We build a set of PDFs $\mathcal{P}_i(\Delta k_0)$ for each bin i in $d\sigma/dk_0$. We assume that the PDFs will be the same for all the interactions,

	K -factor	χ^2/DOF
0π (blue)	1.35	45/11
1π (red)	3.46	24/11

Table 6.1. Fit values referring to the distributions in Figure 6.4.

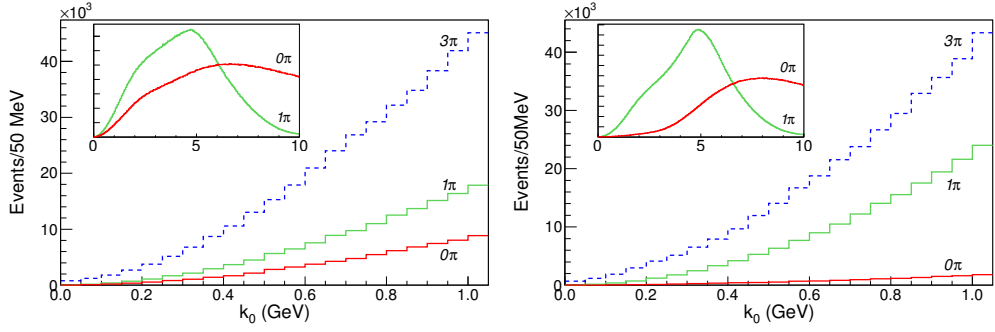


Figure 6.5. Number of $D^0 \bar{D}^{*0}$ pairs (events) counted with Herwig (left panel) and Pythia (right panel) when generating $10^{10} p\bar{p} \rightarrow c\bar{c}$ events at $\sqrt{s} = 1.96$ TeV with the cuts on partons and hadrons described in the text [2]. The histograms named 1π and 3π are related to the elastic scattering of open charm mesons with one or three pions selected as described above. In the insets we report a broader k_0 range.

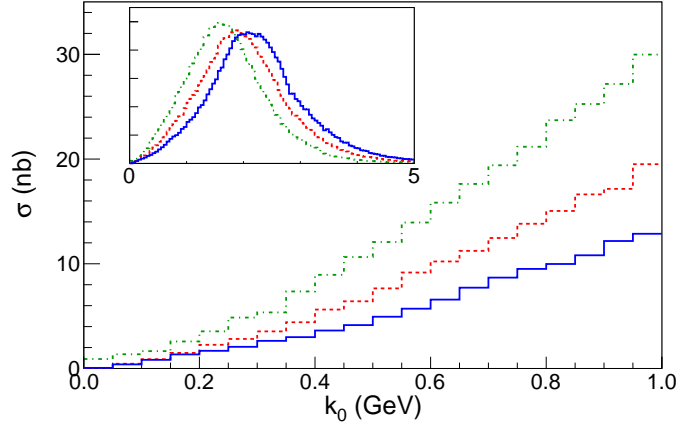


Figure 6.6. Integrated cross section of $D^0 \bar{D}^{*0} + h.c.$ pairs at CDF obtained with HERWIG, without (blue, solid), with one (red, dashed) and with three (green, dot-dashed) interactions with pions [3]. In the inset the same plot on a wider range of k_0 values.

like in a Markov chain. For each event we have a $k_0^{(n)}$, falling in some particular bin i . We randomly extract a Δk_0 according to the distribution $\mathcal{P}_i(\Delta k_0)$ and sum $|k_0^{(n)} + \Delta k_0| = k_0^{(n+1)}$ thus producing a new histogram. We also take into account the ‘lost’ and ‘gained’ would-be-molecules. In each iteration, we generate the number of ‘lost’ and ‘gained’ ones, $l^{(n)}$, $g^{(n)}$, according to Poissonian distributions with mean values $l^{(1)}$, $g^{(1)}$. We implement the following algorithm: *i*) before the n -th interaction, we drop out a number $l^{(n)}$ of pairs, *ii*) we produce the new histogram as a result of the interaction with one more pion, *iii*) after that, we decide to ‘gain’ a $g^{(n)}$ number of pairs. In Table 6.2 we report the values of the integrated cross section for the production of the $X(3872)$ in the full QCD simulation varying both the number of interacting pions and the maximum k_0 allowed for the pair.

As one can see, if one trusts the coalescence model for the $X(3872)$ and hence consider $k_0^{\max} \simeq 50$ MeV, not even the elastic scattering with three consecutive pions

is able to raise the production cross section up to the experimental one ($\sigma \simeq 30$ nb). Moreover, if one considers the (questionable) use of FSI [236, 239] as explained previously, then it should be $k_0^{\max} \simeq 360$ MeV. With this integration region, the simulations produce a cross section after the interaction with one pion – and after a rescaling needed to take into account the different normalization factors between the two works [3, 236]– that is equal to $\sigma(1\pi) \simeq 52$ nb, larger than the experimental one.

6.2 Comparison with deuteron and light nuclei [4]

As we said, the $X(3872)$ is often compared to the deuteron, under the hypothesis that both are loosely bound molecules. It would therefore be of great interest to measure the pp (anti)deuteron production cross section in the same p_\perp region where the X has been observed. Unfortunately, (anti)deuteron production in pp collisions at p_\perp values as high as ≈ 15 GeV (where the X is clearly seen at CMS [122]) has not been measured yet. However, in [3] we studied low- p_\perp preliminary data on anti-deuteron production by ALICE in pp collisions at $\sqrt{s} = 7$ GeV [243]. We tested the validity of the coalescence model for the case of the anti-deuteron using HERWIG. In particular this tool has been used to evaluate the number of $\bar{p}\bar{n}$ pairs produced with small relative momentum ($k_0 < 80$ MeV) in pp collisions at $\sqrt{s} = 7$ TeV in the interval $0.9 \text{ GeV} < p_T < 1.4 \text{ GeV}$. At such small p_\perp a proper tuning of MC to data is not possible, being the absolute cross section not reliable. We ignore therefore the absolute normalization of our deuteron production cross section, and rescale it to match the shape of data. The results of this analysis are reported in Figure 6.7. By anti-deuteron events we mean the number of $\bar{p}\bar{n}$ pairs produced with a momentum smaller than 80 MeV. As one can see in Figure 6.7a, the MC simulation describes reasonably the experimental data, thus providing a proof of the validity of the coalescence model.

In Figure 6.7b we extrapolated the transverse momentum range up to $p_T = 30$ GeV. In order to increase the statistics enough, we allowed the relative momentum between the $\bar{p}\bar{n}$ pair to be up to (300 – 450) MeV since the simulation showed that the shape of the p_T distribution was totally uncorrelated with k_0^{\max} ². This rough estimate shows how the production cross section for anti-deuteron might turn out to be really small at high p_T , in agreement to the intuitive picture mentioned before, and happens to be two orders of magnitude smaller than the $X(3872)$ one. However,

²The $(k_0^{\max})^3$ dependence coming from phase space is reabsorbed in the normalization factor used to tune the distributions on the experimental data.

k_0^{\max}	50 MeV	300 MeV	450 MeV
$\sigma(0\pi)$	0.06 nb	6 nb	16 nb
$\sigma(1\pi)$	0.06 nb	8 nb	22 nb
$\sigma(3\pi)$	0.9 nb	15 nb	37 nb

Table 6.2. Effect of multiple scatterings in $X(3872)$ production cross section. k_0^{\max} indicates the integration region $k_0 \in [0, k_0^{\max}]$.

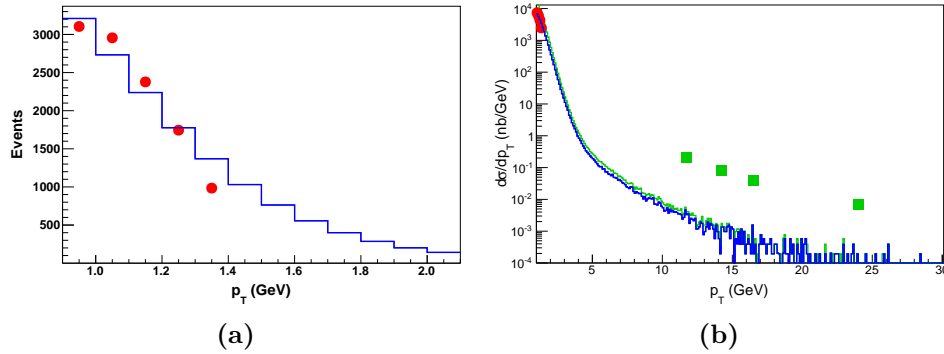


Figure 6.7. Anti-deuteron events produced in pp collisions according to 10^9 HERWIG events with $|\eta| < 0.9$ (blue solid line) and $|y| < 1.2$ (green solid line) as a function of the transverse momentum of the molecule [3]. The MC simulation is compared to the ALICE deuteron production preliminary data [243] (red circles) and with the CMS $X(3872)$ data [122] (green squares).

if we assume that the spin-interactions are second order effects, the yields for the anti-deuteron and for the $X(3872)$ should be similar. Were this confirmed, it would provide the definitive proof of the inconsistency of the molecular interpretation with the experimental data. The uncertainties given by the non-reliability of the MC at low p_\perp and by such a large extrapolation to high p_T prevent us to draw firm conclusions by now.

However, very recently the ALICE collaboration reported results on the production of deuteron, helium-3 (${}^3\text{He}$) and hypertriton (${}^3_\Lambda\text{H}$) light nuclei in relatively high p_\perp bins in Pb-Pb collisions, at $\sqrt{s_{\text{NN}}} = 2.76$ TeV [244, 245].

As a first approximation one can assume that there are no medium effects enhancing or suppressing the production of light nuclei in Pb-Pb collisions. This is equivalent to state that each nucleus-nucleus collision is just an independent product of N_{coll} proton-proton collisions, with N_{coll} computed in a Glauber Monte Carlo calculation as a function of the centrality class. We use the results from [247], which are compatible at 1σ level with the ALICE ones [248], and never more different than 3%. To compare with $\sqrt{s} = 7$ TeV data, we rescale our estimated cross sections by a factor $\sigma_{pp}^{\text{inel}}(7 \text{ TeV})/\sigma_{pp}^{\text{inel}}(2.76 \text{ TeV}) = 1.1$.

Consider for example the production of hypertriton observed by ALICE in Pb-Pb

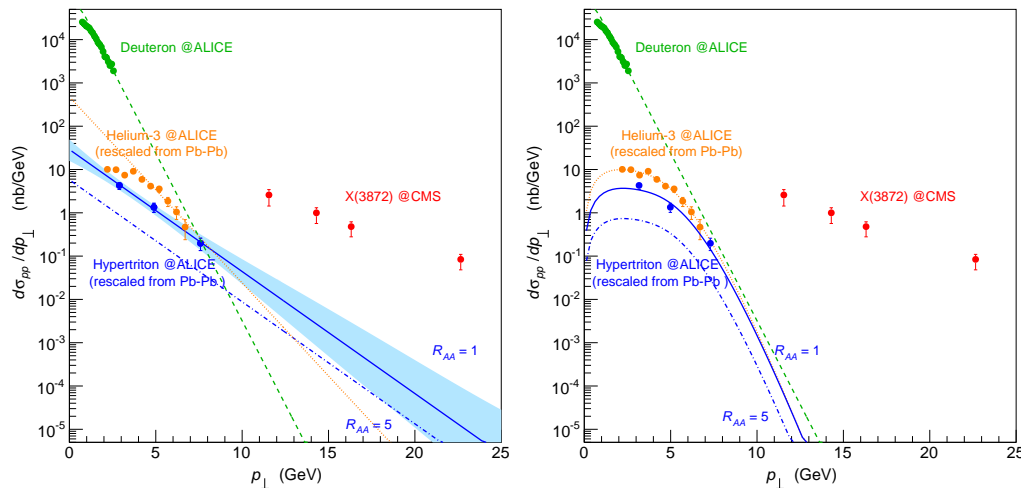


Figure 6.8. Comparison between the prompt production cross section in pp collisions of $X(3872)$ (red), deuteron (green), ${}^3\text{He}$ (orange), and hypertriton (blue) [4]. The X data from CMS [122] are rescaled by the branching ratio $\mathcal{B}(X \rightarrow J/\psi \pi\pi)$. Deuteron data in pp collisions are taken from ALICE [245]. The ${}^3\text{He}$ and hypertriton data measured by ALICE in Pb-Pb collisions [244, 245] have been rescaled to pp using a Glauber model, as explained in the text. The dashed green line is the exponential fit to the deuteron data points in the $p_{\perp} \in [1.7, 3.0]$ GeV region, whereas the dotted orange one is the fit to the ${}^3\text{He}$ data points. The solid and dot-dashed blue lines represent the fits to hypertriton data with $R_{AA} = 1$ (no medium effects) and an hypothetical constant value of $R_{AA} = 5$. The hypertriton data points are horizontally shifted at the bin centers of gravity – being defined as the point at which the value of the fitted function equals the mean value of the function in the bin. (Left Panel) The hypertriton data are fitted with an exponential curve, and the light blue band is the 68% C.L. for the extrapolated $R_{AA} = 1$ curve. ${}^3\text{He}$ data in the $p_{\perp} \in [4.45, 6.95]$ GeV region are also fitted with an exponential curve. (Right Panel) The hypertriton and ${}^3\text{He}$ data are fitted with blast-wave functions [246], whose parameters are locked to the ${}^3\text{He}$ ones obtained in [245].

collisions³. Neglecting medium effects, the pp cross section can be estimated with

$$\begin{aligned}
 & \left(\frac{d\sigma({}^3\text{H})}{dp_{\perp}} \right)_{pp} = \\
 & = \frac{\Delta y}{\mathcal{B}({}^3\text{He} \pi)} \times \frac{1}{\mathcal{L}_{pp}} \left(\frac{d^2 N({}^3\text{He} \pi)}{dp_{\perp} dy} \right)_{pp} = \\
 & = \frac{\Delta y}{\mathcal{B}({}^3\text{He} \pi)} \times \frac{\sigma_{pp}^{\text{inel}}}{N_{\text{evt}}} \left(\frac{d^2 N({}^3\text{He} \pi)}{dp_{\perp} dy} \right)_{pp} = \\
 & = \frac{\Delta y}{\mathcal{B}({}^3\text{He} \pi)} \times \frac{\sigma_{pp}^{\text{inel}}}{N_{\text{coll}}} \left(\frac{1}{N_{\text{evt}}} \frac{d^2 N({}^3\text{He} \pi)}{dp_{\perp} dy} \right)_{\text{Pb-Pb}}.
 \end{aligned} \tag{6.4}$$

ALICE analyzes ${}^3\text{He} \pi$ pairs, thus we need to divide by the branching ratio for the ${}^3\text{H} \rightarrow {}^3\text{He} \pi$ decay – $\mathcal{B}({}^3\text{He} \pi) \approx 25\%$ [249] – in order to deduce the number

³In the following, the average of hypertriton and anti-hypertriton data is understood.

of parent hypertritons. We stress that the experimental data in [244] are indeed normalized to $N_{\text{evt}} = N_{\text{Pb-Pb}}^{0-10\%}$, *i.e.* the total number of inelastic Pb-Pb collisions analyzed (about 20×10^6 events in the 0-10% centrality bin). We use $\sigma_{pp}^{\text{inel}} = 73$ mb, as measured in $\sqrt{s} = 7$ TeV collisions [250, 251], and $\Delta y = 2.4$ to compare with the CMS analysis [122]. In this centrality class, we use $N_{\text{coll}}^{0-10\%} = 1518$ [247].

Similarly, we can estimate the ${}^3\text{He}$ distribution in pp collisions from the ALICE Pb-Pb data in the 0-20% centrality class [245], using $N_{\text{coll}}^{0-20\%} = 1226$ [247]. We remark that the selection of these events rejects any ${}^3\text{He}$ not produced in the primary vertex, *i.e.* the hypertriton decay products. Since the ${}^3\text{He}$ data points with $p_{\perp} < 4.4$ GeV show a deviation from the exponential behavior, likely due to the expansion of the medium, we perform an exponential fit to the points in the region $p_{\perp} \in [4.45, 6.95]$ GeV only. Alternatively, we fit hypertriton and ${}^3\text{He}$ data with the blast-wave model⁴, which describes particle production properties by assuming thermal emission from an expanding source [246]. This model is expected to reproduce correctly the low and medium p_{\perp} regions in Pb-Pb collisions. Since we are rescaling Pb-Pb data to pp by a constant factor, the same shape holds in our estimated pp data, and gives a guess on the asymptotic exponential behavior. The results are shown in Figure 6.8.

Our rescaling to pp collisions does not take into account either medium effects, nor the fact that the coalescence/recombination mechanism can be enhanced in Pb-Pb collisions [252]. In fact, such phenomena are known to favor the production of many-body hadrons with respect to what is expected in vacuum. Medium effects are discussed later.

For the deuteron we use ALICE pp data [245] to estimate

$$\left(\frac{d\sigma(d)}{dp_{\perp}}\right)_{pp} = \Delta y \times \sigma_{pp}^{\text{inel}} \left(\frac{1}{N_{pp}^{\text{inel}}} \frac{d^2N(d)}{dp_{\perp} dy}\right)_{pp} \quad (6.5)$$

N_{pp}^{inel} being the number of pp inelastic collisions collected. We perform the fit to the points in the region $p_{\perp} \in [1.7, 3.0]$ GeV, which shows a good exponential behavior.

The CMS analysis of X production provides the differential cross section times the branching fraction $\mathcal{B}(X(3872) \rightarrow J/\psi \pi^+ \pi^-)$. The latter has not been measured yet, and the lower limit reported in the PDG is $\mathcal{B} > 2.6\%$ [113]. An estimate for the upper limit has been reported, $\mathcal{B} < 6.6\%$ at 90% C.L. [254]; we use instead the more conservative value $\mathcal{B} = 8.1_{-3.1}^{+1.9}\%$ [50]. The comparison in Figure 6.8 shows that, according to the most conservative exponential fit in the left panel, the extrapolated hypertriton production cross section in pp collisions would fall short by about $2 \div 3$ orders of magnitude with respect to the X production, and much more according to the blast-wave fit in the right panel. The drop of the deuteron cross section, which is directly measured in pp collisions, appears definitely faster.

⁴The blast-wave function is

$$\frac{dN}{dp_{\perp}} \propto p_{\perp} \int_0^R r dr m_{\perp} I_0\left(\frac{p_{\perp} \sinh \rho}{T_{\text{kin}}}\right) K_1\left(\frac{m_{\perp} \cosh \rho}{T_{\text{kin}}}\right),$$

where m_{\perp} is the transverse mass, R is the radius of the fireball, I_0 and K_1 are the Bessel functions, $\rho = \tanh^{-1}\left(\frac{(n+2)\langle\beta\rangle}{2}(r/R)^n\right)$, and $\langle\beta\rangle$ the averaged speed of the particles in the medium.

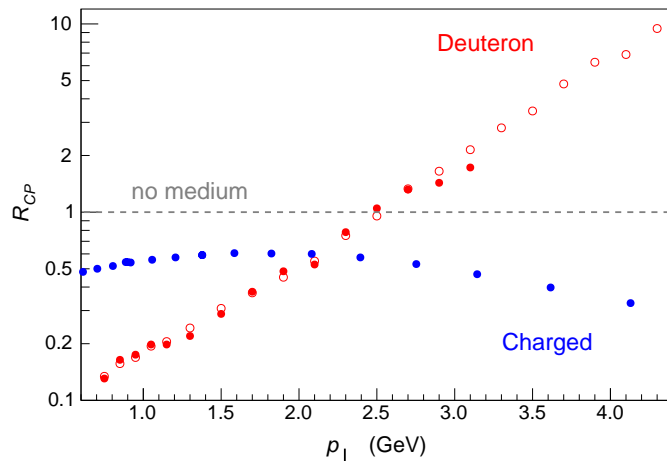


Figure 6.9. Comparison between the nuclear modification factor R_{CP} for deuteron (red) and for generic charged tracks (blue) [253] in central (resp. 0-10% and 0-5%) versus peripheral (60-80%) Pb-Pb collisions. We evaluate R_{CP} either taking the bin-by-bin ratio of ALICE data [245] (full disks), or using the values given by the blast-wave fit for the peripheral Pb-Pb data, and extrapolating up to $p_{\perp} \sim 4.8$ GeV (open disks). The dashed line corresponds to no medium effects, $R_{CP} = 1$. It is worth noticing that $R_{CP}(d)$ gets enhanced at $p_{\perp} \gtrsim 2.5$ GeV.

As we mentioned already, the main problem for the production of loosely bound molecular states in proton-proton collisions is the difficulty in producing the constituents close enough in phase space. However, it is well known that the interaction of elementary partons with the collective hot dense medium causes relevant energy loss of the partons themselves. This effect is usually quantified by the nuclear modification factor [253, 255–258]

$$R_{AA} = \frac{\left(\frac{1}{N_{\text{evt}}} \frac{d^2 N}{dp_{\perp} dy}\right)_{\text{Pb-Pb}}}{N_{\text{coll}} \left(\frac{1}{N_{\text{evt}}} \frac{d^2 N}{dp_{\perp} dy}\right)_{pp}}, \quad (6.6)$$

which compares the particle yield in Pb-Pb collisions with that in pp . It then follows that the method used to obtain Eq. (6.4) corresponds to assume $R_{AA} = 1$.

While for ordinary hadrons medium effects generally lead to a suppression of the particle yield – *i.e.* $R_{AA} < 1$ – conversely they can favor the production of hadronic molecules. The role of the medium would be, in fact, that of decreasing the relative momenta of the components with respect to the zero temperature case due to the well-known jet quenching effect [259–261]. This would favor their coalescence into the final bound state by reducing their relative momenta directly at parton level.

The coalescence model is based on the sudden approximation⁵ and is implemented by calculating the overlap of the density matrix of the constituents with the Wigner function of the final composite particle. In particular, it has the important property of taking into account the inner structure of the considered hadron. If one only

⁵*i.e.* the assumption that the binding of the constituents happens on small time scales and therefore their wave function remains unchanged during the transition to the bound state.

requires the vicinity in momentum space, the p_{\perp} distribution of a composite state with N constituents coming out of a hot QCD medium is roughly given by

$$\frac{dN_b}{dp_{\perp}}(\mathbf{p}_{\perp}) \sim \prod_{i=1}^N \frac{dN_i}{dp_{\perp}}(\mathbf{p}_{\perp}/N), \quad (6.7)$$

where N_b is the number of final bound states and N_i is the number of produced constituents. This would also explain why in Figure 6.8 the cross section for the ${}^3\text{He}$ and hypertriton are several orders of magnitude smaller than the deuteron one: one additional p or Λ , close enough in phase space, must be produced.

It has already been shown that coalescence effects in Pb-Pb collisions can have relevant consequences on the production of multi-quark states. In particular, molecular states with small binding energy are expected to be *enhanced*, *i.e.* $R_{AA} > 1$ [262].

Unfortunately there is no measurement of R_{AA} for the deuteron as a function of p_{\perp} . However, there is another nuclear modification factor which is often used,

$$R_{CP} = \frac{\left(\frac{1}{N_{\text{evt}}} \frac{d^2N}{dp_{\perp}dy}\right)_{\text{Pb-Pb}}^{0-10\%} / N_{\text{coll}}^{0-10\%}}{\left(\frac{1}{N_{\text{evt}}} \frac{d^2N}{dp_{\perp}dy}\right)_{\text{Pb-Pb}}^{60-80\%} / N_{\text{coll}}^{60-80\%}}. \quad (6.8)$$

This quantity is a comparison between the most central and the most peripheral Pb-Pb collisions and therefore provides another valid indicator of the strength of medium effects (which should be absent in the less dense, most peripheral events). The fact that R_{AA} and R_{CP} measurements for hadron species are strongly correlated to each other is shown experimentally by a thorough data analysis reported by ATLAS [253], up to very high $p_{\perp} \sim 100$ GeV.

Using the ALICE data presented in [245] we can compute R_{CP} for the deuteron as a function of p_{\perp} and compare it with that for generic charged tracks, as reported in [253] – see Figure 6.9. We use $N_{\text{coll}}^{60-80\%} = 27.5$ [247]. As one immediately notices, the difference from ordinary hadrons is striking. The presence of the QCD medium is extremely effective at enhancing the production of the deuteron for the reasons explained before. In fact, R_{CP} for this hadronic molecule becomes larger than unity for $p_{\perp} \gtrsim 2.5$ GeV, in particular we have $R_{CP} = 1.7$ at the last point with $p_{\perp} = 3.1$ GeV. Using the blast-wave fitting function for the peripheral data taken from [244], we also extrapolate up to the end point of the central data, confirming the growth of R_{CP} with p_{\perp} .

We expect a similar behavior in R_{AA} , and in particular a value larger than 1 for p_{\perp} large enough.

To get an independent rough estimate for R_{AA} , we assume the deuteron production cross section in pp collisions to scale with \sqrt{s} like the inelastic cross section, and compare the ALICE data in central Pb-Pb collisions at $\sqrt{s_{\text{NN}}} = 2.76$ TeV, with the ones in pp collisions at $\sqrt{s} = 7$ TeV [245]. Indeed, we find that R_{AA} exceeds 1 at $p_{\perp} = 2.1$ GeV, and reaches 5 at $p_{\perp} = 4.3$ GeV. This gives strength to our expectation for $R_{AA} > 1$. To display the size of this effect, we plot also the hypertriton curves for $R_{AA} = 5$ in Figure 6.8.

One naturally expects for a similar enhancement to be even more relevant for 3-body nuclei like ${}^3\text{He}$ and the hypertriton. Its role would be to further *decrease*

the extrapolated cross section in prompt pp collisions. As we already said, indeed, a value of $R_{AA} > 1$ applied to Pb-Pb data implies a pp cross section even smaller than predicted by the Glauber model. Even though qualitative conclusions can already be drawn, a quantitative analysis substantiated by data at higher p_{\perp} is necessary for a definitive comparison with the X case.

Even assuming that only a hot pion gas is excited in Pb-Pb collisions, there would likely be a large number of final state interactions with pions catalyzing the formation of a loosely bound hypertriton along the lines discussed in [3, 8, 50]. In any case, such an environment is present in the Hadron Resonance Gas corona formed when the outer shell of the QCD medium cools down [263].

In summary, the extrapolation of the deuteron and ${}^3\text{He}$ data in pp collisions suggests that loosely bound molecules are hardly produced at high p_{\perp} . The extrapolated curve of hypertriton data from Pb-Pb collisions might lead to milder conclusions although we expect it should be significantly suppressed when medium effects are properly subtracted. Such effects are indeed already sizable for the deuteron as shown in Figure 6.9, and probably even more relevant for 3-body nuclei.

To summarize, the experimental value of the prompt production cross section of the $X(3872)$ casts serious doubts on its possible interpretation in terms of a $D^0\bar{D}^{*0}$ molecule. According to the expectations following from the phenomenological coalescence model – that correctly describes the deuteron – the production of such a weakly bound state should be strongly suppressed in high energy collisions. This is suggested both by MC simulations, and by simple extrapolations of available data. Even though many ideas and models have been proposed during the years none of them has successfully reconciled the theoretical expectations with the experimental results.

It should also be emphasized that the inclusion of possible interactions between comoving pions and final state mesons [2, 3] turned out to improve the accordance between the simulated MC distributions and the experimental ones and hence should be taken into account in future works. Finally, for an unbiased and definitive comparison of light nuclei with X production at p_{\perp} as high as 15 GeV, deuteron (or hypertriton) should be searched in pp collisions rather than in Pb-Pb to avoid the complications of subtracting medium effects. These analyses can be performed by ALICE and LHCb during Run II.

Chapter 7

Tetraquarks

The previously described problem seemed a compelling evidence of the necessity for a new kind of interpretation for these exotic mesons. It has been proposed [264] that these states might actually have a compact (point-like) four-quark structure – the so-called *tetraquark*. In this section we introduce this model starting from its consequences regarding the production of XYZ mesons in high energy collisions, so that a more direct comparison could be done with the previous section.

The constituent quark model has been by far the most successful tool for the classification and interpretation of hadrons. Despite its obvious limitations, the systematic search of $SU(3)$ multiplets provides the most reliable guideline in hadron spectroscopy. Exotic states with nonminimal quark content were forecasted by Gell-Mann in the very first paper on the quark model [13]. One of the simplest and more economic ways (in terms of new states predicted) of forming multiquark states is considering constituent *diquarks*. The proposal of diquarks as effective degrees of freedom inside baryons came out in the late ‘60s: it is based on the observation that a $[q_1 q_2]_{\bar{\mathbf{3}}_c}$ pair in the antisymmetric color configuration binds according to the tree-level calculation (one gluon exchange). Some phenomena, like the $x \rightarrow 1$ of the ratio of proton and neutron PDFs, or the ratio of fragmentation functions to Σ and Λ , can be qualitatively understood assuming the existence of these colored objects. Also, some evidence of a scalar diquark was found in lattice QCD [?]. Diquarks can be the constituent bricks of a new rich multiquark spectroscopy.

In general tetraquark bound states have been proposed a long time ago [265–267] to understand the nature of the light scalar mesons $a_0(980)$ and $f_0(980)$. In 2003, Jaffe and Wilczek [268] proposed a diquark-diquark-antiquark explanation for the positive-strangeness Θ^+ baryon (before that the observation of the state was contested by an higher statistics analysis). An interpretation of light scalar mesons in terms of diquark-antidiquark states was instead proposed for the first time by Maiani *et al.* [35, 269] following the revitalization of interest on the σ meson (reappeared in heavy-light meson decays [270]) and contextually with an interesting reanalysis of $\pi\pi$ scattering [271].

Some aspect of the tetraquark models have been inspired by dibaryons [272, 273], in particular the feasibility of isospin violation [274]. Different extensions of the constituent quark models for the tetraquark spectroscopy have been explored by Valcarce *et al.* [275–279].

As we will show in the next sections, assuming a constituent quark model with color-spin interaction it is possible to study the spectroscopy of these states, in which the $J^{PC} = 1^{+\pm}$ and $J^{PC} = 1^{--}$ states discovered so far can be nicely accommodated. The main problem with this picture is that it also predicts other states which did not (yet?) show up in experimental researches. A possible solution to this problem is also presented.

7.1 Tetraquark production [3, 5]

From the studies on loosely bound molecule production at hadron colliders we are led to consider that multi-quark hadrons should rather be initiated by the formation of compact quark clusters. The seed of a heavy-light tetraquark state could be described by

$$|\psi\rangle = \alpha|[Qq]_{\mathbf{3}_c}[\bar{Q}\bar{q}]_{\mathbf{3}_c}\rangle + \beta|(Q\bar{Q})_{\mathbf{1}_c}(q\bar{q})_{\mathbf{1}_c}\rangle + \gamma|(Q\bar{q})_{\mathbf{1}_c}(\bar{Q}q)_{\mathbf{1}_c}\rangle, \quad (7.1)$$

where by Q and q we represent the heavy and light quarks respectively. In our scheme, the two-meson states will tend to fly apart, as strong Van der Waals-like forces between their meson components are not sufficient to produce bound states like J/ψ ρ or $D\bar{D}^*$ – depending on the spin and orbital quantum numbers of the original four-quark system. In this sense such states are in a “open channel” continuum.

Most authors are convinced instead that some hadron molecule shallow potentials could allow for at least a single discrete level with almost zero energy $\sim -\epsilon$. Small binding energies in quantum field theory are possible and, if g is the *strong* coupling, say in the DD^* interaction, one can connect ϵ to g by [280]

$$\epsilon = \frac{g^4}{512\pi^2} \frac{\mu^5}{M_D^4 M_{D^*}^4}, \quad (7.2)$$

where μ is the reduced mass of the DD^* system (in this formula we are treating D and D^* as if they were spinless particles. Accounting for the spin is simple and does not change our qualitative conclusions). This formula is obtained by resonance scattering theory at low energies supposing that there is a pole term associated with the virtual production of X particle in the $f(DD^* \rightarrow DD^*)$ scattering amplitude

$$\frac{1}{(p_D + p_{D^*})^2 - M_X^2} \quad (7.3)$$

and supposing that \mathcal{E} , the barycentric energy after subtraction of rest energy, is, like ϵ , a *small* quantity. We replace $(p_D + p_{D^*})^2 \rightarrow (M_D + M_{D^*} + \mathcal{E})^2$.

Thus, if \mathcal{E} were indeed small enough, formula (7.2) would hold and, including spin and using the coupling g as deduced in [281], one would get

$$|\epsilon|_{\text{exp}} = 0.1 \text{ MeV} \quad \text{vs.} \quad |\epsilon| = 0.4 \text{ MeV} \quad (7.4)$$

from (7.2).

However in the prompt production of X at large hadron colliders, \mathcal{E} is very far from being small. The fact that the observed prompt production cross section at LHC is so much larger than expectations, as commented at length in previous

sections, suggests then that the X is not a loosely bound state of DD^* , and the rough agreement (7.4) simply occurs outside of the kinematic conditions of X production.

These kind of problems do not exist in the diquark-antidiquark picture for this particle would be kept together by color interactions, the unknown being the effectiveness of the color force at producing diquarks. The diquark-antidiquark belongs to a “closed” channel. The relative size of α, β, γ coefficients in (7.1) is unknown.

We might formulate different hypotheses: *i*) α, β, γ are all of the same order. In this case we should be observing the entire spectrum of diquark-antidiquark states which can be predicted using the color-spin Hamiltonian (see below). In a previous work [264], the Hamiltonian of the diquark-antidiquark model was supposed to contain both spin-spin interaction between quarks within each diquark and quarks in the two different diquarks. The resulting spectrum predicts a rich structure of states with some evident mismatches with the experimental findings.

A ‘type-II’ version of the diquark-antidiquark model, with spin couplings suppressed between different diquarks, allows a remarkable description of the $J^{PC} = 1^{++}$ sector of charged tetraquarks as the $Z(4430)$, $Z_c(4020)$, $Z_c(3900)$ and a good picture of the entire $J^{PC} = 1^{--}$ sector (see next few sections). Some typical problems of the diquark-antidiquark model persist in the type-II model. For example the $X(3872)$ should have charged partners and an hyperfine splitting between two neutral levels, to account for isospin violations [264].

To solve this kind of difficulties we might formulate a different hypothesis for the hierarchy among α, β, γ coefficients. We might indeed assume that, *ii*)

$$|\beta|^2, |\gamma|^2 \gg |\alpha|^2 \quad (7.5)$$

Such an assumption means that, in general, diquark-antidiquark states are less likely to be formed in hadronization but a resonance could emerge as a result of the coupling between open and closed channels. This hypothesis introduces a selection rule in the diquark-antidiquark spectrum: especially those levels which are close enough to open channel thresholds (resonance conditions) are observed as physical resonances.

More specifically, the diquark-antidiquark closed channel provides an effective attraction in the open channel which might lead to produce a resonance. This phenomenon is effective if the energy level E_n , corresponding to the closed channel state $|[Qq]_{\mathbf{3}_c}[\bar{Q}\bar{q}]_{\mathbf{3}_c}, n\rangle_C$, happens to be very close to one, or both, as in the X -particle case, of the open channel thresholds (located, in the case of the X , at $E_O = m_{J/\psi} + m_\rho$ or $E_O = m_{D^0} + m_{\bar{D}^{*0}}$).

Strong interactions provide the discrete spectrum for diquark-antidiquark states, however those levels correspond most likely to physical states once the closed channel is hybridized with the open one, *i.e.* the difference in energy, or detuning parameter ν , is small enough. When this energy matching condition between the total energy in the open channel and the energy level in the closed channel takes place, the two hadrons in one open channel can undergo an elastic scattering, altered by the presence of the near closed channel level. The two hadrons in an open channel can scatter to the intermediate state in the closed channel, which subsequently decays into two particles in one of the open channels.

The contribution to the scattering length due to this phenomenon is of the form [3, 5]

$$a \sim |C| \sum_n \frac{\langle [Qq]_{\mathbf{3}_c} [\bar{Q}\bar{q}]_{\mathbf{3}_c}, n | H_{CO} | (Q\bar{q})_{\mathbf{1}_c} (\bar{Q}q)_{\mathbf{1}_c} \rangle}{E_O - E_n} \quad (7.6)$$

where H_{CO} couples the open and closed channels; the discrete levels of the closed channel are labeled by n . This sum is dominated by the term which minimizes the denominator $E_O - E_n \equiv -\nu$, *i.e.* the one with the smallest detuning. The width of the resulting resonance is naturally proportional to the detuning $\Gamma \sim \sqrt{\nu}$ for phase space arguments.

Since the $X(3872)$ is the narrowest among all XYZ mesons, it must have $\nu \simeq 0$, which means the highest possible hybridization between channels given the (unknown) inter-channel interaction Hamiltonian H_{CO} .

The D^+D^{*-} open channel level is found to be at a mass *above* the X diquark-antidiquark level, by about 8 MeV. Coupling between channels gives rise to a repulsive interaction if the energy of the scattering particles is larger than that of the bound state (and an attractive one if it is smaller). For this reason we might conclude that the neutral particle has no $d\bar{d}$ content in its wavefunction explaining the well-known isospin breaking pattern in X decays.

The diquark-antidiquark X^+ levels (the charged partner of the $X(3872)$), might also fall below $D^+\bar{D}^{*0}$ and \bar{D}^0D^{*+} thresholds by about $3 \div 5$ MeV, which could be enough for inhibiting the resonance phenomenon described. This might be the reason why the X^+ particles, although present in the diquark-antidiquark spectrum, are more difficult to be produced.

The $J/\psi \rho^0$ open channel level is also perfectly matching the closed channel one for the $X(3872)$. However because of the large ρ width, the modification in the scattering length (7.6) is much less effective if compared to the open charm threshold: the sum in (7.6) has to be smeared with an integral convoluting the ρ Breit-Wigner. Therefore we would expect that the X^+ particles are less likely to be formed or they could simply be too broad to be observed. Some examples are shown in Table 7.1.

The mechanism here described is known in nuclear and atomic physics as the Feshbach resonance formation [188].

Recently two *charged* resonances have been confirmed to a high level of precision.

State	Open channel	ν (MeV)	Γ_{th} (MeV)	Γ_{exp} (MeV)
$X(3872)$	$D^0\bar{D}^{*0}$	-0.16 ± 0.31	0	< 1.2
$Z_c(3900)$	$D^+\bar{D}^{*0}$	12.1 ± 3.4	30	35 ± 7
$Z'_c(4020)$	$D^{*+}\bar{D}^{*0}$	6.7 ± 2.4	22	10 ± 6
$Z(4430)$	$\eta_c(2S)\rho$	64 ± 17	$\gtrsim 150$	180 ± 30
$Z_b(10610)$	$B^+\bar{B}^{*0}$	2.7 ± 2.0	14	18.4 ± 2.4
$Z'_b(10650)$	$B^{*+}\bar{B}^{*0}$	1.8 ± 1.5	12	11.5 ± 2.2

Table 7.1. Exotic states in term of Feshbach resonances. The width is related to the detuning by $\Gamma = A\sqrt{\nu}$. An exception is given by the $Z(4430)$, whose width is forced to be larger than its constituent width, *i.e.* $\Gamma_\rho \sim 150$ MeV.

The $Z(4430)$ and the $Z_c(3900)$. These are genuine tetraquark states. We need to recall that the prediction of charged states of this kind was exclusively formulated in the context of compact tetraquark states [264].

In particular, when the first hint of a $Z(4430)$ charged tetraquark was provided by the Belle collaboration in the $\psi(2S)\pi^+$ channel, back in 2007, it was observed that another state at 3880 MeV (*i.e.* lighter by the $\psi(2S) - \psi(1S)$ mass difference) was expected in the tetraquark model [282] with the same quantum numbers (the former being the radial excitation of the latter). The lower state was expected to decay into $J/\psi\pi^+$ or $\eta_c\rho^+$. A charged $Z_c(3900)$ with $J^{PG} = 1^{++}$ decaying into $J/\psi\pi^+$ was discovered by BES III and Belle in 2013 [68]. It was also shown that BES III and Belle data might be compatible with the presence of another peak about 100 MeV below that of the $Z_c(3900)$ [7]. That was also predicted by the tetraquark model.

The tetraquark model in its first diquark-antidiquark version [7, 264] predicts one more $J^{PG} = 1^{++}$ level, at a mass of 3755 MeV (these mass values are locked to the input mass value of the $X(3872)$). We might predict that no resonance will be found at this level because there are no open channels nearby to make the Feshbach mechanism possible. The $Z(4430)$ is instead made possible by the presence of the $\eta_c(2S)\rho$ open channel. The expected width, driven by the ρ , is expected to be as large as 150 MeV, to be compared with the ~ 170 MeV observed.

The tetraquark model in its ‘type-II’ version has no 3755 MeV, but a level perfectly compatible with the observed $Z'_c(4020)$ by the BES III Collaboration [71], which is also compatible with a Feshbach generated state. A $Z(4430)^0$ isosinglet resonance could be due to the vicinity of the $\eta_c(2S)\omega$ open channel, with a narrower width of about 70 MeV.

These considerations about the interplay between a closed (diquark-antidiquark) and open channel (molecular thresholds) are to be considered in a preliminary stage and possibly object of future developments. In the following we will focus instead on the description of the diquark-antidiquark closed channel listing its states by quantum numbers and showing how to estimate expected masses (the position of levels).

We believe that recent experimental findings are clearly spelling in favor of tetraquark particles and the diquark-antidiquark model apparently has many features matching very well the present phenomenology. The Feshbach mechanism here sketched might be a viable way for implementing those selection rules still missing in the tetraquark Hamiltonian approach to be described below.

7.2 Diquarks

One-gluon interaction in the t -channel between two quarks in the $SU(3)_c$ representation $R = \mathbf{3}$ (antiquarks $R = \bar{\mathbf{3}}$) involves a (tensor) product of color charges $T_{R_1} \otimes T_{R_2}$ which can be expressed as the direct sum of diagonal blocks with the dimensions of the irreducible representations S_i in $T_{R_1} \otimes T_{R_2} = S_1 \oplus S_2$. According to the general rule

$$T_{R_1} \otimes T_{R_2} = \bigoplus_i \frac{1}{2}(C_{S_i} - C_{R_1} - C_{R_2})\mathbf{1}_{S_i} \quad (7.7)$$

we only need the Casimir values $C_{\mathbf{3}} = C_{\bar{\mathbf{3}}} = 4/3$ and $C_{\mathbf{1}} = 0$ to appreciate that one-gluon exchange generates a quark-quark *attraction* in the $\bar{\mathbf{3}}$ channel ($-2/3$) which is just half of that in the quark-antiquark singlet channel ($-4/3$). Even if one-gluon-exchange interaction is a primitive model of low energy strong interactions, correlating it with indications from lattice computations [283] on diquarks gives reasonable support to the possibility of diquark-antidiquark hadrons.

Diquarks carry the same color charge of antiquarks. The opposite for antiquark-antiquark pairs. We represent a spin zero diquark with the bispinor notation

$$[cq]_i = \epsilon_{ijk}(c^j)^T \sigma^2 q^k, \quad (7.8)$$

where i, j and k are color indices. In the quadrispinor notation we would have written $\epsilon_{ijk} \bar{c}^j \gamma_5 q^k$, where \bar{c} indicates the charge conjugated spinor. In the next sections color index will be left implicit. Relying on spin-flavor symmetry of heavy-light mesons, a spin-1 heavy-light diquark could equally be formed

$$[cq]_i = \epsilon_{ijk}(c^j)^T \sigma^2 \sigma^\lambda q^k. \quad (7.9)$$

Integrating over the spatial wave function, and absorbing the constant terms into the constituent masses, the relevant Hamiltonian is [284, 285]

$$H = -2 \sum_{i \neq j, a} \kappa_{ij} \mathbf{S}_i \cdot \mathbf{S}_j \frac{\lambda_i^a}{2} \cdot \frac{\lambda_j^a}{2}. \quad (7.10)$$

Here we will discuss the color interaction only, leaving the spin to the next sections. We introduce the (normalized) color singlet/octet states using the following notation which turns out to be rather practical for calculations:

$$|\bar{c}c_{\mathbf{1}}, \bar{q}q_{\mathbf{1}}\rangle := \frac{1}{3} \mathbb{1}_{\bar{c}c} \otimes \mathbb{1}_{\bar{q}q}; \quad (7.11a)$$

$$|\bar{c}c_{\mathbf{8}}, \bar{q}q_{\mathbf{8}}\rangle := \frac{1}{4\sqrt{2}} \lambda_{\bar{c}c}^a \otimes \lambda_{\bar{q}q}^a, \quad (7.11b)$$

where by $\lambda_{\bar{c}c}^a$, for example, we mean $\bar{c}_i (\lambda^a)_j^i c^j$ using latin letters for color indices.

With the notation $|cq_{\bar{\mathbf{3}}}, \bar{c}\bar{q}_{\mathbf{3}}\rangle$ we mean *an overall color singlet* state of a diquark-antidiquark pair:

$$[cq]_i [\bar{c}\bar{q}]^i = c_j \bar{c}^j q_k \bar{q}^k - c_j \bar{q}^j q_k \bar{c}^k. \quad (7.12)$$

Using the relation

$$(\lambda^a)_j^i (\lambda^a)_l^k = 2(\delta_l^i \delta_j^k - 1/3 \delta_j^i \delta_l^k) \quad (7.13)$$

one obtains

$$|cq_{\bar{\mathbf{3}}}, \bar{c}\bar{q}_{\mathbf{3}}\rangle = \frac{2}{3} \mathbb{1}_{\bar{c}c} \otimes \mathbb{1}_{\bar{q}q} - \frac{1}{2} \lambda_{\bar{c}c}^a \otimes \lambda_{\bar{q}q}^a = 2|\bar{c}c_{\mathbf{1}}, \bar{q}q_{\mathbf{1}}\rangle - 2\sqrt{2}|\bar{c}c_{\mathbf{8}}, \bar{q}q_{\mathbf{8}}\rangle, \quad (7.14)$$

i.e. the octet-octet component has *twice the probability* of the singlet-singlet one. The previous state can itself be normalized in the following way (multiply by $1/\sqrt{12}$)

$$|cq_{\bar{\mathbf{3}}}, \bar{c}\bar{q}_{\mathbf{3}}\rangle = \frac{1}{\sqrt{3}} \left(\frac{1}{3} \mathbb{1}_{\bar{c}c} \otimes \mathbb{1}_{\bar{q}q} - T_{\bar{c}c}^a \otimes T_{\bar{q}q}^a \right) \quad (7.15)$$

and use the $T = \lambda/2$ matrices.

Let us represent states of the fundamental representation with the symbol $|i\rangle$ whereas those of the anti-fundamental are $|^j\rangle$. Then we have

$$\langle_j|T^a|i\rangle = (T^a)_i^j; \quad (7.16a)$$

$$\langle^j|T^a|i\rangle = -(T^a)_j^i, \quad (7.16b)$$

i.e. one is the opposite of the transpose (complex-conjugate) of the other.

From the latter equation we get

$$T^a|i\rangle = -|^j\rangle(T^a)_j^i. \quad (7.17)$$

Consider a generic state $|v\rangle$

$$|v\rangle = |^i\rangle v_i, \quad (7.18)$$

then

$$|T^a v\rangle = T^a|v\rangle = T^a|^i\rangle v_i = -|^j\rangle(T^a)_j^i v_i. \quad (7.19)$$

We thus conclude that (multiply the latter by $\langle_k|$ and then rename $k \rightarrow i$)

$$T^a v_i = -(T^a)_i^j v_j, \quad (7.20)$$

whereas

$$T^a v^i = (T^a)_j^i v^j. \quad (7.21)$$

If, for example, we consider the action of the Hamiltonian term $H_{\bar{c}c} \propto T_{\bar{c}}^a T_c^a$, according to (7.20,7.21) we have to replace

$$\mathbb{1}_{\bar{c}c} \longrightarrow -(T^a)_i^j \bar{c}_j (T^a)_k^i c^k = -\bar{c}_j (T^a T^a)_k^j c^k. \quad (7.22)$$

Similarly if we start with some $\bar{c}_i \mathcal{O}_j^i c^j$, where \mathcal{O} is some combination of T 's, we have to replace

$$\bar{c}_i \mathcal{O}_j^i c^j \longrightarrow -\bar{c}_j (T^a \mathcal{O} T^a)_k^j c^k. \quad (7.23)$$

With this rules we can compute the action of H_{cq} on a diquark state defined in (7.15)

$$H_{cq}|cq_{\mathbf{3}}, \bar{c}\bar{q}_{\mathbf{3}}\rangle \propto \frac{1}{\sqrt{3}} \left(\frac{1}{3} T^b \otimes T^b - T^a T^b \otimes T^a T^b \right), \quad (7.24)$$

and thus

$$\langle cq_{\mathbf{3}}, \bar{c}\bar{q}_{\mathbf{3}}|H_{cq}|cq_{\mathbf{3}}, \bar{c}\bar{q}_{\mathbf{3}}\rangle \propto -\frac{1}{3} \left(-2 \frac{2}{3} - \frac{2}{3} \right) = \frac{2}{3}, \quad (7.25)$$

where we have used

$$\text{Tr}(T^a T^b T^c) = \frac{1}{4}(d^{abc} + i f^{abc}) \quad (7.26)$$

and

$$f^{abc} f^{abd} = 3\delta^{ab}, \quad (7.27a)$$

$$d^{abc} d^{abd} = \frac{5}{3}\delta^{ab}. \quad (7.27b)$$

As for the color, taking matrix elements on diquark-antidiquark color-neutral states amounts to redefine the chromomagnetic couplings by some numerical factor: $2/3$

when the H_{cq} and $H_{\bar{c}\bar{q}}$ terms are considered. Actually we assume that the dominant couplings in the Hamiltonian are κ_{cq} and $\kappa_{\bar{c}\bar{q}}$, *i.e.*, intra-diquark interactions. We take them to be equal $\kappa = \kappa_{cq} = \kappa_{\bar{c}\bar{q}}$ ¹.

7.3 Diquark-antidiquark States with $L = 0$

The following discussion is mostly based on a recent paper [286] where, as anticipated, a ‘type-II’ tetraquark model is introduced. The ‘type-I’ is briefly discussed in Sec. 7.7 for historical reasons.

7.3.1 The X tetraquark

Consider a tetraquark made up of two c quarks and two light quarks, with the same flavor: a neutral component. Using explicit spin indices s, b, r, d we write them in the order:

$$c_s \quad q_b \quad \bar{q}_r \quad \bar{c}_d. \quad (7.29)$$

Assume that the cq pair has spin 1 whereas the antidiquark $\bar{q}\bar{c}$ has spin 0. Then the spin indices are saturated by the operators

$$\sigma_{sa}^2 \sigma_{ab}^i \quad (7.30)$$

for the cq pair and

$$\sigma_{rd}^2 \quad (7.31)$$

for $\bar{q}\bar{c}$, where repeated indices are summed. We might write the operators as

$$\sigma_{sa}^2 \sigma_{aq}^i \delta_{qb} \quad \sigma_{rt}^2 \delta_{td} \quad (7.32)$$

and recall that

$$\delta_{qb} \delta_{td} = \frac{1}{2} \delta_{qd} \delta_{tb} + \frac{1}{2} \sigma_{qd}^\ell \sigma_{tb}^\ell. \quad (7.33)$$

Let us consider the first term in (7.33) and plug it into (7.32)

$$\frac{1}{2} \sigma_{sa}^2 \sigma_{ad}^i \quad \sigma_{rb}^2, \quad (7.34)$$

therefore forcing the $c\bar{c}$ pair to be spin 1 and $q\bar{q}$ to be spin 0. Strong interactions are not supposed to change the heavy spin, thus we may assume that the color octet components of the $c\bar{c}$ will maintain spin 1 configuration whereas light quarks can rearrange their spins, when in the octet configuration (twice as probable as the singlet one; see Eq. (7.14)), in such a way to fulfill decay quantum number conservation laws.

¹ If extra-diquark couplings were considered we could determine them, *e.g.* $\kappa_{c\bar{c}}$, from the masses of standard $L = 0$ mesons observing that

$$\langle cq_{\mathbf{3}}, \bar{c}\bar{q}_{\mathbf{3}} | H_{c\bar{c}} | cq_{\mathbf{3}}, \bar{c}\bar{q}_{\mathbf{3}} \rangle = \frac{1}{4} \langle \bar{c}c_1, \bar{q}q_1 | H_{c\bar{c}} | \bar{c}c_1, \bar{q}q_1 \rangle \quad (7.28)$$

Consider now the second term in (7.33) and plug it into (7.32) to obtain

$$\frac{1}{2}\sigma_{sa}^2\sigma_{aq}^i\sigma_{qd}^\ell - \sigma_{rt}^2\sigma_{tb}^\ell. \quad (7.35)$$

Here we use that

$$(\sigma^i\sigma^\ell)_{ad} = \delta^{i\ell}\delta_{ad} + i\epsilon^{ilm}\sigma_{ad}^m. \quad (7.36)$$

Consider the first term in (7.36) and plug it back into (7.35) to obtain

$$\frac{1}{2}\sigma_{sd}^2 - \sigma_{rt}^2\sigma_{tb}^i. \quad (7.37)$$

This term forces the $c\bar{c}$ pair to be spin 0 and the $q\bar{q}$ pair to be spin 1. Inserting the second term on the right-hand-side of (7.36) into (7.35) we have instead

$$-\frac{i}{2}\epsilon^{im\ell}\sigma_{sa}^2\sigma_{ad}^m - \sigma_{rt}^2\sigma_{tb}^\ell, \quad (7.38)$$

forcing both pairs to be spin 1 and the tetraquark to be spin 1.

Here we may introduce the definitions:

$$|1_{\mathbf{q}}, 0_{\bar{\mathbf{q}}}\rangle = \frac{1}{2}\sigma^2\sigma^i \otimes \sigma^2; \quad (7.39a)$$

$$|0_{\mathbf{q}}, 1_{\bar{\mathbf{q}}}\rangle = \frac{1}{2}\sigma^2 \otimes \sigma^2\sigma^i; \quad (7.39b)$$

$$|1_{\mathbf{q}}, 1_{\bar{\mathbf{q}}}\rangle_{J=1} = \frac{i}{2\sqrt{2}}\epsilon^{ijk}\sigma^2\sigma^j \otimes \sigma^2\sigma^k. \quad (7.39c)$$

With the symbol \mathbf{q} we either mean a diquark in the order cq or $\bar{c}\bar{q}$ or a quark-antiquark pair in the order $c\bar{c}$ or $q\bar{q}$. The ordering is relevant. The normalizations in (7.39a,7.39b,7.39c) are obtained using that $\langle Q_a|Q_b\rangle = \delta_{ab}\dots$, where $Q = c, q$. Therefore, taking for example (7.39c), we have (summing over repeated indices)

$$\begin{aligned} & (\delta^{j\lambda}\delta^{k\rho} - \delta^{j\rho}\delta^{k\lambda}) \left[(\sigma^2\sigma^j)_{rs}(\sigma^2\sigma^\lambda)_{rs}(\sigma^2\sigma^k)_{tu}(\sigma^2\sigma^\rho)_{tu} \right] = \\ & = \text{Tr}((\sigma^j)^T\sigma^j)\text{Tr}((\sigma^k)^T\sigma^k) - \text{Tr}((\sigma^j)^T\sigma^k)\text{Tr}((\sigma^k)^T\sigma^j) = \\ & = (2 - 2 + 2)(2 - 2 + 2) - (2 \cdot 2 + 2 \cdot 2 + 2 \cdot 2) = -8, \end{aligned} \quad (7.40)$$

therefore we choose the normalization $i/(2\sqrt{2})$.

According to the quark ordering in (7.29), the spin 0 component will be

$$\bar{q}\sigma^2\bar{c} \quad (7.41)$$

whereas in the definition of a heavy light diquark state, see (7.39a), might also be $\bar{c}\sigma^2\bar{q}$ (heavy quark on the left). On the other hand:

$$\bar{q}\sigma^2\bar{c} = -\bar{c}(\sigma^2)^T\bar{q} = \bar{c}\sigma^2\bar{q}. \quad (7.42)$$

This is not the case if we consider $\bar{q}\sigma^2\sigma^i\bar{c}$:

$$\bar{q}\sigma^2\sigma^i\bar{c} = -\bar{c}(\sigma^2\sigma^i)^T\bar{q} = \bar{c}(\sigma^i)^T\sigma^2\bar{q} = -\bar{c}\sigma^2\sigma^i\bar{q}. \quad (7.43)$$

Therefore, putting together (7.34,7.37,7.38), and keeping in mind that the following states are defined up to an overall minus sign (depending on the initial definition of diquark), we obtain

$$2|1_{cq}, 0_{\bar{c}\bar{q}}\rangle = |1_{c\bar{c}}, 0_{q\bar{q}}\rangle - |0_{c\bar{c}}, 1_{q\bar{q}}\rangle + \sqrt{2}|1_{c\bar{c}}, 1_{q\bar{q}}\rangle_{J=1}. \quad (7.44)$$

On the other hand, if we restart from (7.29) but with cq taken with spin 0 and $\bar{q}\bar{c}$ with spin 1 we get

$$-2|0_{cq}, 1_{\bar{c}\bar{q}}\rangle = |1_{c\bar{c}}, 0_{q\bar{q}}\rangle - |0_{c\bar{c}}, 1_{q\bar{q}}\rangle - \sqrt{2}|1_{c\bar{c}}, 1_{q\bar{q}}\rangle_{J=1}. \quad (7.45)$$

Subtracting (7.45) from (7.44) we therefore obtain the result

$$\frac{|1_{cq}, 0_{\bar{c}\bar{q}}\rangle + |0_{cq}, 1_{\bar{c}\bar{q}}\rangle}{\sqrt{2}} = |1_{c\bar{c}}, 1_{q\bar{q}}\rangle_{J=1} \equiv X. \quad (7.46)$$

Since diquarks are defined to be positive parity states, overall we have $J^P = 1^+$ and $C = +1$. This diquark-antidiquark arrangement is a natural candidate to describe the $X(3872)$, which is a 1^{++} resonance decaying into $J/\psi + \rho/\omega$, compatibly with the $|1_{c\bar{c}}, 1_{q\bar{q}}\rangle_{J=1}$ assignment – especially for what concerns the heavy spin.

If we had started in (7.29) with the ordering

$$c_s \quad q_b \quad \bar{c}_r \quad \bar{q}_d \quad (7.47)$$

then in place of (7.44) and (7.45) (exchange labels $\bar{c} \leftrightarrow \bar{q}$) we would have obtained:

$$2|1_{cq}, 0_{\bar{c}\bar{q}}\rangle = |1_{c\bar{q}}, 0_{q\bar{c}}\rangle - |0_{c\bar{q}}, 1_{q\bar{c}}\rangle + \sqrt{2}|1_{c\bar{q}}, 1_{q\bar{c}}\rangle_{J=1}; \quad (7.48a)$$

$$2|0_{cq}, 1_{\bar{c}\bar{q}}\rangle = |1_{c\bar{q}}, 0_{q\bar{c}}\rangle - |0_{c\bar{q}}, 1_{q\bar{c}}\rangle - \sqrt{2}|1_{c\bar{q}}, 1_{q\bar{c}}\rangle_{J=1}. \quad (7.48b)$$

or

$$\frac{|1_{cq}, 0_{\bar{c}\bar{q}}\rangle + |0_{cq}, 1_{\bar{c}\bar{q}}\rangle}{\sqrt{2}} = \frac{|1_{c\bar{q}}, 0_{q\bar{c}}\rangle - |0_{c\bar{q}}, 1_{q\bar{c}}\rangle}{\sqrt{2}}, \quad (7.49)$$

which is compatible with the DD^* decay mode of the $X(3872)$. Anyway, light quark spins in $Q\bar{q}$ or $\bar{Q}q$ configurations might rearrange also to allow DD or D^*D^* decays although the latter is phase space forbidden and the former is simply forbidden by quantum numbers.

7.3.2 The Z tetraquark

The orthogonal combination to the lhs of (7.46) might be formed, namely:

$$Z = \frac{|1_{cq}, 0_{\bar{c}\bar{q}}\rangle - |0_{cq}, 1_{\bar{c}\bar{q}}\rangle}{\sqrt{2}}. \quad (7.50)$$

This has $J^P = 1^+$ and $C = -1$ for the neutral component (if an isospin triplet is to be considered, the G -parity has to be $G = +1$). Using (7.44) and (7.45) we obtain

$$Z = \frac{|1_{cq}, 0_{\bar{c}\bar{q}}\rangle - |0_{cq}, 1_{\bar{c}\bar{q}}\rangle}{\sqrt{2}} = \frac{|1_{c\bar{c}}, 0_{q\bar{q}}\rangle - |0_{c\bar{c}}, 1_{q\bar{q}}\rangle}{\sqrt{2}}. \quad (7.51)$$

The state in the quark-antiquark basis has $C = -1$ since $C = (-1)^{L+s_{q\bar{q}}+s_{c\bar{c}}}$. In the quark-antiquark basis there is another state with $C = -1$, orthogonal to Z

$$Z' = \frac{|1_{c\bar{c}}, 0_{q\bar{q}}\rangle + |0_{c\bar{c}}, 1_{q\bar{q}}\rangle}{\sqrt{2}}. \quad (7.52)$$

From what just found (reversing the reasoning leading to Eq. (7.46)) this state, in the diquark-antidiquark basis, corresponds to

$$Z' = |1_{cq}, 1_{\bar{c}\bar{q}}\rangle_{J=1}, \quad (7.53)$$

which is indeed a 1^{+-} state. Exchanging the coordinates, spins and charges of two fermions/bosons having each spin s , the total wavefunction has to be completely antisymmetric/symmetric under this exchange:

$$(-1)^L(-1)^{2s+S}C = \mp 1, \quad (7.54)$$

which in the case of (7.53) is

$$(-1)^0(-1)^{2+1}C = +1, \quad (7.55)$$

giving $C = -1$. The case of $X = |1_{c\bar{c}}, 1_{q\bar{q}}\rangle_{J=1}$ is different as the charge conjugation operator concerns the distinct $c\bar{c}$ and $q\bar{q}$ pairs.

Linear combinations of Z and Z' which diagonalize the spin-spin Hamiltonian can be identified with $Z(3900)$ and $Z(4020)$.

If on the other hand we had started with (7.47), using (7.48a,7.48b), we would have found

$$Z = \frac{|1_{cq}, 0_{\bar{c}\bar{q}}\rangle - |0_{cq}, 1_{\bar{c}\bar{q}}\rangle}{\sqrt{2}} = |1_{c\bar{q}}, 1_{q\bar{c}}\rangle_{J=1}, \quad (7.56)$$

suggesting a D^*D^* decay for the color singlet component, which is phase-space suppressed for the $Z(3900)$. Again, light quarks might rearrange their spins and decay into DD^* , so that nothing prevents us to assign $Z = Z(3900)$.

Similarly we obtain that (exchange $q \leftrightarrow \bar{q}$ in (7.48a,7.48b) or simply in (7.56))

$$Z' = |1_{cq}, 1_{\bar{c}\bar{q}}\rangle_{J=1} = \frac{|1_{c\bar{q}}, 0_{q\bar{c}}\rangle + |0_{c\bar{q}}, 1_{q\bar{c}}\rangle}{\sqrt{2}}, \quad (7.57)$$

apart from an overall minus sign (from (7.43)); we will anyway assign $Z' = Z(4020)$ which might preferably decay into D^*D^* rearranging light quark spins.

7.3.3 Scalar and Tensor states

The diquark-antidiquark model also allows for $J^P = 0^+, 2^+$ states with $C = +1$. We have two $J^P = 0^+$ states and a tensor one:

$$X_0 = |0_{cq}, 0_{\bar{c}\bar{q}}\rangle; \quad (7.58a)$$

$$X'_0 = |1_{cq}, 1_{\bar{c}\bar{q}}\rangle_{J=0}; \quad (7.58b)$$

$$X_2 = |1_{cq}, 1_{\bar{c}\bar{q}}\rangle_{J=2}, \quad (7.58c)$$

which are all charge-conjugation even. We use the definitions

$$|0_{\mathbf{q}}, 0_{\mathbf{q}}\rangle = \frac{1}{2}\sigma^2 \otimes \sigma^2; \quad (7.59a)$$

$$|1_{\mathbf{q}}, 1_{\mathbf{q}}\rangle_{J=0} = \frac{1}{2\sqrt{3}}\sigma^2\sigma^i \otimes \sigma^2\sigma^i; \quad (7.59b)$$

$$|1_{\mathbf{q}}, 1_{\mathbf{q}}\rangle_{J=2} = \frac{1}{2}\left(\sigma^2\sigma^{(i} \otimes \sigma^2\sigma^{j)} - \frac{1}{3}\delta^{ij}\sigma^2\sigma^\ell \otimes \sigma^2\sigma^\ell\right), \quad (7.59c)$$

where ij indices are symmetrized; in the latter equation (a factor of $1/2$ has to be included in the symmetrization) and the trace is subtracted.

The normalization $1/\sqrt{N}$ in (7.59b) is chosen in such a way that the square of

$$\frac{1}{\sqrt{N}}(\sigma^2\sigma^i)_{rs}(\sigma^2\sigma^i)_{rs} = \frac{1}{\sqrt{N}}\text{Tr}\left[(\sigma^2\sigma^i)^T(\sigma^2\sigma^i)\right] \quad (7.60)$$

is equal to 1:

$$\frac{1}{N}\left(\text{Tr}\left[(\sigma^2\sigma^i)^T(\sigma^2\sigma^i)\right]\right)^2 \equiv \frac{1}{N}\sum_i\left(\text{Tr}\left[(\sigma^i)^T\sigma^i\right]\right)^2 = 1, \quad (7.61)$$

thus $N = 12$. In the $J = 2$ case we have for the first term in parentheses (7.59c):

$$\frac{2}{4}\text{Tr}\left[(\sigma^i)^T\sigma^i\right]\text{Tr}\left[(\sigma^j)^T\sigma^j\right] + \frac{2}{4}\text{Tr}\left[(\sigma^i)^T\sigma^j\right]\text{Tr}\left[(\sigma^j)^T\sigma^i\right] = 8, \quad (7.62)$$

whereas the second term squared gives $1/9 \times 3 \times 12 = 4$. The crossed term is $-2 \times 1/3 \times 12 = -8$ so that $N = 8 + 4 - 8 = 4$.

Now we recall that

$$\frac{1}{2}\boldsymbol{\sigma}_{ad} \cdot \boldsymbol{\sigma}_{cb} + \frac{1}{2}\delta_{ad}\delta_{cb} = \delta_{ab}\delta_{cd} \quad (7.63)$$

and observe that (7.59a) may be written as

$$\frac{1}{2}(c_s \sigma_{sa}^2 \delta_{ab} q_b) \otimes (\bar{q}_r \sigma_{rc}^2 \delta_{cd} \bar{c}_d), \quad (7.64)$$

which contains $\delta_{ab}\delta_{cd}$. Substituting the completeness relation (7.63) in place of $\delta_{ab}\delta_{cd}$ in the latter expression we get

$$X_0 = \frac{1}{2}|0_{c\bar{c}}, 0_{q\bar{q}}\rangle - \frac{\sqrt{3}}{2}|1_{c\bar{c}}, 1_{q\bar{q}}\rangle_{J=0}, \quad (7.65)$$

where the minus sign arises to preserve the $q\bar{q}$ ordering (instead of $\bar{q}q$ – see discussion before Eq. (7.41)) whereas the factor of $\sqrt{3}$ is introduced in agreement with (7.59b).

Consider now (7.59b) which might be written as (because of (7.43))

$$-\frac{1}{2\sqrt{3}}(c_s \sigma_{sa}^2 \sigma_{ab}^i q_b) \otimes (\bar{q}_r \sigma_{rc}^2 \sigma_{cd}^i \bar{c}_d) \quad (7.66)$$

and make use of the relation

$$\frac{3}{2}\delta_{ad}\delta_{cb} - \frac{1}{2}\boldsymbol{\sigma}_{ad} \cdot \boldsymbol{\sigma}_{cb} = \boldsymbol{\sigma}_{ab} \cdot \boldsymbol{\sigma}_{cd}, \quad (7.67)$$

which immediately leads to

$$X'_0 = \frac{\sqrt{3}}{2} |0_{c\bar{c}}, 0_{q\bar{q}}\rangle + \frac{1}{2} |1_{c\bar{c}}, 1_{q\bar{q}}\rangle_{J=0}, \quad (7.68)$$

up to an inessential overall -1 sign. Considering the conservation of the heavy quark spin, we see that both scalar states found might decay into a spin 0 or spin 1 charmonium.

Finally consider (7.59c):

$$(c\sigma^2\sigma^i q) \otimes (\bar{c}\sigma^2\sigma^j \bar{q}) \quad (7.69)$$

With the usual Fierz transformation, we have

$$\frac{1}{2} (c\sigma^2\sigma^i \bar{c}) \otimes (\bar{q}\sigma^2\sigma^j q) + \frac{1}{2} (c\sigma^2\sigma^i\sigma^l \bar{c}) \otimes (\bar{q}\sigma^2\sigma^j\sigma^l q), \quad (7.70)$$

and symmetrizing and using the Pauli matrices properties, we get

$$- (c\sigma^2\sigma^i \bar{c}) \otimes (q\sigma^2\sigma^j \bar{q}) + \frac{1}{2} \delta^{ij} (c\sigma^2 \bar{c} \otimes q\sigma^2 \bar{q}) + \frac{1}{2} \delta^{ij} (c\sigma^2\sigma^m \bar{c}) \otimes (q\sigma^2\sigma^m \bar{q}). \quad (7.71)$$

The term proportional to δ^{ij} in Eq. (7.59c) after a Fierz transformation cancels the singlet terms in Eq. (7.71). We conclude that

$$|1_{cq}, 1_{\bar{c}\bar{q}}\rangle_{J=2} = |1_{c\bar{c}}, 1_{q\bar{q}}\rangle_{J=2}. \quad (7.72)$$

We summarize these results in Table 7.2.

J^{PC}	$cq \bar{c}\bar{q}$	$c\bar{c} q\bar{q}$	Assig.	Decays
0^{++}	$ 0, 0\rangle$	$(0, 0\rangle + \sqrt{3} 1, 1\rangle_0)/2$	$X_0(\sim 3770)$	$\eta_c, J/\psi + \text{light}$
0^{++}	$ 1, 1\rangle_0$	$(\sqrt{3} 0, 0\rangle - 1, 1\rangle_0)/2$	$X'_0(\sim 4000)$	$\eta_c, J/\psi + \text{light}$
1^{++}	$(1, 0\rangle + 0, 1\rangle)/\sqrt{2}$	$ 1, 1\rangle_1$	$X(3872)$	$J/\psi + \rho/\omega, DD^*$
1^{+-}	$(1, 0\rangle - 0, 1\rangle)/\sqrt{2}$	$(1, 0\rangle - 0, 1\rangle)/\sqrt{2}$	$Z_c(3900)$	$J/\psi \pi, h_c \pi, \eta_c \rho$
1^{+-}	$ 1, 1\rangle_1$	$(1, 0\rangle + 0, 1\rangle)/\sqrt{2}$	$Z'_c(4020)$	$J/\psi \pi, h_c \pi, \eta_c \rho$
2^{++}	$ 1, 1\rangle_2$	$ 1, 1\rangle_2$	$X_2(\sim 4000)$	$J/\psi + \text{light}$

Table 7.2. We list the states obtained together with possible assignments and decay modes.

We refer here to the neutral components. A $G = +1$ parity may be assigned to the Z, Z' particles. Searches by *BABAR* and *Belle* still exclude a $I = 1$ assignment for the $X(3872)$, however a mixed $I = 1$ and $I = 0$ seems possible as well as very broad charged partners of $X(3872)$.

7.4 Spectrum of $L = 0$ states

We assume that the spin-spin interactions within the diquark shells are dominant with respect to quark-antiquark interactions. Then the Hamiltonian would be

$$H \approx 2\kappa(\mathbf{S}_q \cdot \mathbf{S}_c + \mathbf{S}_{\bar{q}} \cdot \mathbf{S}_{\bar{c}}). \quad (7.73)$$

Consider for example

$$4\mathbf{S}_q \cdot \mathbf{S}_c |1_{cq}, 0_{\bar{c}\bar{q}}\rangle = \boldsymbol{\sigma}_{(q)} \cdot \boldsymbol{\sigma}_{(c)} |1_{cq}, 0_{\bar{c}\bar{q}}\rangle := \frac{1}{2}(\sigma^j)^T \sigma^2 \sigma^i \sigma^j \otimes \sigma^2, \quad (7.74)$$

where summation over j is understood. The matrix $(\sigma^j)^T$ works on c whereas σ^j on q . Considering that

$$\frac{1}{2}(\sigma^j)^T \sigma^2 \sigma^i \sigma^j \otimes \sigma^2 = -\frac{1}{2}(\sigma^2 \sigma^j \sigma^i \sigma^j) \otimes \sigma^2 \equiv \frac{1}{2}\sigma^2 \sigma^i \otimes \sigma^2 = |1_{cq}, 0_{\bar{c}\bar{q}}\rangle, \quad (7.75)$$

where we have used $i\epsilon^{ijk}\sigma^j\sigma^k = i\epsilon^{ijk}i\epsilon^{jkl}\sigma^l = -2\sigma^i$. Considering also the antiquark contribution one readily finds

$$4\mathbf{S}_{\bar{q}} \cdot \mathbf{S}_{\bar{c}} |1_{cq}, 0_{\bar{c}\bar{q}}\rangle = -3|1_{cq}, 0_{\bar{c}\bar{q}}\rangle, \quad (7.76)$$

thus

$$4(\mathbf{S}_q \cdot \mathbf{S}_c + \mathbf{S}_{\bar{q}} \cdot \mathbf{S}_{\bar{c}}) |1_{cq}, 0_{\bar{c}\bar{q}}\rangle = -2|1_{cq}, 0_{\bar{c}\bar{q}}\rangle \quad (7.77)$$

and

$$H |1_{cq}, 0_{\bar{c}\bar{q}}\rangle = -\kappa |1_{cq}, 0_{\bar{c}\bar{q}}\rangle. \quad (7.78)$$

Similarly:

$$H |0_{cq}, 1_{\bar{c}\bar{q}}\rangle = -\kappa |0_{cq}, 1_{\bar{c}\bar{q}}\rangle; \quad (7.79a)$$

$$H |1_{cq}, 1_{\bar{c}\bar{q}}\rangle_{J=1} = \kappa |1_{cq}, 1_{\bar{c}\bar{q}}\rangle_{J=1}. \quad (7.79b)$$

We can also determine

$$H |0_{cq}, 0_{\bar{c}\bar{q}}\rangle = -3\kappa |0_{cq}, 0_{\bar{c}\bar{q}}\rangle; \quad (7.80a)$$

$$H |1_{cq}, 1_{\bar{c}\bar{q}}\rangle_{J=0} = \kappa |1_{cq}, 1_{\bar{c}\bar{q}}\rangle_{J=0}. \quad (7.80b)$$

The Hamiltonian (7.73) is diagonal in the diquark-antidiquark basis formed by the 1^{+-} states of Table 7.2:

$$(H)_{1^{+-}} = \begin{pmatrix} -\kappa & 0 \\ 0 & \kappa \end{pmatrix}, \quad (7.81)$$

$|1\rangle = 1/\sqrt{2}(|1, 0\rangle - |0, 1\rangle)$, $|2\rangle = |1, 1\rangle_{J=1}$. This requires $|1\rangle$ to be lighter than $|2\rangle$. Similarly:

$$(H)_{1^{++}} = -\kappa; \quad (7.82a)$$

$$(H)_{2^{++}} = \kappa, \quad (7.82b)$$

so that we conclude that $X(3872)$ and $Z(3900)$ are degenerate in first approximation their masses being twice the diquark mass plus the same spin-spin interaction correction

$$M(X, Z) = 2m_{[cq]} - \kappa. \quad (7.83)$$

The Z' (and the hypothetical tensor state) is instead heavier by a gap of 2κ :

$$M(Z') = 2m_{[cq]} + \kappa. \quad (7.84)$$

As for the scalar case, from (7.80a,7.80b) we have

$$(H)_{0^{++}} = -3\kappa; \quad (7.85a)$$

$$(H)_{0^{++'}} = \kappa, \quad (7.85b)$$

showing what was anticipated in Table 7.2, *i.e.* that $M(X'_0) \sim M(X_2)$.

Considering an average mass value between $X(3872)$ and $Z(3900)$ we can solve finding $m_{[cq]} \simeq 1976$ MeV and $\kappa \simeq 67$ MeV, indicating that $M(0^{++}) \simeq 3750$ MeV and $M(X_2) \sim M(X'_0) \simeq 4000$ MeV – for a pictorial representation see Figure 7.1.

In this scheme we propose that the newly discovered $Z(4430)$ is the first radial excitation of the $Z(3900)$ as $M(Z(4430)) - M(Z(3900)) \simeq M(\psi(2S)) - M(J/\psi)$.

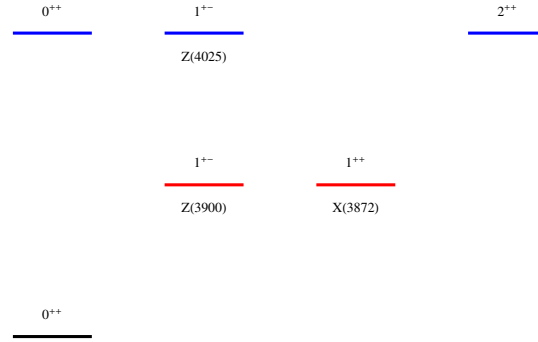


Figure 7.1. The mass pattern dictated by the color-spin Hamiltonian and the construction of states is shown and level degeneracies are highlighted.

7.5 Diquark-antidiquark States with $L = 1$

Tetraquarks with $J^{PC} = 1^{--}$ can be obtained with odd values of the angular momentum; here we set $L = 1$ and select charge-conjugation odd states.

In the diquark-antidiquark basis of $cq \bar{c}\bar{q}$ we have:

$$Y_1 = |0, 0\rangle; \quad C = (-1)^{L=1} \quad (7.86a)$$

$$Y_2 = \frac{|1, 0\rangle + |0, 1\rangle}{\sqrt{2}}; \quad C = (-1)^{L=1} \quad (7.86b)$$

$$Y_3 = |1, 1\rangle_{S=0}; \quad C = (-1)^L (-1)^{2s+S} = (-1)^1 (-1)^{2 \cdot 1 + 0} \quad (7.86c)$$

$$Y_4 = |1, 1\rangle_{S=2}; \quad C = (-1)^1 (-1)^{2 \cdot 1 + 2} \quad (7.86d)$$

Aside from orbital angular momentum considerations we can still make use of Table 7.2 to read the $c\bar{c}$ (conserved) spin; see Table 7.3. Observe that the spin structure of Y_2 and X in (7.46) is exactly the same. The mass difference between Y_2 and X might entirely be attributed to the orbital excitation of Y_2 . The fact that Y_2 and X have the same spin structure also suggests that radiative transitions with $\Delta L = 1$ and $\Delta S_{c\bar{c}} = 0$ might occur:

$$Y_2 \rightarrow \gamma X, \quad (7.87)$$

State	$P(S_{c\bar{c}} = 1) : P(S_{c\bar{c}} = 0)$	Assignment	Radiative Decay
Y_1	3:1	$Y(4008)$	$\gamma + X_0$
Y_2	1:0	$Y(4260)$	$\gamma + X$
Y_3	1:3	$Y(4290)/Y(4220)$	$\gamma + X'_0$
Y_4	1:0	$Y(4630)$	$\gamma + X_2$

Table 7.3. The relative probability of having spin 1 versus spin 0 in the $c\bar{c}$ pair as read by Table 7.2. Observe that Y_3 is predicted to decay preferably in $h_c(1P)$ where $S_{c\bar{c}} = 0$. The states $Y(4290)$ and $Y(4220)$ correspond either to the broad structure in the h_c channel as described by Yuan [91, 92] or the narrow one. In this respects the mass ordering can be reversed Y_3 becoming lighter than Y_2 if the $Y(4220)$ assignment is taken.

as confirmed by the conspicuous radiative decay mode [98]

$$Y(4260) \rightarrow X(3872) + \gamma. \quad (7.88)$$

Other transitions are reported in Table 7.3.

The experimentally well established $Y(4360)$ and $Y(4660)$ are interpreted as radial excitations of $Y_1 = Y(4008)$ (see Table 7.3) and $Y_2 = Y(4260)$. We may note correspondences as $M(\chi_{bJ}(2P)) - M(\chi_{bJ}(1P)) \simeq M(Y(4360)) - M(Y(4008))$ and $M(\chi_{cJ}(2P)) - M(\chi_{cJ}(1P)) \simeq M(Y(4660)) - M(Y(4260))$. For the identification of the Y_3 state as the structures seen in $e^+e^- \rightarrow h_c\pi\pi, \chi_{c0}\omega$, see Sec. 7.6.1.

As for the $Y(4630)$, decaying predominantly into $\Lambda_c\bar{\Lambda}_c$, we recall that there is also the possibility of its assignment to a tetraquark degenerate with $Y(4660)$ [145].

7.6 Spectrum of $L = 1$ states

We use the same Hamiltonian form (7.73) with the addition of a spin-orbit and a purely orbital term – here the chromomagnetic coupling κ' is taken to be different from κ used in (7.73). We have then:

$$H \approx 2\kappa'(S_q \cdot S_c + S_{\bar{q}} \cdot S_{\bar{c}}) - 2A \mathbf{S} \cdot \mathbf{L} + \frac{1}{2}B \mathbf{L}^2, \quad (7.89)$$

in such a way that energy increases for increasing \mathbf{L}^2 and \mathbf{S}^2 , provided κ', A, B are positive; indeed $2\mathbf{L} \cdot \mathbf{S} = 2 - L(L+1) - S(S+1)$ and the masses of Y states will be given by

$$M = M'_0 + \kappa'(s(s+1) + \bar{s}(\bar{s}+1) - 3) + A(L(L+1) + S(S+1) - 2) + B \frac{L(L+1)}{2}, \quad (7.90)$$

where S, \bar{S} are the total spins of diquark and antidiquark. The latter equation can be simplified to

$$M = M_0 + (A + B/2)L(L+1) + AS(S+1) + \kappa'(s(s+1) + \bar{s}(\bar{s}+1)) \quad (7.91)$$

with

$$M_0 = M'_0 - 2A - 3\kappa'. \quad (7.92)$$

From Eq. (7.91), the mass of the state Y_1 in (7.86a) is given by

$$M_1 = M_0 + 2(A + B/2) \quad (7.93)$$

for $s = \bar{s} = 0$, therefore implying $S = 0$, and $L = 1$. The Y_2 state in (7.86b) has $s = 1$ or $\bar{s} = 1$, thus $S = 1$ – considering that M_0 contains $-3\kappa'$ we can determine the mass gap between Y_2 and Y_1 :

$$M_2 - M_1 = 2\kappa' + 2A, \quad (7.94)$$

requiring $M_2 > M_1$. The Y_3 state has both spins $s = \bar{s} = 1$ but $S = 0$ so that

$$M_3 - M_2 = 2\kappa' - 2A, \quad (7.95)$$

which can take either sign depending on $\kappa' - A$ difference; κ' and A have in principle similar size. Finally Y_4 has both spins $s = \bar{s} = 1$ and $S = 2$ so that

$$M_4 - M_3 = 6A \quad (7.96)$$

requiring $M_4 > M_3$. So the mass ordering is M_1, M_2, M_3, M_4 or M_1, M_3, M_2, M_4 from lighter to heavier. Using the assignments in Table 7.3 (choosing $Y_3 = Y(4290)$), from (7.94,7.95) we obtain:

$$4008 + 2\kappa' + 2A = 4260; \quad (7.97a)$$

$$4260 + 2\kappa' - 2A = 4290, \quad (7.97b)$$

in units of MeV, giving

$$\kappa' = 71; \quad A = 56. \quad (7.98)$$

If we had chosen $Y_3 = Y(4220)$ we would have obtained

$$\kappa' = 53; \quad A = 73. \quad (7.99)$$

The values found for κ' have to be compared with the value of $\kappa = 67$ MeV obtained studying the spectrum of $L = 0$ states. Both choices are reasonably consistent with it also in consideration of the simplicity of the model described. With respect to the results found in the original paper [264], we can conclude that diquarks in tetraquarks are expected to behave in a different way from diquarks in baryons: in the latter case the coupling κ is found to be rather smaller $\kappa \simeq 22$ MeV.

As a crosscheck, observe that from (7.96) we get a reasonable agreement with the assigned mass of Y_4 :

$$M(Y_4 = Y(4630)) = 4290(4220) + 6 \times 56(73) = 4626(4658). \quad (7.100)$$

In formula (7.91), the orbital contribution is $2A+B$. Considering that X in (7.46) and Y_2 have the same spin structure, we can conclude that the difference in mass $Y(4260) - X(3872) = 2A + B$, giving a value of B in good agreement with what discussed in [287].

7.6.1 The $Y(4220)$ state [6]

In [6], we analyzed the BES III data of $e^+e^- \rightarrow h_c\pi\pi$ [71] and $\rightarrow \chi_{c0}\omega$ [93] and discussed if the structures seen in these two channels are compatible with each other and with the Y_3 assignment of the tetraquark model (see Sec. 7.6).

In the $h_c\pi^+\pi^-$ invariant mass distribution, we add to the BES dataset the experimental point $\sigma_{h_c\pi^+\pi^-}(4.17 \text{ GeV}) = (15.6 \pm 4.2) \text{ pb}^2$ by CLEO- c [153], with statistical and systematic errors added in quadrature. For the BES data, we take into account only statistical errors, since the systematic ones are common to all points and are not expected to modify the shape of the distribution.

We fit the $h_c\pi^+\pi^-$ and $\chi_{c0}\omega$ data with the sum of a Breit-Wigner corrected for the energy dependence given by PCAC, and a pure phase-space background. To test our hypothesis, the mass and the width of the resonance are constrained to be the same in both channels. Thus, the fitting functions are:

$$\sigma_{h_c\pi^+\pi^-}(m) = \left| A\sqrt{\text{PS}_3(m)} + Be^{i\phi_1}\sqrt{\frac{\text{PS}'_3(m)}{\text{PS}'_3(m_0)}} \text{BW}(m, m_0, \Gamma) \right|^2, \quad (7.101)$$

$$\sigma_{\chi_{c0}\omega}(m) = \left| C + \frac{De^{i\phi_2}}{\sqrt{\text{PS}_2(m_0)}} \text{BW}(m, m_0, \Gamma) \right|^2 \text{PS}_2(m), \quad (7.102)$$

where m_0 and Γ are the mass and width of the resonance, m is the invariant mass of the system, $\text{BW}(m, m_0, \Gamma) = (m^2 - m_0^2 + im_0\Gamma)^{-1}$, $B = \sqrt{12\pi\mathcal{B}_{h_c\pi^+\pi^-}\Gamma_{ee}\Gamma}$, $D = \sqrt{12\pi\mathcal{B}_{\chi_{c0}\omega}\Gamma_{ee}\Gamma}$, PS_n is the n -body phase space, and PS'_3 is the PCAC-corrected phase space [182, 288], namely:

$$\text{PS}'_3 \propto \int d\Phi_3 (E^+p^- + E^-p^+)^2, \quad (7.103)$$

where E^\pm (p^\pm) is the energy (momentum) of π^\pm in the CM frame.

With this model, we get a mass of $4213 \pm 12 \text{ MeV}$ and a width of $52 \pm 24 \text{ MeV}$. The $\chi^2/\text{DOF} = 17.38/15$, corresponding to a $\text{Prob}(\chi^2) = 30\%$ (see Figure 7.2). The fit gives two distinct solutions for the Breit-Wigner amplitudes, corresponding to a constructive and destructive interference in the $h_c\pi^+\pi^-$ channel, respectively.³ The significance with respect to a pure background hypothesis is $> 10\sigma$.

By comparing the Breit-Wigner amplitudes in the two channels, we get the ratio:

$$\frac{\mathcal{B}(Y(4220) \rightarrow \chi_{c0}\omega)}{\mathcal{B}(Y(4220) \rightarrow h_c\pi^+\pi^-)} = 8.3 \pm 4.8 \pm 1.9 \quad (\text{Sol. A}) \quad (7.104a)$$

$$= 0.48 \pm 0.20 \pm 0.11 \quad (\text{Sol. B}) \quad (7.104b)$$

where the second error is the quadrature sum of the systematic uncertainties of 15% for $\sigma_{\chi_{c0}\omega}$ [93] and 18% for $\sigma_{h_c\pi^+\pi^-}$ [71]. In this way, we consider the two BES datasets to have statistically independent systematics, which leads to a conservative estimate of the error.

² $\sigma_f(m)$ indicates the cross section $\sigma(e^+e^- \rightarrow f)$ at $\sqrt{s} = m$.

³This ambiguity does not affect the $\chi_{c0}\omega$ channel, being the background compatible with zero.

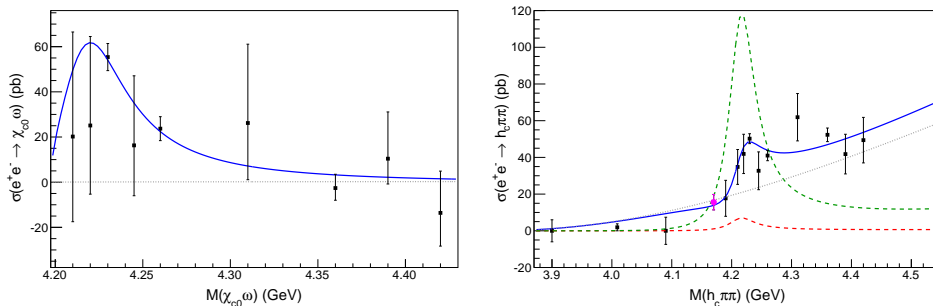


Figure 7.2. Combined fits of $\chi_{c0}\omega$ and $h_c\pi^+\pi^-$ data [6]. The purple disk in the right panel is the CLEO- c data point at $\sqrt{s} = 4.17$ GeV. The red (smaller) and the green (larger) dashed curves are the Breit-Wigner curves for solution A and B, respectively. The dotted grey curve is background.

To further check the predictions within the tetraquark model, we compute the ratio in Eq. (7.104). The same analysis of the $h_c\pi^+\pi^-$ final state showed a resonance, dubbed $Z'_c(4020)$, in the $e^+e^- \rightarrow Z'_c(4020)^\pm\pi^\mp \rightarrow h_c\pi^+\pi^-$ process [71]. From the cross sections in Ref. [71], we can see that the fractions $R_Z = \sigma(e^+e^- \rightarrow Z'_c^\pm\pi^\mp \rightarrow h_c\pi^+\pi^-) / \sigma(e^+e^- \rightarrow h_c\pi^+\pi^-)$ at $\sqrt{s} = 4.23, 4.26$ and 4.36 GeV do not vary with \sqrt{s} . The first point is very close to the $Y(4220)$ peak, and the other ones are slightly above. This would suggest that the same fraction occurs in the resonant events $R_{YZ} = \sigma(Y \rightarrow Z'_c^\pm\pi^\mp \rightarrow h_c\pi^+\pi^-) / \sigma(Y \rightarrow h_c\pi^+\pi^-)$. We therefore can preliminary assume $R_{YZ} = R_Z(\sqrt{s} = 4.23 \text{ GeV}) = (17 \pm 7)\%$. However, we remark that we have no information on R_Z in the left sideband, and a proper multidimensional analysis is due to better establish R_{YZ} . In the following, we will show our results as a function of R_{YZ} . On the other hand, we will not include an intermediate $Z_c(3900)^+\pi^-$ channel, since the signal $Z_c(3900)^+ \rightarrow h_c\pi^+$ is not significant. We also estimate the contribution of a $\pi\pi$ resonance, in particular $Y \rightarrow h_c\sigma \rightarrow h_c\pi^+\pi^-$, whose presence will be verified by a detailed Dalitz analysis when new data will be available by BES III.

We parametrize the matrix elements by enforcing Lorentz invariance and discrete symmetries,

$$\langle \chi_{c0}(p) \omega(\eta, q) | Y(\lambda, P) \rangle = g_\chi \eta \cdot \lambda, \quad (7.105a)$$

$$\langle Z'_c(\eta, q) \pi(p) | Y(\lambda, P) \rangle = g_Z \eta \cdot \lambda \frac{P \cdot p}{f_\pi M_Y}, \quad (7.105b)$$

$$\langle h_c(\eta, q) \sigma(p) | Y(\lambda, P) \rangle = g_h \epsilon_{\mu\nu\rho\sigma} \eta^\mu \lambda^\nu \frac{P^\rho q^\sigma}{P \cdot q}, \quad (7.105c)$$

$$\langle \pi(q) \pi(p) | \sigma(P) \rangle = \frac{P^2}{2f_\pi}, \quad (7.105d)$$

where g_Z, g_h and g_χ are effective strong couplings with dimension of a mass. Applying the reduction formula to the (off-shell) interpolating field of the pion, one obtains

$$\langle \beta \pi | \alpha \rangle \rightarrow -\frac{1}{f_\pi} \langle \beta | \partial \cdot A(0) | \alpha \rangle \rightarrow -\frac{p_\pi^\mu}{f_\pi} \langle \beta | A_\mu(0) | \alpha \rangle \quad (7.106)$$

in the chiral limit. In our case, the latter matrix element is a vector, being α a vector and β an axial-vector. Thus it is either a polarization or a momentum of α , β . An S -wave transition is obtained in the latter case, Eq. (7.105b). Similarly, the emission of two pions implies a factor P^2 in the amplitude $\sigma \rightarrow \pi\pi$, Eq. (7.105d).

Hence, the decay widths in narrow width approximation [281] are:

$$\Gamma(Y(4220) \rightarrow \chi_{c0}\omega) = \frac{1}{3} \frac{p^*(M_Y, m_\chi, m_\omega)}{8\pi M_Y^2} g_\chi^2 \left(3 + \frac{p^{*2}(M_Y, m_\chi, m_\omega)}{m_\omega^2} \right), \quad (7.107a)$$

$$\begin{aligned} \Gamma(Y(4220) \rightarrow Z_c'^{\pm} \pi^{\mp} \rightarrow h_c \pi^+ \pi^-) &= 2 \times \frac{1}{3} \frac{g_Z^2}{8\pi M_Y^2} \int_{(m_\pi+m_h)^2}^{(M_Y-m_\pi)^2} ds p^*(M_Y, \sqrt{s}, m_\pi) \\ &\times \left(3 + \frac{p^{*2}(M_Y, \sqrt{s}, m_\pi)}{s} \right) \frac{E_\pi^2(\sqrt{s})}{f_\pi^2} \frac{1}{\pi} \frac{m_Z \Gamma_Z}{(s - m_Z^2)^2 + m_Z^2 \Gamma_Z^2} \\ &\times \frac{p^{*3}(\sqrt{s}, m_h, m_\pi)}{p^{*3}(m_Z, m_h, m_\pi)} \frac{m_Z^3}{s^{3/2}} \mathcal{B}(Z_c' \rightarrow h_c \pi), \quad (7.107b) \end{aligned}$$

$$\begin{aligned} \Gamma(Y(4220) \rightarrow h_c \sigma \rightarrow h_c \pi^+ \pi^-) &= \frac{1}{3} \frac{g_h^2}{8\pi M_Y^2} \int_{4m_\pi^2}^{(M_Y-m_h)^2} ds p^*(M_Y, \sqrt{s}, m_h) \\ &\times \frac{2p^{*2}(M_Y, \sqrt{s}, m_h)}{m_h^2 + p^{*2}(M_Y, \sqrt{s}, m_h)} \times \frac{1}{\pi} \frac{m_\sigma \Gamma_\sigma}{(s - m_\sigma^2)^2 + m_\sigma^2 \Gamma_\sigma^2} \\ &\times \frac{p^*(\sqrt{s}, m_\pi, m_\pi)}{p^*(m_\sigma, m_\pi, m_\pi)} \frac{s}{m_\sigma^2} \mathcal{B}(\sigma \rightarrow \pi^+ \pi^-), \quad (7.107c) \end{aligned}$$

where $p^*(m_1, m_2, m_3)$ is the decay 3-momentum in the m_1 rest frame. In Eq. (7.107b), the factor of 2 takes into account the incoherent sum over the two charged resonances, being the interference numerically negligible.

For the sake of simplicity, since we are not able to resolve the details of the lineshape within our large uncertainties, we considered the σ resonance to be described by a Breit-Wigner distribution with mass and width $M_\sigma = (475 \pm 75)$ MeV, $\Gamma_\sigma = (550 \pm 150)$ MeV. To obtain the branching ratio $\mathcal{B}(Z_c' \rightarrow h_c \pi)$, we assume the total width of Z_c' to be saturated by the observed decay modes into $h_c \pi$ [71] and $D^* \bar{D}^*$ [72]. We use the BES measurements of production cross sections

$$\sigma(e^+e^- \rightarrow Z_c'^{\pm} \pi^{\mp} \rightarrow h_c \pi^+ \pi^-) = (7.4 \pm 1.7 \pm 2.1 \pm 1.2) \text{ pb}, \quad (7.108)$$

$$\sigma(e^+e^- \rightarrow (D^* \bar{D}^*)^{\pm} \pi^{\mp}) = (137 \pm 9 \pm 15) \text{ pb}, \quad (7.109)$$

and of the cross sections ratio

$$R = \frac{\sigma(e^+e^- \rightarrow Z_c'^{\pm} \pi^{\mp} \rightarrow (D^* \bar{D}^*)^{\pm} \pi^{\mp})}{\sigma(e^+e^- \rightarrow (D^* \bar{D}^*)^{\pm} \pi^{\mp})} = 0.65 \pm 0.09 \pm 0.06, \quad (7.110)$$

to estimate the branching ratio

$$\mathcal{B}(Z_c' \rightarrow h_c \pi) = (8.0 \pm 3.6)\%. \quad (7.111)$$

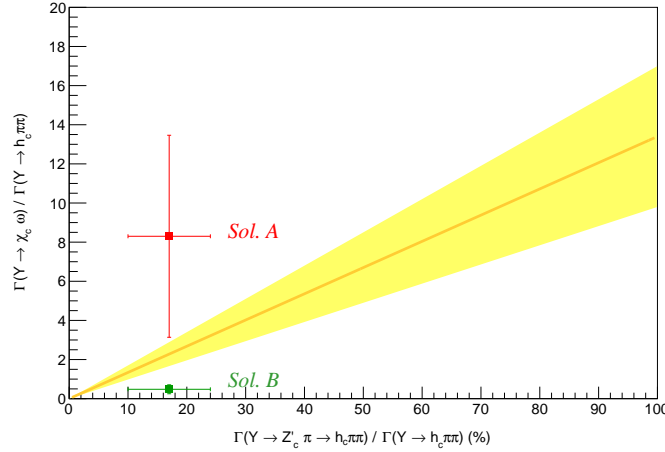


Figure 7.3. Measurements and predictions for $\Gamma(Y \rightarrow \chi_{c0}\omega) / \Gamma(Y \rightarrow h_c\pi^+\pi^-)$ as a function of $R_{YZ} = \sigma(Y \rightarrow Z'_c{}^\pm \pi^\mp \rightarrow h_c\pi^+\pi^-) / \sigma(Y \rightarrow h_c\pi^+\pi^-)$. The solid line is the prediction as a function of R_{YZ} , the colored band the correspondent error. The red and green points are the experimental ratios in Eq. (7.104), plotted at the measured $R_{YZ} = (17 \pm 7)\%$.

The branching fraction $\mathcal{B}(\sigma \rightarrow \pi^+\pi^-)$ can be assumed to be $\simeq \frac{2}{3}$ via isospin symmetry. The effective strong couplings g_χ , g_h , g_Z in Eq. (7.107) are unknown and should be fitted from data.

To obtain a prediction within the diquark-antidiquark model, we assume that a tetraquark couples universally to any charmonia, *i.e.* that the strong effective couplings are equal to a universal constant times a factor depending on heavy quark spin content [8, 286, 289].

In the $|s_{c\bar{c}}, s_{q\bar{q}}\rangle$ basis, we have:

$$\begin{aligned} |Y(4220)\rangle &= \frac{\sqrt{3}}{2} |0, 0\rangle - \frac{1}{2} |1, 1\rangle, \\ |Z'_c\rangle &= \frac{1}{\sqrt{2}} (|1, 0\rangle + |0, 1\rangle) \end{aligned} \quad (7.112)$$

and we recall

$$|h_c\rangle = |s_{c\bar{c}} = 0\rangle, \quad |\chi_{cJ}\rangle = |s_{c\bar{c}} = 1\rangle. \quad (7.113)$$

Hence, we get $g_h : g_\chi = \langle Y|h_c\rangle : \langle Y|\chi_{cJ}\rangle = \sqrt{3} : 1$. The estimate of the ratio $g_Z : g_\chi$ deserves a separate comment. The decay $Y(4220) \rightarrow Z'_c\pi$ is an hadronic transition between tetraquark states. With the additional assumption that the dynamics of tetraquark transitions is the same as that of tetraquark-charmonium decays, one could get $g_Z : g_\chi = \langle Y|Z'_c\rangle : \langle Y|\chi_{cJ}\rangle = \frac{\sqrt{3}-1}{2\sqrt{2}} : \frac{1}{2} \simeq 0.52$. This result is potentially affected by large corrections. Comparisons with new tetraquark candidates decays will allow us to probe the validity of this assumption, and evaluate the errors properly. That said, an order-of-magnitude estimate is given by the ratio:

$$\frac{\Gamma(Y(4220) \rightarrow \chi_{c0}\omega)}{\Gamma(Y(4220) \rightarrow Z'_c{}^\pm \pi^\mp \rightarrow h_c\pi^+\pi^-)} = 13.4 \pm 3.6, \quad (7.114a)$$

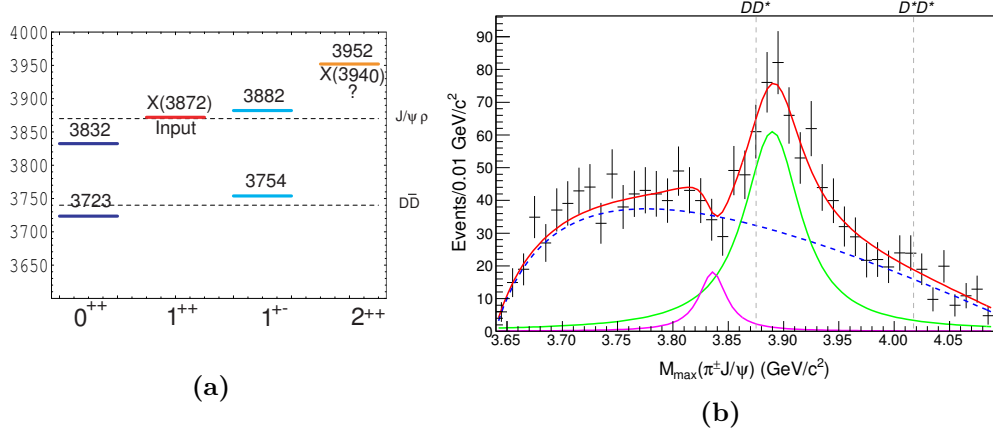


Figure 7.4. (a) The spectrum of ‘type I’ tetraquark model [264]. (b) Fit to BES III data in the $Y(4260) \rightarrow J/\psi \pi^+ \pi^-$ channel. The additional lighter resonance is compatible with data

hence

$$\frac{\Gamma(Y(4220) \rightarrow \chi_{c0}\omega)}{\Gamma(Y(4220) \rightarrow h_c \pi^+ \pi^-)} = (13.4 \pm 3.6) \times R_{YZ} = 2.3 \pm 1.2. \quad (7.114b)$$

In Figure 7.3 we show this result as a function of R_{YZ} . For the quoted value of R_{YZ} , the ratio is compatible with the solution (7.104a) of the fit, even better if R_{YZ} will be discovered to be larger. Similarly, we predict

$$\frac{\Gamma(Y(4220) \rightarrow Z_c'^{\pm} \pi^{\mp} \rightarrow h_c \pi^+ \pi^-)}{\Gamma(Y(4220) \rightarrow h_c \sigma \rightarrow h_c \pi^+ \pi^-)} = 4.8 \pm 3.5, \quad (7.114c)$$

which can be verified by a detailed Dalitz analysis when more data will be available. The errors in Eq. (7.114) are due to the experimental uncertainty on masses, widths and branching fractions of the intermediate resonances. We stress that we are not considering the error on the couplings. The results are summarized in Figure 7.3, and show that the structures seen by BES III in $h_c \pi^+ \pi^-$ and $\chi_{c0}\omega$ can be explained within the diquark-antidiquark model.

7.7 A brief note on the Z_c in the type-I tetraquark model [7]

The original ‘type I’ model made no assumption on the interaction within and outside the diquarks [264]. The hamiltonian was generically

$$H \approx \sum_{i \neq j} \kappa_{ij} (\mathbf{S}_i \cdot \mathbf{S}_j), \quad (7.115)$$

depending on four different chromomagnetic couplings κ_{cq} , $\kappa_{q\bar{q}}$, $\kappa_{c\bar{q}}$, $\kappa_{c\bar{c}}$. These have been extracted from the known spectrum of charmed baryons, light mesons, charmed mesons, and charmonia, respectively. This leads to nondiagonal terms in the

hamiltonian, whence the two Z states mix and are not anymore equal mixtures of $s_{c\bar{c}} = 0, 1$; similarly the two scalar X_0 . The quantum number of the predicted states is obviously the same, but the hierarchy is changed (Figure 7.4a). In these respects, soon after the discovery of the $Z_c(3900)$, we looked for the existence of a lighter Z' state [7], which seemed to be compatible with data (Figure 7.4b). In order to quantify the significance of the second structure included in the fits, we have adopted the statistical approach described in detail in Ref. [1]: from the fit to the data performed assuming only one exotic structure, we have simulated a large number of mock experiments, correctly accounting for statistical fluctuations. On each of them we have performed three fits, one assuming only one exotic resonance, the other one assuming a second resonance with a mass smaller than the dominant one (the ‘‘tetraquark’’ assumption), and the last one assuming a second resonance with a mass larger than the dominant one (the ‘‘molecular’’ assumption). For each mock experiment we have recorded the χ^2 of each fit, called χ_0^2 , χ_{tetra}^2 and χ_{mol}^2 , respectively. From the distribution of $\Delta\chi_{\text{tetra}}^2 = \chi_{\text{tetra}}^2 - \chi_0^2$, we can estimate the probability of a second structure to appear before the main one in absence of a real signal as the fraction of mock experiments where $\Delta\chi_{\text{tetra}}^2 < \Delta\chi_{\text{tetra};\text{data}}^2 = 41 - 50 = -9$. In this way we have estimated that there is only a 12% probability of the second structure as fitted in Figure 7.4b to be a statistical fluctuation. On the other hand, no structure appears close to the D^*D^* threshold, discouraging a molecular interpretation for the state. This was superseded by the discovery of a heavier $Z'_c(4020)$ close to the D^*D^* threshold. However, it is still unclear why no hint of $Z'_c(4020)$ appears in the $J/\psi \pi$ invariant mass.

7.8 The $b\bar{b}$ sector

The two charged Z_b states look like the bottomonium counterparts of the two Z_c resonances. Their tetraquark interpretation was proposed by Ali *et al.* [289, 290]. The two 1^{+-} states have in general diquark content

$$|Z_b\rangle = \frac{\alpha|1_{q\bar{q}}, 0_{b\bar{b}}\rangle - \beta|0_{q\bar{q}}, 1_{b\bar{b}}\rangle}{\sqrt{2}}, \quad (7.116a)$$

$$|Z'_b\rangle = \frac{\beta|1_{q\bar{q}}, 0_{b\bar{b}}\rangle + \alpha|0_{q\bar{q}}, 1_{b\bar{b}}\rangle}{\sqrt{2}}, \quad (7.116b)$$

with $|\alpha|^2 + |\beta|^2 = 1$. Assuming heavy quark spin symmetry, the effective couplings $g_{Z^{(\prime)}} (f_{Z^{(\prime)}})$ of $Z_b^{(\prime)} \rightarrow h_b(nP)\pi$ ($Z_b^{(\prime)} \rightarrow \Upsilon(nS)\pi$) can be evaluated:

$$g_Z = g(\Upsilon(5S) \rightarrow Z_b\pi)g(Z_b \rightarrow h_b\pi) \propto -\alpha\beta\langle h_b|1_{q\bar{q}}, 0_{b\bar{b}}\rangle\langle 0_{q\bar{q}}, 1_{b\bar{b}}|\Upsilon\rangle \quad (7.117a)$$

$$g_{Z'} = g(\Upsilon(5S) \rightarrow Z'_b\pi)g(Z'_b \rightarrow h_b\pi) \propto \alpha\beta\langle h_b|1_{q\bar{q}}, 0_{b\bar{b}}\rangle\langle 0_{q\bar{q}}, 1_{b\bar{b}}|\Upsilon\rangle \quad (7.117b)$$

$$f_Z = f(\Upsilon(5S) \rightarrow Z_b\pi)f(Z_b \rightarrow \Upsilon(nS)\pi) \propto |\beta|^2\langle \Upsilon(nS)|0_{q\bar{q}}, 1_{b\bar{b}}\rangle\langle 0_{q\bar{q}}, 1_{b\bar{b}}|\Upsilon\rangle \quad (7.117c)$$

$$f_{Z'} = f(\Upsilon(5S) \rightarrow Z'_b\pi)f(Z'_b \rightarrow \Upsilon(nS)\pi) \propto |\alpha|^2\langle \Upsilon(nS)|0_{q\bar{q}}, 1_{b\bar{b}}\rangle\langle 0_{q\bar{q}}, 1_{b\bar{b}}|\Upsilon\rangle, \quad (7.117d)$$

which implies $g_Z = -g_{Z'}$ and $f_Z = |\frac{\beta}{\alpha}|^2 f_{Z'}$. The Dalitz plot analyses reported in Table 3.4 [107] show a 180° between the $Z_b \rightarrow h_b(nP)\pi$ and the $Z'_b \rightarrow h_b(nP)\pi$

amplitudes. Moreover, the ratio of the absolute values of the $Z'_b \rightarrow \Upsilon(nS)\pi$ and $Z'_b \rightarrow \Upsilon(nS)\pi$ amplitudes favors $|\alpha| = |\beta|$. Thus one can fix $\alpha = \beta = 1$, so that the Z'_b have the same diquark structure as the $Z_c^{(\prime)}$. The mass splitting and the correspondent chromomagnetic couplings are expected to scale as the inverse of the quark mass, *i.e.*

$$\frac{M(Z'_b) - M(Z_b)}{M(Z'_c) - M(Z_c)} = \frac{2\kappa_b}{2\kappa_c} = 0.38 \quad (7.118)$$

which agrees with

$$\frac{M_c}{M_b} = \frac{1.27}{4.18} = 0.30 \quad (7.119)$$

The Z_b tetraquark interpretation calls for a X_b state with $J^{PC} = 1^{++}$ and a mass $M(X_b) \sim M(Z_b) \sim 10.6$ GeV. This state has been searched both in the isospin conserving ($X_b \rightarrow \Upsilon(1S)\omega$ by Belle [291]) and isospin violating channels ($X_b \rightarrow \Upsilon(1S)\rho(\pi\pi)$ by ATLAS [292]), without success. In Refs. [293, 294], the existence of a $L = 1$ vector tetraquark $Y_b(10890)$ has been discussed. Hints of a narrow state close to the $\Upsilon(5S)$ appear in the $\sigma(e^+e^- \rightarrow B\bar{B})$ analysis by BABAR [295], and in the $\sigma(e^+e^- \rightarrow \Upsilon(nS)\pi\pi)$ analysis by Belle [296], but not in the recent $\sigma(e^+e^- \rightarrow B\bar{B})$ analysis by Belle [297], leaving the existence of such a state an unanswered question.

7.9 Multi-diquark states

As we already stated, the diquark model was originally proposed by Jaffe and Wilczek to explain pentaquark baryons [268]. The observation by LHCb of two baryonic resonances decaying into $J/\psi p$ [101] immediately calls for a diquark-diquark-antiquark description, *i.e.* the \bar{c} antiquark, one heavy-light diquark, $[cq]$, and one light-light diquark, $[q_1q_2]$ [298]. We recall the preferred parameters for the two states (for errors and details see Sec. 3.4):

$$P_c(4380) : \quad M = 4380 \text{ MeV} \quad \Gamma = 205 \text{ MeV} \quad J^P = 3/2^- \quad (7.120)$$

$$P_c(4450) : \quad M = 4449.8 \text{ MeV} \quad \Gamma = 39 \text{ MeV} \quad J^P = 5/2^+ \quad (7.121)$$

The consequent spectroscopy is expected to be very rich, not dissimilar from the baryon spectrum, with the **56** positive parity baryons followed by the **70**, $L = 1$ multiplet of negative parity baryons. Although a precise description of pentaquark spectroscopy has to wait for more resonances to be found, the two observed states fit the expected scheme and corroborate the diquark role in the exotic landscape.

It is worth noticing that, while ground-state baryons carry positive parity, ground-state pentaquarks have negative parity because of the constituent antiquark. The lighter observed state has indeed negative parity, but the ~ 70 MeV difference between the two masses does not go well with the energy associated to orbital excitation. One orbital excitation in mesons and baryons carries an energy difference which is typically of order 300 MeV, (*e.g.* $\Lambda(1405) - \Lambda(1116) \sim 290$ MeV). Mass formulae for the orbital excitation in XYZ mesons are discussed in Sec. 7.6 and the associated energy difference is estimated to be $\Delta M(L = 0 \rightarrow 1) \sim 280$ MeV. However, the mass difference between light-light diquarks with spin $s = 1, 0$ [299], estimated from charm

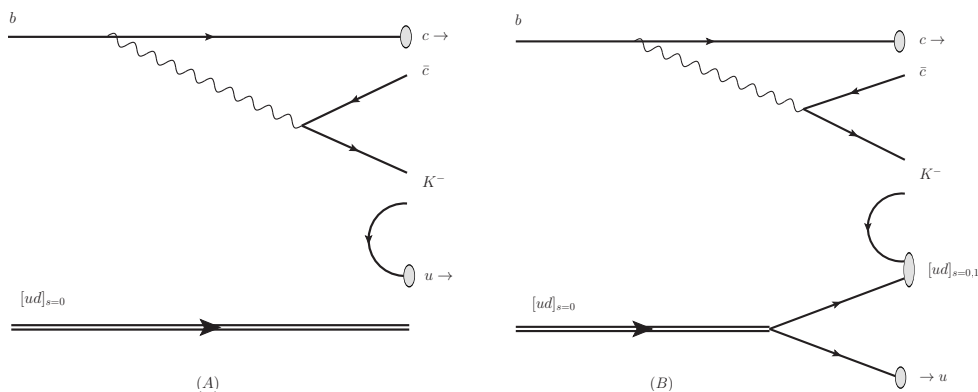


Figure 7.5. (A): The $[ud]$, good diquark in the Λ_b^0 is transmitted to the good pentaquark ($P_c(4380)$ -like). (B) The u quark from the vacuum participates in the formation of the light-light diquark: spin zero and one are both permitted. Mechanism (B) may also produce a flavor-symmetric $[uu]_{s=1}$ diquark ($P_c(4450)$ -like).

and beauty baryon spectra, is of order 200 MeV, *e.g.* $\Sigma_c(2455) - \Lambda_c(2286) \simeq 170$ MeV, $\Sigma_b(5811) - \Lambda_b(5620) \simeq 190$ MeV.

If we assume the compositions

$$P_c(4380) = \{\bar{c}[cq]_{s=1}[q_1q_2]_{s=1}, L = 0\} \quad (7.122a)$$

$$P_c(4450) = \{\bar{c}[cq]_{s=1}[q_1q_2]_{s=0}, L = 1\} \quad (7.122b)$$

the orbital gap is reduced to about 100 MeV, consistent with the observation. Following Jaffe [285], we call “good” (“bad”) diquark the scalar (vector) light-light diquark, and extend these names to the pentaquarks containing good and bad diquarks. The bad diquarks, while conspicuously absent in light meson spectroscopy, are well established in baryons as indicated by the $\Sigma - \Lambda$ mass difference [299] and confirmed by $\Sigma_{c,b} - \Lambda_{c,b}$ mass differences [264].

Given the composition of the $\Lambda_b^0 = \{b[ud]_{s=0}, L = 0\}$, one might ask if the light-light vector diquark in Eq. (7.122a) can actually be produced. In fact two possible mechanisms lead to the pentaquark production: In the first one (Figure 7.5, left panel) the b -quark spin is shared between the kaon and the \bar{c} and $[cu]$ components. Barring angular momentum transfer due to gluon exchanges between the light diquark and light quarks from the vacuum, the final $[ud]$ diquarks has to have spin zero. In the second mechanism, however (Figure 7.5, right panel), the $[ud]$ diquark is formed from the original d quark and the u quark from the vacuum. Angular momentum is shared among all final components and the $[ud]$ diquark may well have spin one. Concerning heavy quark spin conservation, one can also show that both pentaquarks states have heavy quark spin components with either $s_{c\bar{c}} = 0, 1$, hence the decay into J/ψ is allowed. The extension to $SU(3)_f$ is also discussed in Ref. [298]. The generalization to dibaryons (6-quark states) is discussed in Ref. [300]. For other works on the pentaquark interpretation of the P_c states, see Refs. [301–303].

7.10 Amplitudes in the compact tetraquark model

Although one can use the phenomenological constituent quark model to predict the mass spectrum of the tetraquark states, our lack of knowledge on the actual internal structure of such particles is still almost total. The exact solution of this problem would require to solve a four-body problem, having at least a hint on the nature of the strong potential binding the four constituents. This implies that, until now, we have no methods to compute scattering amplitudes for these states from first principles.

The typical approach is to gain as much information as possible from available experimental data. In particular, one usually takes into account the kinematics of a decay parameterizing the matrix elements in terms of an *unknown* effective strong coupling times the most general Lorentz-invariant combination of polarization and momenta with the right behavior under parity and charge conjugation. The effective strong coupling is typically fitted from experimental data when available or, otherwise, it can be estimated by dimensional analysis and under the assumption for it to be of “natural size”. In the latter case one can clearly just give an order of magnitude estimate of the amplitude considered.

To be more definite let us make a classic example: the decay $X(3872) \rightarrow D^0 \bar{D}^{*0}$. This is a $1^+ \rightarrow 0^- 1^-$ strong decay and its matrix element can be parametrized in the following way:

$$\langle D^0(q) \bar{D}^{*0}(k, \lambda) | X(P, \epsilon) \rangle = g_{XDD^*} \epsilon \cdot \lambda, \quad (7.123)$$

where g_{XDD^*} is the effective coupling and ϵ and λ are the polarization vectors of the $X(3872)$ and of the \bar{D}^{*0} respectively. This decay already conserves total angular momentum and parity when happening in S -wave. The next parity-conserving contribution to the matrix element would be the D -wave one, which however must be proportional to a momentum squared and hence is suppressed by the small Q -value for the reaction. Therefore, we want a Lorentz-invariant combination of the available quantities with no momentum dependence. Such combination is clearly just the product of the polarization. The effective coupling can be fitted from the known experimental width for the process considered, obtaining [7] $g_{XDD^*} \simeq 2.5$ GeV.

Very recently, an interesting paper by Brodsky *et al.* [304] proposed a model for the internal dynamics of a tetraquark to compute the effective coupling of the exotic states to quarkonia ($Q\bar{Q}$). The idea is that after the diquark-antidiquark pair is created, it tends to convert all its kinetic energy into potential energy of the color flux tube until it comes to rest at a relative distance \bar{r} . Such distance must satisfy $V(\bar{r}) = M - 2m_{Qq}$, where M is the mass of the exotic particle, m_{Qq} is the constituent diquark mass and $V(r)$ is the spinless Cornell potential. This essentially means that the mass difference between the exotic meson and its diquark-antidiquark constituents is given by the potential energy at $r = \bar{r}$. Once \bar{r} is computed, one can evaluate the quarkonium component of the diquark-antidiquark wave function, *i.e.* the overlap $\langle \psi h | \delta\bar{\delta} \rangle$, ψ being a generic quarkonium, h a light hadron and $\delta\bar{\delta}$ the diquark-antidiquark pair. The larger is this component at \bar{r} the more probable the decay of the exotic state into that particular quarkonium – see Figure 7.6. In other

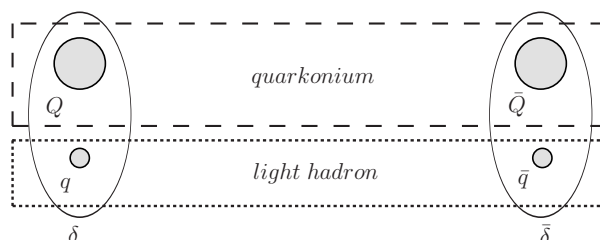


Figure 7.6. Pictorial representation of the overlapping region between the diquark-antidiquark pair and the quarkonium wave function. The larger this overlapping, the more probable the decay.

words, the effective squared coupling can be taken to be proportional to $|\psi_{Q\bar{Q}}(\bar{r})|^2$. The extension to pentaquark decays is discussed in [301]. This might explain why the $Z(4430)$ prefer to decay into $\psi(2S)\pi$ rather than $J/\psi\pi$, indeed

$$\left| \frac{\psi_{\psi(2S)}(r_Z)}{\psi_{J/\psi}(r_Z)} \right|^2 \sim 75.6, \quad \frac{\Gamma(Z(4430) \rightarrow \psi(2S)\pi)}{\Gamma(Z(4430) \rightarrow J/\psi\pi)} \sim 28 \quad (7.124)$$

roughly compatible with the observation [90].

The same authors discuss the modification of the spectrum due to the nearby thresholds in [305].

7.10.1 Constituent Counting Rules

According to the QCD constituent counting rules [306, 307], the cross sections and form factors at large \sqrt{s} and fixed scattering angle θ_{cm} are expected to scale as a power of s determined by the total number n of fundamental constituents (incoming plus outgoing) appearing in the hard scattering. In particular, the invariant amplitude \mathcal{M} for such a process scales as [308]

$$\mathcal{M} \propto \frac{1}{s^{\frac{n}{2}-2}}. \quad (7.125)$$

In [308], the authors propose to look for the production of charged tetraquarks in e^+e^- collisions at large \sqrt{s} . The power law the cross section scales with is sensitive to the nature of the states. The electromagnetic form factor of a charged noncompact (molecular) tetraquark state Z , with 4 fundamental constituents, is indeed

$$F_Z(s) \rightarrow \frac{1}{s^{\frac{1}{2}(1+1+4+4)-2}} = \frac{1}{s^3}. \quad (7.126)$$

However, if the Z contains diquarks that are so tightly bound that they act as fundamental units in high-energy scattering processes, then one expects $F_Z(s) \rightarrow 1/s^1$.

While the scaling rules strictly hold only for large s (presumably several GeV above production threshold), their reach may be extended to lower energies by taking the ratios of cross sections of processes that differ primarily through the number of fundamental constituent components, thus eliminating systematic corrections

common to both processes. As an example, the ratio

$$\frac{\sigma(e^+e^- \rightarrow Z^+(\bar{c}c\bar{d}u) + \pi^-(\bar{u}d))}{\sigma(e^+e^- \rightarrow \mu^+\mu^-)} = |F_{Z_c,\pi}(s)|^2 \propto \frac{1}{s^{n-4}}, \quad (7.127)$$

scales as $1/s^4$ if Z acts as a two-quark, two-antiquark bound state, while if the diquarks are particularly tightly bound and act as fundamental constituents in the hard scattering, the scaling drops to $1/s^2$. Similarly, consider the ratio

$$\frac{\sigma(e^+e^- \rightarrow Z^+(\bar{c}c\bar{d}u) + \pi^-(\bar{u}d))}{\sigma(e^+e^- \rightarrow \Lambda_c(cud)\bar{\Lambda}_c(\bar{c}\bar{u}\bar{d}))} \propto \frac{1}{s^0}, \quad (7.128)$$

such that the same number of constituents, as well as the same heavy-quark ($\bar{c}c$) constituents, appear in both processes. In this case, not only the high- s scaling but also corrections due to the heavy-quark mass cancel in the ratio. One expects the absolute numerical value of the ratio to be substantially smaller if Z behaves as a meson-meson molecule than a diquark-antidiquark state since the color forces in the former are of the residual van der Waals type and hence much weaker.

7.10.2 Brief review on QCD sum rules

Another technique used to compute the mass, widths and coupling constants for these exotic states is to employ the well-known QCD Sum Rules (QCDSR) [309]. As we will see shortly, their use is not limited to tetraquarks only but they can be used also assuming different internal structures or even a mixture of them.

The method of QCDSR was introduced for the first time by Shifman, Vainshtein and Zakharov [310] and used to study the properties of mesons. The main concept⁴ is based on the evaluation of a two-point correlation function given by

$$\Pi(q) \equiv i \int d^4x e^{iq \cdot x} \langle 0 | T (j(x) j^\dagger(0)) | 0 \rangle, \quad (7.129)$$

where $j(x)$ is a current with the quantum numbers of the hadron we want to study. The important assumption is that this correlator can be evaluated both at the quark level (the so-called *OPE side*) and at the hadron level (the so-called *phenomenological side*). On the OPE side, as the name suggests, one expands the function as a series of local operators:

$$\Pi(q^2) = \sum_n C_n(Q^2) \hat{\mathcal{O}}_n, \quad (7.130)$$

with $Q^2 = -q^2$ and where the set $\{\hat{\mathcal{O}}_n\}$ includes all the local, gauge-invariant operators that can be written in terms of the gluon and quark fields. As usual, the information about the short-range (perturbative) part of the correlator is contained in the $C_n(Q^2)$. The matrix elements for the operators $\hat{\mathcal{O}}_n$ are non-perturbative and must be evaluated through Lattice QCD or using some phenomenological model.

⁴Here we just review very quickly the main concepts about QCDSR. For a deeper understanding one should refer to a review on the topic [309].

On the phenomenological side, instead, one writes the two-point function in terms of a spectral density $\rho(s)$:

$$\Pi(q^2) = - \int ds \frac{\rho(s)}{(q^2 - s + i\epsilon)} + \dots, \quad (7.131)$$

with the dots representing subtraction terms. One usually assumes that, over a set of hadrons with certain quantum numbers, the spectral density has a pole correspondent to the mass of the ground-state hadron, while higher mass states are contained in a smooth, continuous part:

$$\rho(s) = \lambda^2 \delta(s - m^2) + \rho_{\text{cont}}(s), \quad (7.132)$$

λ being the coupling of the current to the lowest mass hadron, H , $\langle 0|j|H\rangle = \lambda$. The main assumption is that in a certain range of Q^2 (to be determined) the OPE and phenomenological sides can be matched to extrapolate the values of the mass and width of the hadrons of interest.

The choice of the current $j(x)$ is only dictated by the $(I^G)J^{PC}$ quantum numbers of the hadron and by the assumptions on its internal structure. For example, the currents for a pure $J^{PC} = 1^{++}$ tetraquark and molecule can be written as

$$j_\mu^{(4q)} = \epsilon_{abc} \epsilon_{dec} \frac{i}{\sqrt{2}} \left((q_a^T C \gamma_5 c_b) (\bar{q}_d \gamma_\mu C \bar{c}_e^T) + (q_a^T C \gamma_\mu c_b) (\bar{q}_d \gamma_5 C \bar{c}_e^T) \right); \quad (7.133a)$$

$$j_\mu^{(\text{mol.})} = \frac{1}{2} ((\bar{q} \gamma_5 c) (\bar{c} \gamma_\mu q) - (\bar{q} \gamma_\mu c) (\bar{c} \gamma_5 q)), \quad (7.133b)$$

where C is the charge conjugation matrix and lower case latin letters are color indices. As we mentioned before, one can also build a current for a pure $c\bar{c}$ state or even take a current for a mixture of these states through a certain mixing angle [311].

Lastly, one can estimate decay widths, *i.e.* coupling constants, through the study of an analogous three-point function. To be definite, let us consider the decay of the $X(3872)$ into J/ψ plus a vector mesons V (say, ρ or ω). One can compute the coupling constant, $g_{X\psi V}$, for this process using the following correlator:

$$\Pi_{\mu\nu\alpha}(p, q) \equiv \int d^4x d^4y e^{ip \cdot x} e^{iq \cdot y} \Pi_{\mu\nu\alpha}(x, y), \quad (7.134)$$

with

$$\Pi_{\mu\nu\alpha}(x, y) \equiv \langle 0|T \left(j_\mu^\psi(x) j_\nu^V(y) j_\alpha^{X^\dagger}(0) \right) |0\rangle, \quad (7.135)$$

and j_μ^ψ , j_ν^V and j_α^X are the interpolating currents for the J/ψ , the vector meson and the $X(3872)$ respectively.

7.11 Probing the nature of the Z_c via the $\eta_c \rho$ decay [8]

In [8] we show how the $Z_c^{(\prime)} \rightarrow \eta_c \rho$ decay channel can be used as a tool to differentiate between two of the possible internal structures of these charged resonances. We evaluate indeed some ratios of branching ratios according to the tetraquark model (in

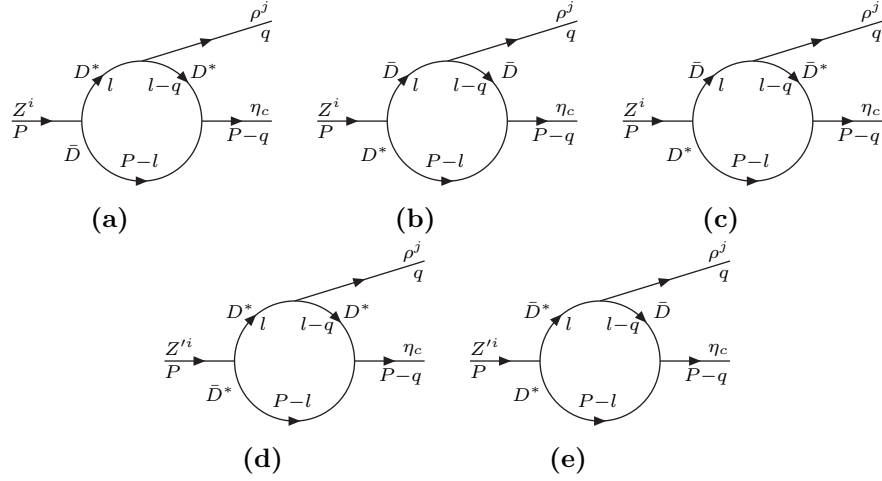


Figure 7.7. Possible one-loop diagrams for the Z_c (upper figures) and the Z'_c (lower figures) decaying into $\eta_c \rho$. The charge conjugate diagrams are omitted.

both type-I and type-II versions), and according to the molecular-inspired NREFT (see Sec. 5.1.2). As far as the decays of tetraquarks are concerned, we have discussed in this chapter how one can resort to the heavy quark spin symmetry [286, 289] to write the amplitudes for the decay into charmonia as a Clebsch-Gordan spin factor times a transition matrix element [8]. This is valid up to corrections of order $\Lambda_{QCD}/m_c \simeq 25\%$, where $m_c \simeq 1.5$ GeV is the constituent charm quark mass.

For the processes of interest, the most general Lorentz-invariant matrix elements that behave properly under parity and charge conjugation are

$$\langle J/\psi(\eta, p) \pi(q) | Z(\lambda, P) \rangle = g_{Z\psi\pi} \lambda \cdot \eta, \quad \langle \eta_c(p) \rho(\epsilon, q) | Z(\lambda, P) \rangle = g_{Z\eta_c\rho} \lambda \cdot \epsilon, \quad (7.136a)$$

$$\langle h_c(p, \eta) \pi(q) | Z(\lambda, P) \rangle = \frac{g_{Zh_c\pi}}{M_Z^2} \epsilon^{\mu\nu\rho\sigma} \lambda_\mu \eta_\nu P_\rho q_\sigma, \quad (7.136b)$$

where λ , η and ϵ are polarization vectors, p , q and P are four-momenta and the g s are effective couplings with dimension of a mass.

	Kinematics only		Dynamics included	
	type I	type II	type I	type II
$\frac{\mathcal{BR}(Z_c \rightarrow \eta_c \rho)}{\mathcal{BR}(Z_c \rightarrow J/\psi \pi)}$	$(3.3^{+7.9}_{-1.4}) \times 10^2$	$0.41^{+0.96}_{-0.17}$	$(2.3^{+3.3}_{-1.4}) \times 10^2$	$0.27^{+0.40}_{-0.17}$
$\frac{\mathcal{BR}(Z'_c \rightarrow \eta_c \rho)}{\mathcal{BR}(Z'_c \rightarrow h_c \pi)}$	$(1.2^{+2.8}_{-0.5}) \times 10^2$		$6.6^{+56.8}_{-5.8}$	

Table 7.4. Predicted ratios of branching fractions for the $Z_c^{(\prime)}$ states according to the main tetraquark models [8]. The first and second columns are computed under the assumptions (a) and (b) respectively, as explained in the text. Both type I and type II models give the same predictions for the $\mathcal{BR}(Z'_c \rightarrow \eta_c \rho) / \mathcal{BR}(Z'_c \rightarrow h_c \pi)$, since both h_c and η_c have spin $s_{c\bar{c}} = 0$. The errors are estimated via a toy MC simulation.

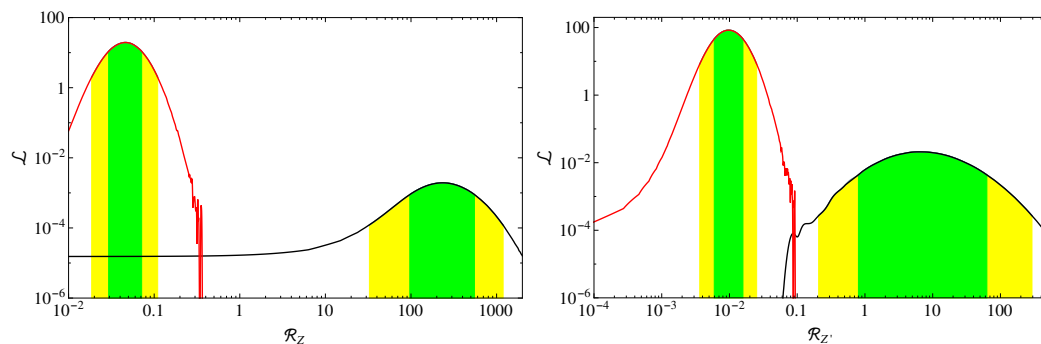


Figure 7.8. Likelihood curves for $\mathcal{BR}(Z_c \rightarrow \eta_c \rho)/\mathcal{BR}(Z_c \rightarrow J/\psi \pi)$ (left) and $\mathcal{BR}(Z'_c \rightarrow \eta_c \rho)/\mathcal{BR}(Z'_c \rightarrow h_c \pi)$ (right). The red curve is the molecular prediction, whereas the black one gives the predictions for the dynamical type I tetraquark model. The green (yellow) bands represent the 68% (95%) confidence region.

Since we have no information on the couplings, some kind of ansatz is required here as well. To test the degree of model dependence of our calculation we make two different assumptions: (a) we neglect the spatial dependence of the wave functions and hence assume that the couplings are universal, the differences between the different matrix elements being only of kinematical nature; (b) we use the dynamical model by Brodsky *et al.* [304] described in Sec. 7.10.

In Table 7.4 we report the predictions obtained within the tetraquark model.

On the other hand, in the molecular picture the $Z_c^{(\prime)}$ is interpreted as a $D^{(*)}\bar{D}^*$ loosely bound state. The complete Lagrangian of interest for our study is fully reported in [8], together with the choice of couplings for the interaction between the different fields. The term describing the interaction between the $Z_c^{(\prime)}$ and the charmed mesons is given by

$$\mathcal{L}_{Z_c^{(\prime)}} = \frac{z^{(\prime)}}{2} \left\langle \mathcal{Z}_{\mu,ab}^{(\prime)} \bar{H}_{2b} \gamma^\mu \bar{H}_{1a} \right\rangle + h.c., \quad (7.137)$$

where $\mathcal{Z}_{\mu,ab}^{(\prime)}$ and \bar{H}_{ia} are the HQET fields for the doubly heavy Z_c 's states and for the D mesons respectively. The $z^{(\prime)}$ are, instead, unknown effective couplings. In principle, such an effective theory is a valid description of the decays of the $Z_c^{(\prime)}$ regardless of its internal structure since the form of the interaction is only dictated by symmetry considerations. The molecular nature of a state is imposed by forcing it to couple to its own constituents only. Therefore, the decays into final states different from the latter ones (charmonia in our case) can only happen via heavy meson loops. The most relevant one-loop diagrams for the $Z_c^{(\prime)} \rightarrow \eta_c \rho$ process are reported in Figure 7.7.

Moreover, since the molecular states are near threshold, the velocities of the mesons inside the loops are given by $v_X \simeq \sqrt{|M_Z - 2M_D|/M_D}$ and are typically small. This allows to perform a power counting procedure in order to estimate the relevance of a certain diagram [193–196, 198]. Using this technique, one finds that the omission of diagrams with more than one loop introduces a 15% relative error on each single amplitude.

Given the previous set up, the predictions obtained within the meson molecule framework are:

$$\frac{\mathcal{BR}(Z_c \rightarrow \eta_c \rho)}{\mathcal{BR}(Z_c \rightarrow J/\psi \pi)} = \left(4.6_{-1.7}^{+2.5}\right) \times 10^{-2}; \quad \frac{\mathcal{BR}(Z'_c \rightarrow \eta_c \rho)}{\mathcal{BR}(Z'_c \rightarrow h_c \pi)} = \left(1.0_{-0.4}^{+0.6}\right) \times 10^{-2}. \quad (7.138)$$

As an additional result one can also assume that the total width of the $Z_c^{(\prime)}$ is saturated by the $D^{(*)}\bar{D}^*$, $\eta_c \rho$, $h_c \pi$, $J/\psi \pi$ and $\psi(2S) \pi$ final states and therefore fit the couplings to the constituents from the experimental data. This gives

$$|z| = \left(1.26_{-0.14}^{+0.14}\right) \text{ GeV}^{-1/2} \quad \text{and} \quad |z'| = \left(0.58_{-0.19}^{+0.22}\right) \text{ GeV}^{-1/2}. \quad (7.139)$$

Once these couplings are given one can also make the following predictions for the comparison between the two charged resonances decaying into the same final states:

$$\frac{\mathcal{BR}(Z_c \rightarrow h_c \pi)}{\mathcal{BR}(Z'_c \rightarrow h_c \pi)} = 0.34_{-0.13}^{+0.21}; \quad \frac{\mathcal{BR}(Z_c \rightarrow J/\psi \pi)}{\mathcal{BR}(Z'_c \rightarrow J/\psi \pi)} = 0.35_{-0.21}^{+0.49}. \quad (7.140)$$

We can now properly compare the predictions obtained within the two models presented — see Fig. 7.8. As one can see, according to the dynamical type I tetraquark model the $Z_c \rightarrow \eta_c \rho$ decay should be enhanced with respect to the already observed $Z_c \rightarrow J/\psi \pi$. The opposite is expected in the meson molecule picture and the two predictions are separated by more than 2σ (95% C.L.). A similar thing holds for the $Z'_c \rightarrow \eta_c \rho$ decay with respect to the $Z'_c \rightarrow h_c \pi$ one. In the last case, however, the predictions for the type I and type II models are the same and hence the result is more model independent. The values obtained under the assumption of no dynamics for the tetraquark turn out to be even more separated from the molecular ones. For the Z_c in the type II paradigm, instead, the two models give predictions which are compatible within 2σ .

Lastly, the results reported in Eq. (7.140) show that in the molecular picture one expects $\mathcal{BR}(Z_c \rightarrow h_c \pi)/\mathcal{BR}(Z'_c \rightarrow h_c \pi) < 0.88$ and $\mathcal{BR}(Z_c \rightarrow J/\psi \pi)/\mathcal{BR}(Z'_c \rightarrow J/\psi \pi) < 1.86$ at 95% C.L.. This means that the two charged resonances should be seen in both the $h_c \pi$ and $J/\psi \pi$ final states with comparable rates. While this seems to agree with the data in the first case, where a small hint of Z_c is seen, it might be at odds with the experiments for the $J/\psi \pi$ channel, where no Z'_c has been observed so far.

In conclusion, we showed how the analysis of the $Z_c^{(\prime)} \rightarrow \eta_c \rho$ decay can be used as a probe of the internal structure of these charged states and hence provide a tool to discriminate between two of the most accepted models for the exotic XYZ mesons. Experimental data on this channel could therefore shed some light on the now long-standing question about the nature of the Z_c and Z'_c resonances.

Chapter 8

Production of exotic states at hadron colliders

Now that we have introduced a large spectrum of possible interpretations for the exotic XYZ states we can describe a couple of circumstances that might give some hint on the real nature of such particles. In particular, we will focus on their production mechanisms, showing how they can give some criteria to distinguish between a compact tetraquark and a loosely bound molecule.

In Sec. 8.1 we focus on the potential appearance of exotic states carrying a double flavor charge (*e.g.* cc or bb). We show how the production branching fractions and decay widths of these particles are of the right order of magnitude to allow them to be detected by the current experimental facilities. In particular, the spectrum of such states contains doubly charged particle. If they were to be observed that would be almost a full-proof of the existence of compact tetraquarks since, because of the strong Coulomb repulsion, hadronic molecules would be forbidden.

In Sec. 8.2, instead, we describe a few models used to predict the production rate of exotic particles, in particular the $X(3872)$, in relativistic heavy ion collisions as those performed at RHIC and LHC. As it will be clear soon, the production cross sections for a molecular states and for a compact tetraquark are expected to be largely different, thus providing a good way to discriminate between the two.

8.1 Possible production of doubly charmed states [9, 10]

The key for the discrimination between the molecular and the compact tetraquark model might be the search for particles with even more exotic properties. It has been pointed out [9, 312–314] that such exotic particles might appear in doubly charmed/bottomed configurations. Because of their peculiar flavor quantum numbers such particles would be clearly distinguished from ordinary mesons and would have a very neat experimental signature. Moreover, as we will show briefly, their spectrum allows the presence of doubly charged states that can only be interpreted in terms of a compact four-quark particle, since the Coulomb repulsion between the two (like-charged) mesons would prevent any possible molecular binding.

In the following section we will focus on doubly charmed states [9]. Their existence is predicted within the constituent diquark-antidiquark model [285]:

$$\mathcal{T} \equiv [cc][\bar{q}_1\bar{q}_2], \quad \text{with } q_1, q_2 = u, d, s. \quad (8.1)$$

The one-gluon-exchange model suggests that the two quarks (antiquarks) combine in the attractive $\bar{\mathbf{3}}_c$ ($\mathbf{3}_c$) color representation. The total wave function for the diquark (antidiquark) must be completely anti-symmetric because of Fermi statistics. For the $[cc]$ diquark we only have one possibility since the flavor wave function can only be symmetric:

$$[cc] = \left| \bar{\mathbf{3}}_c(A), J^P = 1^+(S) \right\rangle, \quad (8.2)$$

where with (S) and (A) we indicate the symmetry and anti-symmetry of a configuration. For the light antidiquark, instead, we can have

$$[\bar{q}_1\bar{q}_2]_G = \left| \mathbf{3}_c(A), \mathbf{3}_f(A), J^P = 0^+(A) \right\rangle; \quad (8.3a)$$

$$[\bar{q}_1\bar{q}_2]_B = \left| \mathbf{3}_c(A), \mathbf{6}_f(S), J^P = 1^+(S) \right\rangle, \quad (8.3b)$$

where with the subscript f we indicate the flavor $SU(3)$ group. According to the phenomenological color-spin Hamiltonian, the “good” (G) scalar state is expected to be lighter than the “bad” (B) vectorial state, and hence should be more likely produced.

Combining the 1^+ diquark with both good and bad antidiquarks one obtains the configurations reported in Table 8.1. As previously pointed out among those states we can find the very peculiar doubly charged ones. Moreover, while the good states can only be produced with $J^P = 1^+$, the bad ones can be found with $J = 0, 1, 2$, although one expects the scalar configuration to be the lighter and, hence, more probable one.

The allowed decay channels for doubly charmed tetraquarks depend crucially on whether or not their masses lie above the open charm threshold. Many analyses [313–317] have been studying the case in which \mathcal{T} particles are below threshold, one of

\mathcal{T} states	
“Good”, $\mathbf{1}^+$	“Bad”, $\mathbf{0}^+, 1^+, 2^+$
$\mathcal{T}^+ \left([cc][\bar{u}\bar{d}]_A \right)$	$\mathcal{T}^0 \left([cc][\bar{u}\bar{u}] \right)$
$\mathcal{T}_s^+ \left([cc][\bar{u}\bar{s}]_A \right)$	$\mathcal{T}^{++} \left([cc][\bar{d}\bar{d}] \right)$
$\mathcal{T}_s^{++} \left([cc][\bar{d}\bar{s}]_A \right)$	$\mathcal{T}_{ss}^{++} \left([cc][\bar{s}\bar{s}] \right)$
	$\mathcal{T}^+ \left([cc][\bar{u}\bar{d}]_S \right)$
	$\mathcal{T}_s^+ \left([cc][\bar{u}\bar{s}]_S \right)$
	$\mathcal{T}_s^{++} \left([cc][\bar{d}\bar{s}]_S \right)$

Table 8.1. Expected \mathcal{T} states. A and S stand for the anti-symmetric and symmetric flavor configurations. Quantum numbers in **red** are the most likely produced.

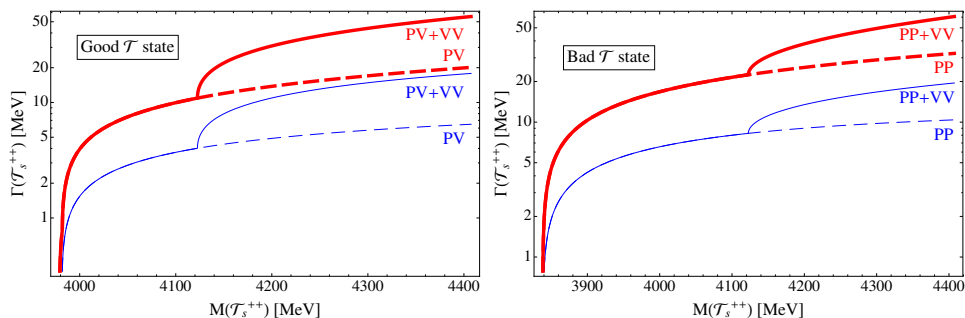


Figure 8.1. Width of good 1^+ (left panel) and bad 0^+ (right panel) \mathcal{T}_s^{++} as a function of the mass for both $g_{\mathcal{T}} = M_{\mathcal{T}}$ (red thick) and $g_{\mathcal{T}} = 2.5$ GeV (blue thin), from Esposito *et al.* [9]. With P and V we indicate the $D_{(s)}$ and $D_{(s)}^*$ final states respectively.

the reasons being that, under this assumption, they would be stable against the (flavor conserving) strong and electromagnetic interactions, hence favoring lattice studies – see also the Large- N discussion in Sec. 2.3. However, in this case, the weak decay channels would present a too complicated pattern, making an experimental analysis very challenging. Since we are interested in the possible detection of these multi-quark states in hadronic colliders we will assume that they lie above the open-charm threshold [9, 10]. Also, for a matter of simplicity, we will focus our study on the \mathcal{T}_s^{++} , the extension to the other states being straightforward. In Table 8.2 we report the S -wave decay channels into the lightest 0^+ and 1^+ open charm mesons (P -wave decays are forbidden by parity conservation).

As explained in Sec. 7.10, the decay amplitudes can be parametrized in terms of a color Fierz coefficient, a kinematical term and an unknown strong effective coupling, $g_{\mathcal{T}}$. The lack of theoretical understanding on the internal structure of tetraquarks makes impossible to exactly compute the value of this coupling. However, one can obtain an order of magnitude estimate by setting $g_{\mathcal{T}} \simeq M_{\mathcal{T}}$ by dimensional analysis and under the assumption for the coupling to be of “natural” size. Another possible choice could be to set $g_{\mathcal{T}}$ to be the same as in the $X(3872) \rightarrow D^0 D^{*0}$ case – which can be estimated from experimental data [7] – that is $g_{\mathcal{T}} \simeq g_{XDD^*} = 2.5$ GeV. In Figure 8.1 we report the computed decays widths as a function of the \mathcal{T}_s^{++} mass for both good and bad states and for both choices of the coupling. It is worth noting that the value of $g_{\mathcal{T}}$ does not change the order of magnitude of such widths.

\mathcal{T}_s^{++} decays			
0⁺ bad	1⁺ good	1 ⁺ bad	2 ⁺ bad
$D_s^+ D^+$	$D_s^{*+} D^+$	$D_s^{*+} D^+$	$D_s^{*+} D^{*+}$
$D_s^{*+} D^{*+}$	$D_s D^{*+}$	$D_s D^{*+}$	
	$D_s^{*+} D^{*+}$		

Table 8.2. Possible \mathcal{T}_s^{++} decay channels. The configurations in **red** are the most likely ones. The 1^+ bad configuration cannot decay into a vector-vector state because of heavy quark spin conservation.

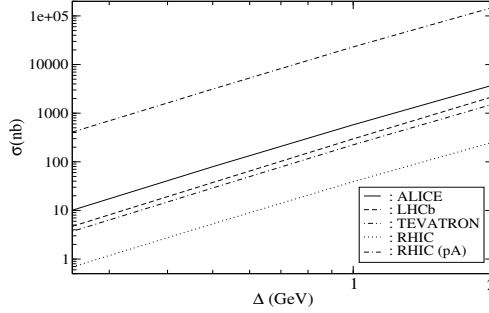


Figure 8.2. Estimated production cross section of two c quarks in momentum space Δ for different experimental facilities at LHC, Tevatron and RHIC. From Del Fabbro *et al.* [313].

Moreover, they are narrow enough to be experimentally measured in the present hadronic experimental facilities.

We can now turn on the study of the production of these particles. They could be created both promptly from the main partonic interaction or from the decay of some other particle. The prompt production has been studied as a three-step process [313]:

1. *Creation of a cc pair from the main interaction.* The two analyzed possibilities are the single parton interaction, dominated by gluon-gluon fusion $gg \rightarrow c\bar{c}c\bar{c}$, and double parton interaction, dominated by $(gg) + (gg) \rightarrow (c\bar{c}) + (c\bar{c})$, where the two distinct interactions occur in the same hadronic event. These processes are dominant in the small transverse momenta region and the presented results are computed in that range. In particular, the cross section for the production of a cc pair has been calculated [313] for quarks with relative momentum $|p_{1i} - p_{2i}| < \Delta$, with $i = x, y, z$. The result as a function of Δ is shown in Figure 8.2. The chosen kinematical cuts for the different experiments are: ($\sqrt{s} = 14$ TeV, $1.8 < \eta < 4.9$) for LHCb, ($\sqrt{s} = 14$ TeV, $|\eta| < 0.9$) for ALICE, ($\sqrt{s} = 1.8$ TeV, $|y| < 1$) for Tevatron and ($\sqrt{s} = 200$ GeV, $|\eta| < 1.6$) for RHIC.
2. *Binding of the two charm quarks into a diquark.* To compute that, one can consider the overlap between the two quarks wave function with the diquark one. In particular, the wave function for the two quarks can be taken to be gaussian and expressing it as a function of the relative, \mathbf{r} , and of the center-of-mass, \mathbf{R} , coordinates one gets, aside from a normalization factor:

$$\psi_{cc}(\mathbf{r}, \mathbf{R}) \propto e^{-\mathbf{R}^2/2(B/\sqrt{2})^2 + i\mathbf{P}\cdot\mathbf{R}} e^{-(\mathbf{r}-\mathbf{r}_a)^2/2(B\sqrt{2})^2 + i\mathbf{p}\cdot\mathbf{r}}, \quad (8.4)$$

with the “oscillator parameter” being $B = 0.69$ fm [313]. Moreover, $\mathbf{r}_a = 1$ or 0 fm depending if we are dealing with a proton-nucleus or a proton-proton collision.

Approximating the diquark wave function with a gaussian with an oscillator parameter $\beta = 0.41$ fm, one gets an amplitude for the conversion of the cc pair

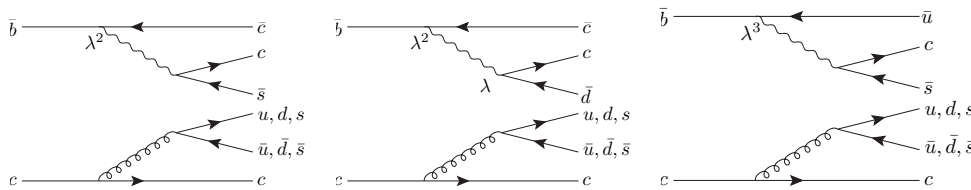


Figure 8.3. Feynman diagrams for the production of \mathcal{T} particles from B_c^+ . $\lambda = \sin \theta_C$ is the sine of the Cabibbo angle associated to each vertex. From Esposito *et al.* [9]

into a diquark equal to

$$\mathcal{M}(p) \propto \int d^3r e^{-(r-r_a)^2/2(B\sqrt{2})^2 - i\mathbf{p}\cdot\mathbf{r}} e^{-r^2/2\beta^2}, \quad (8.5)$$

while the cross section is given by

$$\sigma(cc \rightarrow [cc]) \simeq \frac{1}{4} \frac{d\sigma_{cc}}{d^3p} \left(\frac{2\sqrt{\pi}}{\sqrt{2B^2 + \beta^2}} \right)^3 e^{-r_a^2/2B^2}, \quad (8.6)$$

where $d\sigma_{cc}/d^3p$ is the (approximately constant) cross section in Figure 8.2.

3. *Dressing of the heavy diquark with two light antiquarks.* Neglecting the possible dissociation of the diquark into a DD pair – and hence providing an upper estimate for the production of \mathcal{T} particles – one can assume the probability for “dressing” the diquark with a light antiquark to be 0.1. Such probability has been estimated in analogy with the single heavy quark fragmentation. In particular, it has been assumed to be the same as in the $b \rightarrow \Lambda_b$ case at Tevatron [318].

Putting these three steps together, the expected yield for the \mathcal{T} particles are 20900, 9700, 600 and 1 events/hour for LHC at luminosity $10^{33} \text{ cm}^{-2}\text{s}^{-1}$, Tevatron at luminosity $8 \times 10^{31} \text{ cm}^{-2}\text{s}^{-1}$ and RHIC at d-Au luminosity $0.2 \times 10^{28} \text{ cm}^{-2}\text{s}^{-1}$, respectively.

However, as we previously mentioned, \mathcal{T} particles might also be produced from the decay of other particles. In particular, it seems reasonable to expect this production to be more likely if from particles that already contain a charm quark. In what follows we will consider the possible production from B_c decays [9]. In Figure 8.3 we report the Feynman diagram for these decays.

We will focus on the $B_c^+ \rightarrow \mathcal{T}_s^{++} D^{(*)-}$ decay, avoiding the use of specific models. Heavy meson decays into two baryons are particularly suitable to extract the effective strong coupling which we expect to determine also the process we are interested in – both indeed contain six quarks confined in a two-hadron final state. In particular, one can consider [319–321]

$$\mathcal{BR}(B^0 \rightarrow \bar{\Lambda}_c^- p) = (2.0 \pm 0.4) \times 10^{-5}; \quad (8.7a)$$

$$\mathcal{BR}(B^+ \rightarrow \bar{\Sigma}_c^0 p) = (3.7 \pm 1.5) \times 10^{-5}. \quad (8.7b)$$

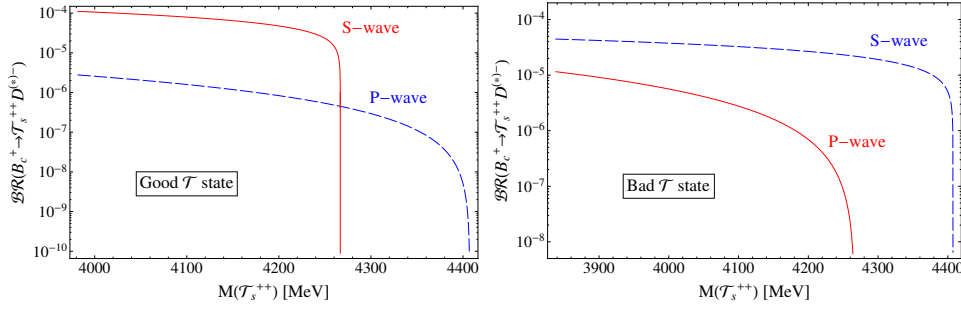


Figure 8.4. Branching ratios for the production of $B_c^+ \rightarrow \mathcal{T}_s^{++} D^-$ (dashed curve) and $B_c^+ \rightarrow \mathcal{T}_s^{++} D^{*-}$ (solid curve) for the good 1^+ state (left panel) and for the bad 0^+ state (right panel) as a function of the mass of \mathcal{T}_s^{++} , in the above-threshold region. From Esposito *et al.* [9].

These interactions can be described by mean of the following heavy meson chiral Lagrangian [199]:

$$\mathcal{L}_{eff} = \frac{g_B}{2M_B^2} \partial_\mu B \bar{P} \gamma^\mu \left(1 - \frac{g_A}{g_V} \gamma_5 \right) \Lambda, \quad (8.8)$$

where g_B is a strong effective coupling and we take $g_A/g_V \simeq 1.27$ as for the β -decay. Λ represents both the $\bar{\Lambda}_c^-$ and the $\bar{\Sigma}_c^0$, the dynamics of the two processes being the same. Fitting from the experimental data in Eqs. (8.7) one finds

$$g_{B^0} = (4 \pm 1) \times 10^{-3} \text{ MeV}; \quad (8.9a)$$

$$g_{B^+} = (5 \pm 3) \times 10^{-3} \text{ MeV}, \quad (8.9b)$$

which are compatible within the errors, thus suggesting that the internal dynamics might indeed be similar.

Extending this assumption to the $B_c^+ \rightarrow \mathcal{T}_s^{++} D^{(*)-}$ decay we can take the effective coupling for this case, $g_{B_c^+}$, to be the average of the previous two. The decay amplitudes can again be parametrized in terms of color structure, kinematics and the effective coupling. In Figure 8.4 we report the obtained results for both good and bad states and for a production associated with both a D^- and a D^{*-} . One can notice that, if the \mathcal{T} is near threshold, than the branching ratio for an S -wave production is just one order of magnitude smaller of the observed $B_c^+ \rightarrow J/\psi D_s^{(*)+}$ decays [322].

We performed a preliminary search of the good \mathcal{T}^+ state via lattice QCD [10]. We use 128 CLS gauge configurations on a $32^3 \times 64$ lattice, with $N_f = 2$ sea flavors, non-perturbatively $\mathcal{O}(a)$ improved. The bare gauge coupling is $\beta = 5$, reproducing a lattice spacing $a = 0.075$ fm. The pion mass is 490 MeV. The charm mass we used is lighter than the physical charm mass, $m_D \sim 1.5$ GeV. Each operator analyzed is doubled using 50 gaussian smearing steps on fermion fields, $\hat{S} = \frac{1+\alpha\Delta}{1+6\alpha}$, with Δ is the spatial laplacian and $\alpha = 0.6$. Preliminarily, we determined the mass of the charmed pseudoscalar D and vector D^* mesons, studying the respective meson-meson correlator. We then solve the Generalized Eigenvalue Problem for the

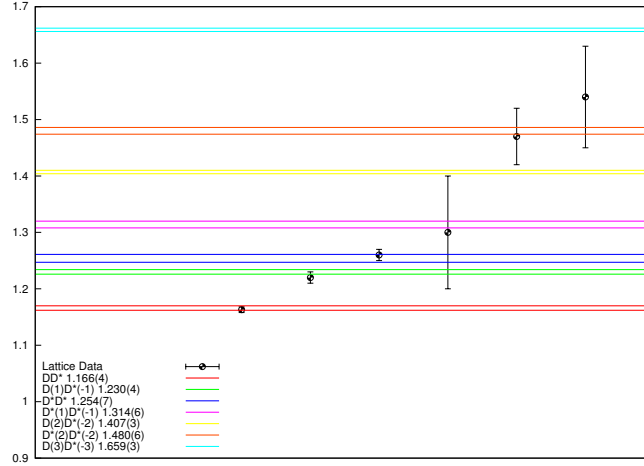


Figure 8.5. Spectrum of the $J^P = 1^+$, $I = 0$ channel extracted from the basis of operators $\mathcal{O}_1\mathcal{O}_2\mathcal{O}_3$ [10]. Notice that we extract the state $D(1)D^*(-1)$, without inserting the corresponding operator. This is due to the presence of correlators constructed with point-like inverted propagators.

correlators $\int d^3x \langle \mathcal{O}_i(0, x) \mathcal{O}_j^\dagger(0, 0) \rangle$, where the operators are given by

$$\mathcal{O}_1 = \varepsilon^{ijk} \varepsilon^{lmk} \bar{c}_c^i(x) \gamma^A c^j(x) (\bar{u}^l(x) \gamma^5 d_c^m(x) - \bar{d}(x)^l \gamma^5 u_c^m(x)) \quad (\text{good } \mathcal{T}^+) \quad (8.10)$$

$$\mathcal{O}_2 = \bar{u}(x) \gamma^A c(x) \bar{d}(x) \gamma^5 c(x) - \bar{d}(x) \gamma^A c(x) \bar{u}(x) \gamma^5 c(x) \quad (D^0 D^{*+} - D^{*0} D^+) \quad (8.11)$$

$$\mathcal{O}_3 = \bar{u} \gamma^A c [\vec{p} = \vec{0}] \bar{d} \gamma^5 c - \bar{d} \gamma^A c [\vec{p} = \vec{0}] \bar{u} \gamma^5 c \quad (D^0 D^{*+} - D^{*0} D^+) \quad (8.12)$$

$$\mathcal{O}_4 = \varepsilon^{ABC} \bar{u}(x) \gamma^B c(x) \bar{d}(x) \gamma^C c(x) \quad (D^{*0} D^{*+}) \quad (8.13)$$

$$\mathcal{O}_5 = \varepsilon^{ABC} \bar{u} \gamma^B c [\vec{p} = \vec{0}] \bar{d} \gamma^C c \quad (D^{*0} D^{*+}) \quad (8.14)$$

The observed levels are reported in Figure 8.5. We do not observe any unknown energy level. This does not exclude the possibility that a resonance could appear in one of the channel considered in this analysis. In order to clarify the situation, more statistics and a larger basis of operators is needed.

Summarizing, the theoretical study and the experimental search for possible exotic mesons with double flavor quantum numbers might be an interesting idea to further understand the nature of these particles. In particular, such particles might appear with double electric charge, in which case the only possible interpretation would be that of a compact tetraquark.

We also showed that their widths and production branching fractions are large enough to be accessible at the present hadron facilities such as LHCb, ALICE, Tevatron and RHIC.

8.2 Compact tetraquarks and meson molecules in heavy ion collisions

Another possible tool to gain some insight about the nature of candidate tetraquarks is to study their behavior in the extreme conditions of relativistic heavy ion collisions at RHIC and LHC.

When two nuclei (Au+Au and Pb+Pb for RHIC and LHC respectively) collide at relativistic speed, the resulting system reaches extremely high temperatures. In particular, if those temperatures are higher than a critical value [323], $T_C = (154 \pm 9)$ MeV, quark and gluons are liberated from hadrons and a new state of matter is created, the so-called Quark-Gluon-Plasma (QGP). It is a QCD plasma of deconfined quarks and gluons which seems to behave as a nearly perfect fluid [324, 325]. After a certain amount of time this “fire-ball” expands and cools down to temperatures below T_C and hence the partons confine again. In this phase the system looks like an expanding gas of interacting hadrons, the so-called Hadron Resonance Gas (HRG). When the temperature drops below the so-called freeze-out temperature, $T_F \simeq 120$ MeV [262], these hadrons simply fly apart without interacting anymore. In the following we will indicate with the subscripts C , H and F quantities at the critical, hadronization and freeze-out temperatures respectively (see for example Table 8.3).

It has been proposed [143, 262, 326, 327] that the study of the produced number of exotic mesons, and in particular the time-honored $X(3872)$, in heavy ion collisions might help to distinguish between the compact tetraquark picture and the molecular one. In particular, the two main techniques to estimate the yield of a particle in hot QGP are:

- *The statistical model [328]:* it assumes that the matter produced in heavy ion collisions is in thermodynamical equilibrium and it is known to describe the relative yields of ordinary hadrons very well. In this model the number of hadrons of a given type, h , produced is given by

$$N_h^{\text{stat}} = V_H \frac{g_h}{2\pi^2} \int_0^\infty \frac{p^2 dp}{\gamma_h^{-1} e^{E_h/T_H} \pm 1}, \quad (8.15)$$

with g_h being the degeneracy of h and $V_H (T_H)$ the volume (temperature) of the source when the statistical production of the hadron occurs. $\gamma_h = \gamma_c^{n_c + n_{\bar{c}}} e^{(\mu_B B + \mu_S S)/T_H}$ is the fugacity, with n_c and $n_{\bar{c}}$ the number of charm and anti-charm in the hadron, B and S the baryon and strangeness numbers of the hadron and μ_B and μ_S the corresponding chemical potentials.

This model does not contain any information about the actual internal structure of h and, in the following, it will be used as a normalization factor.

- *The coalescence model [252]:* it is based on the sudden approximation by calculating the overlap of the density matrix for the constituents of the hadron h with the Wigner function for the produced particle. It is built to take into account the inner structure of h , such as angular momentum, multiplicity of quarks, etc. This picture has successfully explained many different experimental data (*e.g.* enhancement of baryon production in the intermediate p_T

region [329], quark number scaling of the elliptic flow [330]). In this context, the number of hadrons produced is given by

$$N_h^{\text{coal}} \simeq g_h \prod_{j=1}^n \frac{N_j}{g_j} \prod_{i=1}^{n-1} \frac{(4\pi\sigma_i^2)^{3/2}}{V(1+2\mu_i T\sigma_i^2)} \left[\frac{4\mu_i T\sigma_i^2}{3(1+2\mu_i T\sigma_i^2)} \right]^{l_i}, \quad (8.16)$$

if one uses the non-relativistic approximation, neglect the transverse flow and considers only the unit rapidity. Moreover, one assumes an harmonic oscillator ansatz for the hadron internal structure. Here g_j and N_j are the degeneracy and number of the j -th constituent and $\sigma_i = 1/\sqrt{\mu_i\omega}$, with ω the oscillator frequency and μ_i the reduced mass given by $\mu_i^{-1} = m_{i+1}^{-1} + \left(\sum_{j=1}^i m_j\right)^{-1}$. Lastly $l_i = 0, 1$ for a S -wave and a P -wave constituents respectively.

Note that from Eq. (8.16) follows that hadrons with more constituents are, in general, more suppressed and that S -wave coalescence is favored with respect to the P -wave one.

A large part of the information about the nature of the considered hadron is hence somehow embedded in the frequency ω of the harmonic oscillator. In the case of a compact multi-quark state one can fit ω by requiring the coalescence model to reproduce the reference normal hadron yields in the statistical model. For the case of interest, the $X(3872)$ with light and charm quarks, one finds $\omega_c = 385$ MeV by requiring the matching with the yield of $\Lambda_c(2286)$ [262]. The final result is a yield $N_X^{4q} = 4.0 \times 10^{-5}$.

For the case of a meson molecule, instead, one can fix ω by using $\omega = 3/(2\mu_1\langle r^2 \rangle)$ for a two-body S -wave state, together with the equation that relates the binding energy of a loosely bound molecule with its scattering length, a , $E \simeq 1/(2\mu_1 a^2)$ and $\langle r^2 \rangle \simeq a^2/2$. For the case of the X one gets $\omega = 3.6$ MeV [262]. It is worth noting that $\omega \propto E$ and hence, according to Eq. (8.16), the smaller the binding energy of the molecule, the smaller ω and thus the larger is the N_h^{coal} . In this case it turns out to be $N_X^{\text{mol}} = 7.8 \times 10^{-4}$.

In Figure 8.6 the predicted yield for different hadrons in the coalescence model are shown [262]. As one immediately notices, the predictions for the compact tetraquark and for the molecule are completely different. In particular, a molecular structure for the $X(3872)$ implies a yield which is higher than ordinary hadrons, while a compact structure implies a lower yield. This difference is essentially due to the small binding energy of the molecular state and to the high number of constituents of the compact states. There is also another extremely striking feature, *i.e.* the predicted behaviors for the molecule and the compact tetraquark in relativistic heavy ion collisions are opposite to those predicted for pp collisions, as discussed in Chapter 6. Also note that both yields are close enough to the ordinary ones to be experimentally measured at RHIC and LHC.

The previous description of exotic mesons in heavy ion collision can be further improved [327]. So far we only studied the production during the QGP phase. However, the number of exotic mesons can also vary during the HRG phase, when disintegration/creation processes due to the interaction with other particles can

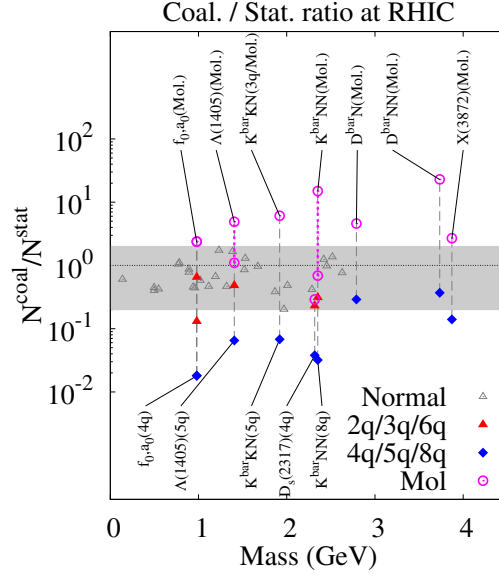


Figure 8.6. Hadron yields in the coalescence model normalized with respect to the statistical one at RHIC, from ExHIC Collaboration [262]. Note the sharp difference between the predictions for a compact four-quark structure and for a molecular structure of the $X(3872)$. The gray band represents the range of yields for ordinary hadrons.

occur. In particular, the most effective processes are – see Figure 8.7:

$$X\pi \rightarrow \bar{D}^*D^*; \quad X\pi \rightarrow \bar{D}D; \quad X\rho \rightarrow \bar{D}^*D; \quad (8.17a)$$

$$X\rho \rightarrow D^*\bar{D}; \quad X\rho \rightarrow D\bar{D}; \quad X\rho \rightarrow D^*\bar{D}^*, \quad (8.17b)$$

and the inverse ones for the creation of a $X(3872)$. The vertices for such reaction can be obtained from an effective Lagrangian approach, with a combination of Heavy Quark Effective Theory (HQET) and chiral theory [281, 327]. In Figure 8.8 we report the cross sections for the processes in Eq. (8.17).

The computed cross sections can be used to estimate the change of the number of $X(3872)$ in the HRG as a function of the proper time, τ , by mean of kinetic

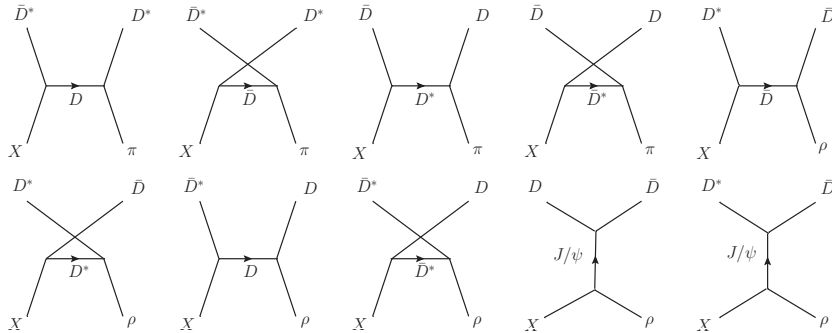


Figure 8.7. Possible disintegration processes of the $X(3872)$ in the hadron resonance gas phase.

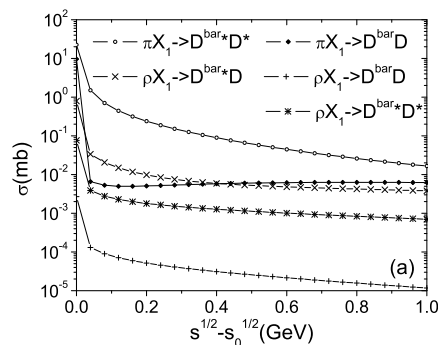


Figure 8.8. Cross sections for the absorption of a $X(3872)$ with $J^{PC} = 1^{++}$ as a function of the difference between the total center-of-mass energy \sqrt{s} and the energy threshold for the process $\sqrt{s_0}$. From Cho and Lee [327].

theory [327]:

$$\frac{dN_X}{d\tau} = R_{QGP}(\tau) + \sum_{\ell, c, c'} (\langle \sigma_{cc' \rightarrow \ell X} v_{cc'} \rangle n_c(\tau) N_{c'}(\tau) - \langle \sigma_{\ell X \rightarrow cc'} v_{\ell X} \rangle n_\ell(\tau) N_X(\tau)), \quad (8.18)$$

where the subscripts ℓ , c and c' stand for a light meson and the two charmed mesons respectively. $n_a(\tau)$ and $N_a(\tau)$ are the density and abundance of the particle a at proper time τ calculated using the statistical model Eq. (8.15) with τ -dependent volume and temperature [327]:

$$V(\tau) = \pi \left[R_C + v_C (\tau - \tau_C) + a_C/2 (\tau - \tau_C)^2 \right]^2 \tau_C, \quad (8.19)$$

$$T(\tau) = T_C - (T_H - T_F) \left(\frac{\tau - \tau_H}{\tau_F - \tau_H} \right)^{4/5}.$$

These equations are obtained following the boost invariant Bjorken picture with an accelerated transverse expansion [331]. In particular, R_C is the radius of the system at T_C , and v_C and a_C are its expansion velocity and acceleration. In Table 8.3 we report the values used for the present analysis.

	Temp. (MeV)	Time (fm/c)
$R_C = 8.0$ fm	$T_C = 175$	$\tau_C = 5.0$
$v_C = 0.4c$	$T_H = 175$	$\tau_H = 7.5$
$a_C = 0.02c^2/\text{fm}$	$T_F = 125$	$\tau_F = 17.3$

Table 8.3. Values for the volume and temperature profiles in the schematic model of Eq. (8.19).

The averages in Eq. (8.18) can be evaluated by mean of the kinetic theory:

$$\langle \sigma_{ab \rightarrow cd} v_{ab} \rangle = \frac{\int d^3 p_a d^3 p_b f_a(\mathbf{p}_a) f_b(\mathbf{p}_b) \sigma_{ab \rightarrow cd} v_{ab}}{\int d^3 p_a d^3 p_b f_a(\mathbf{p}_a) f_b(\mathbf{p}_b)}, \quad (8.20)$$

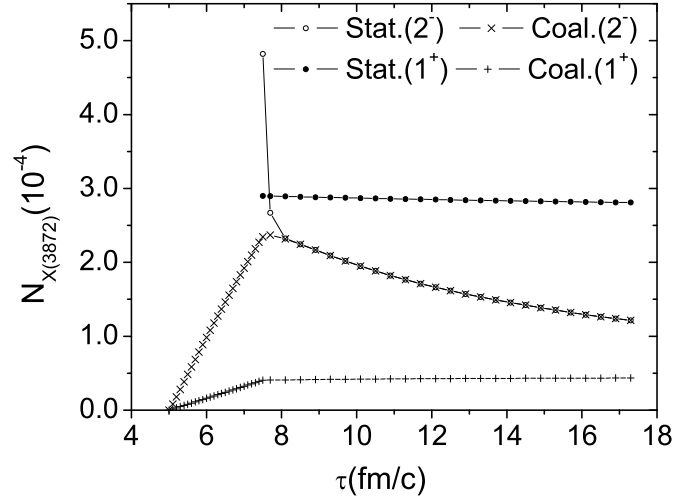


Figure 8.9. Number of $X(3872)$ as a function of proper time under the assumption of a compact tetraquark and of a molecular nature, from Cho and Lee [327]. For comparison, the prediction obtained with a pure statistical approach (which is blind to the internal structure) is drawn as well.

with $f_a(\mathbf{p}_a)$ being the single particle density in momentum space. Lastly, the term $R_{QGP}(\tau)$ is included to take into account the effect of the production of the $X(3872)$ through hadronization from the quark-gluon-plasma and is given by

$$R_{QGP}(\tau) = \begin{cases} N_X^0 / (\tau_H - \tau_C), & \tau_C < \tau < \tau_H ; \\ 0, & \text{otherwise} \end{cases} \quad (8.21)$$

N_X^0 is the number of $X(3872)$ produced by the quark-gluon-plasma as explained in Eqs. (8.15) and (8.16). Once all the ingredients are set one can compute the number of X as a function of proper time, *i.e.* of the evolution of the hot expanding system. In Figure 8.9 we report the results for central Au-Au collisions at $\sqrt{s_{NN}} = 200$ GeV.

The number of $X(3872)$ in the assumption of a $D^0\bar{D}^{*0}$ molecular nature can be computed by solving the evolution equation (8.18) backward in time, starting from the yield found before using the coalescence model, $N_X^{\text{mol}} = 7.8 \times 10^{-4}$. The result is again shown in Figure 8.9.

As one can see, the inclusion of this further possible mechanism of creation/destruction of the $X(3872)$, *i.e.* the interaction of this meson in the hadron resonance gas, leads to a yield for an eventual molecular state which is a factor of ~ 18 larger than that for a compact four-quark structure.

It should be noted that the previous discussion completely neglects transverse flow effects. However, this phenomena turned out to be the key ingredient to explain some puzzling experimental results like, for example, the observation made at RHIC that medium-induced suppression for values of the transverse momentum $p_T \simeq 2$ GeV is not as effective on protons as it is for pions [332, 333]. Particularly surprising was

the fact that the ratio p/π^+ of protons over charged pions for transverse momenta above 2 GeV reaches or even exceeds unity. The explanation to this phenomenon was the following. The expectation from the use of coalescence model is that it is less likely to bind states made by a larger number of components simply because the convolution of their wave functions is smaller. In other words, it is hard to find the components at small value of the relative momentum *and* at small relative positions. However, if one takes into account flow effects it turns out that, exactly because of collectivity, if the previously mentioned components are found close in momentum space, they are also likely to be close in coordinate space, thus increasing the yield of states with higher number of constituents. As we said, this effect turned out to be relevant at explaining the observed p/π^+ ratio for $p_T \simeq 2$ GeV.

In our case, this phenomenon might be quite important at increasing the number of tetraquarks produced with respect to the number of molecules [334, 335]. Therefore, in our view, the conclusions drawn in Figure 8.6 are merely partial.

In conclusion, we showed how the study of the yield of $X(3872)$ – and possibly of other exotic mesons – in heavy ion collisions might have an impact on the determination of its nature. In particular, it turns out that, according to the coalescence model [252], the number of X produced should be much larger if it is a loosely bound molecule than if it is compact tetraquark, in striking contrast to what expected for pp collisions. Moreover, the predicted yields [262, 327] are large enough to be measurable by the current experimental facilities, RHIC and LHC. Future studies should try to include collective flow effects as well.

Conclusions

The field of XYZ phenomenology has impressively been growing on the experimental side. On the other hand it seems that the theoretical models to explain the rich amount of information nowadays available on these states are lagging behind. The comprehension of this sector is tightly related to our understanding of the internal structure of hadrons.

In this thesis we have tried to highlight the reasons for the most fundamental quark picture, suggesting these states to be new kinds of hadrons with respect to standard mesons and baryons, namely new bodyplans of quarks arranged into tetraquarks. The possibility of having long-lived tetraquarks is not excluded by the large number of colors limit of QCD and, in addition, some of the observed charged resonances appear as striking evidence that compact tetraquarks have already been *observed*. The simplified diquark-antidiquark model reviewed in this paper is not the definitive explanation of the XYZ resonances, but we believe it must be at the core of the picture. Within this model, we described the properties of some of the observed states, like the spin of the $X(3872)$ [1], and the identification of the $Z_c(3900)$ as the 1^{+-} partner of the $X(3872)$ [7]. We analyzed BES III $e^+e^- \rightarrow h_c\pi^+\pi^-$ and $\rightarrow \chi_{c0}\omega$ and showed that the structures observed are compatible to be the Y_3 P -wave tetraquark predicted by the updated model [6]. Moreover, we have calculated the $Z_c^{(\prime)} \rightarrow \eta_c\rho$ decays both within a tetraquark assignment, and according to a molecular hypothesis using a Nonrelativistic Effective Theory [8]. We showed that the predictions for the branching ratios are different by orders of magnitude, thus providing a clear signal to discriminate the correct model when data on this channel will be available.

One still has to explain what prevents some of the states predicted by that model to be formed/observed in experiment. We started by looking for the origin of such selection rules in the *accidental* matchings of diquark-antidiquark levels with open charm (beauty) meson thresholds [3, 5]. We do not think that there is anything profound in these matchings, given the huge number of thresholds which can be formed with the known pairs of charmed or beauty mesons. However tetraquark discrete levels might correspond to narrow hadron resonances whenever anyone of these matchings happens to be realized. This is probably the passage to be done to fill the gap between the tetraquark interpretation and the actual phenomenology of these resonances.

Most of the work has been devoted to the understanding of the large $X(3872)$ prompt production cross section at hadron colliders. Were this state a loosely bound molecule, a simple square well model show that the constituent must have a relative momentum $k_0 \sim 50$ MeV. In Ref. [139], MC simulations were used to estimate an

upper limit for the cross section, and found values two orders of magnitude smaller than the experimental one. A controversy on the choice of this k_0 cutoff momentum followed. Some authors proposed this k_0 has to be 10 times larger on the basis of Migdal-Watson theory of Final State Interactions [239], thus making the estimated upper limit for the cross section even larger than the experimental value, but a subsequent paper casted doubts on the applicability of the Migdal-Watson approach in an environment polluted by hundreds of comoving pions, like hadron collisions. In two papers we argued that the rescattering of such pions on molecular candidates might indeed slow down the molecular constituent in their center-of-mass frame, and effectively increase the number of low-momentum meson pairs, and the $X(3872)$ cross section as well. The results obtained in a preliminary sample of simulated $p\bar{p} \rightarrow c\bar{c}$ events went in the right direction [2], but the full QCD simulation show that the effect is not enough to justify the experimental value [3]. We also proposed to compare the differential prompt production cross section $d\sigma/dp_\perp$ of the X with the ones of *bona fide* molecules, *i.e.* light nuclei: if these objects share the same nature, they are expected to have similar behavior as a function of p_\perp , regardless of the details of any mechanism which would be at work to produce large amounts of molecules at high p_\perp . In Ref. [3] we used MC simulations to extrapolate ALICE deuteron preliminary data at $p_\perp \lesssim 3$ GeV up to the 15 GeV region, where the X has been observed. ALICE then published data on deuteron, ^3He and hypertriton differential cross sections in pp and Pb-Pb collisions at $p_\perp \lesssim 10$ GeV. We used Glauber theory to translate the cross sections from Pb-Pb to pp collisions, and then extrapolated with simple functional forms to the $p_\perp \sim 15\text{-}20$ GeV region [4]. In both papers we showed that the $X(3872)$ cross section is at least two orders of magnitude larger than the typical values for light nuclei, thus challenging its molecular interpretation. High p_\perp measurements of deuteron and hypertriton will give a final answer on this topic.

Finally, we used the tetraquark formalism to describe doubly charmed states [9], which might be produced in B_c decays and would be hardly explained by any molecular framework. The \mathcal{T}_s^{++} state, if above the D^*D_s threshold, would be a doubly charged state with a remarkably clean experimental signature. We also started a preliminary search of these states on the lattice [10], which did not find any new level yet.

Finally, it may be that we are looking at different aspects of the same problem using different descriptions, as considered by someone. It may also be true that the definitive answer could be in the non-perturbative intricacies of strong interactions which might eventually be captured only using lattice QCD methods. Yet, in the meanwhile, we think that we made some interesting and solid progress, and especially we believe that there is indeed a problem in XYZ resonance physics: whatever side you are looking at it, it is not a “mirage” made of effects. It looks like there is a pattern behind.

Appendix A

One-loop β of QCD by the background field method

The basic philosophy is as in [336]. Some considerations on the effective action in QCD are in [337].

The partition function of pure YM is:

$$Z = \int \delta A \exp\left(-\frac{1}{2g^2} S_{\text{YM}}\right) \quad (\text{A.1})$$

where:

$$S_{\text{YM}} = \int d^4x \text{Tr} (F_{mn})^2 = \frac{1}{2} \int d^4x (F_{mn}^a)^2 \quad (\text{A.2})$$

The gauge connection is a matrix valued in the fundamental representation of the Lie algebra of $SU(N)$:

$$A_m = A_m^a T^a \quad (\text{A.3})$$

with the Hermitian generators in the fundamental representation normalized as:

$$\text{Tr} (T^a T^b) = \frac{1}{2} \delta^{ab} \quad (\text{A.4})$$

The curvature of the YM connection is:

$$F_{mn} = \partial_m A_n - \partial_n A_m + i [A_m, A_n] \quad (\text{A.5})$$

$$F_{mn}^a = \partial_m A_n^a - \partial_n A_m^a - f^{abc} A_m^b A_n^c \quad (\text{A.6})$$

To perform the one-loop computation of the effective action a linear source term $J_n A_n$ is introduced in the Lagrangian, and the gauge connection is split into a classical background field and a fluctuating quantum field $A_m = \tilde{A}_m + \delta A_m$. The Fourier transform of the quantum field is supposed to be supported on momenta much larger than the momenta of the classical background field. By the splitting of the connection into $A_m = \tilde{A}_m + \delta A_m$ the curvature decomposes as follows:

$$F_{mn}(\tilde{A} + \delta A) = F_{mn}(\tilde{A}) + D_m(\tilde{A})\delta A_n - D_n(\tilde{A})\delta A_m + i [\delta A_m, \delta A_n] \quad (\text{A.7})$$

where the covariant derivative $D_m(\tilde{A}) = \partial_m + i[\tilde{A}_m, \cdot]$ acts in the adjoint representation. We understand the integration on space-time in the following, and we freely

integrate by parts. Since we are performing a one-loop perturbative computation, we keep only up to the quadratic terms in δA_m in the action.

We use the equation of motion $\frac{1}{g^2} D_m(\tilde{A})F(\tilde{A})_{mn} = J_n$ to eliminate the linear term in the fluctuation. The linear term in the background field is eliminated by the Legendre transform. In the following the dependence of the curvature and of the covariant derivatives on the background field is understood. We get:

$$\begin{aligned} F_{mn}^2(\tilde{A} + \delta A) &\sim F_{mn}^2 + (D_m \delta A_n - D_n \delta A_m)^2 + 2iF_{mn} [\delta A_m, \delta A_n] \\ &= F_{mn}^2 + 2(D_m \delta A_n)^2 - 2D_m \delta A_n D_n \delta A_m + 2iF_{mn} [\delta A_m, \delta A_n] \end{aligned} \quad (\text{A.8})$$

Using:

$$(D_m D_n) \delta A_r = (D_n D_m) \delta A_r + i[F_{mn}, \delta A_r] \quad (\text{A.9a})$$

$$\text{Tr}(\delta A_n [F_{mn}, \delta A_m]) = \text{Tr}(F_{mn} [\delta A_m, \delta A_n]) = -\text{Tr}(\delta A_m [F_{mn}, \delta A_n]) \quad (\text{A.9b})$$

the quadratic form in Eq. (A.8) becomes:

$$\begin{aligned} \text{Tr}F_{mn}^2(\tilde{A} + \delta A) &\sim \text{Tr}\left((D_m \delta A_n - D_n \delta A_m)^2 + 2iF_{mn} [\delta A_m, \delta A_n]\right) \\ &= \text{Tr}\left(-2\delta A_m \Delta \delta A_m + 2\delta A_n D_m D_n \delta A_m + 2iF_{mn} [\delta A_m, \delta A_n]\right) \\ &= \text{Tr}\left(-2\delta A_m \Delta \delta A_m + 2\delta A_n D_n D_m \delta A_m + 2i\delta A_n [F_{mn}, \delta A_m] \right. \\ &\quad \left. + 2iF_{mn} [\delta A_m, \delta A_n]\right) \\ &= \text{Tr}\left(-2\delta A_m \Delta \delta A_m - 2(D_m \delta A_m)^2 - 4i\delta A_m [F_{mn}, \delta A_n]\right) \end{aligned} \quad (\text{A.10})$$

where $\Delta = D^2$ and

$$(\Delta)^{ac} = (D_m)^{ad}(D_m)^{dc} = \partial^2 \delta^{ac} - \partial_m A_m^b f^{abc} - 2A_m^b f^{abc} \partial_m + A_m^b f^{abd} A_m^e f^{dec} \quad (\text{A.11})$$

The gauge-fixing is performed by the Faddeev-Popov procedure. It is convenient to choose the Feynman gauge with respect to the background gauge field \tilde{A}_m :

$$D_m \delta A_m - c = 0 \quad (\text{A.12})$$

c is an auxiliary Gaussian field chosen in such a way to cancel the longitudinal term in Eq. (A.10) by adding $\frac{1}{g^2} \int d^4x \text{Tr}(D_m \delta A_m)^2$ to the action. As a consequence the quadratic part of gauge-fixed action is:

$$\frac{1}{2g^2} \int d^4x \text{Tr}(-2\delta A_m \Delta \delta A_m - 4i\delta A_m [F_{mn}, \delta A_n]) \quad (\text{A.13})$$

that in components becomes:

$$\frac{1}{2g^2} \int d^4x \delta A_m^a \left(-(\Delta)^{ac} \delta_{mn} + 2f^{abc} F_{mn}^b \right) \delta A_n^c \quad (\text{A.14})$$

where $\text{ad } F_{mn} = [F_{mn}, \cdot]$, i.e. $(\text{ad } F_{mn})^{ac} = if^{abc} F_{mn}^b$. After integrating on the quadratic fluctuation δA and inserting the FP determinant $\text{Det}(-\Delta)$ the one-loop effective action $\Gamma_{1\text{-loop}}(A)$ reads:

$$e^{-\Gamma_{1\text{-loop}}(A)} = e^{-\frac{1}{2g^2} S_{\text{YM}}(A)} \text{Det}^{-1/2}(-\Delta \delta_{mn} - 2i \text{ad } F_{mn}) \text{Det}(-\Delta) \quad (\text{A.15})$$

The following identity holds:

$$\text{Det}^{-1/2}(-\Delta \delta_{mn} - 2i \text{ad } F_{mn}) = \text{Det}^{-1/2}(-\Delta \delta_{mn}) \text{Det}^{-1/2} \left(1 - 2i (-\Delta)^{-1} \text{ad } F_{mn} \right) \quad (\text{A.16})$$

The first factor gives:

$$\text{Det}^{-1/2}(-\Delta \delta_{mn}) = \text{Det}^{-2}(-\Delta) \quad (\text{A.17})$$

Therefore, the one-loop effective action reads:

$$e^{-\Gamma_{1\text{-loop}}(A)} = e^{-\frac{1}{2g^2} S_{\text{YM}}(A)} \text{Det}^{-1/2} \left(1 - 2i (-\Delta)^{-1} \text{ad } F_{mn} \right) \text{Det}^{-1}(-\Delta) \quad (\text{A.18})$$

The first determinant is the spin contribution while the second determinant is the orbital contribution. We can factorize away a trivial infinite constant from the orbital contribution:

$$\begin{aligned} \text{Det}^{-1}(-\Delta) &= \text{Det}^{-1} \left(-\partial^2 - i\partial_m A_m - 2iA_m \partial_m + A_m A_m \right) \\ &= \text{Det}^{-1}(-\partial^2) \text{Det}^{-1} \left(1 + (-\partial^2)^{-1} (-i\partial_m A_m - 2iA_m \partial_m + A_m A_m) \right) \end{aligned} \quad (\text{A.19})$$

Using:

$$\text{Det}(1 + M) = e^{\text{Tr} \log(1+M)} = e^{\text{Tr } M - \text{Tr}(M)^2/2 + \dots} \quad (\text{A.20})$$

at the lowest non-trivial order we get:

$$\begin{aligned} \text{Det}^{-1}(-\Delta) &= \text{Det}^{-1}(-\partial^2) \exp \left[-\text{Tr} \left[(-\partial^2)^{-1} (-i\partial_m A_m - 2iA_m \partial_m + A_m A_m) \right] \right] \\ &\quad \exp \left[\frac{1}{2} \text{Tr} \left[(-\partial^2)^{-1} (-i\partial_m A_m - 2iA_m \partial_m + A_m A_m) \right. \right. \\ &\quad \left. \left. (-\partial^2)^{-1} (-i\partial_m A_m - 2iA_m \partial_m + A_m A_m) \right] \right] \end{aligned} \quad (\text{A.21})$$

where the trace is over the space-time, the Lie algebra and the vector indices. The term $\text{Det}^{-1}(-\partial^2)$ is an irrelevant constant while the trace in the Lie algebra of the term linear in A_m vanishes. The term $\text{Tr} \left[(-\partial^2)^{-1} A_m A_m \right]$ is a quadratically divergent tadpole that cancels in any gauge-invariant regularization scheme, since it would give rise to a mass counterterm for the gauge connection. Therefore, it can be ignored. There remains the interesting divergence:

$$\text{Det}^{-1}(-\Delta) \sim \exp \left[\frac{1}{2} \text{Tr} \left[(-\partial^2)^{-1} (i\partial_m A_m + 2iA_m \partial_m) (-\partial^2)^{-1} (i\partial_m A_m + 2iA_m \partial_m) \right] \right] \quad (\text{A.22})$$

that evaluated in momentum space leads to:

$$\exp \left[\frac{1}{2} \int \frac{d^4 k}{(2\pi)^4} \int \frac{d^4 p}{(2\pi)^4} \text{Tr} (A_m(-k) A_n(k)) \frac{(2p_m - k_m)(2p_n - k_n)}{p^2 (p - k)^2} \right] \quad (\text{A.23})$$

with the trace Tr on the Lie algebra indices. We are interested in extracting the logarithmic divergences by expanding the denominator in powers of k/p up to the appropriate order:

$$\begin{aligned}
& \int \frac{d^4 p}{(2\pi)^4} \frac{(2p_m - k_m)(2p_n - k_n)}{p^2(p-k)^2} = \int \frac{d^4 p}{(2\pi)^4} \frac{(2p_m - k_m)(2p_n - k_n)}{p^4(1 + (k^2 - 2kp)/p^2)} \\
& \sim \int \frac{d^4 p}{(2\pi)^4} \frac{(4p_m p_n + k_m k_n - 2k_m p_n - 2k_n p_m)}{p^4} \left(1 + \frac{2pk}{p^2} - \frac{k^2}{p^2} + \frac{4(pk)^2}{p^4} \right) \\
& \sim \int \frac{d^4 p}{(2\pi)^4} \frac{-4k^2 \frac{p_m p_n}{p^2} + 16k_r k_s \frac{p_m p_n p_r p_s}{p^4} + k_m k_n - 4k_n k_r \frac{p_m p_r}{p^2} - 4k_m k_r \frac{p_n p_r}{p^2}}{p^4} \\
& = \int \frac{d^4 p}{(2\pi)^4} \frac{-\frac{1}{3}(k^2 \delta_{mn} - k_m k_n)}{p^4} = -\frac{1}{3} (k^2 \delta_{mn} - k_m k_n) \frac{1}{(4\pi)^2} \log \left(\frac{\Lambda}{\mu} \right)^2
\end{aligned} \tag{A.24}$$

where we have integrated symmetrically:

$$p_m p_n \rightarrow \frac{1}{4} p^2 \delta_{mn}, \quad p_m p_n p_r p_s \rightarrow \frac{1}{24} p^4 (\delta_{mn} \delta_{rs} + \delta_{mr} \delta_{ns} + \delta_{ms} \delta_{nr}) \tag{A.25}$$

Hence the orbital contribution to the beta function is:

$$\begin{aligned}
\text{Det}^{-1}(-\Delta) & \sim \exp \left[-\frac{1}{3(4\pi)^2} \log \left(\frac{\Lambda}{\mu} \right)^2 \int \frac{d^4 k}{(2\pi)^4} \frac{1}{2} \text{Tr} \left[A_m (k^2 \delta_{mn} - k_m k_n) A_n \right] \right] \\
& = \exp \left[-\frac{1}{3(4\pi)^2} \log \left(\frac{\Lambda}{\mu} \right)^2 \int \frac{d^4 k}{(2\pi)^4} \frac{1}{2} \left[A_m^b (k^2 \delta_{mn} - k_m k_n) A_n^d \right] (-f^{abc} f^{cda}) \right] \\
& = \exp \left[-\frac{N}{3(4\pi)^2} \log \left(\frac{\Lambda}{\mu} \right)^2 \frac{1}{4} \int d^4 x (F_{mn}^a)^2 \right]
\end{aligned} \tag{A.26}$$

where in the last step we used:

$$f^{abc} f^{abd} = N \delta^{cd} \tag{A.27}$$

and:

$$\frac{1}{4} \int d^4 x F_{mn}^a F_{mn}^a \sim \frac{1}{2} \int \frac{d^4 k}{(2\pi)^4} A_m^a(-k) A_n^a(k) (k^2 \delta_{mn} - k_m k_n) \tag{A.28}$$

at leading order. Now we compute the spin contribution to the effective action. Since $\text{Tr} F_{mn} = 0$, up to the quadratic order in F_{mn} we get:

$$\text{Det}^{-1/2} \left(1 - 2i(-\Delta)^{-1} \text{ad} F_{mn} \right) \sim \exp \left[-\text{Tr} \left((-\Delta)^{-1} \text{ad} F_{mn} (-\Delta)^{-1} \text{ad} F_{nm} \right) \right] \tag{A.29}$$

At the lowest order $(-\Delta) \sim (-\partial^2)$, therefore:

$$\begin{aligned}
& \text{Tr} \left((-\partial^2)^{-1} \text{ad} F_{mn} (-\partial^2)^{-1} \text{ad} F_{nm} \right) \\
& = \int d^4 x \int d^4 y \text{Tr} [G(x-y) \text{ad} F_{mn}(y) G(y-x) \text{ad} F_{nm}(x)] \\
& = -N \int d^4 x \int d^4 y G(x-y)^2 F_{mn}^a(y) F_{mn}^a(x)
\end{aligned} \tag{A.30}$$

where in coordinate space:

$$G(x-y) = \frac{1}{4\pi^2(x-y)^2} \quad (\text{A.31})$$

and:

$$\text{Tr}(\text{ad } F_{mn} \text{ ad } F_{nm}) = F_{mn}^b i f^{abc} F_{nm}^d i f^{cda} = -N F_{mn}^a F_{mn}^a \quad (\text{A.32})$$

Assuming that the background field carries momentum much smaller than the fluctuating field we can expand $F_{mn}(y) = F_{mn}(x) + \dots$ by Taylor series and keep the first term since we are interested only in the divergent terms. Thus defining $z = x - y$

$$\begin{aligned} \text{Tr} \left((-\partial^2)^{-1} \text{ad } F_{mn} (-\partial^2)^{-1} \text{ad } F_{nm} \right) &\sim -\frac{N}{(2\pi)^4} \int \frac{d^4 z}{z^4} \int d^4 x (F_{mn}^a)^2 \\ &= -\frac{N}{(4\pi)^2} \log \left(\frac{\Lambda}{\mu} \right)^2 \int d^4 x (F_{mn}^a)^2 = -\frac{4N}{(4\pi)^2} \log \left(\frac{\Lambda}{\mu} \right) \frac{1}{2} \int d^4 x (F_{mn}^a)^2 \end{aligned} \quad (\text{A.33})$$

Therefore, at this order the divergent part reads:

$$\text{Det}^{-1/2} \left(1 - 2i(-\Delta)^{-1} \text{ad } F_{mn} \right) \sim \exp \left[\frac{4N}{(4\pi)^2} \log \left(\frac{\Lambda}{\mu} \right) \frac{1}{2} \int d^4 x (F_{mn}^a)^2 \right] \quad (\text{A.34})$$

Finally, the local part of the one-loop effective action reads:

$$\begin{aligned} \Gamma_{\text{1-loop}} &= \frac{1}{2g^2} S_{\text{YM}} + \left(\frac{N}{3(4\pi)^2} - \frac{4N}{(4\pi)^2} \right) \log \left(\frac{\Lambda}{\mu} \right) \frac{1}{2} \int d^4 x (F_{mn}^a)^2 \\ &= \left(\frac{1}{2g^2(\Lambda)} - \frac{11N}{3(4\pi)^2} \log \left(\frac{\Lambda}{\mu} \right) \right) S_{\text{YM}} \end{aligned} \quad (\text{A.35})$$

Therefore, the bare coupling constant $g(\Lambda)$ renormalizes as:

$$\frac{1}{2g^2(\Lambda)} = \frac{1}{2g^2(\mu)} + \frac{11N}{3} \frac{1}{(4\pi)^2} \log \frac{\Lambda}{\mu} \quad (\text{A.36})$$

or:

$$g^2(\Lambda) = \frac{g^2(\mu)}{1 + \frac{11N}{3(4\pi)^2} g^2(\mu) \log \left(\frac{\Lambda}{\mu} \right)^2} \quad (\text{A.37})$$

that is the solution at one loop of the equation that defines the β function:

$$\beta(g) = \frac{\partial g}{\partial \log \Lambda} = -\beta_0 g^3 + \dots \quad (\text{A.38a})$$

$$\beta_0 = \frac{11N}{3(4\pi)^2} \quad (\text{A.38b})$$

Eq. (A.36) can be also written as:

$$\Lambda e^{-\frac{1}{2\beta_0 g^2(\Lambda)}} = \mu e^{-\frac{1}{2\beta_0 g^2(\mu)}} \quad (\text{A.39})$$

Thus the combination:

$$\Lambda_{\text{YM}} = \Lambda e^{-\frac{1}{2\beta_0 g^2(\Lambda)}} \quad (\text{A.40})$$

is independent on the cutoff Λ and it is a renormalization group invariant at one loop.

We add now n_f massless Dirac fermions in the fundamental representation. The action reads:

$$S_{\text{QCD}} = \frac{1}{2g^2} S_{\text{YM}} + \sum_{n_f} i \int d^4x \bar{\psi} D_m(A) \gamma^m \psi \quad (\text{A.41})$$

Integrating over the fermion variables, we get the fermion determinant:

$$\mathcal{D}et_\psi = [\det(D_m(A)\gamma^m)]^{n_f} \quad (\text{A.42})$$

At one loop we can simply evaluate the covariant derivative on the background gauge connection. Hence the fermion determinant factors out of the functional integral and it can be evaluated separately. We can put:

$$\begin{aligned} \mathcal{D}et_\psi &\sim \text{Det}^{n_f} (D_m \gamma^m) = \text{Det}^{n_f/2} (D_m D_n \gamma^m \gamma^n) \\ &= \text{Det}^{n_f/2} \left(\frac{1}{2} D_m D_n (\{\gamma^m, \gamma^n\} + [\gamma^m, \gamma^n]) \right) \\ &= \text{Det}^{n_f/2} \left(\Delta \mathbf{1} + i \frac{1}{2} F_{mn} \gamma^m \gamma^n \right) \\ &= \text{Det}^{n_f/2} (-\Delta \mathbf{1}) \text{Det}^{n_f/2} \left(1 - i \frac{1}{2} (-\Delta)^{-1} F_{mn} \gamma^m \gamma^n \right) \end{aligned} \quad (\text{A.43})$$

In order to evaluate the first determinant, we compare with Eq. (A.26) keeping trace of the spinor indices. The local divergent part reads:

$$\text{Det}^{n_f/2} (-\Delta \mathbf{1}) = \text{Det}^{2n_f} (-\Delta) \sim \exp \left[\frac{2n_f T_{\text{F}}}{3(4\pi)^2} \log \left(\frac{\Lambda}{\mu} \right)^2 \frac{1}{4} \int d^4x (F_{mn}^a)^2 \right] \quad (\text{A.44})$$

where T_{F} is the Dynkin index for the fundamental representation. For the spin contribution by comparison with Eq. (A.34), taking the trace over the spinor indices, we get the local divergent part:

$$\begin{aligned} &\text{Det}^{n_f/2} \left(1 - \frac{1}{2} i (-\Delta)^{-1} F_{mn} \gamma^m \gamma^n \right) \\ &\sim \exp \left[\frac{n_f}{16} \text{Tr} \left((-\Delta)^{-1} F_{mn} (-\Delta)^{-1} F_{rs} \gamma^m \gamma^n \gamma^r \gamma^s \right) \right] \\ &= \exp \left[\frac{n_f}{4} \text{Tr} \left((-\Delta)^{-1} F_{mn} (-\Delta)^{-1} F_{rs} (\delta^{mn} \delta^{rs} + \delta^{ms} \delta^{nr} - \delta^{mr} \delta^{ns}) \right) \right] \\ &= \exp \left[\frac{n_f}{2} \text{Tr} \left((-\Delta)^{-1} F_{mn} (-\Delta)^{-1} F_{nm} \right) \right] \\ &\sim \exp \left[-\frac{2n_f T_{\text{F}}}{(4\pi)^2} \log \left(\frac{\Lambda}{\mu} \right)^2 \frac{1}{4} \int d^4x (F_{mn}^a)^2 \right] \end{aligned} \quad (\text{A.45})$$

Finally, the local part of the one-loop effective action reads:

$$\begin{aligned}\Gamma_{\text{QCD}} &= \Gamma_{\text{YM}} + \left(-\frac{2n_f T_{\text{F}}}{3(4\pi)^2} + \frac{2n_f T_{\text{F}}}{(4\pi)^2} \right) \log\left(\frac{\Lambda}{\mu}\right)^2 \frac{1}{4} \int d^4x (F_{mn}^a)^2 \\ &= \left(\frac{1}{2g^2(\Lambda)} - \left(\frac{11N}{3(4\pi)^2} - \frac{4n_f T_{\text{F}}}{3(4\pi)^2} \right) \log\left(\frac{\Lambda}{\mu}\right) \right) \frac{1}{2} \int d^4x (F_{mn}^a)^2\end{aligned}\tag{A.46}$$

Setting $T_{\text{F}} = \frac{1}{2}$ for the fundamental representation, the *QCD* beta function at one loop reads:

$$\beta(g) = \frac{\partial g}{\partial \log \Lambda} = -\beta_0 g^3 + \dots\tag{A.47a}$$

$$\beta_0 = \frac{1}{(4\pi)^2} \left(\frac{11}{3}N - \frac{2}{3}n_f \right)\tag{A.47b}$$

Appendix B

Heavy meson chiral Lagrangians

We report here a brief review on heavy meson chiral Lagrangians in the case of the interaction with light vector mesons [199], with the so-called hidden gauge approach. The interaction Lagrangian is given by

$$\mathcal{L}_{\rho DD^*} = i\beta \langle H_{1b} v^\mu (\mathcal{V}_\mu - \rho_\mu)_{ba} \bar{H}_{1a} \rangle + i\lambda \langle H_{1b} \sigma^{\mu\nu} F_{\mu\nu}(\rho)_{ba} \bar{H}_{1a} \rangle + h.c., \quad (\text{B.1})$$

where $F_{\mu\nu}(\rho) = \partial_\mu \rho_\nu - \partial_\nu \rho_\mu + [\rho_\mu, \rho_\nu]$ and $\sigma^{\mu\nu} = i[\gamma_\mu, \gamma_\nu]/2$. The vector field \mathcal{V}_μ contains information on pion pairs, which are not of interest for the present case. The imposition of Vector Meson Dominance implies $\beta = 0.9 \pm 0.1$. QCD sum rules give $\lambda = (0.56 \pm 0.07) \text{ GeV}^{-1}$ [338]. H_{1a} and H_{2a} are the Heavy Quark Effective Theory bi-spinors for mesons and anti-mesons respectively:

$$\begin{aligned} H_{1a} &= \left(\frac{1+\psi}{2} \right) [V_a^\mu \gamma_\mu + P_a \gamma_5], \quad H_{2a} = [\bar{V}_a^\mu \gamma_\mu - \bar{P}_a \gamma_5] \left(\frac{1-\psi}{2} \right), \quad \bar{H}_{1,2a} = \gamma_0 H_{1,2a}^\dagger \gamma_0 \\ \Psi &= \left(\frac{1+\psi}{2} \right) [\psi_\mu \gamma^\mu - \eta_c \gamma^5] \left(\frac{1-\psi}{2} \right), \quad \chi_\mu = \left(\frac{1+\psi}{2} \right) [\dots + h_{c,\mu} \gamma^5] \left(\frac{1-\psi}{2} \right) \\ \mathcal{Z}_\mu^{(\prime)} &= \left(\frac{1+\psi}{2} \right) Z_\mu^{(\prime)} \gamma^5 \left(\frac{1-\psi}{2} \right), \end{aligned}$$

where v_μ is the heavy meson velocity and a is a flavor index. The fields V^μ (\bar{V}^μ) and P (\bar{P}) annihilate a (anti-)vector and a (anti-)pseudoscalar respectively according to $V^\mu |V(q, \epsilon)\rangle = \epsilon^\mu \sqrt{M_V} |0\rangle$, $P |P(q)\rangle = \sqrt{M_P} |0\rangle$. In the definition of χ_μ , we omit the

Process	Relativistic rule	Non-relativistic rule
$D(P) \rightarrow \rho(k, \eta) D(q)$	$-i\sqrt{2} M_D \beta g_V (v \cdot \eta^*)$	$-i\sqrt{2} M_D \beta g_V (\vec{k} \cdot \vec{\eta}^* / m_\rho)$
$D(P) \rightarrow \rho(k, \eta) D^*(q, \epsilon)$	$-\sqrt{2} M_D M_{D^*} g_V \lambda \epsilon^{\mu\nu\rho\sigma} v_\mu \epsilon_\nu^* k_\rho \eta_\sigma^*$	$\sqrt{2} M_D M_{D^*} g_V \lambda \epsilon^{ijk} k^i \eta^{*j} \epsilon^{*k}$
${}^*(P, \lambda) \rightarrow \rho(k, \eta) D^*(q, \epsilon)$	$i\sqrt{2} M_{D^*} g_V \beta (\epsilon^* \cdot \lambda) (v \cdot \eta^*) +$ $+i\sqrt{2} M_{D^*} g_V \lambda [(\epsilon^* \cdot \eta^*) (\lambda \cdot k) -$ $-(\epsilon^* \cdot k) (\lambda \cdot \eta^*)]$	$-i\sqrt{2} M_{D^*} g_V \beta (\vec{\epsilon}^* \cdot \vec{\lambda}) (\vec{k} \cdot \vec{\eta}^* / m_\rho) +$ $+i\sqrt{2} M_{D^*} g_V \lambda [(\vec{\epsilon}^* \cdot \vec{k}) (\vec{\lambda} \cdot \vec{\eta}^*) -$ $-(\vec{\epsilon}^* \cdot \vec{\eta}^*) (\vec{\lambda} \cdot \vec{k})]$

Table B.1. Feynman rules involving the ρ meson. The charge conjugated of all rules gain an additional minus sign.

$C = +1$ P -wave charmonia. For light vector mesons, we follow the anti-hermitian convention of [199], *i.e.* $\rho_\mu = ig_V \hat{\rho}_\mu / \sqrt{2}$, where:

$$\hat{\rho}_\mu = \begin{pmatrix} \rho_\mu^0 / \sqrt{2} + \omega_\mu / \sqrt{2} & \rho_\mu^+ \\ \rho_\mu^- & -\rho_\mu^0 / \sqrt{2} + \omega_\mu / \sqrt{2} \end{pmatrix}, \quad (\text{B.2})$$

and $g_V \simeq 5.8$ [199, 338]. Starting from the Lagrangians (B.1) one can obtain the Feynman rules for different processes, which we report in Table B.1. The non-relativistic limit can be obtained by letting $v \rightarrow (1, \vec{0})$.

Appendix C

NREFT amplitudes and loop integrals

According to the Feynman rules found in Table B.1 and in [196], the non-relativistic one loop amplitude associated with the processes in Figure 7.7 is:

$$\begin{aligned} \mathcal{A}_{Z_c \eta c \rho} = & 2\sqrt{2M_Z M_\eta} z_{g_V} g_2 \left[\beta \frac{\vec{q}_\rho \cdot \vec{\eta}}{m_\rho} \lambda^i \left(I^i(M_D, M_{D^*}, M_D; q_\rho) + I^i(M_{D^*}, M_D, M_{D^*}; q_\rho) \right) \right. \\ & \left. + \lambda \left((\vec{\lambda} \cdot \vec{\eta}) q_\rho^i - (\vec{\lambda} \cdot \vec{q}_\rho) \eta^i \right) \left(I^i(M_D, M_{D^*}, M_{D^*}; q_\rho) + I^i(M_{D^*}, M_D, M_{D^*}; q_\rho) \right) \right], \end{aligned} \quad (\text{C.1})$$

where $\vec{\lambda}$ and $\vec{\eta}$ are the spatial polarizations of the Z_c and of the ρ respectively and q_ρ is momentum of the outgoing ρ . The overall factor of 2 comes from the charge conjugate diagrams. $I^i(m_1, m_2, m_3; q)$ is the non-relativistic loop integral with three propagators:

$$\begin{aligned} I^i(m_1, m_2, m_3; q) = & \frac{i}{8} \int \frac{d^4 l}{(2\pi)^4} (q - 2l)^i \left(l^0 - \frac{\vec{l}^2}{2m_1} - m_1 + i\epsilon \right)^{-1} \\ & \times \left(M_{Z^{(i)}} - l^0 - \frac{\vec{l}^2}{2m_2} - m_2 + i\epsilon \right)^{-1} \left(l^0 - q^0 - \frac{(\vec{l} - \vec{q})^2}{2m_3} - m_3 + i\epsilon \right)^{-1}. \end{aligned} \quad (\text{C.2})$$

It can be computed with the same techniques explained in [196] and it gives:

$$I^i(m_1, m_2, m_3; q) = q^i [I_0(m_1, m_2, m_3; q) - 2I_1(m_1, m_2, m_3; q)], \quad (\text{C.3})$$

with:

$$I_0(m_1, m_2, m_3; q) = \frac{\mu_{12}\mu_{23}}{16\pi\sqrt{a}} \left[\tan^{-1} \left(\frac{c_{23} - c_{12}}{2\sqrt{ac_{12} - i\epsilon}} \right) + \tan^{-1} \left(\frac{2a + c_{12} - c_{23}}{2\sqrt{a(c_{23} - a) - i\epsilon}} \right) \right], \quad (\text{C.4a})$$

$$I_1(m_1, m_2, m_3; q) = \frac{1}{2a} \left\{ \frac{\mu_{12}\mu_{23}}{2} [B(c_{23} - a) - B(c_{12})] + (c_{23} - c_{12}) I_0(m_1, m_2, m_3; q) \right\}. \quad (\text{C.4b})$$

In particular, μ_{ij} is the reduced mass between m_i and m_j , $a = \left(\frac{\mu_{23}}{m_3}\right)^2 q^2$, $c_{12} = 2\mu_{12}(m_1 + m_2 - M_{Z^{(\prime)}})$ and $c_{23} = 2\mu_{23}\left(m_2 + m_3 + q_0 + \frac{\vec{q}^2}{2m_3} - M_{Z^{(\prime)}}\right)$. Lastly:

$$B(c) = -\frac{\sqrt{c - i\epsilon}}{4\pi}. \quad (\text{C.5})$$

For the case of the Z'_c we have, instead:

$$\begin{aligned} \mathcal{A}_{Z'_c \eta c \rho} = & 2\sqrt{2M_Z M_\eta} z' g_2 g_V \left[\lambda \left((\vec{\lambda} \cdot \vec{\eta}) q_\rho^i - (\vec{\lambda} \cdot \vec{q}_\rho) \eta^i \right) \right. \\ & \times \left(I^i(M_{D^*}, M_{D^*}, M_D; q_\rho) + I^i(M_{D^*}, M_{D^*}, M_{D^*}; q_\rho) \right) \\ & \left. + 2\beta \frac{\vec{q}_\rho \cdot \vec{\eta}}{m_\rho} \lambda^i I^i(M_{D^*}, M_{D^*}, M_{D^*}; q_\rho) \right]. \quad (\text{C.6}) \end{aligned}$$

Bibliography

- [1] R. Faccini, F. Piccinini, A. Pilloni, and A. Polosa, Phys.Rev. **D86**, 054012 (2012), [arXiv:1204.1223 \[hep-ph\]](#).
- [2] A. Esposito, F. Piccinini, A. Pilloni, and A. Polosa, J.Mod.Phys. **4**, 1569 (2013), [arXiv:1305.0527 \[hep-ph\]](#).
- [3] A. Guerrieri, F. Piccinini, A. Pilloni, and A. Polosa, Phys.Rev. **D90**, 034003 (2014), [arXiv:1405.7929 \[hep-ph\]](#).
- [4] A. Esposito, A. L. Guerrieri, L. Maiani, F. Piccinini, A. Pilloni, A. D. Polosa, and V. Riquer, Phys.Rev. **D92**, 034028 (2015), [arXiv:1508.00295 \[hep-ph\]](#).
- [5] M. Papinutto, F. Piccinini, A. Pilloni, A. D. Polosa, and N. Tantalo, in *Proceedings, 6th International Workshop on Charm Physics (Charm 2013)* (2013) [arXiv:1311.7374 \[hep-ph\]](#).
- [6] R. Faccini, G. Filaci, A. Guerrieri, A. Pilloni, and A. Polosa, Phys.Rev. **D91**, 117501 (2015), [arXiv:1412.7196 \[hep-ph\]](#).
- [7] L. Maiani, V. Riquer, R. Faccini, F. Piccinini, A. Pilloni, *et al.*, Phys.Rev. **D87**, 111102 (2013), [arXiv:1303.6857 \[hep-ph\]](#).
- [8] A. Esposito, A. Guerrieri, and A. Pilloni, Phys.Lett. **B746**, 194 (2015), [arXiv:1409.3551 \[hep-ph\]](#).
- [9] A. Esposito, M. Papinutto, A. Pilloni, A. Polosa, and N. Tantalo, Phys.Rev. **D88**, 054029 (2013), [arXiv:1307.2873 \[hep-ph\]](#).
- [10] A. Guerrieri, M. Papinutto, A. Pilloni, A. Polosa, and N. Tantalo, PoS **LATTICE2014**, 106 (2014), [arXiv:1411.2247 \[hep-lat\]](#).
- [11] R. N. Cahn and G. Goldhaber, *The experimental Foundations of Particle Physics* (1989).
- [12] N. Cabibbo, *Meeting of the Italian School of Physics and Weak Interactions Bologna, Italy, April 26-28, 1984*, Phys.Rev.Lett. **10**, 531 (1963), [,648(1963)].
- [13] M. Gell-Mann, Phys.Lett. **8**, 214 (1964).
- [14] G. 't Hooft and M. J. G. Veltman, Nucl.Phys. **B44**, 189 (1972).
- [15] D. J. Gross and F. Wilczek, Phys. Rev. Lett. **30**, 1343 (1973).

- [16] H. D. Politzer, Phys. Rev. Lett. **30**, 1346 (1973).
- [17] S. L. Glashow, J. Iliopoulos, and L. Maiani, Phys.Rev. **D2**, 1285 (1970).
- [18] S. L. Glashow, Nucl.Phys. **22**, 579 (1961).
- [19] J. J. Aubert *et al.* (E598 Collaboration), Phys.Rev.Lett. **33**, 1404 (1974).
- [20] J. E. Augustin *et al.* (SLAC-SP-017 Collaboration), Phys.Rev.Lett. **33**, 1406 (1974), [Adv. Exp. Phys.5,141(1976)].
- [21] T. Appelquist and H. D. Politzer, Phys.Rev.Lett. **34**, 43 (1975).
- [22] G. Goldhaber *et al.*, Phys.Rev.Lett. **37**, 255 (1976).
- [23] S. W. Herb *et al.*, Phys.Rev.Lett. **39**, 252 (1977).
- [24] E. Eichten, K. Gottfried, T. Kinoshita, K. D. Lane, and T.-M. Yan, Phys.Rev. **D17**, 3090 (1978), [Erratum: Phys. Rev.D21,313(1980)].
- [25] N. Brambilla, M. Groher, H. E. Martinez, and A. Vairo, Phys.Rev. **D90**, 114032 (2014), [arXiv:1407.7761 \[hep-ph\]](#).
- [26] Y.-P. Kuang, Front.Phys.China **1**, 19 (2006), [arXiv:hep-ph/0601044 \[hep-ph\]](#).
- [27] G. T. Bodwin, E. Braaten, and G. P. Lepage, Phys.Rev. **D51**, 1125 (1995), [Erratum: Phys. Rev.D55,5853(1997)], [arXiv:hep-ph/9407339 \[hep-ph\]](#).
- [28] N. Brambilla *et al.*, Eur.Phys.J. **C74**, 2981 (2014), [arXiv:1404.3723 \[hep-ph\]](#).
- [29] A. Bevan *et al.* (Belle, BaBar Collaboration), Eur.Phys.J. **C74**, 3026 (2014), [arXiv:1406.6311 \[hep-ex\]](#).
- [30] G. 't Hooft, Nucl.Phys. **B75**, 461 (1974).
- [31] E. Witten, Nucl.Phys. **B160**, 57 (1979).
- [32] S. Coleman, *Aspects of Symmetry* (Cambridge University Press, Cambridge, England, 1985).
- [33] S. Weinberg, Phys.Rev.Lett. **110**, 261601 (2013), [arXiv:1303.0342 \[hep-ph\]](#).
- [34] M. Knecht and S. Peris, Phys.Rev. **D88**, 036016 (2013), [arXiv:1307.1273 \[hep-ph\]](#).
- [35] L. Maiani, F. Piccinini, A. Polosa, and V. Riquer, Phys.Rev.Lett. **93**, 212002 (2004), [arXiv:hep-ph/0407017 \[hep-ph\]](#).
- [36] R. F. Lebed, Phys.Rev. **D88**, 057901 (2013), [arXiv:1308.2657 \[hep-ph\]](#).
- [37] G. Veneziano, Nucl.Phys. **B117**, 519 (1976).

- [38] E. Corrigan and P. Ramond, *Phys.Lett.* **B87**, 73 (1979).
- [39] T. D. Cohen and R. F. Lebed, *Phys.Rev.* **D89**, 054018 (2014), [arXiv:1401.1815 \[hep-ph\]](#).
- [40] S. Prelovsek and L. Leskovec, *Phys.Rev.Lett.* **111**, 192001 (2013), [arXiv:1307.5172 \[hep-lat\]](#).
- [41] S. Prelovsek and L. Leskovec, *Phys.Lett.* **B727**, 172 (2013), [arXiv:1308.2097 \[hep-lat\]](#).
- [42] S. Prelovsek, C. Lang, L. Leskovec, and D. Mohler, *Phys.Rev.* **D91**, 014504 (2015), [arXiv:1405.7623 \[hep-lat\]](#).
- [43] M. Wagner, A. Abdel-Rehim, C. Alexandrou, M. Dalla Brida, M. Gravina, *et al.*, *J.Phys.Conf.Ser.* **503**, 012031 (2014), [arXiv:1310.6905 \[hep-lat\]](#).
- [44] C. Alexandrou, J. O. Daldrop, M. Dalla Brida, M. Gravina, L. Scorzato, *et al.*, *JHEP* **1304**, 137 (2013), [arXiv:1212.1418](#).
- [45] T. D. Cohen and R. F. Lebed, *Phys.Rev.* **D90**, 016001 (2014), [arXiv:1403.8090 \[hep-ph\]](#).
- [46] S. F. Radford and W. W. Repko, *Phys.Rev.* **D75**, 074031 (2007), [arXiv:hep-ph/0701117 \[hep-ph\]](#).
- [47] C.-N. Yang, *Phys.Rev.* **77**, 242 (1950).
- [48] N. Drenska, R. Faccini, F. Piccinini, A. Polosa, F. Renga, and C. Sabelli, *Riv.Nuovo Cim.* **033**, 633 (2010), [arXiv:1006.2741 \[hep-ph\]](#).
- [49] R. Faccini, A. Pilloni, and A. D. Polosa, *Mod.Phys.Lett.* **A27**, 1230025 (2012), [arXiv:1209.0107 \[hep-ph\]](#).
- [50] A. Esposito, A. L. Guerrieri, F. Piccinini, A. Pilloni, and A. D. Polosa, *Int.J.Mod.Phys.* **A30**, 1530002 (2014), [arXiv:1411.5997 \[hep-ph\]](#).
- [51] V. Bhardwaj *et al.* (Belle Collaboration), *Phys.Rev.Lett.* **111**, 032001 (2013), [arXiv:1304.3975 \[hep-ex\]](#).
- [52] S.-K. Choi *et al.* (Belle Collaboration), *Phys.Rev.Lett.* **91**, 262001 (2003), [arXiv:hep-ex/0309032](#).
- [53] S.-K. Choi, S. L. Olsen, K. Trabelsi, I. Adachi, H. Aihara, *et al.*, *Phys.Rev.* **D84**, 052004 (2011), [arXiv:1107.0163 \[hep-ex\]](#).
- [54] B. Aubert *et al.* (BABAR Collaboration), *Phys.Rev.* **D77**, 111101 (2008), [arXiv:0803.2838 \[hep-ex\]](#).
- [55] A. Abulencia *et al.* (CDF Collaboration), *Phys.Rev.Lett.* **98**, 132002 (2007), [arXiv:hep-ex/0612053 \[hep-ex\]](#).
- [56] T. Aaltonen *et al.* (CDF Collaboration), *Phys.Rev.Lett.* **103**, 152001 (2009), [arXiv:0906.5218 \[hep-ex\]](#).

- [57] V. Abazov *et al.* (DØ Collaboration), Phys.Rev.Lett. **93**, 162002 (2004), arXiv:hep-ex/0405004 [hep-ex].
- [58] R. Aaij *et al.* (LHCb Collaboration), Eur.Phys.J. **C72**, 1972 (2012), arXiv:1112.5310 [hep-ex].
- [59] R. Aaij *et al.* (LHCb Collaboration), Phys.Rev.Lett. **110**, 222001 (2013), arXiv:1302.6269 [hep-ex].
- [60] K. Abe *et al.* (Belle Collaboration), (2005), arXiv:hep-ex/0505037 [hep-ex].
- [61] P. del Amo Sanchez *et al.* (BABAR Collaboration), Phys.Rev. **D82**, 011101 (2010), arXiv:1005.5190 [hep-ex].
- [62] V. Bhardwaj *et al.* (Belle Collaboration), Phys.Rev.Lett. **107**, 9 (2011), arXiv:1105.0177 [hep-ex].
- [63] B. Aubert *et al.* (BABAR Collaboration), Phys.Rev.Lett. **102**, 132001 (2009), arXiv:0809.0042 [hep-ex].
- [64] R. Aaij *et al.* (LHCb Collaboration), Nucl.Phys. **B886**, 665 (2014), arXiv:1404.0275 [hep-ex].
- [65] T. Aushev *et al.* (Belle Collaboration), Phys.Rev. **D81**, 031103 (2010), arXiv:0810.0358 [hep-ex].
- [66] B. Aubert *et al.* (BABAR Collaboration), Phys.Rev. **D77**, 011102 (2008), arXiv:0708.1565 [hep-ex].
- [67] M. Ablikim *et al.* (BESIII Collaboration), Phys.Rev.Lett. **112**, 022001 (2014), arXiv:1310.1163 [hep-ex].
- [68] M. Ablikim *et al.* (BESIII Collaboration), Phys.Rev.Lett. **110**, 252001 (2013), arXiv:1303.5949 [hep-ex].
- [69] Z. Liu *et al.* (Belle Collaboration), Phys.Rev.Lett. **110**, 252002 (2013), arXiv:1304.0121 [hep-ex].
- [70] T. Xiao, S. Dobbs, A. Tomaradze, and K. K. Seth, Phys.Lett. **B727**, 366 (2013), arXiv:1304.3036 [hep-ex].
- [71] M. Ablikim *et al.* (BESIII Collaboration), Phys.Rev.Lett. **111**, 242001 (2013), arXiv:1309.1896 [hep-ex].
- [72] M. Ablikim *et al.* (BESIII Collaboration), Phys.Rev.Lett. **112**, 132001 (2014), arXiv:1308.2760 [hep-ex].
- [73] K. Abe *et al.* (Belle Collaboration), Phys.Rev.Lett. **94**, 182002 (2005), arXiv:hep-ex/0408126.
- [74] B. Aubert *et al.* (BABAR Collaboration), Phys.Rev.Lett. **101**, 082001 (2008), arXiv:0711.2047 [hep-ex].

- [75] S. Uehara *et al.* (Belle Collaboration), Phys.Rev.Lett. **104**, 092001 (2010), arXiv:0912.4451 [hep-ex].
- [76] J. P. Lees *et al.* (BABAR Collaboration), Phys.Rev. **D86**, 072002 (2012), arXiv:1207.2651 [hep-ex].
- [77] S. Uehara *et al.* (Belle Collaboration), Phys.Rev.Lett. **96**, 082003 (2006), arXiv:hep-ex/0512035.
- [78] B. Aubert *et al.* (BABAR Collaboration), Phys.Rev. **D81**, 092003 (2010), arXiv:1002.0281 [hep-ex].
- [79] K. Abe *et al.* (Belle Collaboration), Phys.Rev.Lett. **98**, 082001 (2007), arXiv:hep-ex/0507019.
- [80] P. Pakhlov *et al.* (Belle Collaboration), Phys.Rev.Lett. **100**, 202001 (2008), arXiv:0708.3812 [hep-ex].
- [81] C. Z. Yuan *et al.* (Belle Collaboration), Phys.Rev.Lett. **99**, 182004 (2007), arXiv:0707.2541 [hep-ex].
- [82] R. Mizuk *et al.* (Belle Collaboration), Phys.Rev. **D78**, 072004 (2008), arXiv:0806.4098 [hep-ex].
- [83] J. P. Lees *et al.* (BABAR Collaboration), Phys.Rev. **D85**, 052003 (2012), arXiv:1111.5919 [hep-ex].
- [84] T. Aaltonen *et al.* (CDF Collaboration), Phys.Rev.Lett. **102**, 242002 (2009), arXiv:0903.2229 [hep-ex].
- [85] T. Aaltonen *et al.* (CDF Collaboration), (2011), arXiv:1101.6058 [hep-ex].
- [86] C. P. Shen *et al.* (Belle Collaboration), Phys.Rev.Lett. **104**, 112004 (2010), arXiv:0912.2383 [hep-ex].
- [87] R. Aaij *et al.* (LHCb Collaboration), Phys.Rev. **D85**, 091103 (2012), arXiv:1202.5087 [hep-ex].
- [88] S. Chatrchyan *et al.* (CMS Collaboration), Phys.Lett. **B734**, 261 (2014), arXiv:1309.6920 [hep-ex].
- [89] V. M. Abazov *et al.* (DØ Collaboration), Phys.Rev. **D89**, 012004 (2014), arXiv:1309.6580 [hep-ex].
- [90] K. Chilikin *et al.* (Belle Collaboration), Phys.Rev. **D90**, 112009 (2014), arXiv:1408.6457 [hep-ex].
- [91] C.-Z. Yuan, Chin.Phys. **C38**, 043001 (2014), arXiv:1312.6399 [hep-ex].
- [92] C.-Z. Yuan, Int.J.Mod.Phys. **A29**, 1430046 (2014), arXiv:1404.7768 [hep-ex].
- [93] M. Ablikim *et al.* (BESIII Collaboration), Phys.Rev.Lett. **114**, 092003 (2015), arXiv:1410.6538 [hep-ex].

- [94] B. Aubert *et al.* (BABAR Collaboration), Phys.Rev.Lett. **95**, 142001 (2005), arXiv:hep-ex/0506081.
- [95] J. P. Lees *et al.* (BABAR Collaboration), Phys.Rev. **D86**, 051102 (2012), arXiv:1204.2158 [hep-ex].
- [96] T. E. Coan *et al.* (CLEO Collaboration), Phys.Rev.Lett. **96**, 162003 (2006), arXiv:hep-ex/0602034 [hep-ex].
- [97] Q. He *et al.* (CLEO Collaboration), Phys.Rev. **D74**, 091104 (2006), arXiv:hep-ex/0611021 [hep-ex].
- [98] M. Ablikim *et al.* (BESIII Collaboration), Phys.Rev.Lett. **112**, 092001 (2014), arXiv:1310.4101 [hep-ex].
- [99] X. L. Wang *et al.* (Belle Collaboration), Phys.Rev.Lett. **99**, 142002 (2007), arXiv:0707.3699 [hep-ex].
- [100] J. Lees *et al.* (BABAR Collaboration), Phys.Rev. **D89**, 111103 (2014), arXiv:1211.6271 [hep-ex].
- [101] R. Aaij *et al.* (LHCb Collaboration), Phys.Rev.Lett. **115**, 072001 (2015), arXiv:1507.03414 [hep-ex].
- [102] R. Mizuk *et al.* (Belle Collaboration), Phys.Rev. **D80**, 031104 (2009), arXiv:0905.2869 [hep-ex].
- [103] K. Chilikin *et al.* (Belle Collaboration), Phys.Rev. **D88**, 074026 (2013), arXiv:1306.4894 [hep-ex].
- [104] B. Aubert *et al.* (BABAR Collaboration), Phys.Rev. **D79**, 112001 (2009), arXiv:0811.0564 [hep-ex].
- [105] R. Aaij *et al.* (LHCb Collaboration), Phys.Rev.Lett. **112**, 222002 (2014), arXiv:1404.1903 [hep-ex].
- [106] G. Pakhlova *et al.* (Belle Collaboration), Phys.Rev.Lett. **101**, 172001 (2008), arXiv:0807.4458 [hep-ex].
- [107] A. Bondar *et al.* (Belle Collaboration), Phys.Rev.Lett. **108**, 122001 (2012), arXiv:1110.2251 [hep-ex].
- [108] P. Krokovny *et al.* (Belle Collaboration), Phys.Rev. **D88**, 052016 (2013), arXiv:1308.2646 [hep-ex].
- [109] I. Adachi *et al.* (Belle Collaboration), (2012), arXiv:1209.6450 [hep-ex].
- [110] S.-K. Choi *et al.* (Belle Collaboration), Phys.Rev.Lett. **100**, 142001 (2008), arXiv:0708.1790 [hep-ex].
- [111] D. Bugg, J.Phys. **G35**, 075005 (2008), arXiv:0802.0934 [hep-ph].
- [112] M. Ablikim *et al.* (BESIII Collaboration), Phys.Rev.Lett. **115**, 112003 (2015), arXiv:1506.06018 [hep-ex].

- [113] K. Olive *et al.* (Particle Data Group Collaboration), *Chin.Phys.* **C38**, 090001 (2014).
- [114] M. Ablikim *et al.* (BESIII Collaboration), *Phys.Rev.Lett.* **113**, 212002 (2014), [arXiv:1409.6577 \[hep-ex\]](#).
- [115] C. Adolph *et al.* (COMPASS Collaboration), *Phys.Lett.* **B742**, 330 (2015), [arXiv:1407.6186 \[hep-ex\]](#).
- [116] X. Wang, C. Yuan, C. Shen, P. Wang, A. Abdesselam, *et al.* (Belle Collaboration), *Phys.Rev.* **D91**, 112007 (2015), [arXiv:1410.7641 \[hep-ex\]](#).
- [117] K.-F. Chen *et al.* (Belle Collaboration), *Phys.Rev.Lett.* **100**, 112001 (2008), [arXiv:0710.2577 \[hep-ex\]](#).
- [118] I. Adachi *et al.* (Belle Collaboration), *Phys.Rev.Lett.* **108**, 032001 (2012), [arXiv:1103.3419 \[hep-ex\]](#).
- [119] A. Garmash *et al.* (Belle Collaboration), *Phys.Rev.* **D91**, 072003 (2015), [arXiv:1403.0992 \[hep-ex\]](#).
- [120] B. Aubert *et al.* (BABAR Collaboration), *Phys.Rev.* **D71**, 071103 (2005), [arXiv:hep-ex/0406022](#).
- [121] D. Acosta *et al.* (CDF Collaboration), *Phys.Rev.Lett.* **93**, 072001 (2004), [arXiv:hep-ex/0312021 \[hep-ex\]](#).
- [122] S. Chatrchyan *et al.* (CMS Collaboration), *JHEP* **1304**, 154 (2013), [arXiv:1302.3968 \[hep-ex\]](#).
- [123] A. Abulencia *et al.* (CDF Collaboration), *Phys.Rev.Lett.* **96**, 102002 (2006), [arXiv:hep-ex/0512074 \[hep-ex\]](#).
- [124] B. Aubert *et al.* (BABAR Collaboration), *Phys.Rev.* **D74**, 071101 (2006), [arXiv:hep-ex/0607050](#).
- [125] K. Abe *et al.* (Belle Collaboration), (2005), [arXiv:hep-ex/0505038 \[hep-ex\]](#).
- [126] T. J. Burns, F. Piccinini, A. D. Polosa, and C. Sabelli, *Phys.Rev.* **D82**, 074003 (2010), [arXiv:1008.0018 \[hep-ph\]](#).
- [127] C. Hanhart, Y. S. Kalashnikova, A. E. Kudryavtsev, and A. V. Nefediev, *Phys.Rev.* **D85**, 011501 (2012), [arXiv:1111.6241 \[hep-ph\]](#).
- [128] E. Braaten and D. Kang, *Phys.Rev.* **D88**, 014028 (2013), [arXiv:1305.5564 \[hep-ph\]](#).
- [129] S. Dobbs *et al.* (CLEO Collaboration), *Phys.Rev.Lett.* **94**, 032004 (2005), [arXiv:hep-ex/0410038 \[hep-ex\]](#).
- [130] G. Gokhroo *et al.* (Belle Collaboration), *Phys.Rev.Lett.* **97**, 162002 (2006), [arXiv:hep-ex/0606055](#).

- [131] P. Artoisenet, E. Braaten, and D. Kang, Phys.Rev. **D82**, 014013 (2010), arXiv:1005.2167 [hep-ph].
- [132] C. Hanhart, Y. S. Kalashnikova, and A. V. Nefediev, Phys.Rev. **D81**, 094028 (2010), arXiv:1002.4097 [hep-ph].
- [133] C. Hanhart, Y. S. Kalashnikova, and A. V. Nefediev, Eur.Phys.J. **A47**, 101 (2011), arXiv:1106.1185 [hep-ph].
- [134] I. Adachi *et al.* (Belle Collaboration), (2008), arXiv:0809.1224 [hep-ex].
- [135] B. Aubert *et al.* (BABAR Collaboration), Phys.Rev.Lett. **96**, 052002 (2006), arXiv:hep-ex/0510070.
- [136] B. Aubert *et al.* (BABAR Collaboration), Phys.Rev. **D73**, 011101 (2006), arXiv:hep-ex/0507090.
- [137] B. Aubert *et al.* (BABAR Collaboration), Phys.Rev. **D71**, 031501 (2005), arXiv:hep-ex/0412051.
- [138] “The “Lifetime” Distribution of $X(3872)$ Mesons Produced in $\bar{p}p$ Collisions at CDF,” CDF note 7159.
- [139] C. Bignamini, B. Grinstein, F. Piccinini, A. Polosa, and C. Sabelli, Phys.Rev.Lett. **103**, 162001 (2009), arXiv:0906.0882 [hep-ph].
- [140] R. Aaij *et al.* (LHCb Collaboration), Eur.Phys.J. **C73**, 2462 (2013), arXiv:1303.7133 [hep-ex].
- [141] K. Abe *et al.* (Belle Collaboration), Phys.Lett. **B662**, 323 (2008), arXiv:hep-ex/0608037.
- [142] B. Aubert *et al.* (BABAR Collaboration), Phys.Rev.Lett. **93**, 041801 (2004), arXiv:hep-ex/0402025.
- [143] S. Cho *et al.* (ExHIC Collaboration), Phys.Rev. **C84**, 064910 (2011), arXiv:1107.1302 [nucl-th].
- [144] B. Aubert *et al.* (BABAR Collaboration), Phys.Rev.Lett. **98**, 212001 (2007), arXiv:hep-ex/0610057.
- [145] G. Cotugno, R. Faccini, A. Polosa, and C. Sabelli, Phys.Rev.Lett. **104**, 132005 (2010), arXiv:0911.2178 [hep-ph].
- [146] B. Aubert *et al.* (BABAR Collaboration), Phys.Rev.Lett. **99**, 071801 (2007), arXiv:0705.1190 [hep-ex].
- [147] P. del Amo Sanchez *et al.* (BABAR Collaboration), Phys.Rev. **D82**, 052004 (2010), arXiv:1008.0338 [hep-ex].
- [148] G. Pakhlova *et al.* (Belle Collaboration), Phys.Rev. **D80**, 091101 (2009), arXiv:0908.0231 [hep-ex].

- [149] C. Yuan *et al.* (Belle Collaboration), Phys.Rev. **D77**, 011105 (2008), arXiv:0709.2565 [hep-ex].
- [150] X. Wang, Y. Han, C. Yuan, C. Shen, and P. Wang (Belle Collaboration), Phys.Rev. **D87**, 051101 (2013), arXiv:1210.7550 [hep-ex].
- [151] B. Aubert *et al.* (BABAR Collaboration), Phys.Rev. **D76**, 012008 (2007), arXiv:0704.0630 [hep-ex].
- [152] B. Aubert *et al.* (BABAR Collaboration), Phys.Rev. **D77**, 092002 (2008), arXiv:0710.4451 [hep-ex].
- [153] T. Pedlar *et al.* (CLEO Collaboration), Phys.Rev.Lett. **107**, 041803 (2011), arXiv:1104.2025 [hep-ex].
- [154] B. Aubert *et al.* (BABAR Collaboration), Phys.Rev. **D73**, 012005 (2006), arXiv:hep-ex/0512023 [hep-ex].
- [155] J. Brodzicka *et al.* (Belle Collaboration), Phys.Rev.Lett. **100**, 092001 (2008), arXiv:0707.3491 [hep-ex].
- [156] T. Barnes, S. Godfrey, and E. Swanson, Phys.Rev. **D72**, 054026 (2005), arXiv:hep-ph/0505002 [hep-ph].
- [157] F.-K. Guo and U.-G. Meißner, Phys.Rev. **D86**, 091501 (2012), arXiv:1208.1134 [hep-ph].
- [158] S. L. Olsen, Phys.Rev. **D91**, 057501 (2015), arXiv:1410.6534 [hep-ex].
- [159] T. Branz, T. Gutsche, and V. E. Lyubovitskij, Phys.Rev. **D80**, 054019 (2009), arXiv:0903.5424 [hep-ph].
- [160] J. Lees *et al.*, Phys.Rev. **D91**, 012003 (2015), arXiv:1407.7244 [hep-ex].
- [161] M. Ablikim *et al.* (BESIII Collaboration), Phys.Rev. **D91**, 032002 (2015), arXiv:1412.1867 [hep-ex].
- [162] L. Liu *et al.* (Hadron Spectrum Collaboration), JHEP **1207**, 126 (2012), arXiv:1204.5425 [hep-ph].
- [163] M. Luscher and U. Wolff, Nucl.Phys. **B339**, 222 (1990).
- [164] S. Prelovsek, PoS **LATTICE2014**, 015 (2014), arXiv:1411.0405 [hep-lat].
- [165] L. Maiani and M. Testa, Phys.Lett. **B245**, 585 (1990).
- [166] M. Lüscher, Nucl.Phys. **B354**, 531 (1991).
- [167] M. Lüscher, Nucl.Phys. **B364**, 237 (1991).
- [168] S. Sasaki and T. Yamazaki, Phys.Rev. **D74**, 114507 (2006), arXiv:hep-lat/0610081 [hep-lat].

- [169] Y. Chen, M. Gong, Y.-H. Lei, N. Li, J. Liang, *et al.*, Phys.Rev. **D89**, 094506 (2014), [arXiv:1403.1318 \[hep-lat\]](#).
- [170] N. A. Tornqvist, Phys.Rev.Lett. **67**, 556 (1991).
- [171] T. E. O. Ericson and G. Karl, Phys.Lett. **B309**, 426 (1993).
- [172] A. De Rujula, H. Georgi, and S. Glashow, Phys.Rev.Lett. **38**, 317 (1977).
- [173] M. Voloshin and L. Okun, JETP Lett. **23**, 333 (1976).
- [174] N. A. Tornqvist, Z.Phys. **C61**, 525 (1994), [arXiv:hep-ph/9310247 \[hep-ph\]](#).
- [175] A. V. Manohar and M. B. Wise, Nucl.Phys. **B399**, 17 (1993), [arXiv:hep-ph/9212236 \[hep-ph\]](#).
- [176] E. S. Swanson, Annals Phys. **220**, 73 (1992).
- [177] Y. Kalashnikova and A. Nefediev, Pisma Zh.Eksp.Teor.Fiz. **97**, 76 (2013), [arXiv:1212.2004 \[hep-ph\]](#).
- [178] N. A. Tornqvist, Phys.Lett. **B590**, 209 (2004), this report supersedes the unpublished reminder [hep-ph/0308277](#), [arXiv:hep-ph/0402237 \[hep-ph\]](#).
- [179] T. Barnes and E. Swanson, Phys.Rev. **D46**, 131 (1992).
- [180] E. S. Swanson, Phys.Rept. **429**, 243 (2006), [arXiv:hep-ph/0601110 \[hep-ph\]](#).
- [181] E. S. Swanson, Phys.Lett. **B588**, 189 (2004), [arXiv:hep-ph/0311229 \[hep-ph\]](#).
- [182] A. Bondar, A. Garmash, A. Milstein, R. Mizuk, and M. Voloshin, Phys.Rev. **D84**, 054010 (2011), [arXiv:1105.4473 \[hep-ph\]](#).
- [183] F.-K. Guo, C. Hanhart, and U.-G. Meißner, Phys.Rev.Lett. **102**, 242004 (2009), [arXiv:0904.3338 \[hep-ph\]](#).
- [184] F.-K. Guo, C. Hidalgo-Duque, J. Nieves, and M. P. Valderrama, Phys.Rev. **D88**, 054007 (2013), [arXiv:1303.6608 \[hep-ph\]](#).
- [185] A. Tomaradze, S. Dobbs, T. Xiao, K. K. Seth, and G. Bonvicini, (2012), [arXiv:1212.4191 \[hep-ex\]](#).
- [186] M. Voloshin, Phys.Lett. **B579**, 316 (2004), [arXiv:hep-ph/0309307 \[hep-ph\]](#).
- [187] E. Braaten and M. Kusunoki, Phys.Rev. **D69**, 074005 (2004), [arXiv:hep-ph/0311147 \[hep-ph\]](#).
- [188] A. J. Leggett, *Quantum liquids: Bose condensation and Cooper pairing in condensed-matter systems* (Oxford University Press, 2006).

- [189] C. Hanhart, Y. Kalashnikova, A. E. Kudryavtsev, and A. Nefediev, Phys.Rev. **D76**, 034007 (2007), arXiv:0704.0605 [hep-ph].
- [190] E. Braaten and M. Lu, Phys.Rev. **D76**, 094028 (2007), arXiv:0709.2697 [hep-ph].
- [191] E. Braaten and J. Stapleton, Phys.Rev. **D81**, 014019 (2010), arXiv:0907.3167 [hep-ph].
- [192] E. Braaten and M. Lu, Phys.Rev. **D79**, 051503 (2009), arXiv:0712.3885 [hep-ph].
- [193] S. Fleming, M. Kusunoki, T. Mehen, and U. van Kolck, Phys.Rev. **D76**, 034006 (2007), arXiv:hep-ph/0703168 [hep-ph].
- [194] M. Cleven, F.-K. Guo, C. Hanhart, and U.-G. Meissner, Eur.Phys.J. **A47**, 120 (2011), arXiv:1107.0254 [hep-ph].
- [195] M. Cleven, Q. Wang, F.-K. Guo, C. Hanhart, U.-G. Meissner, *et al.*, Phys.Rev. **D87**, 074006 (2013), arXiv:1301.6461 [hep-ph].
- [196] M. Cleven, (2014), arXiv:1405.4195 [hep-ph].
- [197] Q. Wang, C. Hanhart, and Q. Zhao, Phys.Rev.Lett. **111**, 132003 (2013), arXiv:1303.6355 [hep-ph].
- [198] F.-K. Guo, C. Hanhart, U.-G. Meißner, Q. Wang, and Q. Zhao, Phys.Lett. **B725**, 127 (2013), arXiv:1306.3096 [hep-ph].
- [199] R. Casalbuoni, A. Deandrea, N. Di Bartolomeo, R. Gatto, F. Feruglio, *et al.*, Phys.Rept. **281**, 145 (1997), arXiv:hep-ph/9605342 [hep-ph].
- [200] A. Manohar and M. Wise, *Heavy Quark Physics* (Cambridge University Press, 2007).
- [201] C. Z. Yuan, P. Wang, and X. H. Mo, Phys.Lett. **B634**, 399 (2006), arXiv:hep-ph/0511107 [hep-ph].
- [202] F.-K. Guo, C. Hanhart, and U.-G. Meissner, Phys.Lett. **B665**, 26 (2008), arXiv:0803.1392 [hep-ph].
- [203] S. Dubynskiy and M. Voloshin, Phys.Lett. **B666**, 344 (2008), arXiv:0803.2224 [hep-ph].
- [204] S. Dubynskiy, A. Gorsky, and M. Voloshin, Phys.Lett. **B671**, 82 (2009), arXiv:0804.2244 [hep-th].
- [205] S. J. Brodsky, I. Schmidt, and G. de Teramond, Phys.Rev.Lett. **64**, 1011 (1990).
- [206] M. Voloshin, Mod.Phys.Lett. **A19**, 665 (2004), arXiv:hep-ph/0402011 [hep-ph].

- [207] X. Li and M. Voloshin, *Mod.Phys.Lett.* **A29**, 1450060 (2014), [arXiv:1309.1681 \[hep-ph\]](#).
- [208] M. B. Voloshin, *Phys.Rev.* **D87**, 091501 (2013), [arXiv:1304.0380 \[hep-ph\]](#).
- [209] R. Jaffe and K. Johnson, *Phys.Lett.* **B60**, 201 (1976).
- [210] T. Barnes and F. Close, *Phys.Lett.* **B116**, 365 (1982).
- [211] T. Barnes, F. Close, F. de Viron, and J. Weyers, *Nucl.Phys.* **B224**, 241 (1983).
- [212] P. Hasenfratz, R. Horgan, J. Kuti, and J. Richard, *Phys.Lett.* **B95**, 299 (1980).
- [213] Y. Kalashnikova and D. Kuzmenko, *Phys.Atom.Nucl.* **66**, 955 (2003), [arXiv:hep-ph/0203128 \[hep-ph\]](#).
- [214] D. Horn and J. Mandula, *Phys.Rev.* **D17**, 898 (1978).
- [215] M. Tanimoto, *Phys.Lett.* **B116**, 198 (1982).
- [216] M. Tanimoto, *Phys.Rev.* **D27**, 2648 (1983).
- [217] F. Iddir, A. Le Yaouanc, L. Oliver, O. Pene, J. Raynal, *et al.*, *Phys.Lett.* **B205**, 564 (1988).
- [218] S. Ishida, H. Sawazaki, M. Oda, and K. Yamada, *Phys.Rev.* **D47**, 179 (1993).
- [219] S. Ishida, M. Oda, H. Sawazaki, and K. Yamada, *Prog.Theor.Phys.* **82**, 119 (1989).
- [220] T. Barnes, F. Close, and E. Swanson, *Phys.Rev.* **D52**, 5242 (1995), [arXiv:hep-ph/9501405 \[hep-ph\]](#).
- [221] S. Perantonis and C. Michael, *Nucl.Phys.* **B347**, 854 (1990).
- [222] P. Guo, A. P. Szczepaniak, G. Galata, A. Vassallo, and E. Santopinto, *Phys.Rev.* **D78**, 056003 (2008), [arXiv:0807.2721 \[hep-ph\]](#).
- [223] E. Braaten, *Phys.Rev.Lett.* **111**, 162003 (2013), [arXiv:1305.6905 \[hep-ph\]](#).
- [224] E. Braaten, C. Langmack, and D. H. Smith, *Phys.Rev.* **D90**, 014044 (2014), [arXiv:1402.0438 \[hep-ph\]](#).
- [225] E. Kou and O. Pene, *Phys.Lett.* **B631**, 164 (2005), [arXiv:hep-ph/0507119 \[hep-ph\]](#).
- [226] K. Marsh and R. Lewis, *Phys.Rev.* **D89**, 014502 (2014), [arXiv:1309.1627 \[hep-lat\]](#).
- [227] C. Morningstar, K. Juge, and J. Kuti, , 179 (1998), [arXiv:hep-lat/9809015 \[hep-lat\]](#).
- [228] F. E. Close and P. R. Page, *Nucl.Phys.* **B443**, 233 (1995), [arXiv:hep-ph/9411301 \[hep-ph\]](#).

- [229] D. Bugg, Phys.Lett. **B598**, 8 (2004), arXiv:hep-ph/0406293 [hep-ph].
- [230] E. Swanson, Phys.Rev. **D91**, 034009 (2015), arXiv:1409.3291 [hep-ph].
- [231] P. Pakhlov and T. Uglov, Phys.Lett. **B748**, 183 (2015), arXiv:1408.5295 [hep-ph].
- [232] F.-K. Guo, C. Hanhart, Q. Wang, and Q. Zhao, Phys.Rev. **D91**, 051504 (2015), arXiv:1411.5584 [hep-ph].
- [233] A. P. Szczepaniak, Phys.Lett. **B747**, 410 (2015), arXiv:1501.01691 [hep-ph].
- [234] J. Ferretti, G. Galatà, and E. Santopinto, Phys.Rev. **C88**, 015207 (2013), arXiv:1302.6857 [hep-ph].
- [235] L. Csernai and J. I. Kapusta, Phys.Rept. **131**, 223 (1986).
- [236] P. Artoisenet and E. Braaten, Phys.Rev. **D83**, 014019 (2011), arXiv:1007.2868 [hep-ph].
- [237] G. Corcella, I. Knowles, G. Marchesini, S. Moretti, K. Odagiri, *et al.*, JHEP **0101**, 010 (2001), arXiv:hep-ph/0011363 [hep-ph].
- [238] T. Sjostrand, S. Mrenna, and P. Z. Skands, JHEP **0605**, 026 (2006), arXiv:hep-ph/0603175 [hep-ph].
- [239] P. Artoisenet and E. Braaten, Phys.Rev. **D81**, 114018 (2010), arXiv:0911.2016 [hep-ph].
- [240] M. Goldberger and K. Watson, *Collision Theory*, 3rd ed. (Dover Publications, 2004).
- [241] C. Bignamini, B. Grinstein, F. Piccinini, A. Polosa, V. Riquer, *et al.*, Phys.Lett. **B684**, 228 (2010), arXiv:0912.5064 [hep-ph].
- [242] D. Acosta *et al.* (CDF Collaboration), Phys.Rev.Lett. **91**, 241804 (2003), arXiv:hep-ex/0307080 [hep-ex].
- [243] N. Sharma and A. Kalweit (ALICE Collaboration), Acta Phys.Polon.Supp. **5**, 605 (2012).
- [244] J. Adam *et al.* (ALICE Collaboration), (2015), arXiv:1506.08453 [nucl-ex].
- [245] J. Adam *et al.* (ALICE Collaboration), (2015), arXiv:1506.08951 [nucl-ex].
- [246] E. Schnedermann, J. Sollfrank, and U. W. Heinz, Phys.Rev. **C48**, 2462 (1993), arXiv:nucl-th/9307020 [nucl-th].
- [247] D. G. d'Enterria, (2003), arXiv:nucl-ex/0302016 [nucl-ex].

- [248] B. Abelev *et al.* (ALICE Collaboration), Phys.Rev. **C88**, 044909 (2013), arXiv:1301.4361 [nucl-ex].
- [249] H. Kamada, J. Golak, K. Miyagawa, H. Witala, and W. Gloeckle, Phys.Rev. **C57**, 1595 (1998), arXiv:nucl-th/9709035 [nucl-th].
- [250] G. Antchev *et al.* (TOTEM Collaboration), Europhys.Lett. **101**, 21003 (2013).
- [251] B. Abelev *et al.* (ALICE Collaboration), Eur.Phys.J. **C73**, 2456 (2013), arXiv:1208.4968 [hep-ex].
- [252] H. Sato and K. Yazaki, Phys.Lett. **B98**, 153 (1981).
- [253] G. Aad *et al.* (ATLAS Collaboration), JHEP **09**, 050 (2015), arXiv:1504.04337 [hep-ex].
- [254] C.-Z. Yuan (Belle Collaboration), in *29th International Conference on Physics in Collision (PIC 2009) Kobe, Japan, August 30-September 2, 2009* (2009) arXiv:0910.3138 [hep-ex].
- [255] K. Reygers (PHENIX Collaboration), *Proceedings, 20th International Conference on Ultra-Relativistic Nucleus-Nucleus Collisions (QM 2008)*, J.Phys. **G35**, 104045 (2008), arXiv:0804.4562 [nucl-ex].
- [256] J. Adams *et al.* (STAR Collaboration), Phys.Rev.Lett. **91**, 072304 (2003), arXiv:nucl-ex/0306024 [nucl-ex].
- [257] S. Chatrchyan *et al.* (CMS Collaboration), Eur.Phys.J. **C72**, 1945 (2012), arXiv:1202.2554 [nucl-ex].
- [258] K. Aamodt *et al.* (ALICE Collaboration), Phys.Lett. **B696**, 30 (2013), arXiv:1012.1004 [nucl-ex].
- [259] M. Gyulassy and M. Plumer, Phys.Lett. **B243**, 432 (1990).
- [260] M. Gyulassy, I. Vitev, X.-N. Wang, and B.-W. Zhang, (2003), arXiv:nucl-th/0302077 [nucl-th].
- [261] R. Baier, Y. L. Dokshitzer, S. Peigne, and D. Schiff, Phys.Lett. **B345**, 277 (1995), arXiv:hep-ph/9411409 [hep-ph].
- [262] S. Cho *et al.* (ExHIC Collaboration), Phys.Rev.Lett. **106**, 212001 (2011), arXiv:1011.0852 [nucl-th].
- [263] T. Hirano and M. Gyulassy, Nucl.Phys. **A769**, 71 (2006), arXiv:nucl-th/0506049 [nucl-th].
- [264] L. Maiani, F. Piccinini, A. D. Polosa, and V. Riquer, Phys.Rev. **D71**, 014028 (2005), arXiv:hep-ph/0412098 [hep-ph].
- [265] R. L. Jaffe, Phys.Rev. **D15**, 281 (1977).
- [266] R. Jaffe and F. Low, Phys.Rev. **D19**, 2105 (1979).

- [267] M. G. Alford and R. Jaffe, Nucl.Phys. **B578**, 367 (2000), arXiv:hep-lat/0001023 [hep-lat].
- [268] R. L. Jaffe and F. Wilczek, Phys.Rev.Lett. **91**, 232003 (2003), arXiv:hep-ph/0307341 [hep-ph].
- [269] G. 't Hooft, G. Isidori, L. Maiani, A. Polosa, and V. Riquer, Phys.Lett. **B662**, 424 (2008), arXiv:0801.2288 [hep-ph].
- [270] A. Deandrea and A. Polosa, Phys.Rev.Lett. **86**, 216 (2001), arXiv:hep-ph/0008084 [hep-ph].
- [271] I. Caprini, G. Colangelo, and H. Leutwyler, Phys.Rev.Lett. **96**, 132001 (2006), arXiv:hep-ph/0512364 [hep-ph].
- [272] G. Rossi and G. Veneziano, Nucl.Phys. **B123**, 507 (1977).
- [273] L. Montanet, G. Rossi, and G. Veneziano, Phys.Rept. **63**, 149 (1980).
- [274] G. Rossi and G. Veneziano, Phys.Lett. **B70**, 255 (1977).
- [275] N. Barnea, J. Vijande, and A. Valcarce, Phys.Rev. **D73**, 054004 (2006), arXiv:hep-ph/0604010 [hep-ph].
- [276] J. Vijande, E. Weissman, N. Barnea, and A. Valcarce, Phys.Rev. **D76**, 094022 (2007), arXiv:0708.3285 [hep-ph].
- [277] J. Vijande, E. Weissman, A. Valcarce, and N. Barnea, Phys.Rev. **D76**, 094027 (2007), arXiv:0710.2516 [hep-ph].
- [278] T. Fernandez-Carames, A. Valcarce, and J. Vijande, Phys.Rev.Lett. **103**, 222001 (2009), arXiv:1001.4506 [hep-ph].
- [279] J. Vijande, A. Valcarce, and J.-M. Richard, Phys.Rev. **D87**, 034040 (2013), arXiv:1301.6212 [hep-ph].
- [280] A. Polosa, Phys.Lett. **B746**, 248 (2015), arXiv:1505.03083 [hep-ph].
- [281] F. Brazzi, B. Grinstein, F. Piccinini, A. D. Polosa, and C. Sabelli, Phys.Rev. **D84**, 014003 (2011), arXiv:1103.3155 [hep-ph].
- [282] L. Maiani, A. Polosa, and V. Riquer, (2007), arXiv:0708.3997 [hep-ph].
- [283] C. Alexandrou, P. de Forcrand, and B. Lucini, Phys.Rev.Lett. **97**, 222002 (2006), arXiv:hep-lat/0609004 [hep-lat].
- [284] A. De Rujula, H. Georgi, and S. L. Glashow, Phys.Rev. **D12**, 147 (1975).
- [285] R. Jaffe, Phys.Rept. **409**, 1 (2005), arXiv:hep-ph/0409065 [hep-ph].
- [286] L. Maiani, F. Piccinini, A. Polosa, and V. Riquer, Phys.Rev. **D89**, 114010 (2014), arXiv:1405.1551 [hep-ph].

- [287] L. Maiani, V. Riquer, F. Piccinini, and A. Polosa, Phys.Rev. **D72**, 031502 (2005), [arXiv:hep-ph/0507062](#) [hep-ph].
- [288] M. B. Voloshin, Sov.J.Nucl.Phys. **43**, 1011 (1986), [Yad.Fiz.43,1571(1986)].
- [289] A. Ali, L. Maiani, A. Polosa, and V. Riquer, Phys.Rev. **D91**, 017502 (2015), [arXiv:1412.2049](#) [hep-ph].
- [290] A. Ali, C. Hambroek, and W. Wang, Phys.Rev. **D85**, 054011 (2012), [arXiv:1110.1333](#) [hep-ph].
- [291] X. H. He *et al.* (Belle Collaboration), Phys.Rev.Lett. **113**, 142001 (2014), [arXiv:1408.0504](#) [hep-ex].
- [292] G. Aad *et al.* (ATLAS Collaboration), Phys. Lett. **B740**, 199 (2015), [arXiv:1410.4409](#) [hep-ex].
- [293] A. Ali, C. Hambroek, I. Ahmed, and M. J. Aslam, Phys.Lett. **B684**, 28 (2010), [arXiv:0911.2787](#) [hep-ph].
- [294] A. Ali, C. Hambroek, and M. J. Aslam, Phys.Rev.Lett. **104**, 162001 (2010), [Erratum: Phys. Rev. Lett.107,049903(2011)], [arXiv:0912.5016](#) [hep-ph].
- [295] B. Aubert *et al.* (BaBar Collaboration), Phys.Rev.Lett. **102**, 012001 (2009), [arXiv:0809.4120](#) [hep-ex].
- [296] K. F. Chen *et al.* (Belle Collaboration), Phys.Rev. **D82**, 091106 (2010), [arXiv:0810.3829](#) [hep-ex].
- [297] D. Santel *et al.* (Belle Collaboration), (2015), [arXiv:1501.01137](#) [hep-ex].
- [298] L. Maiani, A. D. Polosa, and V. Riquer, Phys.Lett. **B749**, 289 (2015), [arXiv:1507.04980](#) [hep-ph].
- [299] A. De Rujula, H. Georgi, and S. L. Glashow, Phys.Rev. **D12**, 147 (1975).
- [300] L. Maiani, A. D. Polosa, and V. Riquer, Phys.Lett. **B750**, 37 (2015), [arXiv:1508.04459](#) [hep-ph].
- [301] R. F. Lebed, Phys. Lett. **B749**, 454 (2015), [arXiv:1507.05867](#) [hep-ph].
- [302] V. V. Anisovich, M. A. Matveev, J. Nyiri, A. V. Sarantsev, and A. N. Semenova, (2015), [arXiv:1507.07652](#) [hep-ph].
- [303] Z.-G. Wang, (2015), [arXiv:1509.06436](#) [hep-ph].
- [304] S. J. Brodsky, D. S. Hwang, and R. F. Lebed, Phys.Rev.Lett. **113**, 112001 (2014), [arXiv:1406.7281](#) [hep-ph].
- [305] S. H. Blitz and R. F. Lebed, Phys.Rev. **D91**, 094025 (2015), [arXiv:1503.04802](#) [hep-ph].
- [306] S. J. Brodsky and G. R. Farrar, Phys.Rev.Lett. **31**, 1153 (1973).

- [307] V. A. Matveev, R. M. Muradian, and A. N. Tavkhelidze, *Lett.Nuovo Cim.* **7**, 719 (1973).
- [308] S. J. Brodsky and R. F. Lebed, *Phys.Rev.* **D91**, 114025 (2015), [arXiv:1505.00803 \[hep-ph\]](#).
- [309] M. Nielsen, F. S. Navarra, and S. H. Lee, *Phys.Rept.* **497**, 41 (2010), [arXiv:0911.1958 \[hep-ph\]](#).
- [310] M. A. Shifman, A. Vainshtein, and V. I. Zakharov, *Nucl.Phys.* **B147**, 385 (1979).
- [311] R. D. Matheus, F. Navarra, M. Nielsen, and C. Zanetti, *Phys.Rev.* **D80**, 056002 (2009), [arXiv:0907.2683 \[hep-ph\]](#).
- [312] M. A. Moinester, (1995), [arXiv:hep-ph/9503289 \[hep-ph\]](#).
- [313] A. Del Fabbro, D. Janc, M. Rosina, and D. Treleani, *Phys.Rev.* **D71**, 014008 (2005), [arXiv:hep-ph/0408258 \[hep-ph\]](#).
- [314] A. Valcarce, J. Vijande, and T. Carames, *Int.J.Mod.Phys.Conf.Ser.* **2**, 173 (2011), [arXiv:1012.4627 \[hep-ph\]](#).
- [315] M. A. Moinester, *Z.Phys.* **A355**, 349 (1996), [arXiv:hep-ph/9506405 \[hep-ph\]](#).
- [316] T. Hyodo, Y.-R. Liu, M. Oka, K. Sudoh, and S. Yasui, *Phys.Lett.* **B721**, 56 (2013), [arXiv:1209.6207 \[hep-ph\]](#).
- [317] P. Bicudo and M. Wagner (European Twisted Mass Collaboration), *Phys.Rev.* **D87**, 114511 (2013), [arXiv:1209.6274 \[hep-ph\]](#).
- [318] T. Affolder *et al.* (CDF Collaboration), *Phys.Rev.Lett.* **84**, 1663 (2000), [arXiv:hep-ex/9909011 \[hep-ex\]](#).
- [319] B. Aubert *et al.* (BABAR Collaboration), *Phys.Rev.* **D78**, 112003 (2008), [arXiv:0807.4974 \[hep-ex\]](#).
- [320] N. Gabyshev *et al.* (Belle Collaboration), *Phys.Rev.Lett.* **90**, 121802 (2003), [arXiv:hep-ex/0212052 \[hep-ex\]](#).
- [321] N. Gabyshev *et al.* (Belle Collaboration), *Phys.Rev.Lett.* **97**, 242001 (2006), [arXiv:hep-ex/0409005 \[hep-ex\]](#).
- [322] R. Aaij *et al.* (LHCb Collaboration), *Phys.Rev.* **D87**, 112012 (2013), [arXiv:1304.4530 \[hep-ex\]](#).
- [323] A. Bazavov *et al.* (HotQCD Collaboration), *Phys.Rev.* **D90**, 094503 (2014), [arXiv:1407.6387 \[hep-lat\]](#).
- [324] E. Iancu, (2012), [arXiv:1205.0579 \[hep-ph\]](#).
- [325] J. Casalderrey-Solana, H. Liu, D. Mateos, K. Rajagopal, and U. A. Wiedemann, (2011), [arXiv:1101.0618 \[hep-th\]](#).

- [326] S. H. Lee, S. Yasui, W. Liu, and C. M. Ko, *Eur.Phys.J.* **C54**, 259 (2008), [arXiv:0707.1747 \[hep-ph\]](#).
- [327] S. Cho and S. H. Lee, *Phys.Rev.* **C88**, 054901 (2013), [arXiv:1302.6381 \[nucl-th\]](#).
- [328] A. Andronic, P. Braun-Munzinger, and J. Stachel, *Nucl.Phys.* **A772**, 167 (2006), [arXiv:nucl-th/0511071 \[nucl-th\]](#).
- [329] K. Adcox *et al.* (PHENIX Collaboration), *Phys.Rev.Lett.* **88**, 242301 (2002), [arXiv:nucl-ex/0112006 \[nucl-ex\]](#).
- [330] S. Adler *et al.* (PHENIX Collaboration), *Phys.Rev.Lett.* **91**, 182301 (2003), [arXiv:nucl-ex/0305013 \[nucl-ex\]](#).
- [331] L. Chen, C. Ko, W. Liu, and M. Nielsen, *Phys.Rev.* **C76**, 014906 (2007), [arXiv:0705.1697 \[nucl-th\]](#).
- [332] S. Adler *et al.* (PHENIX Collaboration), *Phys.Rev.Lett.* **91**, 072303 (2003), [arXiv:nucl-ex/0306021 \[nucl-ex\]](#).
- [333] S. Adler *et al.* (PHENIX Collaboration), *Phys.Rev.* **C69**, 034909 (2004), [arXiv:nucl-ex/0307022 \[nucl-ex\]](#).
- [334] L. Maiani, A. Polosa, V. Riquer, and C. Salgado, *Phys.Lett.* **B645**, 138 (2007), [arXiv:hep-ph/0606217 \[hep-ph\]](#).
- [335] L. Maiani, A. Polosa, V. Riquer, and C. Salgado, (2007), [arXiv:0707.4578 \[hep-ph\]](#).
- [336] A. M. Polyakov, *Contemp. Concepts Phys.* **3**, 1 (1987).
- [337] M. Bochicchio and A. Pilloni, *JHEP* **09**, 039 (2013), [arXiv:1304.4949 \[hep-th\]](#).
- [338] C. Isola, M. Ladisa, G. Nardulli, and P. Santorelli, *Phys.Rev.* **D68**, 114001 (2003), [arXiv:hep-ph/0307367 \[hep-ph\]](#).